UNIVERSITY OF ALBERTA

MODELING VEHICLE EMISSION FACTORS DETERMINED WITH AN IN-USE & REAL-TIME EMISSION MEASUREMENT SYSTEM

BY

©

JASON DAVID HAWIRKO

A THESIS SUBMITTED TO THE FACULTY OF GRADUATE STUDIES AND RESEARCH IN PARTIAL FULFILMENT OF THE REQUIREMENTS FOR THE DEGREE OF MASTER OF SCIENCE

DEPARTMENT OF MECHANICAL ENGINEERING

EDMONTON, ALBERTA

SPRING 2003

National Library
of Canada

Acquisitions and
Bibliographic Services

395 Wellington Street
Ottawa ON K1A 0N4
Canada

Bibliothèque nationale
du Canada

Acquisitions et
services bibliographiques

395, rue Wellington
Ottawa ON K1A 0N4
Canada

Your file Votre référence

Our file Notre référence

The author has granted a non-exclusive licence allowing the National Library of Canada to reproduce, loan, distribute or sell copies of this thesis in microform, paper or electronic formats.

L'auteur a accordé une licence non exclusive permettant à la Bibliothèque nationale du Canada de reproduire, prêter, distribuer ou vendre des copies de cette thèse sous la forme de microfiche/film, de reproduction sur papier ou sur format électronique.

The author retains ownership of the copyright in this thesis. Neither the thesis nor substantial extracts from it may be printed or otherwise reproduced without the author's permission.

L'auteur conserve la propriété du droit d'auteur qui protège cette thèse. Ni la thèse ni des extraits substantiels de celle-ci ne doivent être imprimés ou autrement reproduits sans son autorisation.

0-612-82287-7

Canada

UNIVERSITY OF ALBERTA

LIBRARY RELEASE FORM

NAME OF AUTHOR: JASON DAVID HAWIRKO

TITLE OF THESIS: MODELING VEHICLE EMISSION FACTORS DETERMINED WITH AN IN-USE & REAL-TIME EMISSION MEASUREMENT SYSTEM

DEGREE: MASTER OF SCIENCE

YEAR THE DEGREE GRANTED: 2003

PERMISSION IS HEREBY GRANTED TO THE UNIVERSITY OF ALBERTA LIBRARY TO REPRODUCE SINGLE COPIES OF THIS THESIS AND TO LEND OR SELL SUCH COPIES FOR PRIVATE, SCHOLARLY OR SCIENTIFIC RESEARCH PURPOSES ONLY.

THE AUTHOR RESERVES ALL OTHER PUBLICATION AND OTHER RIGHTS IN ASSOCIATION WITH THE COPYRIGHT IN THE THESES, AND EXCEPT AS HEREIN BEFORE PROVIDED, NEITHER THE THESIS NOR ANY SUBSTANTIAL PORTION THEREOF MAY BE PRINTED OR OTHERWISE REPRODUCED IN ANY MATERIAL FORM WHATEVER WITHOUT THE AUTHOR'S PRIOR WRITTEN PERMISSION.

MR. JASON DAVID HAWIRKO
16 DONLEVY PLACE
ST. ALBERT, ALBERTA.
T8N 4W3, CANADA

DATE: Nov. 19/2002

UNIVERSITY OF ALBERTA

FACULTY OF GRADUATE STUDIES AND RESEARCH

The undersigned certify that they have read, and recommend to the Faculty of Graduate Studies and Research for acceptance, a thesis entitled Modeling Vehicle Emission Factors Determined with an In-Use & Real-Time Emission Measurement System submitted by Jason David Hawirko in partial fulfillment of the requirements for the degree of Master of Science.

Dr. M. David Checkel

Bob Koch

Dr. Charles R. Koch

Dr. Brian A. Fleck

Dr. W.B. Kindzierski

Date: Nov. 1/2002

ABSTRACT

Vehicle exhaust emissions were measured with a portable measurement system. This system was designed to operate on any automobile to provide real-time / on-road instantaneous emission rates and monitor vehicle operating parameters. The instantaneous emissions (HC, CO and NO_x) rates of the vehicle were then used to determine the emission factors represented in grams per kilometer. In this study, a single test vehicle / driver combination was examined and emission testing occurred during commuting driving sequences throughout one full year of operation. The analysis has shown the presence of two emission factors describing the pre and post-catalyst light-off operating regions. The variables of ambient temperature and non-zero average vehicle speed were used to develop a model allowing the emission factors for this test vehicle to be predicted. This work provides the foundation, including the measurement system and analysis algorithms, to extend this research to any on-road vehicle and testing scenario.

ACKNOWLEDGMENTS

I wish to thank and express my appreciation to the following people for their support and guidance:

> Dr. M David Checkel for providing me with the opportunity to work under his supervision and for all of his support and guidance.
>
> The entire Mechanical Engineering staff for their instruction of both my graduate and undergraduate degrees.
>
> Bernie Faulkner, Don Fuhr, Terry Nord, Wayne Pittman and Albert Yuen for all of their technical assistance.
>
> Jason Olfert for his invaluable help during the beginning stages of this research and for his continued assistance through the completion of my degree.
>
> Paul Rieder for his greatly appreciated contributions during the final stages of this research.
>
> NSERC, Alternative Fuel Systems (AFS) and David Morris for their financial assistance.
>
> The entire Combustion Lab for all their help, encouragement and the numerous "Safety Meetings."
>
> To all of my friends for their encouragement and support throughout this research; you are all very special to me.
>
> Finally to my family, I would like to express a special appreciation to my parents Dave and Dianna and to my brother Wade for all of their love and support.

TABLE OF CONTENTS

CHAPTER 1 **INTRODUCTION TO MODELING VEHICLE EMISSION FACTORS DETERMINED WITH AN IN-USE & REAL-TIME EMISSION MEASUREMENT SYSTEM** **1**
1.0 INTRODUCTION 2
REFERENCES 7
CHAPTER 2 **REVIEW OF CURRENT EMISSION MEASUREMENT TECHNIQUES AND EMISSION INVENTORY MODELS** **9**
2.0 INTRODUCTION 10
2.1 DYNAMOMETER TESTING 11
2.1.1 DESCRIPTION OF FTP CERTIFICATION TESTING 11
2.1.2 EFFECTS OF AMBIENT TEMPERATURE ON VEHICLE EMISSIONS 14
2.1.3 DRIVING CYCLES 14
2.1.4 INSPECTION AND MAINTENANCE (I/M) EMISSION TESTING 19
2.2 REMOTE SENSING PROCEDURE 22
2.3 CURRENT IN-USE, REAL-TIME EMISSION STUDIES 24
2.4 DESCRIPTION OF CURRENT EMISSION FACTOR MODELING SOFTWARE 25
2.5 CONCLUSIONS 27
REFERENCES 35
CHAPTER 3 **REAL-TIME, ON-ROAD MEASUREMENTS OF DRIVING BEHAVIOR, ENGINE PARAMETERS AND EXHAUST EMISSIONS** **39**
3.0 INTRODUCTION 41
3.1 GENERAL TEST SET-UP 42
3.2 EXPERIMENTAL VEHICLE 44
3.3 MEASUREMENT SYSTEM DETAILS 45
3.3.1 VETRONIX FIVE GAS ANALYZER 45
3.3.2 ECM AFRECRDER 2400E 48
3.3.3 MASS AIR FLOW MEASUREMENT 49

3.3.4 TEMPERATURE MEASUREMENTS 49
3.3.5 VEHICLE SPEED MEASUREMENTS 50
3.3.6 PORTABLE DATA ACQUISITION SYSTEM 51
3.3.7 DATA ANALYSIS SOFTWARE 51
3.4 RESULTS 54
3.4.1 DRIVING BEHAVIOR 55
3.4.2 EMISSION CHARACTERISTICS 59
3.5 CONCLUSIONS 63
3.6 FUTURE WORK 64
REFERENCES 74
CHAPTER 4 QUANTIFYING VEHICLE EMISSION FACTORS FOR VARIOUS AMBIENT AND INITIAL ENGINE CONDITIONS USING AN ON-ROAD, REAL-TIME EMISSIONS SYSTEM 78
4.0 INTRODUCTION 80
4.1 EXPERIMENTAL SEP-UP / CONFIGURATION 83
4.2 EXPERIMENTAL VEHICLE 84
4.3 RESULTS 84
4.3.1 INSTANTANEOUS EMISSIONS TRACES 86
4.3.2 CUMULATIVE EMISSION PROFILES 89
4.3.3 CALCULATION OF EMISSION FACTORS FROM CUMULATIVE EMISSION PROFILES 94
4.3.4 EFFECTS OF A WIDE TEMPERATURE RANGE ON MEASURED EMISSION FACTORS 95
4.3.4.1 COLD-START/IDLE EMISSIONS ... THE INTERCEPT 95
4.3.4.2 EMISSION FACTORS FOR THE TWO- AN THREE-EMISSION-FACTOR MODELS 96
4.3.4.3 CHANGE-OVER POINTS FOR THE TWO- AND THREE-EMISSION-FACTOR MODELS 99

4.3.5 EFFECT OF INITIAL ENGINE TEMPERATURE ON VEHICLE EMISSION FACTORS 100

4.3.5.1 COLD-START/IDLE EMISSIONS ... THE INTERCEPT 100

4.3.5.2 EMISSION FACTORS FOR THE TWO- AN THREE-EMISSION-FACTOR MODELS 101

4.3.5.3 CHANGE-OVER POINTS FOR THE TWO- AND THREE-EMISSION-FACTOR MODELS 103

4.3.6 DETECTION AND ANALYSIS OF EMISSION CONTROL FAILURES 104

4.4 CONCLUSIONS 107

4.5 FUTURE WORK 108

REFERENCES 128

CHAPTER 5 ON-ROAD CHARACTERIZATION OF DRIVER BEHAVIOR AND ITS INFLUENCE ON VEHICLE EMISSION FACTORS 131

5.0 INTRODUCTION 133

5.1 EXPERIMENTAL SEP-UP / CONFIGURATION 136

5.2 EXPERIMENTAL VEHICLE 137

5.3 EMISSION FACTORS AS FUNCTIONS OF AMBIENT TEMPERATURES 137

5.4 EXAMPLE OF DRIVING PATTERNS AND RESULTING EMISSION FACTORS 138

5.5 METHOD TO ADJUST EMISSION FACTORS FOR AMBIENT TEMPERATURE 140

5.6 RESULTS OF TEMPERATURE ADJUSTED EMISSION FACTORS AND INFLUENCE OF VEHICLE SPEED 142

5.6.1 CORRELATION OF EMISSION FACTORS FOR THE PRE-LIGHT-OFF REGION WITH NON-ZERO AVERAGE VEHICLE SPEED 143

5.6.2 CORRELATION OF EMISSION FACTORS FOR THE POST-LIGHT-OFF REGION WITH NON-ZERO AVERAGE VEHICLE SPEED 144

5.7 DESCRIPTION OF THE TWO VARIABLE EMISSION FACTOR MODEL 147

5.7.1 IDLE EMISSIONS FOR COLD AND WARM START APPLICATIONS 148

5.7.2 PRE-CATALYST LIGHT-OFF EMISSION FACTORS AND CHANGE-OVER POINTS FOR COLD AND WARM START APPLICATIONS 149

5.7.3 AVERAGE SPEED INFLUENCE ON POST-CATALYST LIGHT-OFF EMISSION FACTORS 150

5.7.4 AMBIENT TEMPERATURE CORRECTION OF THE POST-CATALYST LIGHT-OFF EMISSION FACTORS 150

5.8 CONCLUSIONS 141

5.9 FUTURE WORK 152

REFERENCES 162

CHAPTER 6 CONCLUSIONS 165

APPENDIX A ACCOUNTING FOR THE TIME DELAY OF THE GAS ANALYZER 169

APPENDIX B VEHICLE DYNAMIC MODEL 187

APPENDIX C REAL-TIME EMISSION CALCULATIONS 198

APPENDIX D ERROR ANALYSIS 202

APPENDIX E DETERMINATION OF EMISSION FACTORS AND CHARACTERISTIC POINTS 214

LIST OF TABLES

CHAPTER 2 **LITERATURE REVIEW OF CURRENT EMISSION MEASUREMENT TECHNIQUES AND EMISSION INVENTORY MODELS** **9**

2-1 ASSESSMENT CRITERIA FOR COMPARING DRIVING CYCLES 16

2-2 ASSESSMENT CRITERIA FIGURES FOR SOME WELL KNOWN DRIVING CYCLES 17

2-3 DRIVING CYCLES AND CYCLE DETAILS 19

CHAPTER 3 **REAL-TIME, ON-ROAD MEASUREMENTS OF DRIVING BEHAVIOR, ENGINE PARAMETERS AND EXHAUST EMISSIONS** **39**

3-1 INSTRUMENT SPECIFICATIONS AND CALIBRATION STANDARDS 44

3-2 BASIC DETAILS OF THE THREE COMMUTER TRIPS 55

3-3 DISTANCES AND TIMES FOR THE THREE COMMUTER TRIPS 56

3-4 SUMMARY OF EMISSIONS AND CONSUMPTION BY TRIP AND SEGMENT 61

3-5 TRIP EMISSION AND CONSUMPTION STATISTICS (AVERAGE OF THREE TRIPS) 63

CHAPTER 4 **QUANTIFYING VEHICLE EMISSION FACTORS FOR VARIOUS AMBIENT AND INITIAL ENGINE CONDITIONS USING AN ON-ROAD, REAL-TIME EMISSIONS SYSTEM** **78**

4-1 FOUR SAMPLE 17.4 KM COMMUTER PROFILES AT A RANGE OF TEMPERATURES 85

4-2 COEFFICIENTS FOR THE TWO-EMISSION-FACTOR MODEL: SAMPLE TRIP PER FIGURE 4-7 92

4-3 COEFFICIENTS FOR THE THREE-EMISSION-FACTOR MODEL: SAMPLE TRIP PER FIGURE 4-7 93

CHAPTER 5 **ON-ROAD CHARACTERIZATION OF DRIVER BEHAVIOR AND ITS INFLUENCE ON VEHICLE EMISSION FACTORS** **131**

5-1 DEFINITIONS OF THE FOUR MODAL ANALYSIS VARIABLES 139

5-2 COLD START/IDLE MASS ACCUMULATIONS CORRELATIONS FOR A 50S IDLE TIME (AMBIENT TEMPERATURE RANGE OF -30 TO +20°C) 148

5-3 WARM START/IDLE MASS ACCUMULATIONS CORRELATIONS FOR A 50S IDLE TIME (INITIAL ENGINE TEMPERATURE RANGE OF 0 TO +90°C) 148

5-4 COLD START HC, CO AND NO_x PRE-CATALYST LIGHT-OFF EMISSION FACTOR CORRELATIONS (AMBIENT TEMPERATURE RANGE OF -30 TO +20°C) 149

5-5 WARM START HC, CO AND NO_x PRE-CATALYST LIGHT-OFF EMISSION FACTOR CORRELATIONS (INITIAL ENGINE TEMPERATURE RANGE OF 0 TO +90°C) 150

5-6 POST-CATALYST LIGHT-OFF HC, CO AND NO_x EMISSION FACTOR CORRELATIONS FOR NON-ZERO AVERAGE VEHICLE SPEEDS OF 10 TO 60 KM/HR 150

5-7 COLD START HC, CO AND NO_x POST-CATALYST LIGHT-OFF EMISSION FACTOR CORRELATIONS FOR AN AMBIENT TEMPERATURE RANGE OF -30 TO +20°C 151

APPENDIX A ACCOUNTING FOR THE TIME DELAY OF THE GAS ANALYZER 169

A-1 VARIOUS EXHAUST SYSTEM RESONANCE TIMES FOR EXPERIMENTAL EXHAUST VOLUME FLOW RATES 175

A-2 ILLUSTRATION OF MAXIMUM PERCENT DIFFERENCES DUE TO DIFFERENT TIME SHIFTS 180

APPENDIX B VEHICLE DYNAMIC MODEL 187

B-1 PROCESSED CDA, CD AND CR VALUES DETERMINED FROM COAST DOWN TESTS 194

B-2 FINAL OVERALL AVERAGES DRAG AND ROLLING RESISTANCE COEFFICIENTS 195

APPENDIX E DETERMINATION OF EMISSION FACTORS AND CHARACTERISTIC POINTS 214

E-1 LINEAR EQUATION FIT COEFFICIENTS FOR THE TWO EMISSION FACTOR MODEL 220

E-2 LINEAR EQUATION FIT COEFFICIENTS FOR THE THREE EMISSION FACTOR MODEL 222

LIST OF FIGURES

CHAPTER 1 INTRODUCTION TO MODELING VEHICLE EMISSION FACTORS DETERMINED WITH AN IN-USE & REAL-TIME EMISSION MEASUREMENT SYSTEM 1

1-1 CUMULATIVE EMISSION TRACE AND RESULTING EMISSION FACTORS 6

CHAPTER 2 LITERATURE REVIEW OF CURRENT EMISSION MEASUREMENT TECHNIQUES AND EMISSION INVENTORY MODELS 9

2-1 FTP EMISSION TESTING PARAMETERS 28

2-2 SCHEMATIC REPRESENTATION OF THE FTP EMISSION CERTIFICATION TEST 28

2-3 NORTH AMERICAN FTP 75 DRIVING CYCLE FOR EMISSION CERTIFICATION TESTING BASED ON AN ACTUAL DRIVING SEQUENCE 29

2-4 FTP 75 EMISSION FACTORS OF A 2.0L VEHICLE AT DIFFERENT AMBIENT CONDITIONS 29

2-5 FTP 75 EMISSION FACTORS OF A 1.3L VEHICLE AT DIFFERENT AMBIENT CONDITIONS 30

2-6 THE SYNTHETICALLY CONSTRUCTED EUROPEAN DRIVING SEQUENCE (EDC & EUDC) FOR EMISSION TESTING 30

2-7 SCHEMATIC REPRESENTATION OF THE FTP 75 SPEED/ACCELERATION ENVELOPES 31

2-8 SCHEMATIC REPRESENTATION OF THE EDC SPEED/ACCELERATION ENVELOPES 31

2-9 HC EMISSION FACTOR COMPARISON FOR DIFFERENT DRIVING CYCLES 32

2-10 CO EMISSION FACTOR COMPARISON FOR DIFFERENT DRIVING CYCLES 32

2-11 NO_X EMISSION FACTOR COMPARISON FOR DIFFERENT DRIVING CYCLES 33

2-12 I/M 240 DRIVING SEQUENCE 33

2-13 ILLUSTRATION OF EMISSION FACTORS CALCULATED WITH MOBILE 5 & 6 34

CHAPTER 3 **REAL-TIME, ON-ROAD MEASUREMENTS OF DRIVING BEHAVIOR, ENGINE PARAMETERS AND EXHAUST EMISSIONS** **39**

3-1 SCHEMATIC OF TEST SET-UP ILLUSTRATING SENSORS AND INSTRUMENTS 65

3-2 RESPONSE OF THE PXA-1100 TO VARIOUS HC COMPOUNDS REPRESENTED IN EQUIVALENT HEXANE 65

3-3 VEHICLE SPEED AND NO_x EMISSION RATES FOR TRIP 1 (SEPT 27) 66

3-4 VEHICLE SPEED AND NO_x EMISSION RATES FOR TRIP 2 (OCT 3) 66

3-5 VEHICLE SPEED AND NO_x EMISSION RATES FOR TRIP 3 (OCT 4) 67

3-6 VELOCITY/ACCELERATION ENVELOPES FOR THREE SEGMENTS OF TRIP 1 68

3-7 VELOCITY/ACCELERATION ENVELOPES FOR THREE SEGMENTS OF TRIP 2 69

3-8 VELOCITY/ACCELERATION ENVELOPES FOR THREE SEGMENTS OF TRIP 3 70

3-9 RELATIVE TIME DISTRIBUTION OF POSITIVE POWER LEVELS 71

3-10 RELATIVE ENERGY DISTRIBUTION OF POSITIVE POWER LEVELS 71

3-11 TRENDS OF NO_x PRODUCED WITH FUEL CONSUMED 72

3-12 TRENDS OF CO PRODUCED WITH FUEL CONSUMED 72

3-13 TRENDS OF HC PRODUCED WITH FUEL CONSUMED 73

CHAPTER 4 **QUANTIFYING VEHICLE EMISSION FACTORS FOR VARIOUS AMBIENT AND INITIAL ENGINE CONDITIONS USING AN ON-ROAD, REAL-TIME EMISSIONS SYSTEM** **78**

4-1 COMPONENTS OF THE ON-ROAD, REAL-TIME EMISSIONS SYSTEM 109

4-2 INSTANTANEOUS SPEED AND EMISSION TRACES (+21°C AMBIENT) 110

4-3 INSTANTANEOUS SPEED AND EMISSION TRACES (-26°C AMBIENT) 111

4-4 CUMULATIVE HC EMISSIONS AT FOUR AMBIENT TEMPERATURES 112

4-5 CUMULATIVE CO EMISSIONS AT FOUR AMBIENT TEMPERATURES 112

4-6 CUMULATIVE NO_x EMISSIONS AT FOUR AMBIENT TEMPERATURES 113

4-7 COMMUTATIVE HC EMISSION PROFILE ILLUSTRATING THE TWO AND THREE EMISSION FACTOR MODELS 113

4-8 AMBIENT TEMPERATURE EFFECT ON HC EMISSION DURING A 50S INITIAL IDLE PERIOD 114

4-9 AMBIENT TEMPERATURE EFFECT ON CO EMISSION DURING A 50S INITIAL IDLE PERIOD 114

4-10 AMBIENT TEMPERATURE EFFECT ON HC EMISSION FACTORS (THREE EMISSION FACTOR MODEL) 115

4-11 AMBIENT TEMPERATURE EFFECT ON CO EMISSION FACTORS (THREE EMISSION FACTOR MODEL) 116

4-12 AMBIENT TEMPERATURE EFFECT ON NO_x EMISSION FACTORS (THREE EMISSION FACTOR MODEL) 117

4-13 AMBIENT TEMPERATURE INFLUENCE IN HC AND CO CHANGE-OVER POINTS FOR THE TWO AND THREE EMISSION FACTOR MODEL 118

4-14 AMBIENT TEMPERATURE INFLUENCE IN NO_x CHANGE-OVER POINTS FOR THE TWO AND THREE EMISSION FACTOR MODEL 119

4-15 INITIAL ENGINE TEMPERATURE EFFECT ON HC EMISSIONS DURING A 50S IDLE PERIOD (-20°C AMBIENT TEMPERATURE) 120

4-16 INITIAL ENGINE TEMPERATURE EFFECT ON CO EMISSIONS DURING A 50S IDLE PERIOD (-20°C AMBIENT TEMPERATURE) 120

4-17 INITIAL ENGINE TEMPERATURE EFFECT ON HC EMISSION FACTORS (-20°C AMBIENT TEMPERATURE) 121

4-18 INITIAL ENGINE TEMPERATURE EFFECT ON CO EMISSION FACTORS (-20°C AMBIENT TEMPERATURE) 122

4-19 INITIAL ENGINE TEMPERATURE EFFECT ON NO_x EMISSION FACTORS (-20°C AMBIENT TEMPERATURE) 123

4-20 INITIAL ENGINE TEMPERATURE EFFECT ON HC AND CO CHANGE-OVER POINTS FOR THE TWO AND THREE EMISSION FACTOR MODELS 124

4-21 INITIAL ENGINE TEMPERATURE EFFECT ON NO_x CHANGE-OVER POINTS FOR THE TWO AND THREE EMISSION FACTOR MODELS 125

4-22 CUMULATIVE HC EMISSION PROFILE SHOWING LOSS OF HC EMISSION CONTROL AFTER TEMPERATURE STABILIZED 126

4-23 MAGNITUDE AND FREQUENCY OF HC EMISSION FAILURE 126

4-24 MAGNITUDE AND FREQUENCY OF CO EMISSION FAILURE 127

4-25 MAGNITUDE AND FREQUENCY OF NO_X EMISSION FAILURE 127

CHAPTER 5 ON-ROAD CHARACTERIZATION OF DRIVER BEHAVIOR AND ITS INFLUENCE ON VEHICLE EMISSION FACTORS 131

5-1 COMPONENTS OF THE ON-ROAD, REAL-TIME EMISSION SYSTEM 154

5-2 CUMULATIVE HC EMISSION PROFILE ILLUSTRATING THE TWO EMISSION FACTOR MODEL 154

5-3 CONGESTED VELOCITY PROFILE WITH RESULTING EMISSION FACTORS 155

5-4 FREE-FLOWING VELOCITY PROFILE WITH RESULTING EMISSION FACTORS 156

5-5 MODAL ANALYSIS FOR THE CONGESTED TRAFFIC PROFILE 157

5-6 MODAL ANALYSIS FOR THE FREE-FLOWING TRAFFIC PROFILE 157

5-7 CORRELATION OF TEMPERATURE CORRECTED PRE-CATALYST LIGHT-OFF HC EF WITH NON-ZERO AVERAGE VEHICLE SPEED 158

5-8 CORRELATION OF TEMPERATURE CORRECTED PRE-CATALYST LIGHT-OFF CO EF WITH NON-ZERO AVERAGE VEHICLE SPEED 158

5-9 CORRELATION OF TEMPERATURE CORRECTED PRE-CATALYST LIGHT-OFF NO_X EF WITH NON-ZERO AVERAGE VEHICLE SPEED 159

5-10 CORRELATION OF TEMPERATURE CORRECTED POST-CATALYST LIGHT-OFF HC EF WITH NON-ZERO AVERAGE VEHICLE SPEED 159

5-11 CORRELATION OF TEMPERATURE CORRECTED POST-CATALYST LIGHT-OFF CO EF WITH NON-ZERO AVERAGE VEHICLE SPEED 160

5-12 CORRELATION OF TEMPERATURE CORRECTED POST-CATALYST LIGHT-OFF NO_X EF WITH NON-ZERO AVERAGE VEHICLE SPEED 160

5-13 DERIVED ALGORITHM FOR EMISSION PROFILING USING EXPERIMENTAL EMISSION FACTORS 161

APPENDIX A ACCOUNTING FOR THE TIME DELAY OF THE GAS ANALYZER 169

A-1 RESPONSE TIME OF THE HC MEASUREMENT TO A STEP CHANGE CONCENTRATION WITHOUT SAMPLE LINE 170

A-2 RESPONSE TIME OF THE CO MEASUREMENT TO A STEP CHANGE CONCENTRATION WITHOUT SAMPLE LINE 170

A-3 Response Time of the CO_2 Measurement to a Step Change Concentration without Sample Line 171

A-4 Response Time of the O_2 Measurement to a Step Change Concentration without Sample Line 171

A-5 Response Time of the NO_x Measurement to a Step Change Concentration without Sample Line 171

A-6 Response Time of the HC Measurement to a Step Change Concentration with Sample Line 172

A-7 Response Time of the CO Measurement to a Step Change Concentration with Sample Line 172

A-8 Response Time of the CO_2 Measurement to a Step Change Concentration with Sample Line 173

A-9 Response Time of the O_2 Measurement to a Step Change Concentration with Sample Line 173

A-10 Response Time of the NO_x Measurement to a Step Change Concentration with Sample Line 173

A-11 Exhaust System Delay Time at a MAF Rate of 12.5 g/s 175

A-12 Exhaust System Delay Time at a MAF Rate of 40.0 g/s 175

A-13 The Effects of Varying Time Shifting Constants on HC Emissions 176

A-14 The Effects of Varying Time Shifting Constants on CO Emissions 177

A-15 The Effects of Varying Time Shifting Constants on CO_2 Emissions 178

A-16 The Effects of Varying Time Shifting Constants on O_2 Emissions 178

A-17 The Effects of Varying Time Shifting Constants on NO_x Emissions 179

A-18 Sensitivity of the HC Mass Calculation to Various Time Shift Constants 180

A-19 Sensitivity of the CO Mass Calculation to Various Time Shift Constants 181

A-20 Sensitivity of the CO_2 Mass Calculation to Various Time Shift Constants 181

A-21 Sensitivity of the O_2 Mass Calculation to Various Time Shift Constants 182

A-22 Sensitivity of the NO_x Mass Calculation to Various Time Shift Constants 183

A-23 Illustration of an Original and Shifted NO_x Emission Trace and the Correlation to Vehicle Speed 183

A-24 Correlation of Exhaust and HC Mass Flow Rates 184

A-25 Correlation of Exhaust and NO_x Mass Flow Rates 184

A-26 Correlation of a Measured and Time Shifted A/F Values 185

Appendix B Vehicle Dynamic Model 187

B-1 Schematic of Dynamic Vehicle Resistances 188

B-2 Typical Speed and Tractive Power Trace for a Congested Driving Sequence 190

B-3 Typical Speed-Time Trace of Coast Down Test for the 1992 GM 3/4 Tome Pick-up Truck 191

B-4 Linearized Coast Down Test Illustrating Break Point Velocity Model 192

B-5 Individual Energy Contributions to Overall Positive Tractive Energy 195

Appendix E Determination of Emission Factors and Characteristic Points 214

E-1 The FTP 75 Certification Driving Sequence 215

E-2 Cumulative HC, CO and NO_x Emissions for an Ambient Temperature of -26°C 216

E-3 Linear Regression Analysis for the Pre-Light-Off HC Emission Factor 218

E-4 Linear Regression Analysis for the Post-Light-Off HC Emission Factor 219

E-5 Illustration of the Intersection Point of the Linear Regression Analysis for the Two Emission Factor Model 220

E-6 ILLUSTRATION OF THE TWO AND THREE HC EMISSION FACTOR MODEL 221

E-7 LOSS OF HC EMISSION CONTROL WITHIN THE STABILIZED REGION 223

E-8 NO NO_x EMISSION CONTROL FOR THE ENTIRE EXPERIMENT 224

ABBREVIATIONS

A/F	Air to Fuel Ratio (Mass Based)
ASME	The American Society of Mechanical Engineers
BER	Basic Emission Rate
C_3H_8	Propane
C_6H_{14}	Hexane
Cd	Drag Coefficient
Cr	Rolling Resistance Coefficient
CDT	Coast Down Test
CF	Correction Factor
CNG	Compressed Natural Gas
CO	Carbon Monoxide
CO_2	Carbon Dioxide
CVS	Constant Volume Sample
DAQ	Data Acquisition
EDC	European Driving Cycle
EF	Emission Factor
EPA	Environmental Protection Agency
FA	Frontal Area
FID	Flame Ionization Detector
FTP	Federal Test Program

GUI	Graphical User Interface
H/C	Hydrogen to Carbon Ratio
HC	Hydrocarbons
I/M	Inspection and Maintenance
IR	Infrared
MAF	Mass Air Flow
NDIR	Non-Dispersive Infrared
NGV	Natural Gas Vehicle
NI	National Instruments
NO_x	Oxides of Nitrogen
O_2	Oxygen
OEM	Original Equipment Manufacturer
OMTCF	Operating - Mode / Temperature Correction Factor
OMTTAM	Tamper Offset
PEF	Propane Equivalency Factor
PM	Particulate Matter
RSD	Remote Sensing Device
RPM	Revolutions per Minute
SAE	Society of Automotive Engineers
SALCHF	Speed Correction Factor

TFs	Travel Weighting Factor
UV	Ultraviolet
VMT	Vehicle Miles Traveled

CHAPTER 1

INTRODUCTION TO MODELING VEHICLE EMISSION FACTORS DETERMINED WITH AN IN-USE & REAL-TIME EMISSION MEASUREMENT SYSTEM

Chapter 1 provides the rationale and reasons why vehicle emissions are studied and regulated. This chapter states the objectives of this research and outlines the contents of the following chapters.

1.0 INTRODUCTION

Emissions from internal combustion engines are a major source of urban air quality problems.(1,2) In recent years, tighter vehicle emission standards have led to advancements in pollution control systems which have resulted in emissions that have been lowered on a per vehicle basis. However, even with the advancements in emission control technology, the automobile is still the key contributor to increasing atmospheric air pollution. Expanding urban areas, constantly rising numbers of on-road vehicles and increased mileage on a per vehicle basis have all led to increasing amounts of vehicular air pollution and a decline in air quality levels.(1-5) Concerns of human health and global well-being have led to the implementation and strengthening of emission legislation and regulations.

To help quantify the products of combustion produced by vehicles, numerous emission testing experiments and protocols have been developed and modified over the years. Testing of exhaust emissions mainly include chassis dynamometer (FTP protocols) experiments with many variations, and remote sensing procedures. Dynamometer procedures are currently used as the benchmark for certification and inspection routines of vehicles while remote sensing studies are commonly used to enhance on-road emission understanding. These procedures have led to great efforts and success in reducing vehicle emissions though various forms of technology.(6-8) However, these current studies fail to capture the vehicle's actual emission behavior, magnitude and variability as it is driven in real-world applications.

This thesis describes a measurement system and methods to quantify real-time, on-road vehicle emissions. It provides insight into real-life vehicle operating conditions and resultant pollution impacts on the environment. The objectives of the research presented here are:

1. The development of an in-use and real-time emission measurement system. This system will allow the analysis of vehicular exhaust from real-application and on-road driving.
2. To determination multiple emissions factors of the test vehicle based on the measure emission concentrations. These emission factors will be correlated to measured variables of the experiments.
3. The development of a multi emission factor model. This model will allow complete emission profiling of the test vehicle for any given simulation distance.

The reason for this study was to improve the representativeness of emission factors(9-12) and improve the accuracy of emission inventories. Currently, the emission factors used in emission inventories are:

1. Determined from dynamometer (laboratory) testing procedures.
2. Single valued emission factors. (i.e. only one emission factor describing the emission performance of the vehicle.)

Figure 1-1 schematically illustrates a cumulative emission trace and resulting emission factors. The goal of this research was to describe the vehicle emissions in terms of: (1) a starting emissions or intercept value, (2) a pre-catalyst-light-off emission factor and (3) a change-over point and (4) a post-catalyst-light-off emission factor. This method will allow more accurate and representative emission profiling.

The literature review (Chapter 2), will help illustrate the need for an in-use measurement system by examining the current emission measuring techniques. The techniques to be examined will include the standardized emission certification procedures, more commonly known as FTP testing, and remote sensing studies. The FTP procedures have been altered by numerous researchers to examine how ambient conditions affect vehicle pollution. In addition, nonstandard driving schedules have been utilized to provide more insight to real-world, on-road application behavior. These variations were made with the goal of producing more accurate and representative emission factors. Remote sensing procedures improve the real-life nature of vehicle emissions since the measurements are conducted at on-road site locations. However, this type of analysis has various problems associated with the calculated emission factors due to the number of assumptions which are required. Next, an overview of the current work using in-use and real-time measurement systems will be examined high lighting the main conclusions. Finally, a brief overview of the current emission factor modeling software will be presented.

Following the literature review will be the description of the developed emission measurement system and experimental method, presented as a stand alone paper (Chapter 3). The equipment used and details describing the experimental setup will be presented and discussed. Validation and proof of the system integrity and capabilities will also be illustrated.

The next section, presented as a stand alone paper (Chapter 4), will be concerned with the calculation and presentation of the experiential emission factors for a range of ambient conditions during one full year of driving. Two models will be presented, which use the calculated emission factors and will allow the complete emission profiling for any ambient temperature and given simulation distance. The first model consists of two emission factors for hydrocarbons (HC), carbon monoxide (CO) and oxides of nitrogen (NO_x) emissions, with a single change-over point. The second model incorporates three emission factors and two change-over points to better represent the emissions for short duration trip lengths. As will be shown, the two emission factor model is sufficient for emission profiling purposes.

Following the ambient temperature analysis the next chapter, presented as a stand alone paper (Chapter 5), will focus on the emission profiles for different driving patterns. This analysis uses the temperature model to correct the emission factors to a common temperature and allow them to be described in terms of another independent variable. For this investigation, the non-zero average vehicle speed was used to establish correlations. This allowed predictions of the emission factors based on the type of driving patterns to be modeled.

With the above presented sections, the emission behavior of the test vehicle in any ambient and driving condition will be predictable through the developed emission factor model. This work provides the foundation, including the measurement system and analysis algorithms, to extend this research to any on-road vehicle and testing scenario.

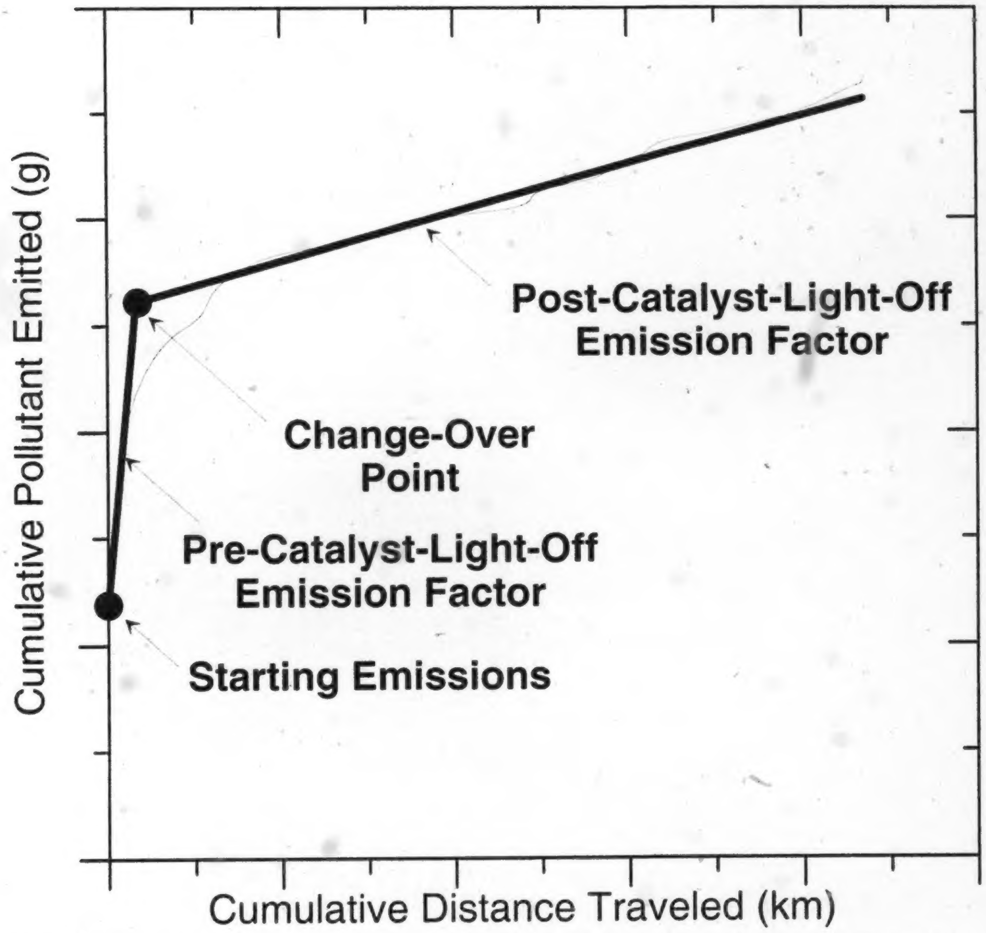

FIGURE 1-1 CUMULATIVE EMISSION TRACE AND RESULTING EMISSION FACTORS

REFERENCES

1. Dhaliwal B.S., "Alternative Fuel Effects on Vehicle Emission and Indoor Air Quality" Master of Science Thesis, University of Albert, Edmonton, Canada. 2000.

2. "Automobile Emissions: An Overview" EPA Office of Mobile Sources Fact Sheet OMS - 5, 1994.

3. Klingenberg H., "Automobile Exhaust Emission Testing," New York, Springer, 1996.

4. "Automobiles and Carbon Monoxide" EPA Office of Mobile Sources Fact Sheet OMS - 3, 1993.

5. "Automobiles and Ozone" EPA Office of Mobile Sources Fact Sheet OMS - 4, 1993.

6. Becker E.R., Watson R.J., "Future Trends on Automotive Emission Control" SAE Technical Paper 980413, Society of Automotive Engineers, 1998.

7. Tudor R.J., "Electronic Throttle Control as an Emission Reduction Device" SAE Technical Paper 930339, Society of Automotive Engineers, 1998.

8. Wenzel T., Ross M., "Emissions from Modern Passenger Cars with Malfunctioning Emissions Controls" SAE Technical Paper 960067, Society of Automotive Engineers, 1996.

9. Goodwin R.W., Ros M.H., "Off-Cycle Exhaust Emissions from Modern Passenger Cars with Properly-Functioning Emissions Controls" SAE Technical Paper 960064, Society of Automotive Engineers, 1996.

10. Watson H.C., Milkins E.E., Preston M.O., Chittleborough C., Beardsley P.A., "In-Use Vehicle Survey of Fuel Consumption and Emissions on Dynamometer and Road" SAE Technical Paper 850524, Society of Automotive Engineers, 1985.

11. Watson H.C., "Effects of a Wide Range of Drive Cycles on the Emissons from Vehicles of Three Levels of Technology" SAE Technical Paper 950221, Society of Automotive Engineers, 1995

12. Gurney M.D., Allsup J.R., "Predictability of Emissions from In-Use Vehicles at Low-Ambient Temperature and Alternate Driving Cycle Based on Standard Tests" SAE Technical Paper 890625, Society of Automotive Engineers,

13. Laurikko J., Nylund N.O., Sipila K., "Automotive Exhaust Emissions at Low Ambient

Temperature" Valtion teknillinen tutkimuskeskus, Tutkimuksia Statens tekniska forskingscentral, Forskingsrapporter Technical Reserch Ventre of Finland, Research Reports, 1987.

14. Laurikko J., Nylund N. "Regulated and Unregulated Emissions frm Catalyst Vehicles at Low Ambient Temperatures" SAE Technical Paper 930946, Society of Automotive Engineers, 1993.

15. Ginberg L., Morgan L. "Effect of Temperature on Exhaust Emissions" SAE Technical Paper 740527, Society of Automotive Engineers, 1974.

16. Larson R.E., "Vehicles Emission Characteristics Under Cold Ambient Conditions"SAE Technical Paper 890021, Society of Automotive Engineers, 1989.

17. Polak J.C., "Cold Ambient Temperature Effects on Emissions from Light-Duty Motor Vehicles" SAE Technical Paper 741051, Society of Automotive Engineers, 1974.

18. Kyriakis N.A., Andre M., "Cold Start of Passenger Cars" International Journal of Vehicle Design, Vol. 20, Nos. 1-4 (Special Issue), pp. 137 - 146, 1998.

19. Eccleston B.H., Hurn R.W, "Ambient Temperature and Trip Length – Influence on Automotive Fuel Economy and Emissions" SAE Technical Paper 780613, Society of Automotive Engineers, 1978.

20. Laurikko J., Erlandsson L., Arbrahamsson R., "Exhaust in Cold Ambient Conditions: Considerations for a European Test Procedure," SAE Technical Paper 950255, Society of Automotive Engineers, 1995.

CHAPTER 2

REVIEW OF CURRENT EMISSION MEASUREMENT TECHNIQUES AND EMISSION INVENTORY MODELS

Currently, emission factors used for emission inventories have been determined from laboratory style experiments with small contributions from field studies. However, the laboratory emissions testing may not necessarily represent the same conditions experienced in real-world applications. These variations from current testing conditions can lead to large deviations between the emission factors measured and those actually produced. This chapter attempts to examine the current emission measurement techniques and the calculation methods. The aim of this chapter is to introduce the need for an on-road and real-time emission measurement system and analysis methods capable of determining emission factors. It also examines how the laboratory emission factors are implemented in current emission inventory models.

2.0 INTRODUCTION

The measurement of exhaust emissions has been carried out in some form for almost the past 40 years.(1) Obviously, several parameters such as emission control systems, ambient conditions, traffic scenarios and power levels demanded by the driver all influence the quantity of emissions entering the atmosphere. It is because of these parameters that standardized tests have been instituted in various countries to: (1) allow emission levels to be set, (2) offer a basis for comparison between vehicles and emission technologies, and (3) to help quantify any improvements in automotive emissions. The focus of this thesis and literature review will be on the calculation of emission factors since these parameters are used directly in emission inventories.

This literature review will first examine the two main types of vehicle emissions testing procedures, including dynamometer and remote sensing experiments. The review of dynamometer testing literature will include a detailed examination of the procedures currently used to certify vehicle emissions. Modifications to the standardized procedure, such as different ambient conditions and drive cycles, will be examined. This section will also include a description of the improved Inspection and Maintenance (I/M 240) routine testing procedure, as a result of the 1990 Clear Air Act.

Remote sensing procedures will then be examined by first introducing the procedures and equipment for these experiments. As will be explained, the remote sensing procedure improves the real-life nature of exhaust emissions, but do not allow the direct measurements of emission factors.

The next section will focus on recent studies using in-use and real-time measurement systems to monitor and record the operational characteristics of test vehicles. This will include a review of results obtained from this work.

The final section of the literature review will examine the current emission inventories models developed by the Environmental Protection Agency (EPA); Mobile 5 and 6. A comparison of the two models will be made and a description of how the models modify emission factor for different conditions will be presented.

2.1 DYNAMOMETER TESTING

As will be discussed in more detail in the forthcoming sections, dynamometer testing has been the main source for determining emission factors. As a result, a discussion of the types of dynamometer testing will be provided with the corresponding emission factors analysis methods.

2.1.1 DESCRIPTION OF FTP CERTIFICATION TESTING

Chassis dynamometer experiments are currently the standards in emission certification and fuel consumption testing. Figure 2-1⁽¹⁾ illustrates the important parameters of the emission testing procedure including: the test vehicle, test fuel, driver, driving cycle, chassis dynamometer, and ambient conditions. The two parameters that will be studied in detail in this thesis include the influence of different ambient conditions and driving cycles.

A schematic view of an FTP exhaust emission test facility including all of the required emission measurement equipment is illustrated in Figure 2-2.(1) The exhaust sampling system used in these experiments is known as Constant Volume Sampling (CVS) and consists of a dilution tunnel, isokinetic sampling probes, and sample bags for collecting the exhaust emissions. The basis behind the CVS system is to keep the total volume of exhaust flow and dilution air constant throughout the sampling process. The measurement system also includes exhaust analyzers to measure concentrations of HC, CO, NO_x, carbon dioxide (CO_2), oxygen (O_2), and particulate matter (PM) for diesel measurements. The testing process begins with the vehicle placed onto the chassis dynamometer which serves as a simulated load on the engine (i.e. the total resistance to vehicle motion). The vehicle is then driven according a specified driving cycle which includes numerous phases of accelerations, decelerations, constant speeds and idling within specified tolerances. In the North America, one of the cycles used to measure vehicle emissions is known as the FTP 75 and is illustrated in Figure 2-3.(1)

As the vehicle is driven through the driving cycle, the exhaust sample is diverted into the dilution tunnel where the exhaust is mixed and diluted with filtered ambient air. This mixture of exhaust and dilution air is drawn out of the dilution tunnel and in the case of the FTP 75 procedure, is collected into three bags corresponding to the three test sections illustrated in Figure 2-3.(1) To compensate for background concentrations of the measured emissions, ambient air is also drawn into three separate bags, again for the FTP 75 procedure.

Once the driving cycle has been completed, the average concentrations of the pollutants from the bag samples are measured with the analyzers shown in Figure 2-2.(1) The background concentrations are subtracted from each of the corresponding bags providing the true volumetric exhaust emission concentrations. In addition to this measurement, the total volume of exhaust and dilution air is also recorded. Together, these measurements allow the mass calculation of the exhaust components and fuel consumption. Since the distance traveled for each section is known, an emission factor in units of g/km or g/kg$_{fuel}$ can be easily determined for each section of the FTP sequence. To calculate the overall or "composite" emission factor, the three factors are independently weighted (i.e. 43% and 57% for the cold and warm starts respectively and 100% for the stabilized phase).(1)

Some advantages of using the CVS measurement system include:(1)

- After each test, the results can be calculated.
- The dilution tunnel reduces condensation and chemical reaction within the exhaust probe.
- Even though considerable space is required for the experimental set-up the equipment can be moved to other locations.
- The emission measurement circuits are simple meaning that dead volume time and resolutions are minimized.

Some disadvantages of using the CVS measurement system are:(1)

- Real-time measurements of exhaust components are not possible with the system shown in Figure 2-2,(1) and thus require additional equipment.
- Analyses of unregulated emissions or exact speciation of HC are difficult because of the dilution process.

2.1.2 EFFECTS OF AMBIENT TEMPERATURES ON VEHICLE EMISSIONS

Ambient conditions are well-known parameters which affect the emissions emitted by vehicles. At low temperatures internal engine friction and cylinder leakage increases, catalytic converters have prolonged warm-up times and reduced fuel volatility all lead to increased emissions.(2,3) Various studies have been conducted to determine the operational characteristics of vehicles functioning in these situations.

As an example, Figures 2-4 and 2-5 show the results of a temperature study conducted by Laurikko and Nylund.(4) This research examined the emission factor behavior of two vehicles with engine sizes of 2.0 and 1.3 L. The dynamometer tests were conducted in a cold test chamber with temperature conditions of +20, -7 and -20°C. For the 2.0L engine illustrated in Figure 2-4, the -20°C HC emission factors increased approximately 6.5 times compared to the +20°C values. Similarly, the CO emission factors increased by approximately 10.5 times for the 2.0L engine. Comparing the NO_x emissions for this engine, no significant increases were measured over the range of ambient temperatures. Other temperature studies have shown similar trends in the relationships to ambient conditions.(5-13)

2.1.3 DRIVING CYCLES

Standardized driving cycles developed for dynamometer experiments are used to characterize the exhaust emissions and fuel economy behavior of test vehicles. The premise behind the driving cycle is one of simulating actual on-road behavior and assuming that the emissions and fuel consumption will be the same on a dynamometer as would be experienced in on-road applications. This of course is only feasible if the test cycle properly emulates on-road behavior in terms of the sequence driven and if the mean magnitude forces are similar in both situations.(1,14-17) Thus, the driving cycles developed are ideally representative of the "mean" driving behavior. However, different cycles were developed to represent different driving conditions since it is impossible to represent all driving patterns in a single driving sequence.(1)

Driving sequences were developed using one of two methods.(1,17) The first method is to manufacture a sequence based on actual velocity profiles of a test vehicle.(14,15,18) This method allows the direct characterization of actual in-use driving behavior and can be tailored to simulated different traffic profiles. The traffic conditions to be simulated are directly proportional to the exhaust emissions and fuel economy measured. The FTP 72 driving cycle, which consists of the first two sections of the FTP 75 cycle shown in Figure 2-3(1) was developed using this method, and was a representation of morning rush hour traffic in Los Angeles.(18)

The second method for developing driving sequences is the synthetic construction of a number of actual driving profiles.(1,14,17) It results in sequences of constant acceleration / deceleration phases and constant speed sections. This is accomplished by subdividing measured driving profiles into modes and then, based on a frequency of occurrence, are combined into a representative driving cycle. This method requires much computing but allows for easy modification of the driving sequence. An example of a synthetically manufactured sequence is shown for the European emission testing in Figure 2-6.(1)

It is important to note that in the US the current emission certification procedure is the FTP 75 cycle. The use of different certification driving sequences around world decreases the shipping and selling of domestic vehicles due to different emission legislation. This has led to suggestions for a standard worldwide driving schedule, however this has been impossible so far.(1,16)

Simply comparing the velocity profiles of the driving sequences is insufficient to compare the properties of different driving patterns. To aid in the analysis, a number of assessment criteria shown in Table 2-1,(1) has been developed to characterize the velocity profiles.

TABLE 2-1 ASSESSMENT CRITERIA FOR COMPARING DRIVING CYCLES(1,19)

No	Criterion	Abbreviation	Unit
1	Average speed over the entire driving cycle	v_1	km/hr
2	Average speed during actual driving (idle time excluded)	v_2	km/hr
3	Average acceleration all acceleration phases ($a > 0.1$ m/s^2)	a^+_{avg}	m/s^2
4	Average deceleration all deceleration phases ($a < -0.1$ m/s^2)	a^-_{avg}	m/s^2
5	Mean duration of a driving period (from start to standstill)	T	s
6	Average number of acceleration-deceleration changes (and vice versa) within one driving period	M	N/A
7	Proportion of idle time ($v \leq 3$ km/hr and $\lvert a \rvert \geq 0.1$ m/s^2)	I	%
8	Proportion of acceleration time ($a > 0.1$ m/s^2)	A	%
9	Proportion of deceleration time ($a < -0.1$ m/s^2)	D	%
10	Proportion of constant speed time ($\lvert a \rvert \leq 0.1$ m/s^2)	C	%

Of the parameters listed above, v_2 is one of the most important in describing any particular cycle since it offers a very simple description of the average speeds at which the test vehicle was driven. The remainder of the parameters offer further insight as to how aggressively the vehicle was driven throughout the test cycle. For an in depth analysis of the testing sequences, Table 2-2(1) displays the calculated parameters for various cycles.

TABLE 2-2 ASSESSMENT CRITERIA FIGURES OF SOME WELL KNOWN DRIVING CYCLES(1)

Criterion	EDC	Former Californian	FTP 72	FTP 75	Japan 10 Mode	Japan 11 Mode	Mean
v_1	18.8	35.6	31.5	34.1	17.7	28.9	27.8
v_2	26.4	41.7	38.1	41.2	23.7	38.4	34.9
$a_{ave,+}$	0.64	0.64	0.58	0.59	0.63	0.52	0.60
$a_{avg,-}$	0.71	0.65	0.69	0.70	0.62	0.58	0.66
T	46.3	117	63.0	67.4	50.3	95.0	73.2
M	1.0	3.0	3.9	4.2	2.0	5.0	3.2
I	28.7	14.6	17.3	17.4	25.4	24.8	21.4
A	21.5	32.8	34.0	33.7	25.9	33.3	30.2
D	30.3	21.2	20.0	20.5	22.2	11.9	21.0
C	19.5	31.4	38.6	28.5	26.4	30.1	27.4

NOTE: Refer to Table 2-2 for description of criteria.

From this table, it is evident that the driving cycles used in other countries are not only different in terms of the actual speed traces but also vary significantly in terms of the prescribed criteria. Examining the EDC (European Drive Cycle without the high speed phase) parameters such as v_1, length of drive cycle, number of acceleration phase changes and portions of idle times show distinctly different values. Comparing the v_1 (average vehicle speed) parameter, the FTP 72 and 75 cycles show relative high values when compared to the EDC and Japanese sequences. These lower average speeds are not only due to slower peak velocities, which lower the v_2 (average non-zero vehicle speed) parameter, but are also a result of the prolonged idle and constant speed times, which increase the I (idle time) and C (constant speed time) parameters respectively. Lastly, if comparisons are made to the velocity-acceleration envelopes, comparing an actual driving sequence to a synthetically derived schedule as shown schematically in Figures 2-7 and 2-8,(1) differences can be seen. Figure 2-7 illustrates a general representation of the FTP 75 speed/acceleration envelope. The shaded regions represent the occurrences of speed/acceleration points obtained in the drive cycle. As shown, the FTP 75 cycle has characteristic large rounded distributions, indicating a large variance in the driving profile. In contrast, Figure 2-8 representing the synthetically derived EDC, a significantly narrower range of operation is noted. In addition, it is noticeable that acceleration rates for vehicle speeds up to 30 km/hr in the actual speed profiles, are higher that those experienced in the synthetic cycles.

Research presented by Rijkeboer et al,(20) illustrates the differences between driving cycles used in dynamometer testing. This work examined the emission performance of five late model vehicles with accumulated mileages between 3000 and 12500 km over four driving sequences presented in Table 2-3.(20)

TABLE 2-3 DRIVING CYCLES AND CYCLE DETAILS[(20)]

Cycle	Start	Length (km)	Max Speed (km/hr)	Average Speed (km/hr)	Number of Stops per km
Dutch - Urban	Cold	7.56	63.0	34.1	1.3
Dutch - Traffic Jam	Warm	0.71	21.0	7.3	37
European Drive Cycle (UDC + EUDC)	Cold & Warm	11.01	120	33.6	1.2
US - FTP 75	Cold	17.94	63	34.1	1.3

Figures 2-9 to 2-11 display the average emission factors for the five test vehicles as a result of the different driving sequences.(20) The results show a 5, 10 and 3 times difference between the emission factors of HC, CO and NO_x respectively for the various driving profiles. Clearly, this research indicates that using a single driving sequence to determine emission factors for inventory purposes will produce inaccurate results. Other research examining driving cycles has also shown differences in calculated emission factors corresponding to different driving profiles.(16)

2.1.4 INSPECTION AND MAINTENANCE (I/M) EMISSION TESTING

The concept of Inspection and Maintenance (I/M) testing was to provide an annual standardized check on vehicle emission control systems. As was described previously, all new vehicles are required to pass an emission certification test, but these low pollution profiles are only attainable on new vehicles (i.e. 0 Vehicle Miles Traveled; VMT) and with new emission control systems. Thus, the I/M programs were developed to identify malfunctioning emission controls and help to discourage tampering of the systems. The EPA has suggested that I/M programs, depending on their sophistication, can reduce HC and CO emissions by 5% to more than 30% and NO_x emissions up to 10%.(21)

Past I/M procedures consisted of two testing criteria. The first part of the test involved an emissions test while the vehicle was idling or with the engine rotating at 2500 rpm (i.e. with no load). The exhaust emissions, consisting of HC and CO, were then measured and reported on a concentration basis, that is, reported in percent or ppm. The second phase of the test involved a check to ensure critical emission control components were present and operational.(22)

As a result of the 1990 Clean Air Act, a new I/M program has been developed and is known as the I/M 240. This new procedure allows for more compressive testing and was specifically designed to measure the emissions from today's high-tech vehicles. This new procedure consists of three distinct elements:(22) 1) A transient, mass-based emission tailpipe test, 2) A purge flow test of the evaporative canister, and 3) A pressure test of the evaporative system.

The transient section of the procedure is conducted similarly to the FTP certification tests described above as the vehicle is driven over a special cycle as illustrated in Figure 2-12.(2) The main difference with the I/M testing is that the emissions are analyzed and calculated in real-time as opposed to being collected in sample bags and analyzed after completion of the test. The mass of emissions is determined with the CVS system and is calculated by multiplying the flow rate of the diluted sample by the measured concentration of the pollutants in the mixture. This new procedure allows for a faster analysis of the vehicle emissions and through the use of pass / fail algorithms, completing the entire 4 minute drive cycle is usually not necessary. The pass / fail criteria vary between model years but generally are 2 to 3 times higher than the new vehicle certification emission levels. This new stringent testing protocol monitors not only HC and CO as in the previous versions but also NO_x emissions.(22)

The evaporative system purge test was designed to analyze the effectiveness of the vehicle charcoal canister. The charcoal canister was one of the first emission controlling devices installed on vehicles to reduce the amount of HC vapors exiting from the fuel system.(1) This test is conducted at the same time as the transient portion and involves measuring the flow rate of air drawn through the canister. This procedure only requires the installation of a flow meter transducer between the canister and engine and conditioning components. A pass for this test is given if one liter of ambient air is drawn through the canister before the transient test is finished. In general, most vehicles will accumulate as much as 25 liters of air though the canister before the transient test is completed.(22)

The last test conducted in the revamped I/M routine examines the evaporative system for leaks, again eliminating HC from escaping into the atmosphere. A pressure decay method is used to monitor for leaks in the fuel delivery system. This procedure involves disconnecting the vapor line from the charcoal canister and pressurizing the remaining components of the system to 3.5 kPa with nitrogen. If the pressure in the system remains above 2 kPa after two minutes the vehicle passes the test.(22)

2.2 REMOTE SENSING PROCEDURES

Remote sensing of vehicle emissions was developed to improve the real-life nature of vehicle emission testing. This is accomplished by making no direct contact between the vehicle and emission measuring equipment, and allowing the vehicle to be driven in any manner dictated by the driver. Current remote sensing devices (RSD) are capable of measuring volumetric concentrations of HC, CO, CO_2 and NO_x. Because of this, RSD data serve to complement other mobile emission measurement programs.

The experimental setup of the remote sensing procedure is relatively simple thus allowing different locations to be measured with ease.(23-26) It mainly consists of an infrared (IR) source and an IR detector on either side of a single lane roadway. In the case where NO_x measurements are made, an ultraviolet (UV) source and detector are also required. The IR (and UV) source projects a beam of radiation across the roadway approximately at the height of the average vehicle exhaust pipe. As the vehicle passes through the beam, the device measures the ratio of exhaust CO (HC and NO_x) to CO_2 concentrations in front of the vehicle and in the exhaust plume. The measurements made before the exhaust plume are used as baselines. The vehicles CO and HC emission rates are calculated by comparing the total carbon content of the exhaust (i.e. HC, CO and CO_2) to the total carbon content of the gasoline fuel.

Other features incorporated into the RSD commonly include the use of radar guns and video cameras.(23) Radar guns are used to determine the vehicle speed at the time of measurement and a camera is used to capture the licence plate number for identification purposes.

The use of RSDs has some advantages. The real-life nature of vehicle emissions are better represented with this method since the vehicles are driven "freely" and not confined to a specified cycle. This type of procedure also allows for the measurement of numerous vehicles per day and is generally an automated process.

However, RSD systems have numerous drawbacks and difficulties associated with the analysis of the measurements. The major complication of the analysis are the required assumptions needed to calculate an emission factor in g/km. A g/kg_{fuel} emission factor is calculated by estimating the fuel properties and assuming that no O_2 is present in the exhaust, which may or may not be the case. In addition, a vehicle fuel mileage estimate is required to obtain an emission factor in terms of g/km. This analysis leads to questionable emission factors for inventory purposes. Within the context of most RSD measurements, no indication of vehicle operating parameters are recorded.(25) These include parameters such as whether the vehicle was accelerating, decelerating, cruising, operating with a cold or warm engine and other emissions affecting variables. Current RSD technology is capable of only measuring emissions of vehicles on single lane roadways due to the placement of the measurement equipment. This not only limits measurement locations but if multiple lane roadways are filtered into single lanes, practicality may be limited and the procedure loses its real-life advantages. Lastly, the inability of some systems to measure NO_x poses a major drawback to the emissions measurements.

It has been estimated by the EPA that the RSD have misidentified high emitters by as much as 20% for CO and 60% for HC. More importantly, it was indicated that the procedure missed 80 to 90% of high emitter vehicles.(26)

2.3 CURRENT IN-USE, REAL-TIME EMISSION STUDIES

In-use emission measurement systems have been designed,(27,28) and implemented in past studies.(27-31) Studies conducted by Vojtisek-Lom et al.(27,28) have examined the emission behavior of a fleet of gasoline and compressed natural gas (CNG) fueled vans. They found, using the real-time measurement system that, the CNG fueled vehicles had lower cold start emissions than the gasoline vans. Vojtisek-Lom et al. also found that the CNG vans produced comparable HC and CO emissions on daily routes, however the NO_x emissions varied greatly.

Research conducted by Frey et al.(29-31) used the same portable measurement system as Vojtisek-Lom et al., but examined the effects of traffic flow on vehicle emissions. These studies evaluated the relationship between vehicle emission and control delay (i.e. the difference in time it takes a vehicle to reach cruising speed at a distance down stream of an intersection, after slowing down and stopping at the intersection, to the time taken had the vehicle maintained its cruising speed through the intersection).(30) The main conclusion of these studies was that instantaneous vehicle emission rates are the highest during acceleration events, where as idling emissions are very low in comparison.

This work while interesting on the basis of micro modeling (i.e. determining the mass emissions for a single intersection) provides little insight as to the emission factors for entire trip lengths. It will be the focus of this research to develop the methodology to improve the emission factors used for inventory purposes.

2.4 DESCRIPTION OF CURRENT EMISSION FACTOR MODELING SOFTWARE

Emission data collected from dynamometer testing and field testing from remote sensing studies have enabled the development of emission inventory software. Mobile 6,(32,33) developed by the EPA, is the most current emission inventory modeling software. Mobile 5(34,35) modeling software, the predecessor of Mobile 6, distributes the current on-road vehicle fleet into eight main weight categories. Mobile 6 further expands the eight categories into twenty-eight vehicle weight sections.

Figure 2-13 shows an example of a HC cumulative emission trace for a -26°C cold start. This figure illustrates, while not necessarily to scale, the emission factors estimated by the two models. Mobile 5, calculates a composite emission factor essentially based on the mass of the pollutant emitted divided by the distance traveled. This is shown with the solid line in Figure 2-13. Mobile 6 calculates two emission values. This first value describes the "starting emissions"(36,37) shown as the intercept. The second value describes the "running emission factor"(37,38) of the vehicle shown with the dashed line. Clearly, the Mobile 6 model will better estimate vehicle emissions since the single emission factor calculated with Mobile 5 is only accurate for simulation distances near 16 km. This poses a major drawback when accurate emission estimates are required for other simulation distances.

The basic premiss of this modeling software is to calculate the emission factors for groups or fleets of vehicles based on numerous conditions, and distributions of vehicle miles traveled (VMT). The calculated emission factors are based upon six main inputs that are locality-specific to the region in question consisting of:(34,35)

1. Daily minimum and maximum ambient temperatures.
2. Statistical data on average vehicle or fleet annual mileage accumulation rates and model years.
3. The VMT mix (i.e. the distribution of the fleets VMT accumulations).
4. Fractions of VMT in cold, transitional and warm-start operating modes.
5. The calendar year of evaluation.
6. Fuel volatility values.

Once these variables have been defined, the Mobile model then uses a collection of data tables containing emission factor values consisting of HC, CO and NO_x. These values are known as the basic emission rates (BER) expressed as g/km. These BER values were measured and obtained in laboratory environments under a standard set of conditions. The BER values are usually determined from certification testing conducted with new (non-aged) vehicles. These emission rates are then adjusted using experimentally determined deterioration rates (found from I/M testing) to account for vehicle age and accumulated mileage. The BER values are then corrected based upon the six inputs described earlier. The correction factors include an Operating-Mode /

Temperature Correction Factor (OMTCF), a Tamper Offset (OMTTAM), a Speed Correction Factor (SALCHF), and a Travel Weighting Factor (TFs). Once these correction factors have been determined, the basic emission factor (BEF) can be calculated for the three major pollutants:

$$BEF_{exhaust} = (BER * OMTCF + OMTTAM) * SACHCF * TF)$$

This equation calculates the tailpipe emission factors for pollutants of CO and NO_x. However, because HC emissions also include other losses (i.e. crankcase, evaporative, refueling, running, and resting losses) the BEF value for HC is modified to include these estimates:

$$BEF = BEF_{exhaust} + TFs * (\text{ Evaporative} + \text{Refueling} + \text{Running} + \text{Resting})$$

This algorithm allows the emission factors to be estimated and then used for inventory purposes.

2.5 CONCLUSIONS

With the background presented in this chapter, it is clear that valuable insight will be gained by measuring vehicle emissions from on-road applications. The remainder of this thesis describes a system to make these measurements and develops algorithms to process the data with the intention of developing an emission factor model based on in-use emission traces.

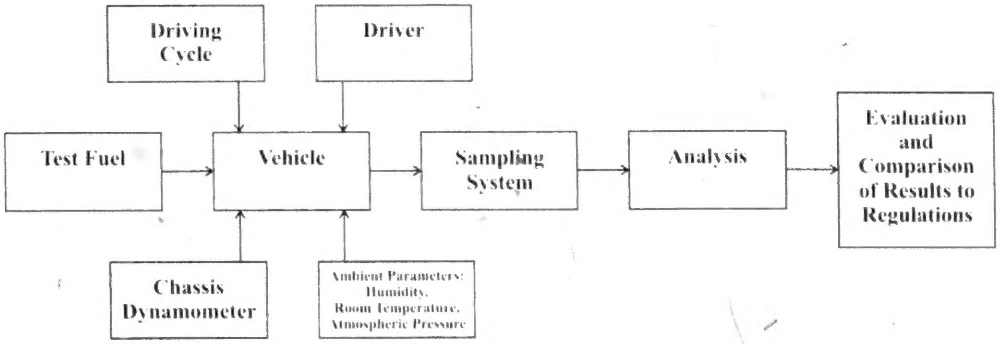
Driving Cycle
Driver
Test Fuel
Vehicle
Sampling System
Analysis
Evaluation and Comparison of Results to Regulations
Chassis Dynamometer
Ambient Parameters: Humidity, Room Temperature, Atmospheric Pressure

FIGURE 2-1 FTP EMISSION TESTING PARAMETERS(1)

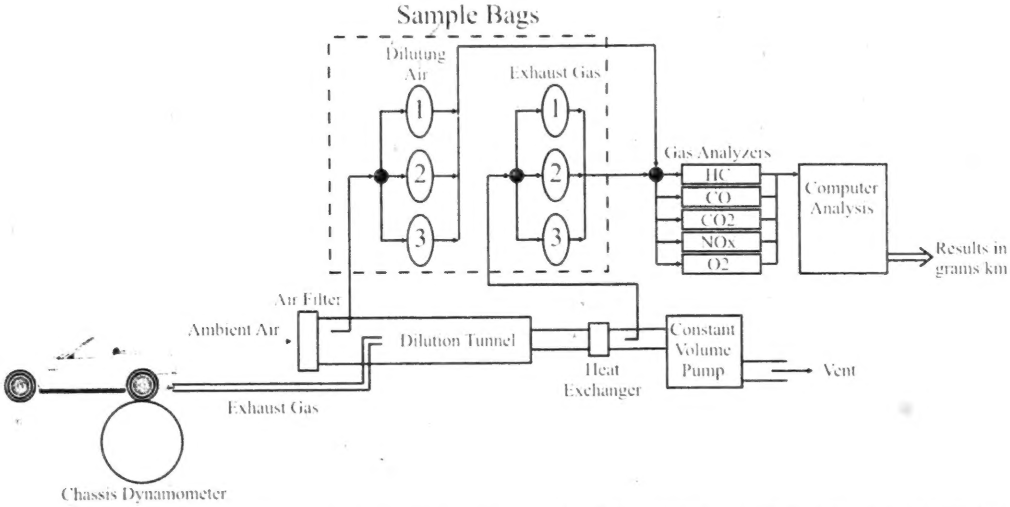

FIGURE 2-2 SCHEMATIC REPRESENTATION OF THE FTP EMISSION CERTIFICATION TEST(1)

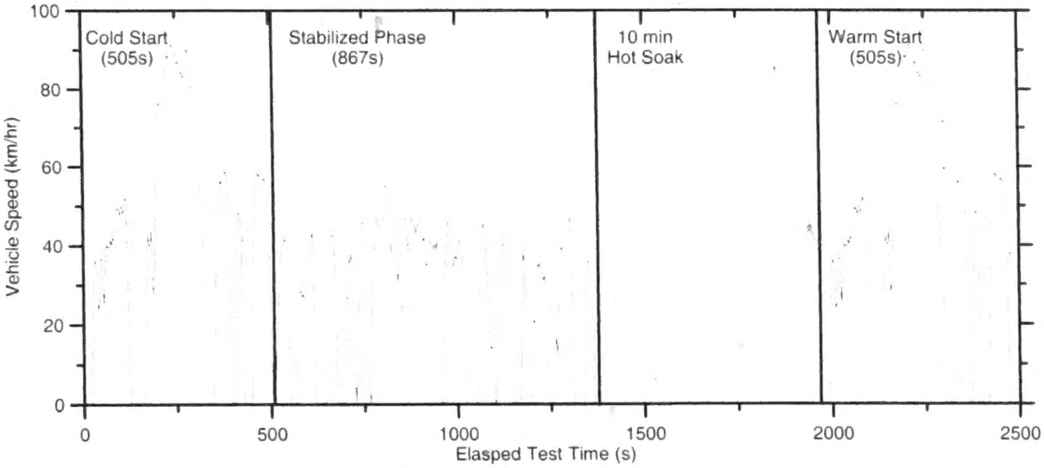

FIGURE 2-3 NORTH AMERICAN FTP 75 DRIVING CYCLE FOR EMISSION CERTIFICATION TESTING BASED ON AN ACTUAL DRIVING SEQUENCE(1)

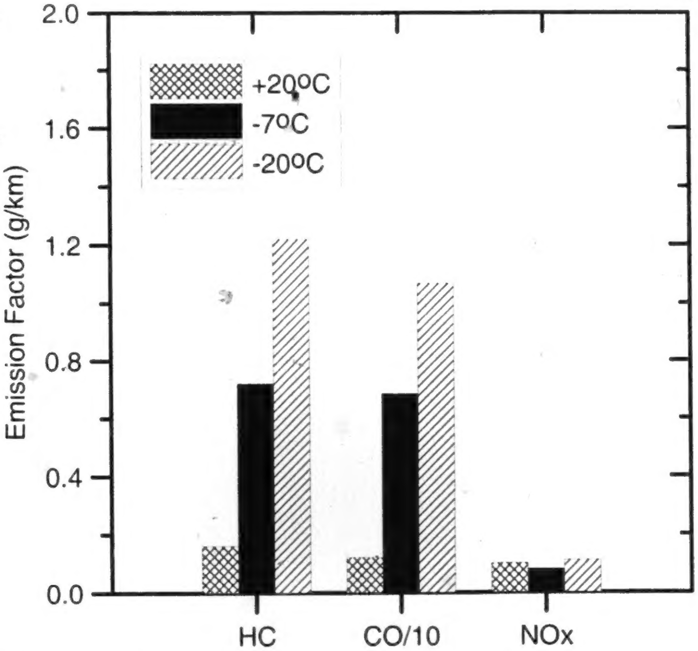

FIGURE 2-4 FTP 75 EMISSION FACTORS OF A 2.0L VEHICLE AT DIFFERENT AMBIENT CONDITIONS(4)

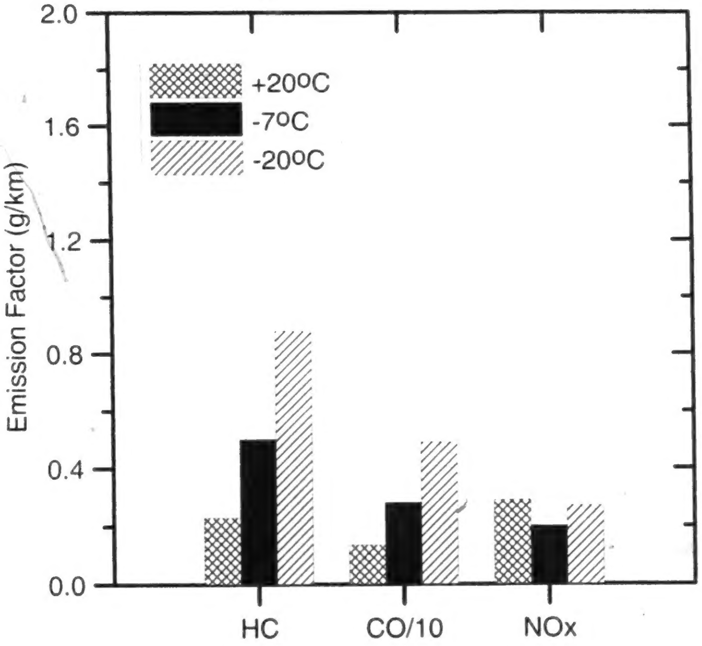

FIGURE 2-5 FTP 75 EMISSIONS FACTORS OF A 1.3L VEHICLE AT DIFFERENT AMBIENT CONDITIONS(4)

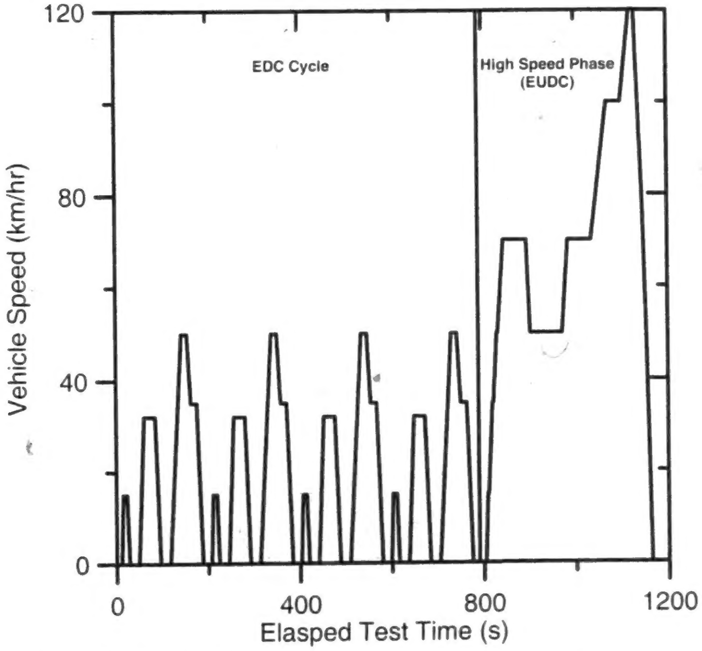

FIGURE 2-6 THE SYNTHETICALLY CONSTRUCTED EUROPEAN DRIVING SEQUENCE (EDC & EUDC) FOR EMISSION TESTING(1)

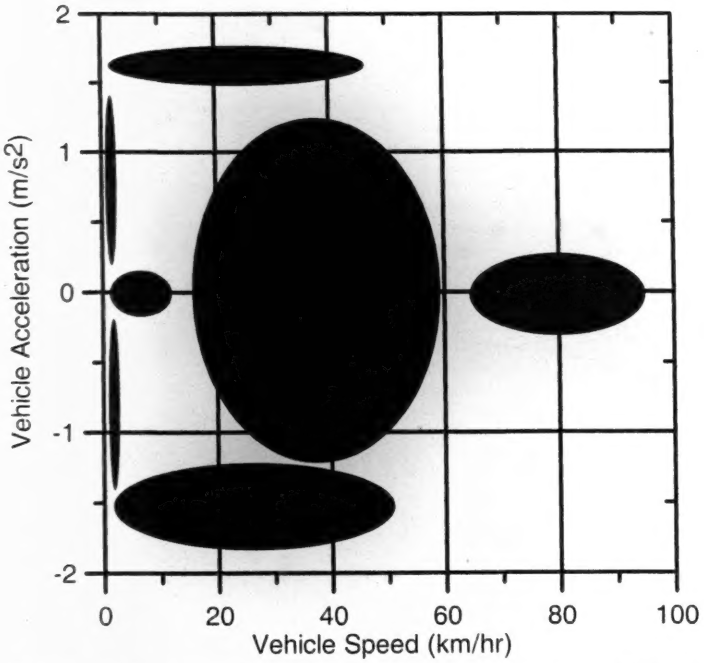

FIGURE 2-7 SCHEMATIC REPRESENTATION OF THE FTP 75 SPEED/ACCELERATION ENVELOPES

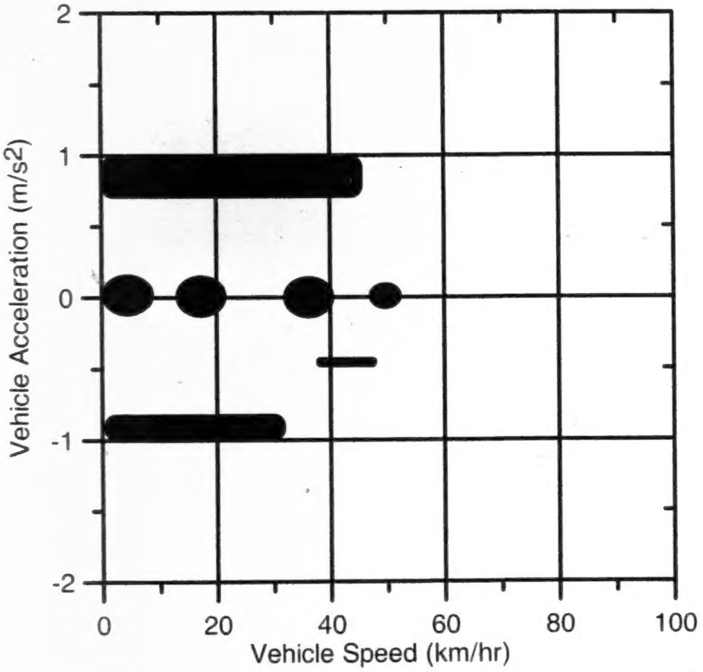

FIGURE 2-8 SCHEMATIC REPRESENTATION OF THE EDC SPEED/ACCELERATION ENVELOPES

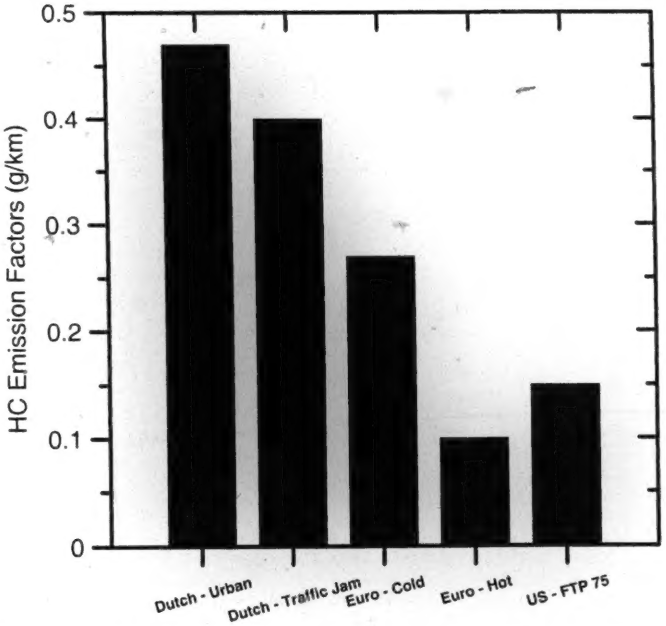

FIGURE 2-9 HC EMISSION FACTOR COMPARISON FOR DIFFERENT DRIVING CYCLES(20)

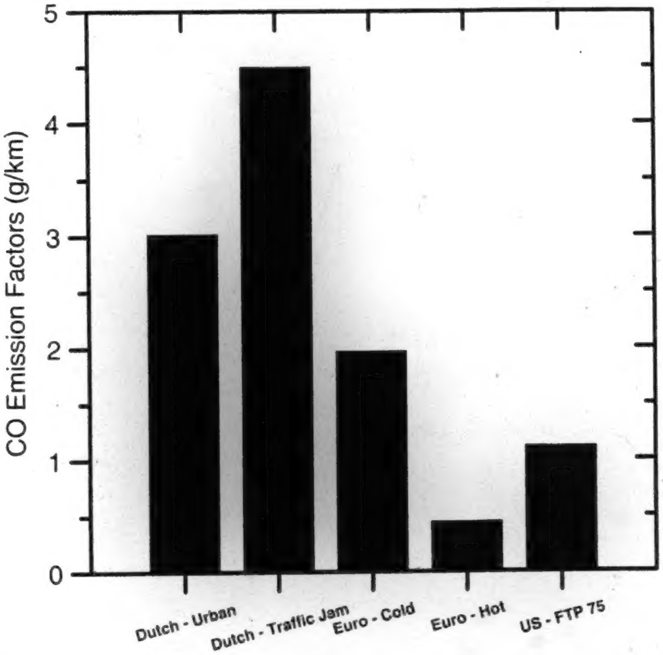

FIGURE 2-10 CO EMISSION FACTOR COMPARISON FOR DIFFERENT DRIVING CYCLES(20)

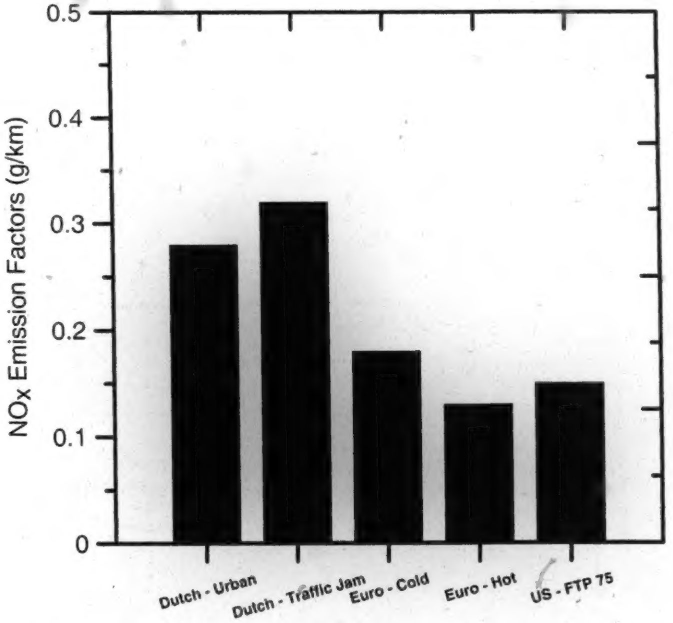

FIGURE 2-11 NO_x EMISSION FACTOR COMPARISON FOR DIFFERENT DRIVING CYCLES[(20)]

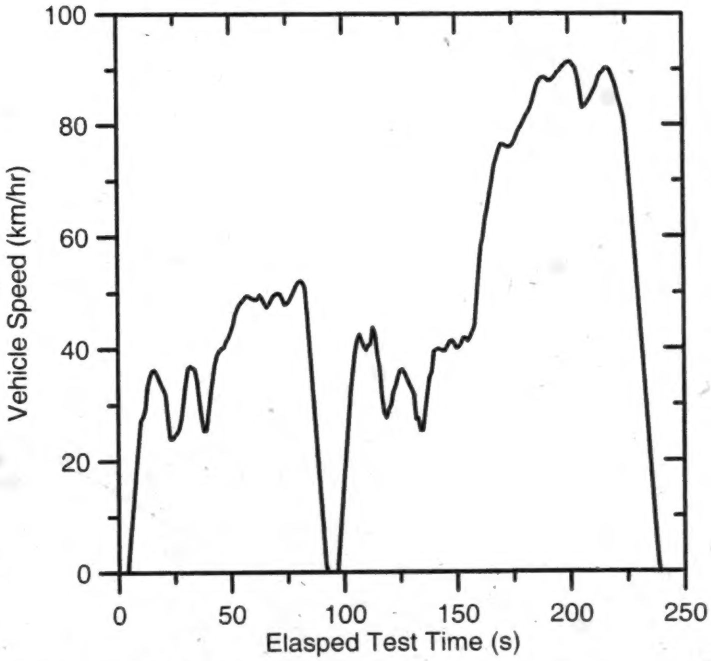

FIGURE 2-12 I/M 240 DRIVING SEQUENCE[(2)]

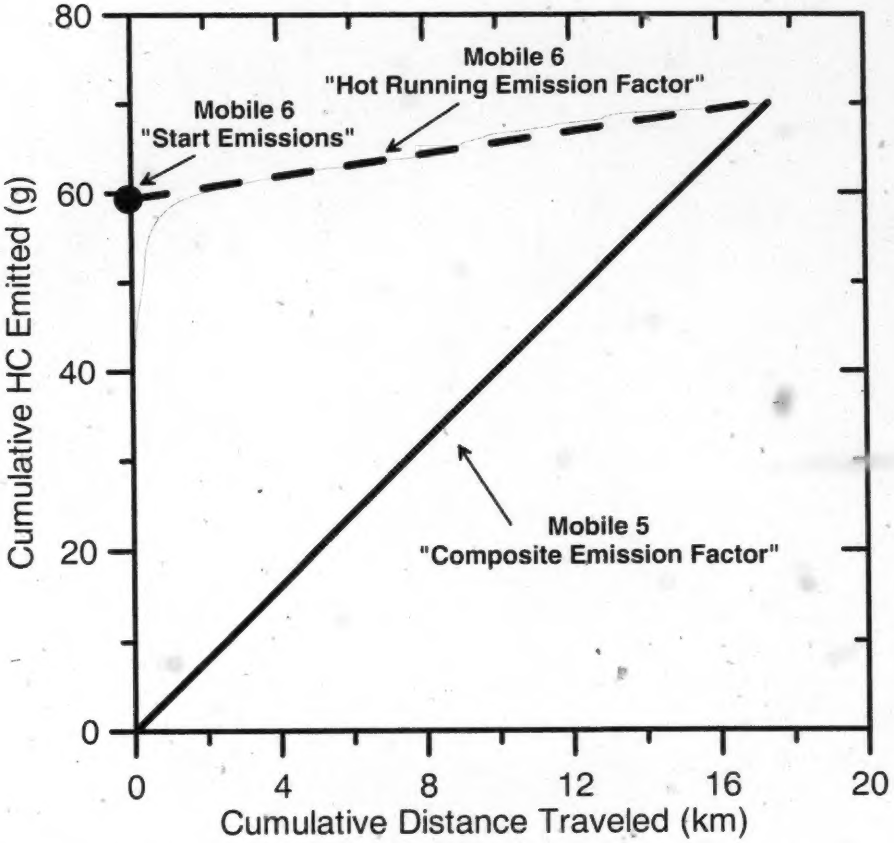

FIGURE 2-13 ILLUSTRATION OF EMISSION FACTORS CALCULATED WITH MOBILE 5 & 6 (NOTE EMISSION FACTORS NOT TO SCALE)

REFERENCES

1. Klingenberg H., "Automobile Exhaust Emission Testing," New York, Springer-Verlag, 1996.

2. Dhaliwal B.S., "Alternative Fuel Effects on Vehicle Emission and Indoor Air Quality" Master of Science Thesis, University of Alberta, Edmonton, Canada, 2000.

3. Bielaczyc P., Merkisz J., "Cold Start Emissions Investigation at Different Ambient Temperature Conditions" SAE Technical Paper 980401, Society of Automotive Engineers, 1998.

4. Laurikko J., Nylund N. "Regulated and Unregulated Emissions frm Catalyst Vehicles at Low Ambient Temperatures" SAE Technical Paper 930946, Society of Automotive Engineers, 1993.

5. Laurikko J., Erlandsson L., Arbrahamsson R., () "Exhaust in Cold Ambient Conditions: Considerations for a European Test Procedure," SAE Technical Paper 950255, Society of Automotive Engineers, 1995

6. Laurikko J., Aakko P., "The Effect of Ambient Temperature on the Emissions of Some Nitrogen Compounds: A Comparative Study on Low-, Medium- and High Mileage Three-Way Catalyst Vehicles" SAE Technical Paper 950933, Society of Automotive Engineers, 1995.

7. Gurney M.D., Allsup J.R., "Predictability of Emissions from In-Use Vehicles at Low-Ambient Temperature and Alternate Driving Cycle Based on Standard Tests" SAE Technical Paper 890625, Society of Automotive Engineers, 1989.

8. Larson R.E., "Vehicles Emission Characteristics Under Cold Ambient Conditions" SAE Technical Paper 89002, Society of Automotive Engineers, 1989.

9. Polak J.C., "Cold Ambient Temperature Effects on Emissions from Light-Duty Motor Vehicles" SAE Technical Paper 741051, Society of Automotive Engineers, 1974.

10. Ginberg L., Morgan L. "Effect of Temperature on Exhaust Emissions" SAE Technical Paper 740527, Society of Automotive Engineers, 1974.

11. Braddock J.N., "Impact of Low Ambient Temperature on 3-Way Catalyst Car Emissions" SAE Technical Paper 810280, Society of Automotive Engineers, 1981.

12. Springer K.J., Dickinson A.G., "Car Cold-Start Hydrocarbon Control Considerations"

Presented at Energy-sources Technology Conference & Exhibition, Jan 31 - Feb 4, Houston, TX, 1993.

13. Bielaczyc P., Merkisz J., "Cold Start Emissions Investigation at Different Ambient Temperature Conditions" SAE Technical Paper 980401, Society of Automotive Engineers, 1998.

14. Andre M., Hickman A.J., Hassel D., Joumard R., "Driving Cycles for Emission Measurements Under European Conditions" SAE Technical Paper 950926, Society of Automotive Engineers, 1995.

15. Enns P., German J., Markey J., "EPA's Survey of In-Use Driving Patterns: Implications for Mobile Source Emission Inventories" USEPA Ann Arbor MI, 1993.

16. Milkins E., Watson H., Comparison of Urban Driving Patters" SAE Technical Paper 830939, Society of Automotive Engineers, 1983.

17. Dembski N., Guezennec Y., Soliman A., "Analysis and Experimental Refinement of Real-World Driving Cycles" SAE Technical Paper 2002-01-0069, Society of Automotive Engineers, 2002.

18. Kruse R.E., Huls T., "Development of the Federal Urban Driving Schedule" SAE Technical Paper 730553, Society of Automotive Engineers, 1973.

19. German J., "Observations Concerning Current Motor Vehicle Emissions" SAE Technical Paper 950812, Society of Automotive Engineers, 1995.

20. Rijkeboer R.C., Hendriksen P., Hollemans B., van der Weide J., "Potential Impact of Four Different Car Fuels on the Dutch Environment" SAE Technical Paper 941914, Society of Automotive Engineers, 1994.

21. "Clean Cars for Clean Air: Inspection and Maintenance Programs" US EPA Office of Mobile Sources Fact Sheet OMS - 14, 1994.

22. "High-Tech Inspection and Maintenance Tests" US EPA Office of Mobile Sources Fact Sheet OMS - 16, 1994.

23. Unal A., Dalton R., Frey H.C., Rouphail N.M., "Simultaneous Measurement of On-Road Vehicle Emissions and Traffic Flow Using Remote Sensing and an Area-Wide Detector" Paper # 99-712, 1999.

24. Bishop G.A., Zhang Y., McLaren S.E., Guenther P.L., Beaton S.P., Peterson J.E.,

Stedman D.H., "Enhancements of Remote Sensing for Vehicle Emissions in Tunnels" Journal of Air and Waste Management, Vol. 44, pp 169 - 175, 1994.

25. Swayne K.L., "Infrared Remote Sensing of On-Road Motor Vehicle Emission in Washington State" Washington State Department of Ecology. March 1999, Publication #99-204.

26. "Remote Sensing: A Supplemental Tool for Vehicle Emission Control" US EPA Office of Mobile Sources Fact Sheet OMS - 15, 1993

27. Vojtisek-Lom M., Cobb T. "Vehicle mass emissions measurements using a portable 5-gas exhaust analyser and engine computer data" Presented at at: Emission Inventory: Planning for the Future, Research Triangle Park, NC, October 29, 1997.

28. Vojtisek-Lom M., Cobb T. "Measurement, variance and reduction of real-world emissions of 20 dedicated CNG vans" Presented at: Air & Waste Management Association's 91st Annual Meeting & Exhibition, San Diego, California, June 14-18, 1998..

29. Frey H.C., Rouphail N., Unal A., Colyar J. "Emissions and Traffic Control: An Empirical Approach" Presented at CRC On-Road Vehicle Emissions Workshop, San Diego, CA., March 2000,.

30. Rouphail N.M., Frey H.C., Colyar J.D., Unal A. "Vehicle Emissions and Traffic Measures: Exploratory Analysis of Field Observations at Signalized Arterials" Presented at the 80th Annual Meeting of the Transportation Research Board, Washington D.C., Jan 7-11 2001.

31. Frey H.C., Rouphail N.M., Unal A., Colyar J.D. "Measurement of On-Road Tailpipe CO, NO, and Hydrocarbon Emissions Using a Portable Instrument" Presented at the Annual Meeting of the Air and Waste Management Association, June 24-28, Orlando Florida, 2001.

32. Environmental Protection Agency, Mobile 6, http: www.epa.gov/otaq/m6.htm.

33. Environmental Protection Agency, "User's Guide to Mobile 6.0 (Mobile Source Emission Factor Model)" EPA420-R-02-001, 2002.

34. Environmental Protection Agency, Mobile 5, http: www.epa.gov/otaq/m5.htm.

35. Environmental Protection Agency, "User's Guide to Mobile 6 (Mobile Source Emission Factor Model)" EPA-AA-TEB-94-01, 1994.

36. Glover E., Carey P., "Determination of Start Emission as Function of Mileage and Soak Time for 1981-1993 Model Year Light-Duty Vehicles" Assessment and Modeling Division, Office of Mobile Sources, U.S. Environmental Protection Agency, M6.STE.003, 1999.

37. Carey P., Lorang P., "Overview of Methodology for Tier 0 In-Use Deterioration and Key Issues for Comment" Assessment and Modeling Division, Office of Mobile Sources, U.S. Environmental Protection Agency, M6.EXH.008, 1999.

38. Brzezinski D.J., Glover., Enns P., "The Determination of Hot Running Emission from FTP Bag Emissions" Assessment and Modeling Division, Office of Mobile Sources, U.S. Environmental Protection Agency, M6.STE.002, 1999.

CHAPTER 3

REAL-TIME, ON-ROAD MEASUREMENTS OF DRIVING BEHAVIOR, ENGINE PARAMETERS AND EXHAUST EMISSIONS

As was discussed in Chapter 2, various modifications have been implemented in laboratory studies to improve the real-world representativeness of the experimental emission factors. Remote sensing experiments were developed to enhance the real-world nature of emission factors. However, both of these test methods produce questionable emission factors used in emission inventories. Chapter 3 describes a measurement system and analysis algorithms which are capable of determining the emission factors of vehicles in real-world applications. This chapter also identifies the capabilities of the entire measurement system.

Chapter 3 is a paper which was published by the Society of Automotive Engineers (SAE 2002-01-1714) and was presented at the Spring Fuel and Lubricants conference in Reno, Nevada in May of 2002. It is presented here in a lengthened version with references to various appendices.

ABSTRACT

Automotive tailpipe emissions are a significant contribution to urban air quality problems. However, it is difficult to quantify the extent of that contribution and to quantify any progress in solving the problem. Emissions inventories are commonly based on vehicle registrations, assumed mileage and a set of emission factors. The emission factors are based on dynamometer testing of selected vehicles under tightly controlled conditions. Actual vehicle operation in any urban area encompasses a wider range of vehicles, operating conditions and ambient conditions. Given the highly tuned nature of current engine management systems, the actual in-use emissions levels can be highly sensitive to nonstandard ambient and operating situations.

This paper describes an on-board system used to record ambient conditions, driving behavior, vehicle operating parameters, fuel consumption and exhaust emissions. The system uses a laptop computer data acquisition system and a number of add-on sensors, (which include a five-gas analyzer and fast-response lambda sensor). Recorded data files are post-processed to measure values ranging from simple vehicle speed and distance traveled to emission rates in grams per kilometer. In addition, using the vehicle speed trace as input to a vehicle dynamic model, the tractive power requirements could be calculated.

This paper presents results for a small set of repeated commuting trips to illustrate the capabilities and repeatability of the in-use measurement system. Also included are diagnoses of emission control system anomalies which significantly affected emissions but were not detectable by the

driver.

3.0 INTRODUCTION

Current vehicle emission inventories are generally based on chassis or engine dynamometer testing protocols and sometimes include information from remote sensing studies. Chassis dynamometer speed-time driving schedules were developed from actual measurements of real-time driving traces(1) and provide a standardized means of comparison between vehicles running in tightly controlled test conditions. Transients more (and less) extreme than those specified in standard driving schedules,(2-6) combined with degradation of the vehicle systems can lead to major deviations between the emissions produced on a dynamometer and those produced in on-road applications. In addition, variations in ambient conditions are known to affect pollutant emissions but are difficult to specify and reproduce in lab environments.(7-17) Remote sensing studies improve the real-life nature of emission measurements by covering a broad spectrum of in-use vehicles, (sometimes hundreds or thousands of vehicles per day). However, they only measure the instantaneous emissions at a specified location and provide no insight as to the operating parameters of the test vehicle itself or its emissions under other operating conditions.(18-21)

There has been a need for a real-time emission measurement system that could provide instantaneous measurements of the products of combustion as well as the engine parameters and driving behaviors that lead to those emissions. Earlier chemistry-based emission measurement technologies for exhaust gas composition made it difficult to design portable devices for accurate emission measurements and also to coordinate their output with simultaneous measurements of vehicle operating parameters. Current technology has allowed the design of relatively simple and accurate gas composition instruments(22-27) and flexible data acquisition systems which have the capability to measure and record several vehicle operating parameters simultaneously. This paper describes the development and use of a real-time measurement system capable of simultaneously monitoring emission rates, fuel consumption rates, ambient conditions and driving traces. Exhaust gas composition was measured using a five-gas analyzer, exhaust mass flow rate was measured using a mass air flow sensor plus a fast-response lambda sensor to infer the air/fuel ratio. Using these values, the instantaneous mass emission rate of each exhaust gas component could be calculated on a second-by-second basis and correlated with actual vehicle operation in a range of real-world driving conditions. The paper (chapter) describes the implementation and testing of this system on a bi-fuel test vehicle which operated using either gasoline or natural gas in a variety of driving conditions in the region of Edmonton, Canada. Typical results and preliminary findings are presented.

3.1 GENERAL TEST SET-UP

The arrangement of sensors and connections with the data acquisition system are shown schematically in Figure 3-1. The emissions measurements were based on a Vetronix PXA - 1100 five-gas analyzer which used a combination of infrared absorption and fast response chemical cells to measure NO_x, HC, CO, CO_2 and O_2. Air mass consumption rate was measured by a Siemens HFM 62B mass air flow (MAF) sensor which had been calibrated against an ASME standard nozzle. An instantaneous fuel consumption rate was inferred using an ECM AFRecorder 2400E fast response lambda sensor in combination with the mass air consumption rate. Measured vehicle parameters included speed, (measured by a signal conditioning circuit on the stock vehicle speed sending unit), and coolant temperature, (measured by an AD590 temperature probe in the manifold crossover water jacket). Ambient temperatures were measured by two AD590 temperature probes, one in the vehicle's intake system under-hood before the throttle valve, and one attached to the vehicle's radio antenna. Specific instrument details as well as range, sensitivity and accuracy are presented in Table 3-1. Communication with all of the instruments and sensors was conducted through a Fujitsu laptop computer running National Instruments (Austin, Texas) Labview 6i. The five-gas analyzer composition data were communicated over a serial line and the other parameters were measured as analog signals using a National Instruments PCMCIA DAQCard-AL-16E-4 data acquisition (DAQ) card.

TABLE 3-1 INSTRUMENT SPECIFICATIONS AND CALIBRATION STANDARDS

VALUE	RANGE	RESOLUTION	SENSITIVITY	ACCURACY (RATED)	CALIBRATION	MAX. % DEVIATION
5 Gas HC	0 - 20,000ppm	1 ppm	N/A	5% of reading	One Point Propane 1267 ppm	5.5
5 Gas CO	0 - 10%	0.01 %	N/A	5% of reading	One Point CO 3.90 %	5.6
5 Gas CO_2	0 - 20%	0.1 %	N/A	5% of reading	One Point CO_2 12.00 %	6.7
5 Gas O_2	0 - 25%	0.01 %	N/A	5% of reading	One Point Air 20.9 %	4.3
5 Gas NO_x	0 - 4000 ppm	1 ppm	N/A	32 ppm at 0 - 1000 ppm 60 ppm at 1001 - 2000 ppm 120 ppm at 2001 - 4000 ppm	One Point NO_x 2030 ppm	8.2
AD590	-55 - 150 °C	0.12 °C	1000 °C/V	0.5 °C	Three Point (Boiling, Room, Ice Bath)	N/A
Siemens HFM 62B	10 - 70 g/s	27.7 mg/s	22.7 (g/s) / V	1.0 g/s	ASME Standard Nozzle	N/A
Engine Speed	0 - 5000 RPM	1.22 RPM	1000 RPM/V	20 RPM	Internal Calibration	N/A
Air to Fuel Ratio	10 to 25	0.004 A/F Units	3.0 (A/F) / V	0.25 A/F units	Internal Calibration	N/A
Vehicle Speed	0 - 80 km/hr	0.01 km/hr	0.057 km/hr / Hz	0.25 km/hr	Chassis Dynamometer	N/A

3.2 EXPERIMENTAL VEHICLE

The test vehicle used during system development was a 1992 GMC three-quarter ton regular cab pickup with 5.7L (350ci), automatic transmission and long box bed. The dry vehicle weight was approximately 2,100 kg (4,700 lbs.) and, at the start of testing in early June of 2001, the odometer read approximately 187,000 km. Approximately 2,000 km were accumulated during experimental testing. This test vehicle was originally the University of Alberta entry in the 1993 NGV Challenge.(28) Subsequent to that event, the engine had been returned to stock gasoline configuration and a Natural Gas Vehicle (NGV) fuel injection system developed by Alternative Fuel Systems of Calgary, Canada was installed. This system allowed operation in either gasoline or natural gas mode with stock gasoline settings and similar levels of sophistication in the fuel injection tables, block learn system and feedback control on natural gas. The vehicle was chosen for development of the on-road emissions measurement system because it represented a fairly large portion of the on-road fleet which, due to original standards and age, provides an even more significant fraction of the on-road emissions. To avoid the complications of a severely aged catalyst, a replacement OEM catalytic converter was installed during the test period.

3.3 MEASUREMENT SYSTEM DETAILS

3.3.1 VETRONIX FIVE GAS ANALYZER

The Vetronix (Santa Barbara, California) PXA-1100 portable five-gas analyzer is a self-contained device which operates from vehicle power (12V). It includes a built-in vacuum pump sample system with valving and control logic for sample line purging, auto-zeroing and water separation as well as exhaust gas sampling. Samples are analyzed by two methods: non-dispersive infrared (NDIR) for HC, CO and CO_2 composition and two electro-chemical detectors for O_2 and NO_x detection. Microprocessor logic is used to calculate and display exhaust gas volumetric concentrations using a calibration based on automatic zero (using air) and a one-point calibration (using a fixed multi-component sample gas). A built-in RS-232 serial link was used to transmit the calibrated readings to the laptop computer.

Emission monitoring depends heavily on an accurate and consistent measurement of exhaust gas composition. As a result, attention had to be paid to the zeroing and calibration of the five-gas analyzer to ensure such accuracy. The analyzer has the capability to adjust its zero levels for NO_x, HC, CO and CO_2 using ambient air as a zero gas. This re-zeroing process halts exhaust gas sampling for approximately 1.5 minutes and it is desirable to avoid frequent re-zeroing during vehicle testing. This was accomplished in this study by warming up the test instrument for a minimum of 15 minutes before each test. The instrument then gave a minimum of 10 minutes and usually 30 minutes of operation before requesting a re-zero. In addition, the unit would warn that a re-zero was required but deferred the procedure until triggered manually. This permitted orderly completions of each test run. Periodic checks showed that there were no detectable changes in zero values with ambient air when the unit was operated for a few minutes beyond its request for a re-zero.

The one-point calibration procedure was performed every week after approximately 10 to 15 hours of operation using the calibration gases listed in Table 3-1. To monitor the accuracy of the analyzer, checks using the calibration gases were run before and after the weekly calibration. The results of these checks showed no significant drift in instrument calibrations and the maximum percent differences are shown in Table 3-1.

NDIR techniques for concentration measurement of CO and CO_2 are well-defined since the gases and their absorption characteristics are well characterized. However, using infrared absorption to measure the exhaust hydrocarbon level leads to uncertainties due to the range of hydrocarbons present and differing absorption constants for carbon-hydrogen, carbon-carbon and multiple carbon-carbon bonds.(21,29,30) Typically, these instruments express HC output in terms of equivalent hexane (C_6H_{14}) content but are calibrated using propane (C_3H_8). The relative output for the same molar concentration of propane as hexane is expressed as a propane equivalence factor (PEF). An ideal PEF value would be 0.5 since propane has half as much carbon as hexane. The actual PEF value is 0.480 for this instrument, illustrating some of the sensitivities mentioned above. The difference becomes more significant for unsaturated hydrocarbons, (having multiple carbon-carbon bonds), and for methane (with no carbon-carbon bonds). The PXA-1100 gas analyzer was tested with calibration gases having known levels of methane, propane and hexane as well as comparison tested against a flame ionization detector (FID) HC analyzer with real engine exhaust. Figure 3-2 illustrates the response of the PXA-1100 to methane, propane and hexane calibration gases after pre-calibration using propane gas. (Calibration gas concentrations are adjusted to equivalent hexane value using 0.480 for propane and 1/6 for methane.) As shown in the figure, the response to equivalent carbon content in the form of propane is good, (since it was calibrated on propane). The instrument over-responds by 11% when measuring actual hexane samples. Although the infrared-based HC measurement does not provide the same carbon content sensitivity as a FID-based instrument, its results are reasonably consistent for any single engine fuel.

The sensitivity of methane measurements (a hydrocarbon compound with no carbon-carbon bonds) was only 22% of the correct reading. This low sensitivity to methane is a concern for any NGV HC emission analysis, however no natural gas testing was conducted in this thesis.

3.3.2 ECM AFRECORDER 2400E

The ECM (Sunnyvale, California) AFRecorder 2400E is a fast-response instrument using a wide-range lambda sensor and operating on 12V vehicle power. It was used to monitor the air/fuel ratio and engine speed (RPM) of the test vehicle. A proprietary lambda sensor was installed into the vehicle's exhaust pipe for the air/fuel ratio measurement and an inductive pick-up assembly was connected to the distributor coil wire to determine the engine speed. The ECM provided analog outputs of the two measurements to the DAQ system.

To ensure that sensor warm-up effects were eliminated for the air/fuel ratio measurement, power to the lambda sensor was enabled for two minutes before the start of the experiment. The lambda sensor was placed at a mid-wall location along a horizontal section of exhaust pipe to prevent puddling of condensation around the probe. In addition, the sensor was positioned approximately ten centimeters downstream of the V8 Y-pipe junction to provide a representative measurement of the average air/fuel ratio from all cylinders.

The calibration of the air/fuel ratio measurement was conducted on a weekly basis. The process involved exposing the lambda sensor to ambient air and a resulting O_2 measurement being made. If an O_2 measurement of 20.9% was not obtained, then an ambient air calibration could be selected and the instrument would re-calibrate automatically. The analog outputs for the two measurements were calibrated internally to the ECM instrument. That is, endpoint values were required for the two measurements and the ECM would compensate for nonlinear effects of the transducers and produce a linear voltage output over a 0 to 5 volt range.

3.3.3 MASS AIR FLOW MEASUREMENT

Engine air consumption was measured using a Siemens (New York, New York) HFM 62B MAF sensor mounted in the engine air intake system. Using hot film anemometry principles and an internal temperature compensation, the device operates on the vehicle 12V system and produces an analog output voltage. This was converted to mass air flow rate using a calibration curve derived from comparison with an ASME standard nozzle per SAE standard J244. Before each test, as with the other instruments, the MAF sensor was warmed up for a minimum of fifteen minutes. This was to ensure that instrument warm-up transients did not affect operation during the cold-start phase of the test. To enure that accurate and consistent measurements would be obtained over the months of operation, monthly inspections of the sensor were conducted. This involved simple inspection and cleaning (if required) of the flow straightening devices and thin metal wires.

3.3.4 TEMPERATURE MEASUREMENTS

Three identical, Intersil (Milpitas, California) AD590 temperature transducers were used to measure engine coolant, intake air, and ambient air temperature. The AD590 sensors consist of an integrated circuit in a small metal canister which produces a linear current output of 1 μA/K over the temperature range of -55 to 150°C. The three sensors were all powered by the vehicle 12V system and output read directly by the data acquisition system. The engine coolant temperature sensor was mounted in contact with the engine coolant through a plug in the coolant crossover through the V8 intake manifold. This location was chosen to provide the coolant temperature most relevant to gasoline vaporization and mixture formation in this throttle-body injected engine. The intake air temperature sensor was inserted into the under-hood air ducting upstream of the air filter. This provided a position which responded to high under-hood temperatures during a hot soak. The ambient air temperature sensor was mounted on the radio antenna where it would be directly exposed to ambient air flow and a significant distance from any hot vehicle surfaces.

3.3.5 VEHICLE SPEED MEASUREMENTS

The test vehicle's road speed was obtained by conditioning the signal of the stock speed sending unit in the automatic transmission. The magnetic pick-up sensor produced a sine wave with both frequency and amplitude proportional to vehicle speed. Signal conditioning circuitry was developed to amplify and trim the sine wave, producing an approximately square wave output. However, at vehicle speeds below 2 km/hr the amplitude was too low to measure accurately. The pulse width of the transformed signal was measured using the 20 MHz counter within the data acquisition system. The calibration of the vehicle speed sending unit was conducted on a chassis dynamometer at various wheel speeds ranging from 0 to 80 km/hr and the output was also cross referenced with the vehicle's stock speedometer at speeds up to 120 km/hr.

3.3.6 PORTABLE DATA ACQUISITION SYSTEM

A Fujitsu laptop computer equipped with a National Instruments (NI) DAQCard-AL-16E-4 PCMCIA DAQ card collected and logged all recorded signals. The data acquisition card was capable of monitoring eight differential channels of analog inputs with twelve bit resolution and selectable gains of 1, 2, 5 10, 20, 50 or 100. The DAQ card was also equipped with two counter/timers capable of measuring periods or frequencies of digital signals. Labview 6i program code was written to process the analog inputs from the data acquisition card as well as communicate with the five gas analyzer via RS 232 serial connection. The sampling frequency of the DAQ system was dictated by the communication rate of the five gas analyzer, resulting in a variable sampling frequency which averaged 1.5 Hz. If a serial communications error occurred, the maximum time between successive data entries was 3 seconds.

3.3.7 DATA ANALYSIS SOFTWARE

Raw experimental files were processed using a dedicated MATLAB (Natick, Massachusetts) program which included a Graphical User Interface (GUI) to provide onscreen options. The program incorporated filtering algorithms to eliminate electrical interference spikes from the temperature transducers and smoothing routines to eliminate unrealistic jumps in the velocity profile.

The electrical noise filtering routine for the temperature measurements was based on a running average/despike scheme. The algorithm considered seven consecutive data points with the fourth value being the point of interest. The highest and lowest values were discarded and the average of the remaining five values was calculated. If the original data point differed from this average by more than a specified tolerance (±2.0 °C) that point was replaced by this average value.

Vehicle speeds above 50 km/hr were filtered in a similar manner except the tolerance range was specified to be ±0.15 km/hr. In addition to this averaging scheme, two other routines were developed to remove data outliers. The first algorithm set all vehicle speeds below 2 km/hr to 0 km/hr since the system only erratically responded to less than 2 km/hr speeds. The second algorithm removed false velocity spikes attributed to shifting gears (park to reverse or reverse to drive). Slack in the drive train caused the transmission-mounted speed sensor to produce velocity spikes when the vehicle was stationary so these spikes were replaced with a zero velocity value.

The smoothing of the velocity profile was important since the acceleration of the vehicle was calculated from the slope of this curve using the simple formula:

$$\text{Accel}(i) = \frac{\text{Speed}(i+1) - \text{Speed}(i-1)}{\text{Time}(i+1) - \text{Time}(i-1)}$$

Where:

Accel = test vehicle's acceleration [m/s^2]
Speed = test vehicle's speed [m/s]
Time = elapsed test time

Once the acceleration of the vehicle had been determined at each time step, the possibility arose to have a non-zero acceleration associated with a zero vehicle speed. To prevent biasing the speed

/ acceleration profiles, these situations were handled by changing the vehicle speed from 0 to 1 km/hr. This replacement also helped to compensate for the inability of the system to accurately measure vehicle speeds below 2 km/hr.

Another data adjustment was to synchronize the timing of the exhaust gas composition measurements with other measurements due to the transport delay from the tail pipe to the five gas analyzer. Experimental tests where conducted to measure the response time for a step change in gas concentration. The analysis of the time shift constants is presented in Appendix A. The combined system transport and first-order time constant for the NDIR measurements of CO, CO_2 and HC was 8 seconds and that for chemical cell measurements of O_2 and NO_x was 10 seconds. The first order time constants for the NDIR measurements were found to be approximately 1 second. However, the time constants for the chemical cells were 4 and 7 seconds for the measurements of O_2 and NO_x respectively. This leads to some uncertainty which is difficult to quantify as explained in Appendix A. Since sampling frequency varied, a linear interpolation algorithm was developed to shift the emissions data by the experimentally determined time delay while also accounting for the non-uniform sample timing.

A dynamic vehicle model was incorporated in the analyzing program to calculate the vehicle tractive power(31-33) at each time step. Tractive power is a measure of actual power transmitted to the road by the test vehicle based on the aerodynamic drag, rolling and inertial resistance of the vehicle. The complete set of calculations is illustrated in Appendix B. With second-by-second values of fuel consumption rate, emissions rates and tractive power, the fuel consumption and emissions values could be calculated in various format such as g/s, g/kWhr and g/kg$_{fuel}$. Calculation of parameters such as Air to Fuel ratio, Hydrogen to Carbon ratio (H/C) and molecular weight of the exhaust were performed to check data integrity and monitor for unusual conditions. These equations are illustrated in Appendix C.

With vehicle performance, consumption and emissions measured on a second-by-second basis, many integrations could be computed to measure values over a distance, time or trip. Trapezoidal integration functions were used to integrate:

1. Vehicle speed to give total distance traveled
2. Fuel flow rate to give total fuel consumed
3. Air flow rate to give total air consumed
4. Pollutant emission rates to give total mass of pollutants emitted
5. Positive tractive power to give total drive-train energy output.

A complete error analysis of all the measured and calculated variables is presented in Appendix D. This analysis has shown that the expected error in the calculated emission factors is approximately 12% over the 17.4 km commute.

3.4 RESULTS

This section displays analysis of a set of three tests to illustrate the capabilities and repeatability of the in-use measurement system. These tests were repeats of a 17.4 km morning commute along the same route from suburban St. Albert to the University of Alberta in Edmonton, Canada. These tests were chosen for similar ambient weather conditions and similar driving patterns so as to compare the ability of the measurement system to measure driving patterns and emission characteristics. Test times and details are provided in Table 3-2.

TABLE 3-2 BASIC DETAILS OF THE THREE COMMUTER TRIPS

Trip #	Date (2001)	Start Time	Ambient Conditions	
		hh:mm	°C	kPa
1	Sep 27	07:30	10.5	93.3
2	Oct 3	07:30	3.9	94.6
3	Oct 4	07:25	2.7	95.3

3.4.1 DRIVING BEHAVIOR

Figures 3-3, 3-4 and 3-5 illustrate the similarity of the vehicle speed traces for the three morning commutes. Each trip includes three main segments:

I. A cold start followed by about 500 seconds of un-congested driving on suburban roads with sustained speeds around 70 km/hr.
II. A congested period, (about 500 to 1700 sec), of stop-and-go city driving with speed seldom exceeding 50 km/hr.
III. A free-flowing period near the end of the trip with top speeds around 70 km/hr.

Table 3-3 provides details for each segment of the three commuter trips. Vehicle fuel consumption and emissions can be considered for the overall trip or performance in the shorter segments can also be examined to illustrate the effects of driving and traffic conditions.

TABLE 3-3 DISTANCES AND TIMES FOR THE THREE COMMUTER TRIPS

Trip #	Segment I		Segment II		Segment III		Total Trip	
	dist (m)	time (s)	dist (m)	time (s)	dist (m)	time (s)	dist (m)	time (s)
1	6143	515	6650	1175	4578	424	17370	2115
2	6149	505	6187	1150	5042	447	17380	2102
3	6210	580	6134	1606	5022	410	17370	2596
Average	6167	533	6323	1310	4880	427	17370	2271
Average Speed	41.8 km/hr		17.8 km/hr		41.2 km/hr		27.8 km/hr	
Std. Deviation	2.8 km/hr		3.6 km/hr		2.7 km/hr		3.23 km/hr	

The first and third segments were similar in terms of free-flowing traffic conditions and similar average speed. However, the first segment was a "cold-start and warm-up" region, with the engine consistently reaching operating temperature near the end of the first segment. The second segment was through a series of traffic lights on a major arterial road. Frequent stops and traffic congestion kept the speeds and acceleration rates low. Varying amounts of congestion could significantly change the travel time through this segment and it will be shown later that this had a notable effect on emissions. (For example, due to the low speed and tractive power requirements during Segment II on Trip 3, the catalytic converter dropped below the light-off temperature leading to an increase in all of the measured emissions).

Vehicle acceleration / speed envelope diagrams are a visualization of the driving pattern that allows rapid comparison of the vehicle demands due to differing traffic conditions and driver behavior.[4,34]

Each vehicle movement generally draws a clockwise loop on the acceleration / speed diagram as the vehicle starts from rest with positive acceleration as it increases speed, then drops to zero acceleration at cruise speed, and eventually moves to negative acceleration as the speed drops back toward zero. The acceleration / speed envelope is generally arrow head-shaped, with higher accelerations at low speeds and near-zero accelerations at the highest speeds. Aggressive driving with high power demands produces a wider acceleration/speed envelope while economy-oriented driving gives a narrower envelope. Figures 3-6 through 3-8 show the acceleration / speed envelopes for each of the three trips and three trip segments. On each trip, the differing nature of Segments I, II and III are easily seen. Segment I consists of a series of acceleration / deceleration loops with fairly consistent top speed, Segment II has many small acceleration / deceleration loops with generally lower peak speed, and Segment III generally shows a single clockwise loop with low accelerations but most of the time spent at cruise speed.

Comparing the same trip segment for different trips, Trips 1 and 2 had very similar acceleration / speed envelopes implying very similar driving conditions. Trip 3 generally showed lower acceleration values and lower speeds in all segments implying more traffic congestion. This was particularly confirmed in the stop-and-go urban region, Segment II, where the 'arrow head' shape was generally shorter and thinner.

While the acceleration / speed envelope provides a visual indication of driving patterns, more quantitative values are obtained from vehicle tractive energy modeling which provides second-by-second tractive power levels. For example, Figure 3-9 shows the fraction of test time that the vehicle spent in each of eight (non-uniformly distributed) power bands on the three trips being analyzed. The similarities between Trips 1 and 2 are clear since the tractive power duty cycles for the two trips overlap almost perfectly. In contrast, Trip 3 spent a much higher fraction of time at idle; (49% of the time in Trip 3 was spent at 0>1 kW compared with 34% of the time for Trips 1 and 2). Clearly, ensuring low idle emission rates would become more critical for overall emission levels in the traffic conditions representative of Trip 3. While idle occupied the greatest fraction of time on all three commutes, the low speed cruise power band at 10>20 kW occupied the second greatest fraction of time; (24% for Trips 1 and 2 and 17% for Trip 3). High power levels (over 50 kW) were virtually never required for this lightly loaded vehicle running in commuter traffic.

While the distribution of time spent in each tractive power band can be informative, the distribution of tractive energy is also important since energy correlates well with total fuel consumption and exhaust mass production. Tractive energy, (power * time = energy), is illustrated in Figure 3-10 for the same 3 commuter trips. This diagram illustrates similar overall profiles with 40 to 50% of the vehicle's tractive energy output produced in the 10>20 kW band for these trips. However, there were some differences. The more congested trip produced less tractive energy in the 10>20 kW band, (43% vs 48% average for Trips 1 and 2), and more in the 30>50 kW band, (11% vs 5.5% average for Trips 1 and 2).

3.4.2 EMISSION CHARACTERISTICS

To illustrate the second-by-second capabilities of the emission measurement system to trace the time pollutants, Figures 3-3 through 3-5 show the NO_x emission rate in grams per second. (Similar traces exist for CO, CO_2, HC and O_2 but the NO_x emission rate was used for illustration since it was highly correlated with vehicle speed and the emission rate dropped but remained significant even after the catalyst exceeded light-off temperature). Each of these curves shows two distinctive operating periods: cold start to catalyst light-off and post-light-off operation. In the first period, (about 500 seconds at these ambient temperatures), emission rates of CO, HC and NO_x are all significant and strongly affected by vehicle tractive power levels. In the post-light-off period, the combination of fuel system control and 3-way catalyst operation normally reduces emission rates to a small fraction of their pre-light-off level. In Figures like 3-3 through 3-5, this reduction is best illustrated by the lack of emission rate 'spikes' for accelerations after the first 400 seconds. However, various anomalies in emission control system performance can appear in these emission rate traces. For example, during Trip 1 significant NO_x emission spikes continued after the catalyst should have reached light-off temperature. This, combined with low CO and HC emission rates plus high O_2 emission rates implied that the vehicle was temporarily operating with a lean mixture. Whatever situation caused that problem was eventually corrected by the engine control system, eliminating the emission spikes after about 750 seconds of operation. During Trip 3, the combination of low driving speeds and prolonged idle apparently allowed the catalytic converter to drop back below light-off temperature. This was illustrated by the reappearance of simultaneous spikes of NO_x, CO and HC near the end of the congested driving period, (Segment II).

'Spikes' in the second-by-second emission rates are a good visual indication of emission problems but are difficult to quantify. Figures 3-11 through 3-13 show the integrated result of these emission rates, cumulative trip emissions, plotted against cumulative trip fuel use. This graphical format clearly illustrates differences between emission performance of the test vehicle in these relatively similar commuter trips. For example, the NO_x traces in Figure 3-11 clearly show identical trends of high initial NO_x/(fuel consumption) ratio during the cold start / pre-light-off period of driving. After about 400 grams of fuel were consumed, the catalyst started to work and cumulative NO_x emission flattened out dramatically (for Trips 2 and 3). During Trip 1, the high NO_x production rate continued until about 1100 grams of fuel were used before flattening out. Figures 3-12 and 3-13 show related trends in the CO and HC emission rates for the same 3 trips. Trip 1 had lower CO emissions right from the cold start, implying a leaner mixture. The catalyst appeared to reach catalyst light-off for CO and HC emissions at a similar time as Trips 2 and 3, corresponding to 400 grams of fuel consumed. However, lower CO and HC emission rates over the period until 1000 grams of fuel were consumed resulted in significantly lower cumulative emissions for Trip 1. After 1000 grams of fuel consumed, the vehicle control system had rectified the lean situation, resulting in a similar rate of emissions accumulation for Trip 1.

Another type of emissions control anomaly is illustrated in the Trip 3 cumulative emission traces. In this low-power congested driving case, it appears that catalytic converter effectiveness dropped during the prolonged idle periods. The HC emission rate began to increase after 1500 grams of fuel consumed and the CO emission rate after 2000 grams of fuel consumed. The ratios of CO and HC emissions to fuel consumption were similar to those with a cold catalyst, providing further evidence of the cause. Once the vehicle reached Segment III of the trip where it ran continuously at a significant power level, the CO and HC emission rates dropped back to normal, implying that the catalyst had warmed up again. The net result of this cooling off during a period of congested operation was a significant increase in cumulative CO and HC emissions for Trip 3 compared with Trips 1 and 2.

Table 3-4 displays cumulative emissions and fuel consumption measured for the 3 full trips as well as the values measured in each trip segment. These numbers are given in the form of g/km and could also be easily expressed as g/kg_{fuel} since those are two forms commonly used as input for the calculation of emissions inventories.

TABLE 3-4 SUMMARY OF EMISSIONS AND CONSUMPTION BY TRIP AND SEGMENT

Trip	Segment	CO		CO_2		NO_x		HC		FUEL	
		g	g/km	g	g/km	g	g/km	g	g/km	g	g/km
# 1 27 - Sept	Full Trip	221	12.7	7150	411	10.6	0.610	9.63	0.55	2534	146
	I	139	22.6	2230	363	6.95	1.13	4.80	0.78	828	135
	II	60.6	9.11	3440	518	3.02	0.45	3.52	0.53	1193	179
	III	21.7	4.73	1470	322	0.633	0.14	1.30	0.29	514	112
# 2 3-Oct	Full Trip	264	15.2	7020	404	7.44	0.43	11.1	0.64	2562	147
	I	194	31.6	2290	373	4.95	0.81	5.64	0.92	906	147
	II	43.7	7.07	3150	509	1.39	0.23	3.99	0.65	1099	178
	III	26.4	5.24	1580	313	1.10	0.22	1.45	0.29	557	110
# 3 4-Oct	Full Trip	320	18.4	7900	455	7.87	0.45	15.4	0.89	2900	167
	I	200	32.2	2380	384	4.65	0.75	5.83	0.94	939	151
	II	87.0	14.2	3960	646	2.20	0.36	8.56	1.40	1407	229
	III	32.9	6.55	1560	310	1.02	0.20	1.10	0.21	554	110

As expected, the cold-start segments of each trip show substantially higher CO, HC and NO_x

emission rates on a g/km basis. The second and third segments generally illustrate the progressively reduced emission rates expected for warmed up operation (II better than I) and for steady cruising (III better than II). However, the emission rate anomalies mentioned above are visible in the emission rate statistics drawn from these trips. For example, Trip 1 had a substantially higher NO_x emission rate due to leaner operation in Segments I and II. Trip 3 produced a substantially higher HC emission rate due to the catalyst cool-down which made its HC emissions higher in the mid-trip (Segment II) than the cold-start (Segment I).

The emphasis in this paper has primarily been on detecting and diagnosing differences in driving patterns and vehicle emission/consumption performance based on in-use emission monitoring. While this is illustrative of the capabilities of a second-by-second vehicle monitoring system, use of such a system for those purposes is not really justified. One of the ultimate purposes of the data being collected is to contribute better input values for vehicle emission models used in urban air quality simulations. The simplest vehicle emission models used in those simulations use vehicle emission rates in terms of g/km or g/kg_{fuel}. Table 3-5 presents the averages and standard deviations of such emission/consumption rate values, (in g/km), for this vehicle based on the full and segmented data files.

TABLE 3-5 TRIP EMISSION AND CONSUMPTION STATISTICS (AVERAGE OF THREE TRIPS)

	Statistics							
	Average				Standard Deviation			
	Full Trip	Segment			Full Trip	Segment		
		I	II	III		I	II	III
CO (g)	268	178	63.8	27.0	49.5	33.6	21.8	5.65
(g/km)	15.5	28.8	10.1	5.51	2.85	5.35	3.66	0.94
CO_2 (g)	7360	2300	3520	1540	479	76.6	412	55.3
(g/km)	423	373	557	315	27.7	10.3	76.7	6.02
NO_x (g)	8.64	5.52	2.20	0.92	1.71	1.25	0.82	0.25
(g/km)	0.50	0.90	0.35	0.19	0.10	0.21	0.12	0.04
THC (g)	12.1	5.43	5.36	1.27	3.02	0.55	2.78	0.21
(g/km)	0.69	0.88	0.86	0.26	0.17	0.09	0.47	0.05
FUEL (g)	2666	891	1233	542	204	57.3	158	24.2
(g/km)	153	144	195	111	11.8	8.64	29.3	1.05

As shown in this table, despite the small sample size and various emission system anomalies, the standard deviations are modest relative to the computed average values. This implies that the measurement system is able to adequately quantify vehicle emission/consumption performance. However, the variability between trip segments points out the weakness of any emission inventories based on a single emission constant for each pollutant. Much greater variability can be expected as a wider range of vehicles, weather conditions, road conditions and drivers are covered.

3.5 CONCLUSIONS

This paper has described the development and application of a real-time, on-road measurement system for driving behavior, engine parameters and exhaust emissions. The measurement system was based on a portable computer monitoring on-board sensors which included a speed sensor, temperature sensors, a mass air flow sensor, wide-range lambda sensor and a portable five-gas analyzer. The package was designed for installation on any vehicle with minimal installation effort and no permanent vehicle modifications.

Use and capability of the measurement system was demonstrated by analyzing a series of repeated commuter trips along one route. The measured vehicle performance and emission / consumption traces clearly showed how the vehicle was being operated and how the operating mode affected vehicle pollutant emission and fuel consumption rates. Varying emissions system anomalies were detected in virtually identical trips and were shown to have a significant effect on the overall emission rates from the vehicle.

3.6 FUTURE WORK

This system is being used to measure the impact of varying weather and traffic conditions on the driver behavior and emissions rates for a range of vehicles, including those fueled with alternative fuels. Future results will provide both single-value emission rate models (i.e. g/kg_{fuel} and g/km) and more detailed functional models.

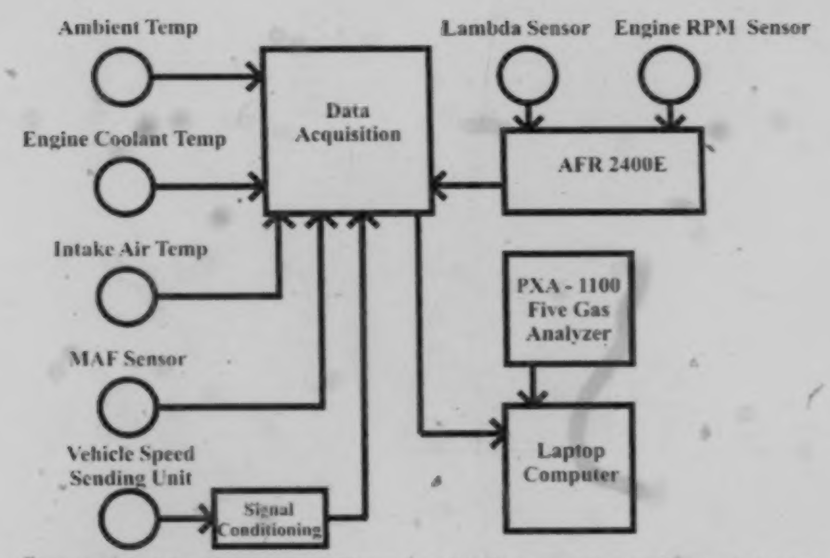

FIGURE 3-1 SCHEMATIC OF TEST SET-UP ILLUSTRATING SENSORS AND EQUIPMENT

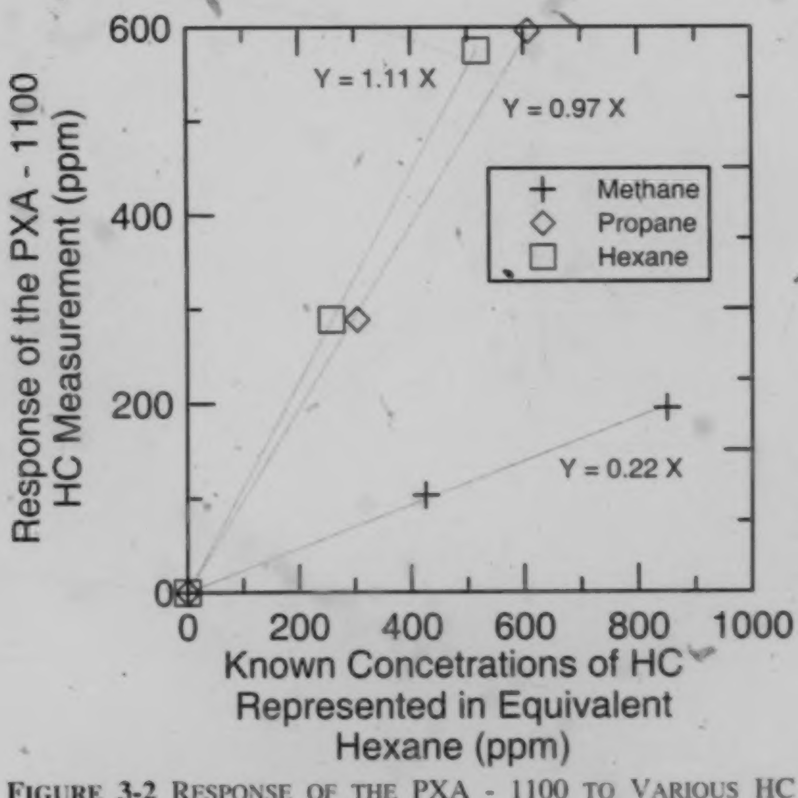

FIGURE 3-2 RESPONSE OF THE PXA - 1100 TO VARIOUS HC COMPOUNDS REPRESENTED IN EQUIVALENT HEXANE

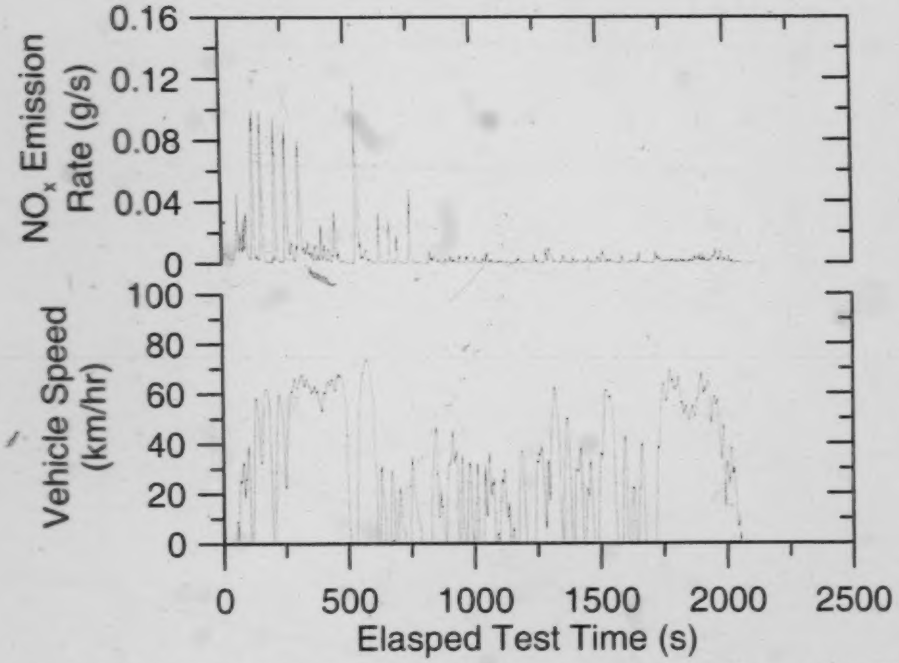

FIGURE 3-3 VEHICLE SPEED AND NO$_x$ EMISSION RATES FOR TRIP 1 (SEPT 27)

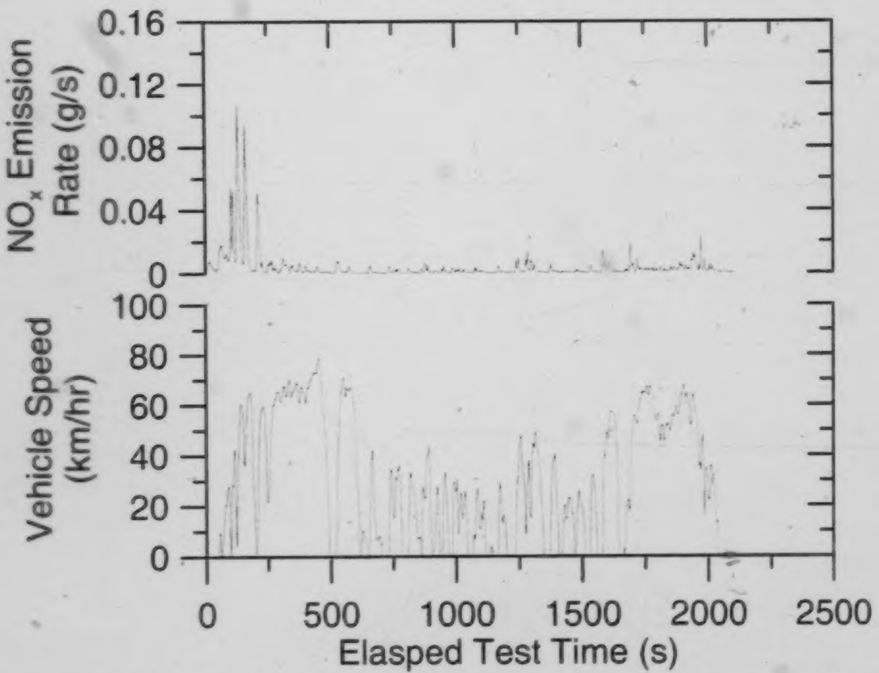

FIGURE 3-4 VEHICLE SPEED AND NO$_x$ EMISSION RATES FOR TRIP 2 (OCT 3)

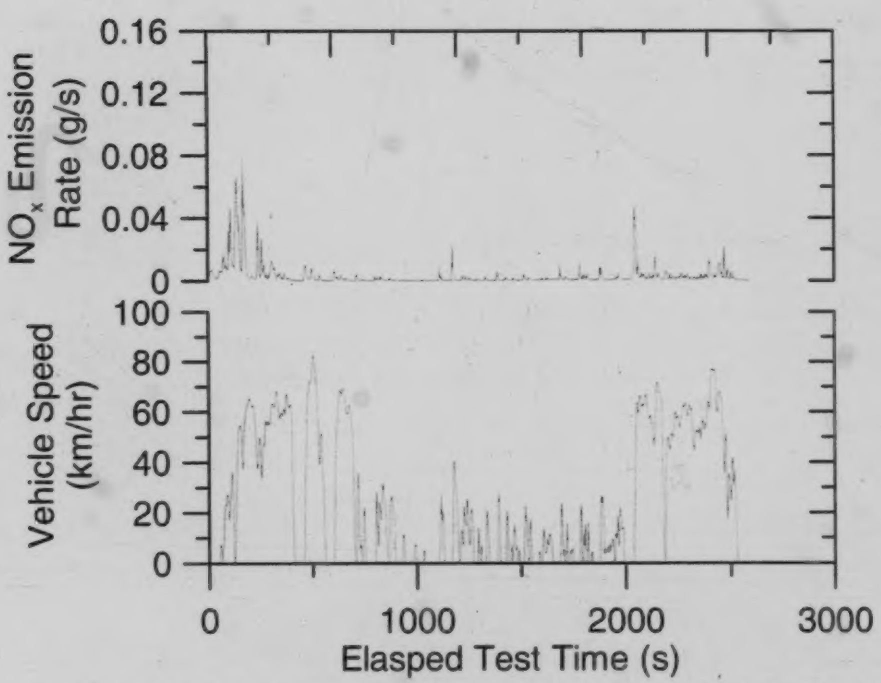

FIGURE 3-5 VEHICLE SPEED AND NO_x EMISSION RATES FOR TRIP 3 (OCT 4)

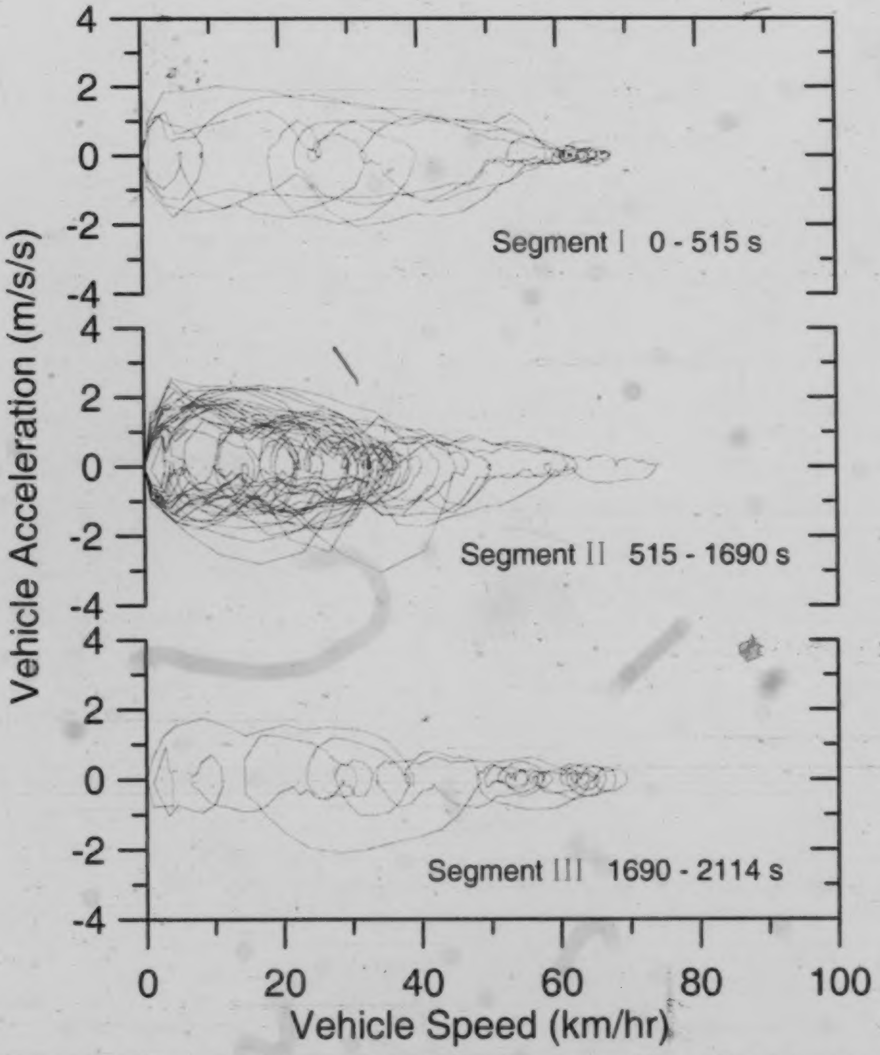

FIGURE 3-6 VELOCITY / ACCELERATION ENVELOPES FOR THREE SEGMENTS OF TRIP 1

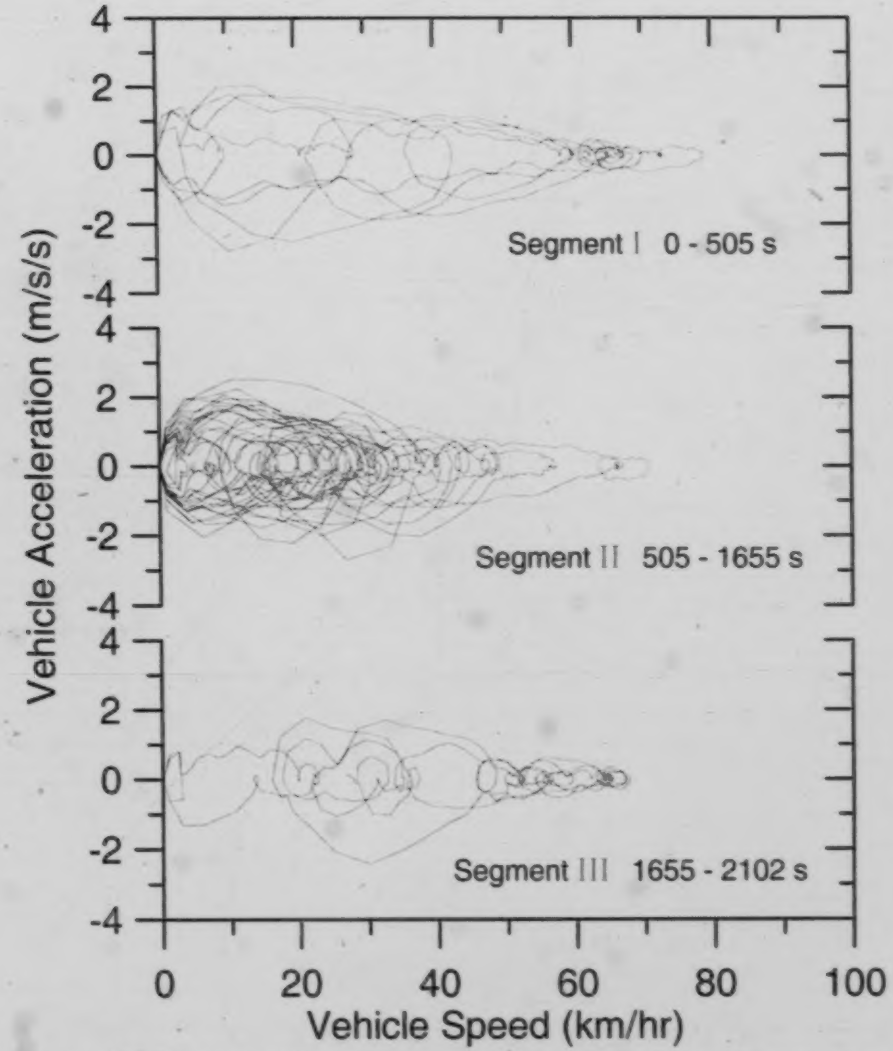

FIGURE 3-7 VELOCITY / ACCELERATION ENVELOPES FOR THREE SEGMENTS OF TRIP 2

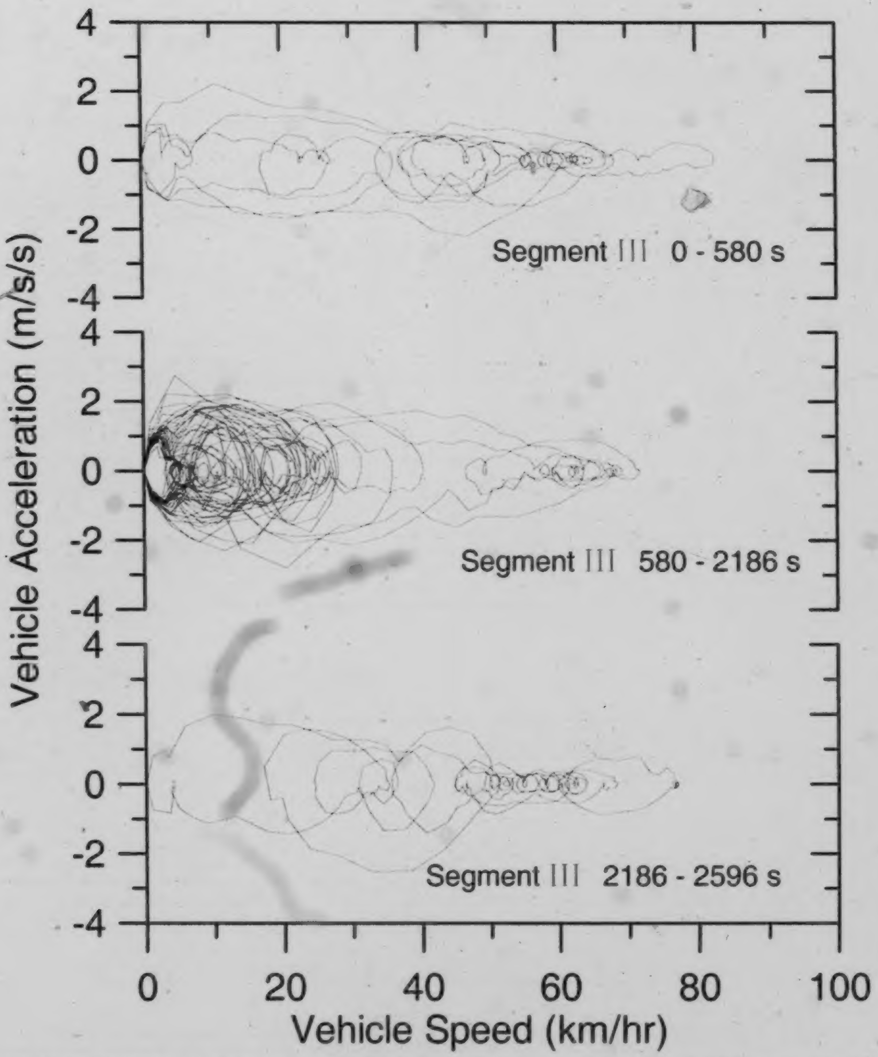

FIGURE 3-8 VELOCITY / ACCELERATION ENVELOPES FOR THREE SEGMENTS OF TRIP 3

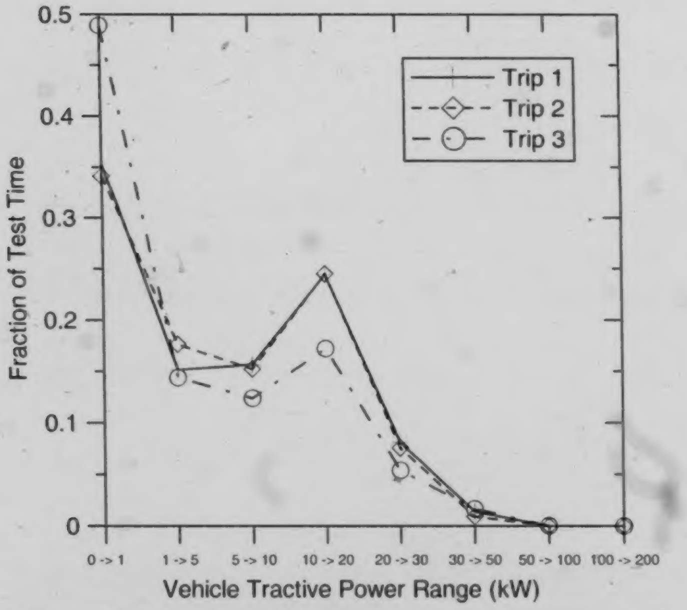

FIGURE 3-9 RELATIVE TIME DISTRIBUTION OF POSITIVE POWER LEVELS (3 ENTIRE TRIPS)

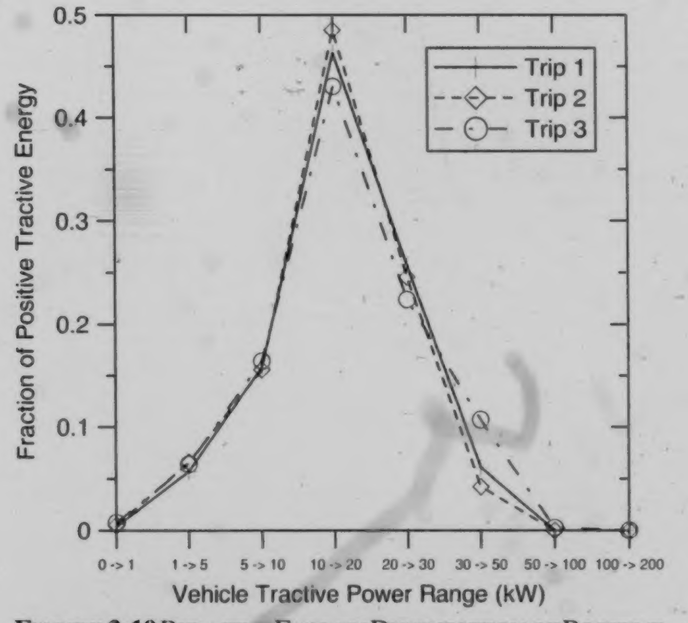

FIGURE 3-10 RELATIVE ENERGY DISTRIBUTION OF POSITIVE POWER LEVELS (3 ENTIRE TRIPS)

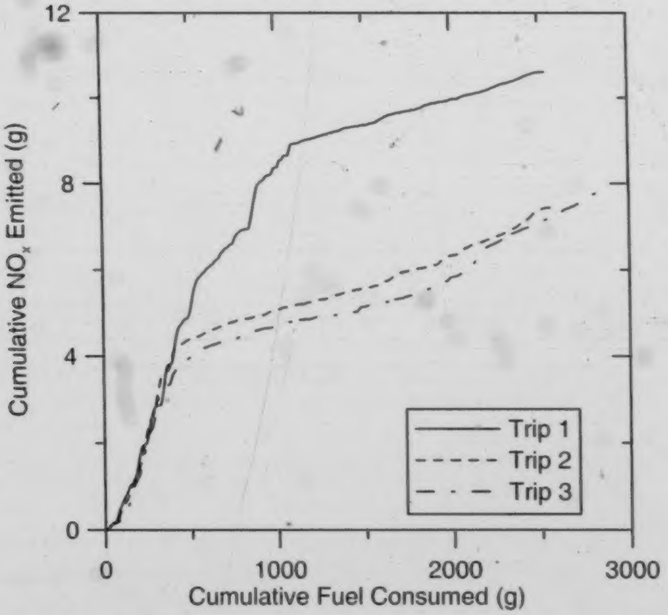

FIGURE 3-11 TRENDS OF NO$_X$ PRODUCED WITH FUEL CONSUMED

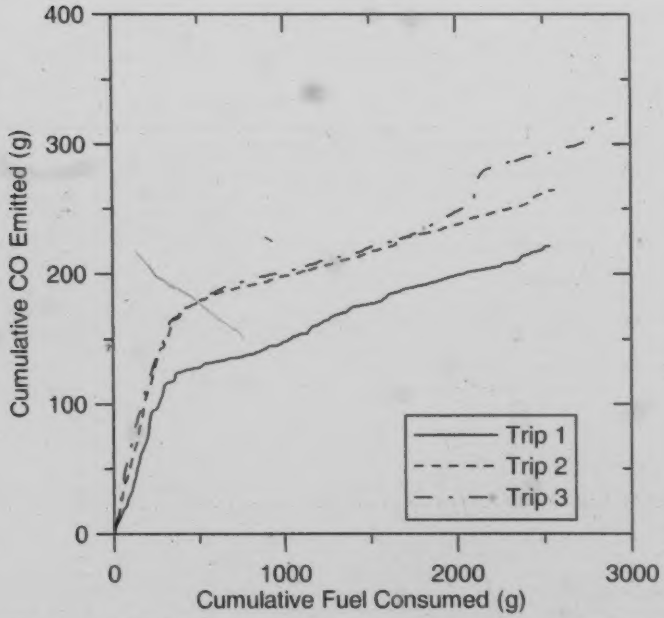

FIGURE 3-12 TRENDS OF CO PRODUCED WITH FUEL CONSUMED

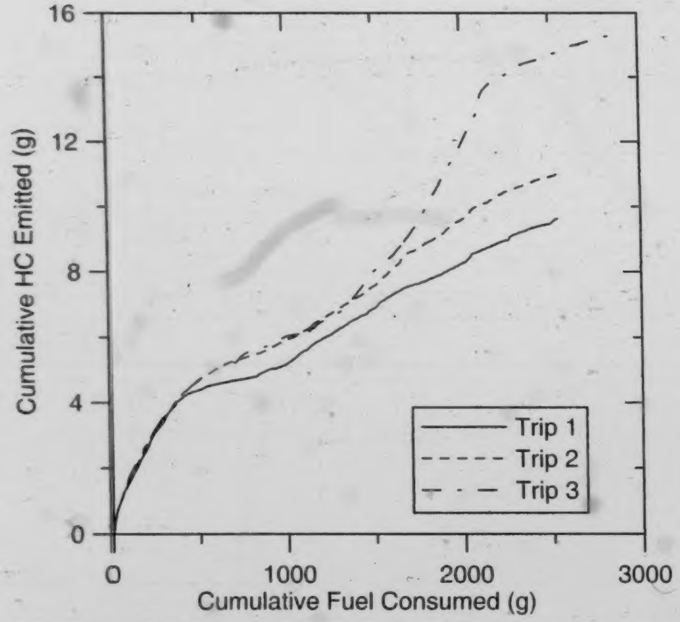

FIGURE 3-13 TRENDS OF HC PRODUCED WITH FUEL CONSUMED

REFERENCES

1. Kruse R.E., Huls T., "Development of the Federal Urban Driving Schedule," SAE Technical Paper 730553, Society of Automotive Engineers, 1973.

2. St. Denis M.J., Winer A.M., "Prediction of On-Road Emissions and Comparison of Modelled On-Road Emissions to Federal Test Procedures Emissions," Environmental Science and Engineering Program. Environmental Health Sciences Department. School of Public Health. University of California, Los Angles. (310) 825 - 3161.

3. Goodwin R., Ross M.H., "Off-Cycle Exhaust Emissions from Modern Passenger Cars with Properly-Functioning Emission Controls," SAE Technical Paper 960064, Society of Automotive Engineers, 1996.

4. Watson H.C., Milkins E.E., Preston M.O., Chittleborough C., Beardsley P.A., "In-Use Vehicle Survey of Fuel Consumption and Emissions on Dynamometer and Road," SAE Technical Paper 850524, Society of Automotive Engineers, 1985

5. St. Denis M.J., Cicero-Fernandez P., Winer A.M., Butler J.W., Jension G., "Effects of In-Use Driving Conditions and Vehicle/Engine Operating Parameters on "Off-Cycle" Events: Comparison with Federal Test Procedure Conditions," Journal of Air and Waste Management Technical Paper, Vol 44, Pages 31-38, January, 1994.

6. Enns P., German J., Markey J., "EPA's Survey of In-Use Driving Patterns: Implications for Mobile Source Emission Inventories," USEPA Technical Report, 1993.

7. Laurikko J., Erlandsson L., Arbrahamsson R., "Exhaust in Cold Ambient Conditions: Considerations for a European Test Procedure," SAE Technical Paper 95923, Society of Automotive Engineers, 1995.

8. Laurikko J., Aakko P., "The Effect of Ambient Temperature on the Emissions of Some Nitrogen Compounds: A Comparative Study on Low-, Medium- and High Mileage Three-Way Catalyst Vehicles," SAE Technical Paper 950933, Society of Automotive Engineers, 1995.

9. Eccleston B.H., Hurn R.W, "Ambient Temperature and Trip Length – Influence on Automotive Fuel Economy and Emissions," SAE Technical Paper 780613, Society of Automotive Engineers, 1978.

10. Taylor G.W.R., Stewart S., "Cold Start Impact on Vehicle Energy Use," SAE Technical Paper 2001-01-0221, Society of Automotive Engineers, 2001.

11. Gurney M.D., Allsup J.R., "Predictability of Emissions from In-Use Vehicles at Low-Ambient Temperature and Alternate Driving Cycle Based on Standard Tests," SAE Technical Paper 890625, Society of Automotive Engineers, 1989 .

12. Larson R.E., "Vehicles Emission Characteristics Under Cold Ambient Conditions," SAE Technical Paper 890021, Society of Automotive Engineers, 1989.

13. Polak J.C., "Cold Ambient Temperature Effects on Emissions from Light-Duty Motor Vehicles," SAE Technical Paper 741051, Society of Automotive Engineers, 1974.

14. Ginberg L., Morgan L., "Effect of Temperature on Exhaust Emissions," SAE Technical Paper 740527, Society of Automotive Engineers, 1974.

15. Laurikko J., Nylund N. "Regulated and Unregulated Emissions from Catalyst Vehicles at Low Ambient Temperatures," SAE Technical Paper 930946, Society of Automotive Engineers, 1993.

16. Laurikko J., Nylund N.O., Sipila K., "Automotive Exhaust Emissions at Low Ambient Temperature," Valtion teknillinen tutkimuskeskus, Tutkimuksia Statens tekniska forskingscentral, Forskingsrapporter Technical Research Center of Finland, Research Reports, 1987.

17. Braddock J.N., "Impact of Low Ambient Temperature on 3-Way Catalyst Car Emissions," SAE Technical Paper 810280, Society of Automotive Engineers, 1981.

18. Stephens R.D., Giles M.T., Groblicki P.J., Gorse R.A., McAlinden K.J., Hoffman D.B., James R., Smith S., "Real World Emissions Variability as Measured by Remote Sensors," SAE Technical Paper 940582, Society of Automotive Engineers, 1994.

19. Staab J., Schurmann D., "Measurement of Automobile Exhaust Emissions under Realistic Road Conditions," SAE Technical Paper 871986, Society of Automotive Engineers, 1987.

20. Unal A., Dalton R., Frey H.C., Rouphail N.M., "Simultaneous Measurement of On-Road Vehicle Emissions and Traffic Flow Using Remote Sensing and an Area-Wide Detector," Paper # 99-712, 1999.

21. Stephens R.D., "Remote Sensing Data and a Potential Model of Vehicle Exhaust Emissions," Journal of Air & Waste Management, Vol 44, pp 1284-1292, 1994.

22. Frey H.C., Rouphail N., Unal A., Colyar J., "Emissions and Traffic Control: An Empirical Approach," Presented at CRC On-Road Vehicle Emissions Workshop, March 2000, San Diego, CA.

23. Rouphail N.M., Frey H.C., Colyar J.D., Unal A., "Vehicle Emissions and Traffic Measures: Exploratory Analysis of Field Observations at Signalized Arterials," Presented at the 80th Annual Meeting of the Transportation Research Board, Jan 7-11 2001, Washington D.C.

24. Frey H.C., Rouphail N.M., Unal A., Colyar J.D., "Measurement of On-Road Tailpipe CO, NO, and Hydrocarbon Emissions Using a Portable Instrument," Presented at the Annual Meeting of the Air and Waste Management Association, June 24-28, 2001. Orlando Florida.

25. Vojtisek-Lom M., Cobb T., "Vehicle mass emissions measurements using a portable 5-gas exhaust analyzer and engine computer data," Presented at at: Emission Inventory: Planning for the Future, Research Triangle Park, NC, October 29, 1997.

26. Vojtisek-Lom M., Cobb T., "Measurement, variance and reduction of real-world emissions of 20 dedicated CNG vans," Presented at: Air & Waste Management Association's 91st Annual Meeting & Exhibition, June 14-18, 1998, San Diego, California.

27. Guenther P.L., Stedman D.H., Lesko J.M., "Prediction of IM240 Mass Emissions Using Portable Exhaust Analyzers," Journal of Air & Waste Management, Vol 46, pp 343-348, 1996.

28. Salt W., Checkel M.D., "A Fully Functional Natural Gas Pickup Truck - The University of Alberta 1993 NGV Challenge," Department of Energy, Austin, 1993.

29. Guenther P.L., Stedman D.H., Lesko J.M., "Prediction of IM240 Mass Emissions Using Portable Exhaust Analyzers," Journal of Air & Waste Management, Vol 46, pp 343-348, 1996.

30. Kelly N.A., Groblicki P.J., "Real-World Emissions from a Modern Production Vehicle Driven in Los Angeles," Journal of Air & Waste Management, Vol 43, pp1351-1357, 1993.

31. Checkel M.D., Brownlee A., Doblanko L., "Pollution Inventories using Second-by-Second Vehicle Modeling and Traffic Planning Models," Combustion and Global Climate Change, Combustion Canada 99, Natural Resources Canada, 11 pages, 1999.

32. Yung V., Checkel M.D., "Energy Use and Emissions Effects of Operating a Hybrid Electric Vehicle," Presented at The Combustion Institute, Canadian Section. May 25-28, 1997.

33. Checkel M.D., "Emission Functions for Motor Vehicle Emission Audits Based on Traffic Modeling," Presented at CI/CS Spring Technical Meeting, Waterloo, May 27-29, 1996.

34. Milkins, E., Watson H., "Comparison of Urban Driving Patterns," SAE Technical Paper

830939, Society of Automotive Engineers, 1983.

CHAPTER 4

QUANTIFYING VEHICLE EMISSION FACTORS FOR VARIOUS AMBIENT AND INITIAL ENGINE CONDITIONS USING AN ON-ROAD, REAL-TIME EMISSIONS SYSTEM

Chapter 3 described the development of the measurement system and processing algorithms. This system was used to study a typical commuter style of driving patterns for the region of Edmonton, Alberta, Canada. Chapter 4 extends this study to include cold-start applications and resulting emissions over a wide range of ambient conditions. Also, included are a small set of warm-start experiments. This chapter further develops the processing algorithms to calculate both a two and three emission factor model as functions of ambient / initial engine temperatures.

Chapter 4 is a paper which was accepted for publication to the Society of Automotive Engineers for the 2003 World Congress held in Detroit, Michigan and is presented here in a lengthened version. Because this chapter is based on a stand-alone paper, there is some repetition. Specifically, this chapter includes a summary the work presented in Chapter 3 and presents similar arguments and justifications for the development of an in-use and real-time measurement system.

ABSTRACT

This paper examines vehicle emission behavior and the effects of ambient temperature, initial engine temperature and occasional emission system failures on vehicle emission factors. Vehicle operating parameters, fuel consumption and emissions were measured on-road using a portable system. Although this system was designed for ease of use with a range of vehicles, drivers and driving situations, the data reported come from repeated trips over a 17.4 km urban / suburban commute with a particular vehicle that could meet Tier 1 standards at normal conditions. As such, the resulting emission models do not represent the current on-road fleet. Instead, they show the importance of ambient temperature, initial engine temperature and emission system glitches in determining emissions. This leads to an appreciation of the value of on-road testing.

A series of trips, (with an ambient temperature range of -25 to +20°C), were analyzed to develop emission factor models with one, two or three emission factors. The results emphasize the inadequacy of using a single emission factor (based on the total mass of emissions and distance traveled) to describe the pollution characteristics of vehicles operating in a range of trip lengths and ambient / initial engine conditions. A two-emission-factor model provides adequate sensitivity to cold start conditions while a three-emission-factor model is generally not required. Ambient temperatures below the standard test conditions were shown to produce dramatically higher emission rates. Lastly, many temporary failures or "glitches" in emission control were noted and the frequency and magnitude of those failures are reported.

4.0 INTRODUCTION

Automotive tailpipe emissions are known be a major source of urban pollution, contributing significantly to urban air quality problems.(1) Emission inventories are used to estimate and predict the amount of pollution that automobiles release into the atmosphere. Inventories are generally based on a simple equation multiplying the number of current on-road vehicles, the number of vehicle miles traveled and sets of emission factors. The number of active on-road vehicles can be estimated from vehicle registries and the number of vehicle miles traveled can be further estimated with traffic models. The emission factors used in the equation however, are known with less certainty, leading to some questionable emission inventory estimates. Currently, emission factors are determined from chassis dynamometer experiments and sometimes include information from remote sensing studies. Engine and chassis dynamometer experiments offer an excellent controlled, repeatable and comparable experiment however, concerns have been raised with the representative nature of the emission factors determined with this procedure. Actual vehicle operation in any urban area encompasses a wider range of ambient conditions and driving profiles.(2-6) Vehicle operating parameters and emission behavior can be measured on-road using a portable system to record vehicle operating parameters, fuel consumption and emissions.(2) This paper examines the influence of ambient and initial engine conditions on vehicle emission factors.

Both ambient conditions and vehicle driving profiles can have a dramatic effect on vehicle emissions and there is some difficulty in capturing these effects accurately using dynamometer testing based on standard test procedures. For example, varying ambient temperature conditions are known to influence vehicular exhaust emissions.(7-17) The effect of ambient temperature on exhaust emissions has been studied in laboratory environments(7-17) using specialized facilities (i.e. environmental chambers large and powerful enough to accommodate vehicles). These difficulties limit the number and variety of tests with varying ambient conditions but the results have shown the importance. For example, research has shown that emissions at ambient conditions of -20°C can increase by 650% for HC, 800% for CO and 10% for NO_x emissions when compared to standard certification values (i.e. at +25°C).(15) To account for this trend of sharply higher emissions at nonstandard ambient temperatures, colder "cold-start" tests at -7°C (20°F) were added to some certification requirements. However, much of the current fleet preceded these standards and there is still uncertainty over how vehicles which comply truly behave at colder or hotter starting conditions. Hence, despite improved certification procedures there are concerns about how well the on-road emission behavior of the current fleet is represented in current emission inventories.

Driving behavior is also known to have a large effect on vehicular emissions.(18,19) The majority of the testing for current emission factor's is based on a single driving sequence which happens to be the same cycle used for vehicle tuning and certification testing, (i.e. FTP-75). This test cycle was originally derived from an on-street speed-time trace,(20,21) (measured in 1973 Los Angeles traffic and edited to limit the peak accelerations to values that any vehicle could attain). However, given increases in traffic congestion and varying vehicle capability, there is some doubt about how representative this cycle is for current driving patterns. Also, given the highly tuned nature of current engine controllers, it is questionable how well emission factors measured on the precisely controlled FTP-75 dynamometer cycle represent emission performance with slightly different operating parameters on the road. It is important to consider that all dynamometer studies are only simulations of on-road driving behavior and resulting tailpipe emissions.

Remote sensing studies improve the real-life behavior of emission measurements by covering a broad spectrum of in-use vehicles, (sampling hundreds or thousands of vehicles per day).(22-25) However, they only give indications of instantaneous emissions at a specific location, generally without measuring any vehicle operating parameters and of course, giving no indication of vehicle emissions under different operating conditions.

Research of the sort presented here improves the real-life nature of the measured exhaust emissions and resulting emission factors by using an on-road emission measurement system in a variety of ambient conditions.(2) The focus of this paper is to examine the effect of ambient conditions on emission factors measured on a repeated 17.4 km commute using a constant driver / vehicle configuration with a vehicle capable of meeting Tier 1 emission standards. Over a full year of operation, ambient conditions ranging from -25 to +20°C were experienced. In addition, a set of temperature correction factors relating the vehicle emission factors to ambient temperature was constructed. These correction factors allow the user to adjust emission factors for any ambient temperature. (This analysis is expanded in a Chapter 5, which uses a multi-variable approach to calculate the emission factors).

Also, presented in this paper will be a small set of experiments conducted at -20°C to investigate the influence of warm re-start behavior on emission factors under cold conditions. Finally, several minor emission control failures were observed and these are analyzed to indicate the frequency and magnitude of emission effects due to the failures.

4.1 EXPERIMENTAL SET-UP / CONFIGURATION

The arrangement of sensors and connections with the data acquisition system is shown schematically in Figure 4-1. The emission measurements were based on a Vetronix PXA - 1100 five-gas analyzer which used a combination of infrared absorption and fast response chemical cells to measure Oxides of Nitrogen (NO_X), Hydrocarbons (HC), Carbon Monoxide (CO), Carbon Dioxide (CO_2) and Oxygen (O_2). Air mass consumption rate was measured by a Siemens HFM 62B mass air flow (MAF) sensor which had been calibrated against an ASME standard nozzle. Instantaneous fuel consumption rate was inferred using an ECM AFRecorder 2400E fast response lambda sensor in combination with the mass air consumption rate. Measured vehicle parameters included speed, (measured by a signal conditioning circuit on the stock vehicle speed sending unit), and coolant temperature, (measured by an AD590 temperature probe in the manifold crossover water jacket). Ambient temperatures were measured by two AD590 temperature probes, one in the vehicle's intake system under-hood before the throttle valve, and one attached to the vehicle's radio antenna. Barometric pressure was measured using a lab barometer at one end of the trip. Communication with all of the instruments and senors was conducted through a Fujitsu laptop computer running National Instruments Labview 6i. The five-gas analyzer composition data was communicated over a serial line and the other parameters were measured as analog signals using a National Instruments PCMCIA DAQCard-AL-16E-4 data acquisition (DAQ) card. Further measurement system and processing details are provided in SAE paper 2002-01-1717.(2) (Chapter 3).

4.2 EXPERIMENTAL VEHICLE

A 1992 GMC 2500-series, two-wheel drive, regular cab pickup with 5.7L (350ci), automatic transmission and long box bed was used for this study. This vehicle class represents a significant fraction of the Edmonton, Alberta on-road fleet and, due to original standards and age, provides an even more significant fraction of the on-road emissions. The dry vehicle weight was approximately 2,100 kg (4,700 lbs.) and, at the start of testing in early July of 2001, the odometer read approximately 187,000 km. At the end of the data collecting phase, June of 2002, approximately 10,000 km were accumulated on the test vehicle. To avoid the complications of a severely aged catalyst, a replacement OEM catalytic converter was installed near the start of the test period. Multimode dynamometer testing showed that the vehicle would probably meet US Tier 1 standards in this condition. (This test vehicle was originally the University of Alberta entry in the 1993 NGV Challenge.(26) Before this test period, the engine and emission control systems were returned to stock gasoline configuration.)

4.3 RESULTS

Basic test results are in the form of time traces for vehicle speed, fuel consumption rate and tailpipe mass emission rates. These traces can be integrated to provide cumulative consumption and emissions against vehicle distance traveled. Vehicle emission factors can be obtained from the graphs of cumulative emissions against distance traveled. The intent of this paper is to illustrate ambient temperature and engine temperature effects on vehicle emission factors measured using this on-road system. The presentation begins with a comparison of basic traces recorded across a wide range of ambient temperatures: (+21°C to -25°C). Then, cumulative emission traces are shown for typical trips at temperatures across this range (as shown in Table 4-1). A procedure for extracting vehicle emission factors from these cumulative emission traces is developed and the effects of emission control anomalies on these emission factors is illustrated. The major contribution of this paper is then to compare measured vehicle emission factors from a large number of trips over a range of ambient temperatures and to present a simple relationship. Two further items are presented. The first is a comparison which illustrates the effect of engine initial temperature on vehicle emission factors at cold ambient temperature (-20°C). The second is an analysis of the frequency and magnitude of emission control "failures" where the vehicle's emissions were higher than the levels it was capable of achieving.

TABLE 4-1 FOUR SAMPLE 17.4 KM COMMUTER PROFILES AT A RANGE OF TEMPERATURES

Trip#	Date	AmbientTemp (°C)	Ambient Pressure (kPa)	Duration (s)
1	Sept 26, 2001	+21	92.2	2545
2	Oct 3, 2001	+4	94.6	2100
3	Jan 17, 2002	-9	94.4	1970
4	Mar 7, 2002	-26	94.4	2070

4.3.1 INSTANTANEOUS EMISSION TRACES

Figures 4-2 and 4-3 illustrate the velocity profile and instantaneous mass emission rates of HC, CO and NO_x for two typical commutes run at an ambient temperatures of +21°C and -26°C. Examination of the speed and emission profiles, shows that each trip consists of three sections with a different traffic pattern. The first section consists of a cold start followed by un-congested suburban roadway driving with sustained vehicle speeds near 60 to 65 km/hr. The free flowing conditions typically ended near 750s into the morning commute (by which time the engine was at full operating temperature). The second region is a typical congested (stop and go) urban driving profile with average vehicle speeds in the 10 to 20 km/hr range. The congested region for Trip 1 (at +21°C) had a duration of 1250s whereas for Trip 4 (at -26°C) the congested region duration was only 1000s. This implies that more traffic congestion was experienced during Trip 1 than in Trip 4. The final trip section, (which was from 2000 to 2500s for Trip 1 and from 1750 to 2000s for Trip 4), is an un-congested urban road with sustained high vehicle speeds similar to the starting section. This similarity between the starting and ending region of the commute allows direct comparison of the emission profiles for cold and warm-stabilized engine operation.

Figures 4-2 and 4-3 show the second-by-second HC, CO and NO_x emission traces (in g/s) above the speed-time trace. The HC trace at the time of startup initially shows a spike of 0.07 g/s for the +21°C trip and 2.5 g/s for the -26°C trip. *(The startup spike is shown in the subplot of Figure 4-3. Note the 10x scale difference between the HC plots in Figures 4-2 and 4-3 and that the HC emission trace in Figure 4-3 still had to be clipped in the main plot to avoid scaling* *problems*). Very cold weather operation resulted in a 3500% increase in the HC emission rate for the starting phase of the test vehicle. The range of these measurements provides one illustration of the on-board measurement system's ability to capture the vehicle emissions on a second-by-second basis. Closer examination of both HC emission profiles shows distinctive pre-catalyst light-off and post-light-off regions. The pre-light-off region where emissions were not substantially reduced by the emission control system lasted approximately 250s with a more gradual tail-down at +21°C than at -26°C. Within this region (excluding the startup phase), HC emission rates at +21°C averaged 0.01 g/s and reached peak rates of 0.04 g/s. At -26°C, HC emission rates were substantially higher, averaging 0.24 g/s, (a 2300% increase), and peaking at 0.8 g/s, (a 1900% increase). The second region of the -26°C commute (i.e. after 250 s with the catalytic converter working), gave a running emission HC rate of 0.006 g/s. This was about 200% higher than the 0.002 g/s running warmed-up emission rate generally achieved at +21°C, showing the strong effect of extreme ambient temperature, even for fully warmed-up vehicles.

Figure 4-2 also illustrates that the vehicle's running emission rate was not always consistent. The trace shows a significant rise in the HC emission rate between 1000s and 2000s, indicating a loss of emission control in the catalyst. Over this time period, the average HC rate rose to 0.01 g/s and peaked at values of 0.04 g/s. These rates are similar to the emission rates before catalyst light-off and about five times higher than the expected emission rate. This 1000s to 2000s time period coincided with the congested urban section of the commute, represented by long periods of idling and occasional accelerations. After 2000s, when the test vehicle entered the un-congested, higher-speed urban area, the average HC emission rate returned to 0.002 g/s. (Such failures are even more visible in the cumulative emission traces of Figures 4-4 though 4-6 and are discussed in section 4.3.2).

The CO emission traces show trends similar to the HC emission profiles. At 21°C, emission rates peaked at 3.0 g/s and averaged 0.5 g/s before catalyst light-off. At -26°C, emission rates peaked at 8.0 g/s during the starting phase, (250% increase), and averaged 1.6 g/s (220% increase) in the pre-light-off period. After catalyst light-off, the +21°C CO emission rate averaged 0.03 g/s. However, as with the HC profile, during the elapsed time range of 1250 to 2000s frequent CO emission spikes up to 0.5 g/s were visible. At -26°C, the CO emission rate averaged 0.06 g/s (100% increase) once the catalyst was operational.

The NO_x emission traces also showed pre- and post- catalyst light-off behavior but were less affected by ambient temperature. During the pre-catalyst light-off phase, significant NO_x spikes appeared at the tailpipe, associated with each vehicle acceleration. Peak values were about 0.1 g/s at +21°C and 0.09 g/s at -26°C, indicating little ambient temperature influence for a cold engine. Once the catalyst became operational, the average emission rate dropped to approximately 0.001 g/s. However, the vehicle emission controls took about twice as long to gain control of NO_x at -26°C (500s vs. 250s), leading to higher total emissions of NO_x. Also, in the test runs at both temperatures, there were some emission control anomalies. After 750 - 1000s of consistently low NO_x emissions, control apparently slipped with periodic bursts of NO_x emission up to 0.02 g/s from 1250s to the end of both trips. This comparison of NO_x emissions for the two trips with widely varying ambient conditions indicates that ambient temperature only influences the delay time for the emission control / catalyst to become fully functionality.

These instantaneous emission rate traces illustrate the vehicle emission control characteristics (such as starting, pre-light-off and post-light-off periods) and the influence of ambient temperature on those systems. While emission rate traces (in g/s) can be useful diagnostic tools for vehicle and emission control systems, measurement of actual vehicle emission factors (in g/km or g/mi) requires integration of the instantaneous emission rate to present cumulative emission with distance traveled. The emission factors are then the slopes of such plots of cumulative mass emission against distance traveled.

4.3.2 CUMULATIVE EMISSION PROFILES

Figures 4-4 through 4-6 present cumulative mass emissions, (of HC, CO and NO_x respectively), for four repeated commutes along the same route at different ambient temperatures. Trips 1 and 4, (at +20°C and -26°C), were presented as instantaneous emission rate traces above and Trips 2 and 3 represent intermediate temperatures of +4°C and -9°C respectively. These cumulative mass emission curves clearly show the effect of ambient temperature on the three measured pollutants.

The intercept values on each curve measure the mass of pollutant emitted during the startup and initial idling period (which was 50s for all trips). Figure 4-4 shows that the start-and-50s-idle HC emission values were 1.0, 1.4, 4.8 and 34 g for temperatures of +20, +4, -9 and -26°C respectively. For the same ambient temperatures, Figure 4-5 shows that CO start-and-50s-idle emissions were 20, 40, 105 and 180 g. The initial intercept values on Figure 4-6 were very similar showing that start-and-idle NO_x was not significantly affected by ambient temperature.

The slopes of these cumulative mass emission curves represent emission factors, (in g/km units). All of the curves generally show a similar pattern which starts with a high initial slope during open-loop operation followed by a transition period and then a lower slope after full catalyst light-off. The magnitudes of these slopes generally increase for cold ambient temperatures indicating that cold temperatures raise the vehicle emission factors. However, despite ambient temperature changes, the transition points from high initial emission factors to lower stabilized emission factors were fairly consistent. The steep initial slope of the earliest cold-running period ends at about 0.5 km for all three pollutants in all four commutes, probably indicating a consistent start of closed-loop control. The progressive transition to a lower, stabilized slope indicating a fully functional catalyst has generally occurred by 2 km. A transition region with a progressively decreasing slope is visible between 0.5 and 2 km.

Figures 4-4 through 4-6 show that the cumulative emission trace features described above were generally consistent for HC, CO and NO_x cumulative emission traces on most trips over a wide range of temperatures. However, the figures also show that anomalous emissions control failures appeared during some trips. These failures, represented by jumps or anomalously steep slopes in the cumulative emissions will be discussed in section 4.3.6.

4.3.3 CALCULATION OF EMISSION FACTORS FROM CUMULATIVE EMISSION PROFILES

A generalized algorithm was developed to consistently extract emission factors from the cumulative emission curves. This algorithm is briefly discussed here and the details are presented in Appendix E.

The first step in analyzing cumulative emission traces was to use a 60 second rolling average to smooth out steps and jumps associated with specific acceleration events. Then, linear regression was used to fit straight lines to two regions of the curve: the pre-catalyst-light-off and post-catalyst-light-off regions. The first of these regions was generally identified as 0 to 250m and the second as 500m to end-of-trip. User input was used to confirm or adjust this for each analysis. With straight-line emission rates calculated for the pre-light-off and post-light-off regions, the program identified the points where the cumulative emission trace separated by 2% from the linear fit as the change-over points. (See Figure 4-7 for an illustration of the smoothed cumulative emission trace with straight lines fitted to the pre-light-off and post-light-off regions.) The first change-over point (at about 250m) separated the pre-light-off region from the transition region where the catalyst started to become active. The second change-over point marked the end of the transition region and the start of the, (hopefully stable), post-light-off region. The slopes of straight line fits in each region provide vehicle emission factors (in grams/km) for that region. If the two straight lines for the pre- and post- light-off regions were extended across the transition region, a single change-over point would be defined at their intersection and a two emission factor vehicle model could be developed. If a more accurate model was required (for short trips where the transition region was significant), a three emission factor model could be developed by fitting a straight line between the original 2% deviation points and using the slope of that line to define the emission factor for the transition region. Figure 4-7 shows the change-over points and straight line fits used for both two-emission-factor and three-emission-factor models. Tables 4-2 and 4-3 display the equations for both the two and three emission factor models as well as the associated change-over points.

TABLE 4-2
COEFFICIENTS FOR THE TWO-EMISSION-FACTOR MODEL: SAMPLE TRIP PER FIGURE 4-7

	Cold Start	Pre-Light-Off Region		Post-Light-Off Region	
	Intercept (g)	Range (km)	Slope (g/km)	Range (km)	Slope (g/km)
HC	32.6	0 to 0.48	55.7	0.48 to x	0.65
CO	172	0 to 0.72	632	0.72 to x	8.74
NO_x	0.20	0 to 1.64	3.84	1.64 to x	0.18

TABLE 4-3
COEFFICIENTS FOR THE THREE-EMISSION-FACTOR MODEL: SAMPLE TRIP PER FIGURE 4-7

	Cold Start	Pre-Light Off Region		Light-Off or Transition Region		Post-Light Off Region	
	Intercept (g)	Range (km)	Slope (g/km)	Range (km)	Slope (g/km)	Range (km)	Slope (g/km)
HC	32.6	0 to 0.40	55.7	0.40 to 1.31	5.74	1.31 to x	0.65
CO	172	0 to 0.43	632	0.43 to 3.01	78.5	3.01 to x	8.74
NO_x	0.20	0 to 1.17	3.84	1.17 to 3.52	0.92	3.52 to x	0.18

The two-emission-factor and three-emission-factor models shown in Tables 4-2 and 4-3 are essentially piecewise models for describing the vehicle's emission behavior during its trip. For instance, using the two-emission-factor model, calculated HC emissions would be 60 g if the vehicle traveled only 1 km, (HC = 32.6 g + 55.7 g/km * 0.48 km + 0.65 g/km * 0.52 km = 59.6 g) and if the vehicle traveled 50 km the expected emission would be 92 g. The three-emission-factor model would estimate 58 g and 92 g for the same distance trips. After 1 km of travel, there is some difference between the two models since the vehicle is in its transition region. However, the two models inherently agree once the vehicle is in the post-light-off region since they use the same straight-line-fit to the cumulative emission curve in the post-light-off region. This means that the complexity of the three-emission-factor model would only be justifiable where accurate emissions data were required for vehicles making very short trips or areas where most vehicles were in the early stages of trips. (One example would be modeling localized emissions in enclosed parking areas where all of the departing vehicles are all in the early stages of warm-up).

The two-emission-factor model can also be compared with two types of models using only one emission factor. For example, older emission simulation programs (such as Mobile 5(27)) used one emission factor based on measuring the cumulative emissions over an FTP test and dividing by the test distance. This approach ignored the huge initial emissions offset, so it was really only accurate for trips the same length as the test cycle on which the emission factor was measured. To illustrate, the sample commute of Figure 4-7 would give an overall HC emission factor of 4.0 g/km, (70 g of HC over 17.4 km). This model would grossly under-predict emissions at 1 km, (4 g rather than 58 g) and also grossly over-predict emissions at 50 km, (200 g rather than 92 g). The other sort of single emission factor model, as used in Mobile 6(28), consists of the post-light-off emission factor and a zero-distance intercept that accounts for the excess emissions in the cold-start, pre-light-off and post-light-off regions of the trip. For the commute of Figure 4-7, this sort of single-emission-factor model would use an intercept of 59.0 g and an emission factor of 0.65 g/km. This model would over-predict emissions for a very short trip, (60 g at 1 km rather than 58 g), but would provide the same results as the two- or three-emission-factor model for all trips longer than the end of the catalyst-light-off region.

This examination of one-, two- and three-emission factor models has shown that:

1. The three-emission-factor model provides the most detailed and accurate simulation of vehicle emission performance during warm-up. However, this level of accuracy could only be justified if the situation simulated is highly sensitive to cold-start emissions.
2. The two-emission-factor model provides suitable accuracy for virtually all emission simulation and inventory work since it is sensitive to both the cold-start region and the stabilized, post-light-off region.
3. The one-emission-factor model, (of the intercept + emission-factor type), provides essentially the same accuracy as a two-emission-factor model except in situations where

a significant fraction of vehicles are in the pre-light-off and light-off regions.

4. If a two-emission-factor model is available, the corresponding one-emission-factor model can be easily derived from its parameters.

Based on this analysis, the authors have looked at developing two-emission-factor models and the sensitivity of such models to ambient temperature, initial engine temperature and failures of emission control systems.

4.3.4 EFFECTS OF A WIDE AMBIENT TEMPERATURE RANGE ON MEASURED EMISSION FACTORS

The results presented in this section represent repeated runs on the commuter profile shown in Figures 4-2 and 4-3 with the test vehicle conditioned to ambient temperature before the initial start. Emission factors for the two-emission-factor and three-emission-factor models were measured using the algorithms described above. As previously mentioned, the two-emission-factor model is sufficient for emission modeling in virtually all cases. The three-emission-factor parameters are provided for comparative purposes.

4.3.4.1 COLD-START/IDLE EMISSIONS ... THE INTERCEPT

Figures 4-8 and 4-9 illustrate the temperature effect on the mass of HC and CO emitted in the cold start and initial 50s idle phase. Each of the 30+ data points represents a separate trip and the curves are least-square regression fits. Figure 4-8, for HC emissions, shows both the time-averaged emission rate, (in g/s), and the cumulative emission over the start and 50s idle period, (in g). (The measured average idle emission rates could be used in a model to explore the effect of different idle times. However, caution is advised since altering the idle time on a real vehicle would also affect the catalyst warm-up rate and thus transition times). Figure 4-9 and subsequent figures present only the cumulative emission which is the actual intercept for the two- and three-emission-factor models.

Figure 4-8 shows that the mass of HC emitted on a start-and-idle increased exponentially with decreasing ambient temperature, primarily due to fuel enrichment starting strategies with this throttle-body-injected system and lack of effective after-burning in exhaust manifold or catalyst.(21,30) Figure 4-9 shows a more linear trend in the start-and-50s-~~idle~~ CO mass emission over the same ambient temperature range.

The mass of NO_x emitted during the starting and idling phases was negligible and a zero value is assumed for the NO_x intercept in modeling emissions.

4.3.4.2 EMISSION FACTORS FOR THE TWO- AN THREE-EMISSION-FACTOR MODELS

Emission factors and change-over points for HC, CO and NO_x were extracted from the cumulative emission curves for the same set of 31 commuting trips covering a wide temperature range. Figures 4-10, 4-11 and 4-12 illustrate the experimentally determined emission factors for HC, CO and NO_x emissions respectively. Each figure presents measured data points and fitted curves for three emission factors: pre-light-off, transition (or light-off) and post-light-off. The pre- and post-light-off emission factors are used for either two- or three-emission-factor models and the transition emission factor would be used only for the three-emission factor model. Note the differing scales in each figure ranging from high scales for the pre-light-off period at the bottom to lower scales for the post-light-off period at the top. This difference in scale shows the importance of the cold-start, pre-light-off emission rates relative to stabilized, post-light-off emission rates.

(In Figures 4-10, 4-11 and 4-12, the values of post-light-off emission factor for certain trips have been identified as "Cat Failure". The term "Cat Failure" means that the tailpipe emissions during that trip were significantly higher than expected for at least part of the trip. This is really an emissions system failure rather than a catalyst failure per se. The issues and effects of emissions system failures are discussed later in this paper. The ambient temperature effects presented here are based on the fraction of trips without failures, that is, the attainable emission factors which are represented by crosses in the figures.)

Figure 4-10 shows that, (like the intercept), the HC emission factors increase dramatically at lower ambient temperatures. Exponential fits were used for the pre-light-off and transition emission factors while a linear fit was appropriate for the post-light-off emission factor. In the pre-light-off period, the HC emission factor was 19 g/km at -20°C compared with 2.6 g/km at +20°C ... a 7.4 times difference. In the post-light-off period, the difference looks relatively small but is still a significant ratio. At -20°C, the post-light-off HC emission factor was 0.44 g/km compared with 0.07 g/km at +20°C ... a 6.3 times difference.

Figure 4-11 provides a similar picture for the effect of temperature on CO emission factors. Linear fits were used for the temperature effect on both the pre-light-off and post-light-off emission factors. In the pre-light-off period, the emission factor increased from 126 g/km at 20°C to 440 g/km at -20°C ... a 3.5 times increase. The post-light-off emission factors had a much lower magnitude but the drop in temperature had a similar effect. Post-light-off emission factors increased from 1.6 g/km at +20°C to 6.3 g/km at -20°C ... a 3.9 times increase.

The measured NO_x emission factors are shown in Figure 4-12. *(A further symbol to indicate emission system anomalies appears in this figure. In cases where the post-light-off emission factor was higher than expected, the pre-light-off emission factor was consistently low. These points, identified as diamonds on the figure, were not included in calculating the pre-light-off NO_x emission factor.)* Since NO_x production in combustion is associated with high temperatures, you might expect NO_x emission factors to be decreased at low temperatures. However, many factors combine to produce higher NO_x emission factors as temperature drops. Some factors might include lean mixture transients due to poor vaporization, decreased humidity, a more aggressive spark schedule, and higher vehicle power requirements for cold start operation. The relationships in Figure 4-12 show that the NO_x emission factor in the pre-light-off period rises from 1.9 g/km to 3 g/km as temperature drops from +20°C to -20°C. This 60% rise is a similar magnitude to the 75% rise from 0.09 g/km to 0.16 g/km in the post-light-off period.

4.3.4.3 Change-Over Points for the Two- and Three-Emission-Factor Models

The range over which the above emission factors should be used is set by the change-over points in each model. The two-emission-factor model has a single change-over point from pre-light-off to post-light-off emission factor. The three-emission-factor model has two change-over points separating pre-light-off, transition and post-light-off behavior. Figures 4-13 and 4-14 show the measured change-over points for HC, CO and NO_x and the trends with ambient temperature.

Figure 4-13 presents change-over points for both HC and CO emission factors since these values behave identically. The two change-over points for the three-emission-factor model, (presented in the lower and middle part of Figure 4-13), are virtually constant over the range of ambient temperatures tested. This indicates that the emission system warm-up processes are relatively insensitive to cold ambient surroundings. For the vehicle and trip profile in these tests, the first change-over point always occurred close to 0.4 km after starting and the second change-over point was generally between 2 and 3 km from the start. In contrast, the single change-over point for the two-emission-factor model drops dramatically at low temperature, (top of Figure 4-13). This is an artifact of extending pre- and post-light-off emission curves across the transition region and placing the change-over-point at the intersection. The pre-light-off emission factor is a steep slope and becomes much steeper at low temperature. By comparison, the post-light-off emission factor is flatter and less affected by temperature. As a result, the intersection of these two lines moves closer to the origin at low temperatures and this is reflected by the top curve in Figure 4-13.

Figure 4-14 presents change-over points for NO_x emission factors as measured over a range of ambient temperatures. Note that only 16 individual trip data points are presented and trips where the emission control system didn't substantially control NO_x emissions are excluded. This figure shows negligible temperature effect on the change-over points for NO_x emission implying that the data points can be averaged rather than fitting a trend line. The top curve shows that the average two-emission-factor change-over point was 1.8 km. The lower two figures show that, for a three-emission-factor model, the pre-light-off period lasts from 0 to 1.2 km and the transition period lasts from 1.2 to 3.3 km with negligible ambient temperature effect.

4.3.5 EFFECT OF INITIAL ENGINE TEMPERATURE ON VEHICLE EMISSION FACTORS

This section presents results of a secondary study carried out using the same vehicle and commuter route. The objective was to measure the effect of pre-start engine temperature, (0°C to 90°C), on emission factors and change-over points for both the two and three emission factor models. A series of nine commuter runs was completed at -20°C ambient temperature. Results are presented in the same form as the cold start emission section. It seems apparent that, once the vehicle has run long enough to reach the post-light-off emission rates, initial engine temperature has no "remembered" effect and the vehicle emissions are dominated by ambient temperature.

4.3.5.1 COLD-START / IDLE EMISSIONS ... THE INTERCEPT

Figures 4-15 and 4-16 present the cumulative mass of HC and CO emitted during the cold start and 50s idle period for these trips with varying initial engine coolant temperature. A quick comparison of the scales of Figures 4-8 and 4-15 shows that only about 1/10th as much HC is emitted from a partially warm engine as from a pure cold start situation. A similar comparison of Figures 4-9 and 4-16 shows that the effect for CO emissions is substantial but less with reductions of ½ for the start scenarios where the engine retained some heat. The mass of NO_x emitted during the warm starting and idling phases was negligible and a zero value is assumed for the NO_x intercept in modeling emissions regardless of initial engine temperature.

4.3.5.2 EMISSION FACTORS FOR THE TWO- AND THREE-EMISSION FACTOR MODELS

Emission factors and change-over points were calculated from the cumulative data sets for the warm-start engine temperature study. Figures 4-17, 4-18 and 4-19 present the experimentally determined emission factors (pre-light-off, transition and post-light-off) for the HC, CO and NO_x emissions respectively. Also note the scaling differences in each figure ranging from high scales for the pre-light-off emission factors to lower scales for the post-light-off emission factors. In addition, some post-light-off emission factors values have been termed "*Cat Failure*", implying the same definition given before.

Figure 4-17 shows that HC emission factors decrease substantially at higher initial engine temperatures. Exponential curve fits were used to describe the emission factors for all three segments of operation (pre-light-off, transition and post-light-off emission factors). At -20°C ambient temperature, a full cold start produced 19 g/km HC emissions, an engine initially at 0°C produced 4.3 g/km and an engine initially at 90°C produced 1.5 g/km of HC. These emission rates are substantially lower, corresponding to a 4.5 times decrease for the 0°C engine and 13 times decrease for the 90°C engine. As expected, the post-light-off HC emission factors remained similar regardless of pre-start engine temperature.

Figure 4-18 shows the effect of initial engine temperature on the CO emission factors. Exponential fits were used to describe the pre-light-off and transitional emission factors whereas a linear fit was sufficient for the post-light-off emission factor. At -20°C ambient temperature, a full cold start produced 450 g/km CO emissions. With the engine initially at 0°C, the CO emission was 2.6 times less (170 g/km) and at 90°C it was 15 times less (30 g/km). Again, the post-light-off CO emission factors were consistent regardless of pre-start engine temperature.

The effect of initial engine temperature on the NO_x emission factors is presented in Figure 4-19. This figure shows decreasing emission factor magnitudes as the engine start temperature increases. The pre-light-off emission factor decreases by 3.5 times over the temperature range of 0 to 90°C, whereas the post-light-off emission factor decreases by 1.3 times for the same temperature range. Note that the graph scales used for displaying emission factors values were the same for the warm and cold start studies. This implies that emission factor value is affected more by the state of the emission control system than by the residual engine temperatures.

4.3.5.3 CHANGE-OVER POINTS FOR THE TWO- AND THREE-EMISSION-FACTOR MODELS

As described previously, the range over which each emission factor applies is limited by the change-over points. Figures 4-20 and 4-21 describe the change-over points for HC, CO and NO_x emissions for the two and three emission factor models.

Figure 4-20 illustrates the HC and CO change-over points. The two change-over points for the three emission factor model (presented in the lower and middle part of Figure 4-20) are relatively constant over the range of temperatures and similar to the cold start study. For these experiments, the first change-over point consistently occurred in the range of 0.4 to 0.8 km whereas the second change-over point occurred in the range of 2.0 to 3.0 km; with neither showing any clear trends. The single change-over point for the two emission factor model (the upper plot of Figure 4-20) showed more scatter over the range of 0.6 to 1.2 km. The average distance was calculated to be 0.89 and 0.84 km for the HC and CO emission factors respectively.

The effect of initial engine starting temperature on the NO_x change-over points is shown in Figure 4-21. (This analysis only considers the data files where NO_x control was obtained). The first change-over point for the three emission factor model was found to average 0.65 km. The second change over-point tended to increase with increasing pre-start engine temperature. The reason for this increase was not clear. The change-over point for the two emission factor model averaged 1.3 km and there was no significant trend with initial engine temperature.

The analysis of trips starting at different ambient temperature and different initial engine temperature has shown that:

1. The mass of emissions produced by the start and idle phase increases dramatically with decreasing temperatures (both ambient and initial engine temperatures). This can have a profound impact on inventories due to various idling times.
2. The three cold start HC and CO emission factors (for pre-light-off, transition and post-light-off driving), differ by approximately an order of magnitude. This implies that the majority of emissions are emitted during the "warm-up and transitional" phases of the engine and emission control systems.
3. With a pre-warmed engine, the HC and CO emission factors showed substantially lower pre-light-off and transitional emission factors when compared to the cold start. This was a result of the engine/emission control system being partially warmed up. The post-light-off emission factors were of similar magnitude. The three warm start NO_x emission factors were of comparable magnitudes to the cold start values so engine warming did not significantly affect NO_x emissions.
4. The change-over points for the two- and three emission factor models were relatively consistent over the temperature ranges (i.e. ambient and initial engine temperatures).

4.3.6 DETECTION AND ANALYSIS OF EMISSION CONTROL FAILURES

As was mentioned previously, numerous emission control failures were observed during the data analysis. These emission control anomalies are most visible in cumulative emission plots such as Figures 4-4, 4-5 and 4-6. For example, Figure 4-4 shows a loss in HC control for the +20°C test at approximately 8.5km into the trip. For the same experiment, a loss in CO control (Figure 4-5) was also noted at the same distance. To measure the effect on these occurrences on emission factors, a procedure was developed as shown in Figure 4-22. The basic (best attainable) emission factor was measured by fitting a straight line only through the initial part of the post-light-off region before the emission control failure. A second and more representative emission factor was then calculated based on the slope of a line drawn through the start of the post-light-off region and the final mass emission value. For this example, the best attainable HC emission factor found was found to be 0.38 g/km (solid line). The actual emission factor including the failure, (represented by the dashed line), was 0.56 g/km which is a 47% increase. In the post-light-off emission factor graphs, these actual emission factors are reported as "Cat Failure" points.

The second type of emission control anomaly only affected NO_x emissions. As shown in Figure 4-6 for the -9°C experiment, this mode of failure was a total inability of the emission control system to reduce NO_x emissions. This resulted in no apparent "catalyst-light-off" point and a continuous and a steady rise in the cumulative NO_x emission profile. For these situations, a single linear regression analysis applied to the entire cumulative plot produced a single NO_x emission factor for the entire trip. These emission factor values are presented as diamonds (and labeled 'Non-Function Cat') in the pre-light-off emission factor analysis (Figure 4-12).

The frequency of emission failures was determined by comparing the two calculated emission factors in the post-light-off sections of the cumulative emission profiles. Recall that one represented the achievable emission rate and the other was the actual emission rate.

Figure 4-23 illustrates the magnitude and frequency of the HC emission failures. The "Baseline" values were the emission factors of a "functioning control system" where a maximum 10% difference was found between the two emission factors calculated in the post-light-off region. As show in the figure, the test vehicle attained these emission factors only for 6.5% of the experiments. This means that 93.5% of the experiments had "true" emission factors more than 10% above the attainable values. Figure 4-24 shows that the CO emissions performance was similar: only 6.5% of trips avoided some level emission system failure and stayed within 10% of the attainable value.

Figure 4-25 shows the NO_x failure rate for the 52% of experiments where some reduction was measured. Basically, all NO_x cumulative emission curves showed some sign of emission failure. Only 6.3% of the experiments fell within 20% increase of the attainable post-light-off emission factor.

Comparisons were made between the actual emissions produced by the vehicle to the attainable emissions (found from using the emission factors for the "functioning emission control system.") It was found that a 14, 7 and 9% increase was found for the emissions of HC, CO and NO_x respectively. This means that although emission-control losses occurred frequently, the impact of the anomalies was relatively modest.

The detection and frequency/magnitude of emission control failures has shown:

1. HC and CO emission control anomalies in the post-light-off regions occur as sharp (and short duration) increases in the cumulative emission profiles. Only 6.5% of the experiments consistently kept post-light-off emissions factors within 10% of the attainable values. However, only 14 and 7% increases in the final mass accumulations were found for HC and CO emissions as a result of the emission control anomalies.
2. Complete failure to control NO_x emission occurred 48% of the time. Even in the remaining trips, there were significant failures of NO_x control during every trip. However, only a 9% increase in the final mass accumulation of NO_x emissions was found as a result of the emission control anomalies.
3. The exact cause of the emission control anomalies is unclear since the problems were transitory and no codes were set. Essentially, the anomalies were only detectable because the vehicle was instrumented to measure them.

4.4 CONCLUSIONS

This paper has examined the impact of ambient temperature and to a lesser extent initial engine temperature on the emission profiles (and resulting emission factors) for a single vehicle / driver configuration. The emission measurements were conducted in real-time and in an on-road applications to improve the analysis of real-world vehicle emissions.

The paper demonstrated the development of one-, two- and three-emission factor models to represent the cumulative vehicle emissions. Properly developed one-emission factor models provided adequate accuracy outside the initial cold start region and two-emission factor models adequately covered the cold start and warmed-up regions.

The emission factors for the test vehicle were found to correlate with ambient temperature allowing the characterization of emission behavior for cold start applications. Comparing the cold-start pre- and post-catalyst light-off emission factors, it was determined that typical magnitude increases of 100, 60 and 10 were calculated for HC, CO and NO_x respectively over the temperature range of +20°C to -25°C. In addition, the effect of initial engine temperature was also examined and an initially warm engine was found to substantially reduce HC and CO emissions.

The research also showed that frequent emission control failures were occurring in the on-road application and that these failures significantly increased the corresponding emission factor. However, these failures only increased the final mass values modestly when compared to the attainable values.

4.5 FUTURE WORK

This paper has demonstrated the strong influence of ambient and initial engine temperatures on the corresponding emission factors. Chapter 5 focuses on this topic and explores the effects of driving patterns. This will result in the development of two variable emission factor model of this test vehicle consisting of: 1) ambient / initial engine temperature (as describe in this paper) and 2) non-zero average vehicle speed.

With the development of the measurement system and algorithms to analyze the data, numerous other test vehicles will be explored. This will allow the emission characterization of newer vehicles with more sophisticated emission control systems. In addition, older vehicles with aged or non-functioning emission control systems will be tested to determine their impact on air pollution.

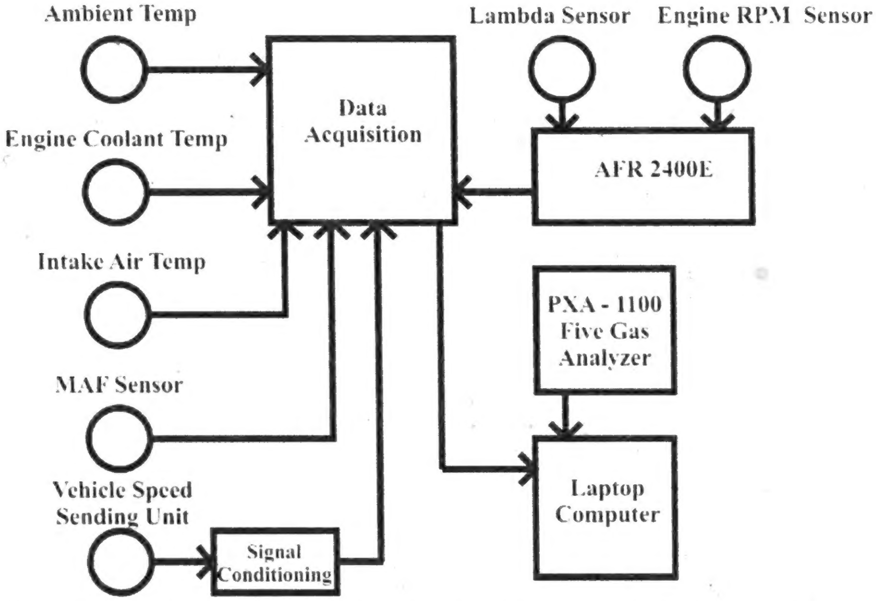

FIGURE 4-1 COMPONENTS OF THE ON-ROAD, REAL-TIME EMISSIONS SYSTEM

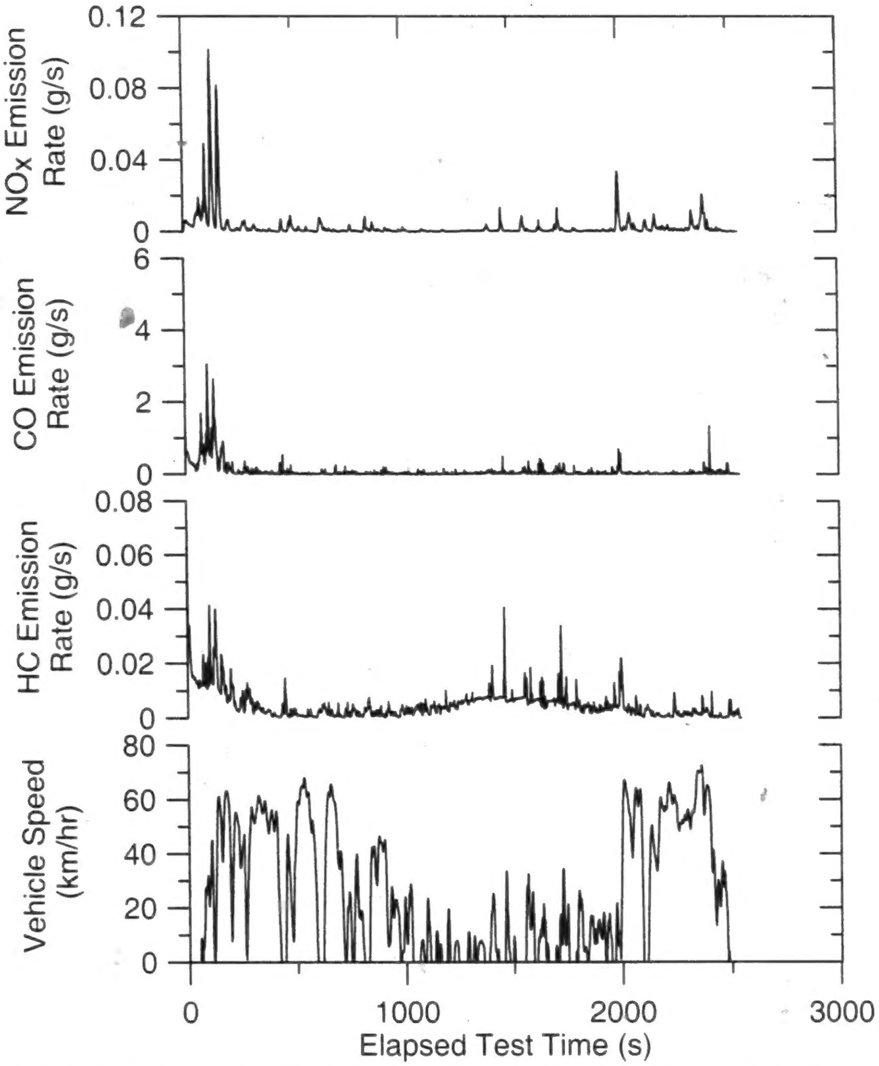

FIGURE 4-2 INSTANTANEOUS SPEED AND EMISSION TRACES (+21°C Ambient)

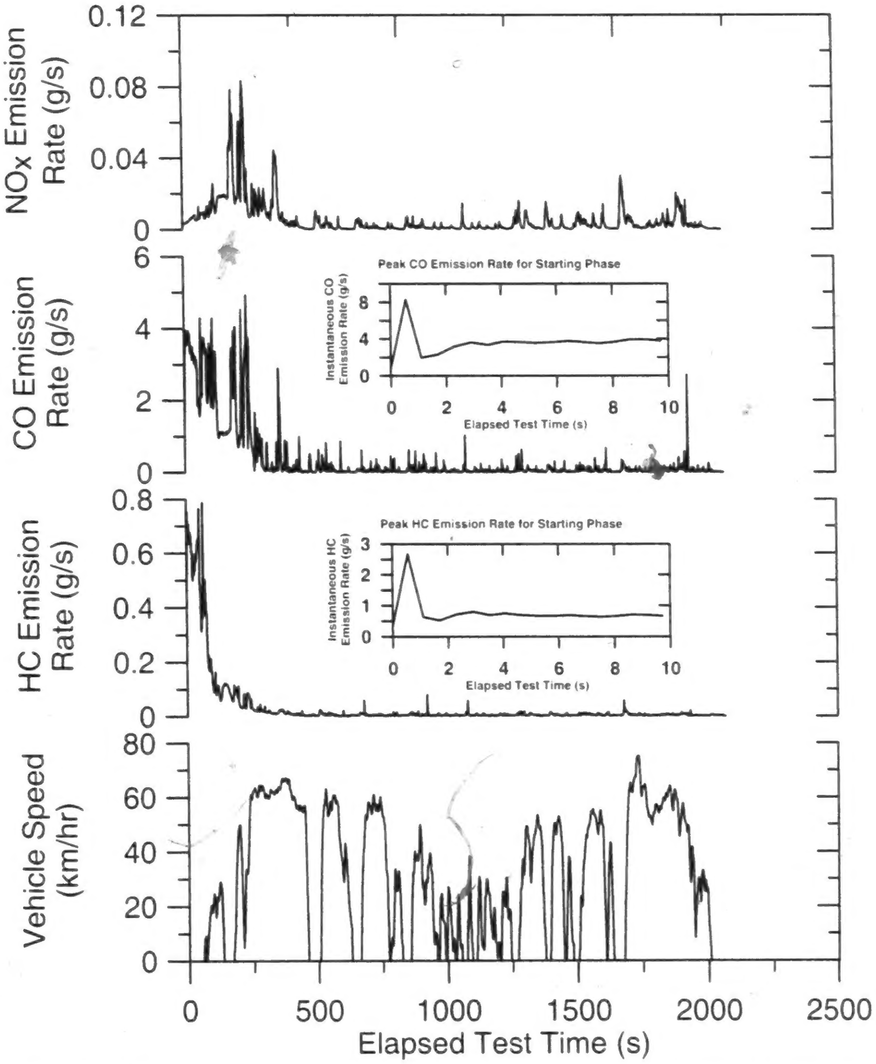

FIGURE 4-3 INSTANTANEOUS SPEED AND EMISSIONS TRACES (-26°C AMBIENT) (Note 10x change of HC scale from Figure 4-2)

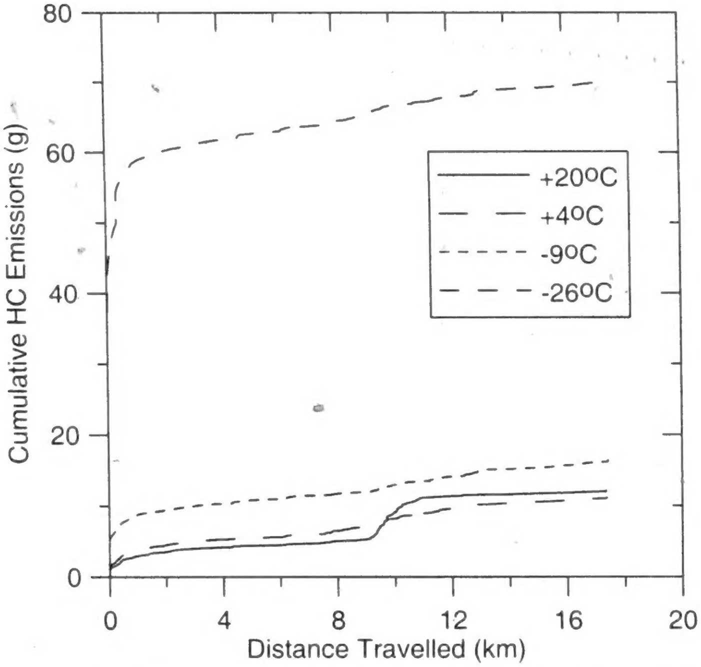

FIGURE 4-4 CUMULATIVE HC EMISSIONS AT FOUR AMBIENT TEMPERATURES

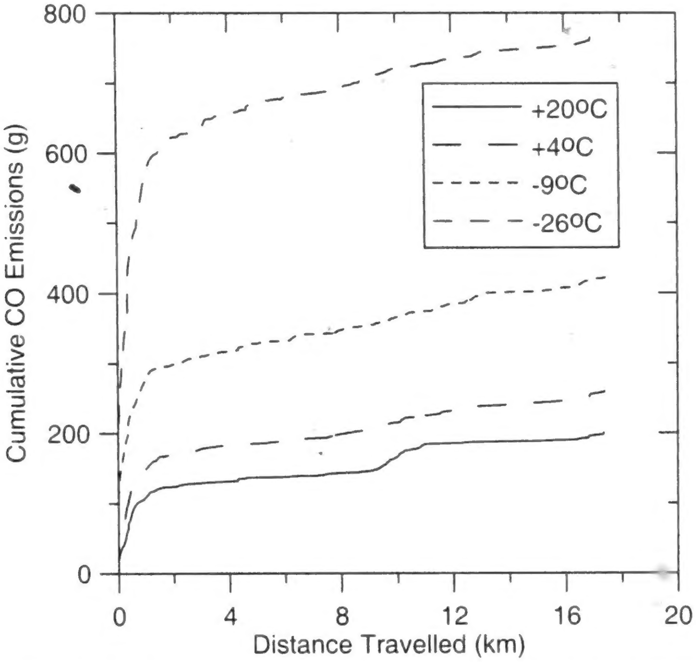

FIGURE 4-5 CUMULATIVE CO EMISSIONS AT FOUR AMBIENT TEMPERATURES

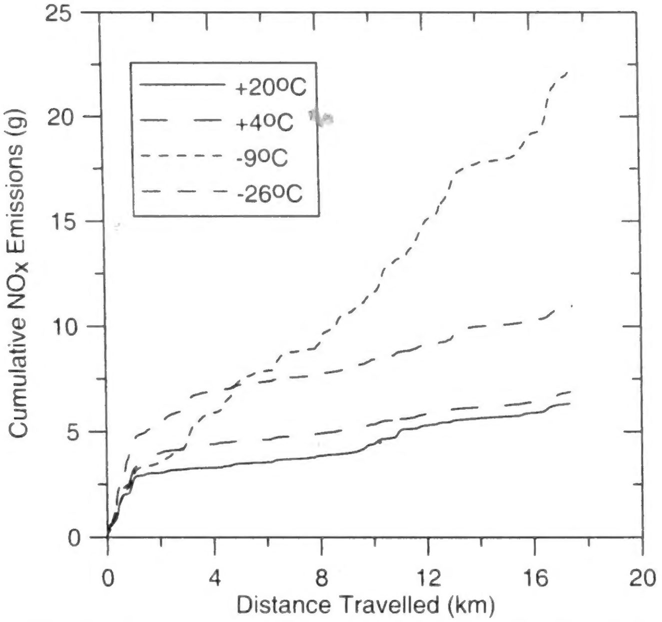

Figure 4-6 Cumulative NO$_x$ Emissions At Four Ambient Temperatures

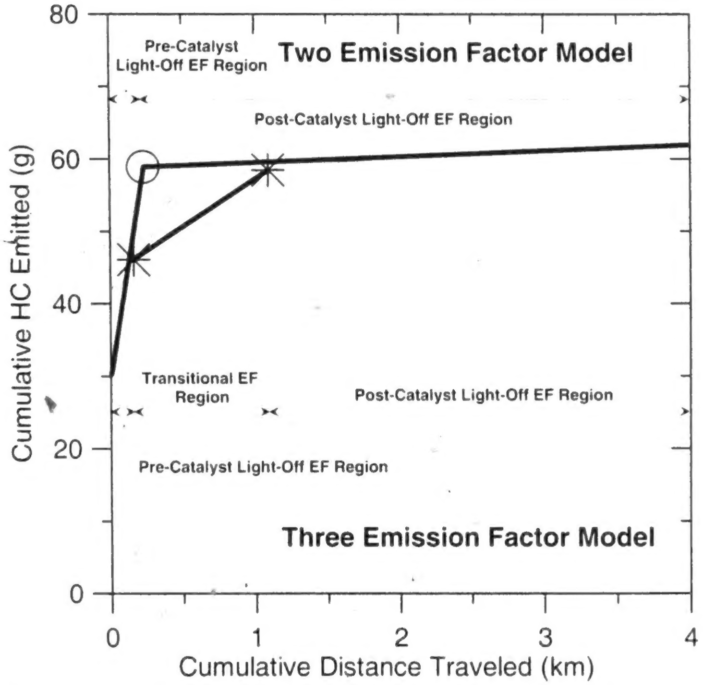

Figure 4-7 Cumulative HC Emission Profile Illustrating the Two and Three Emission Factor Models

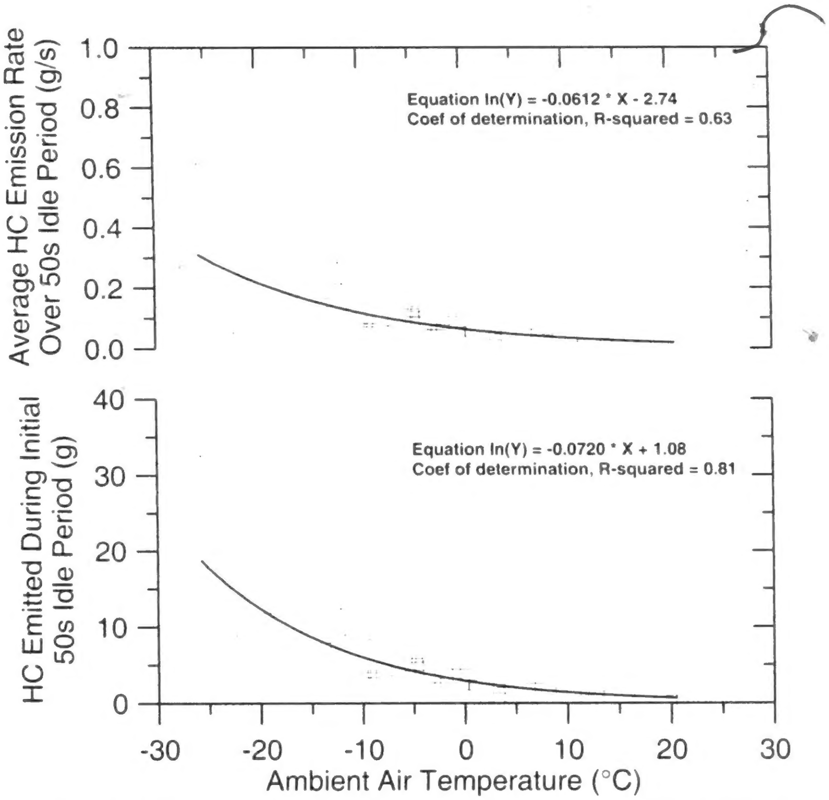

FIGURE 4-8 AMBIENT TEMPERATURE EFFECT ON HC EMISSION DURING A 50S INITIAL IDLE PERIOD

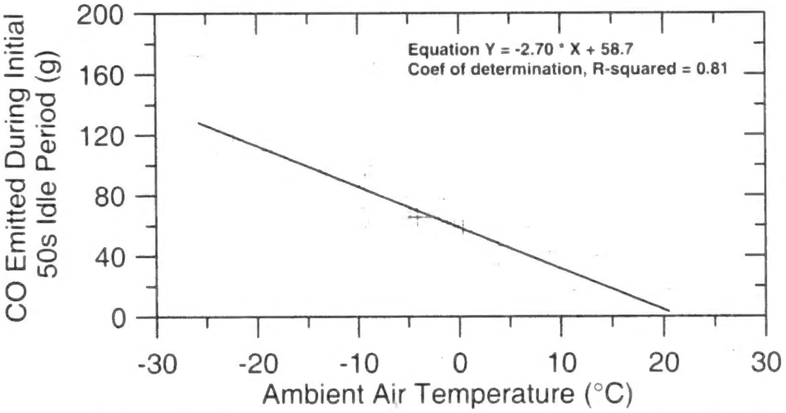

FIGURE 4-9 AMBIENT TEMPERATURE EFFECT ON CO EMISSION DURING A 50S INITIAL IDLE PERIOD

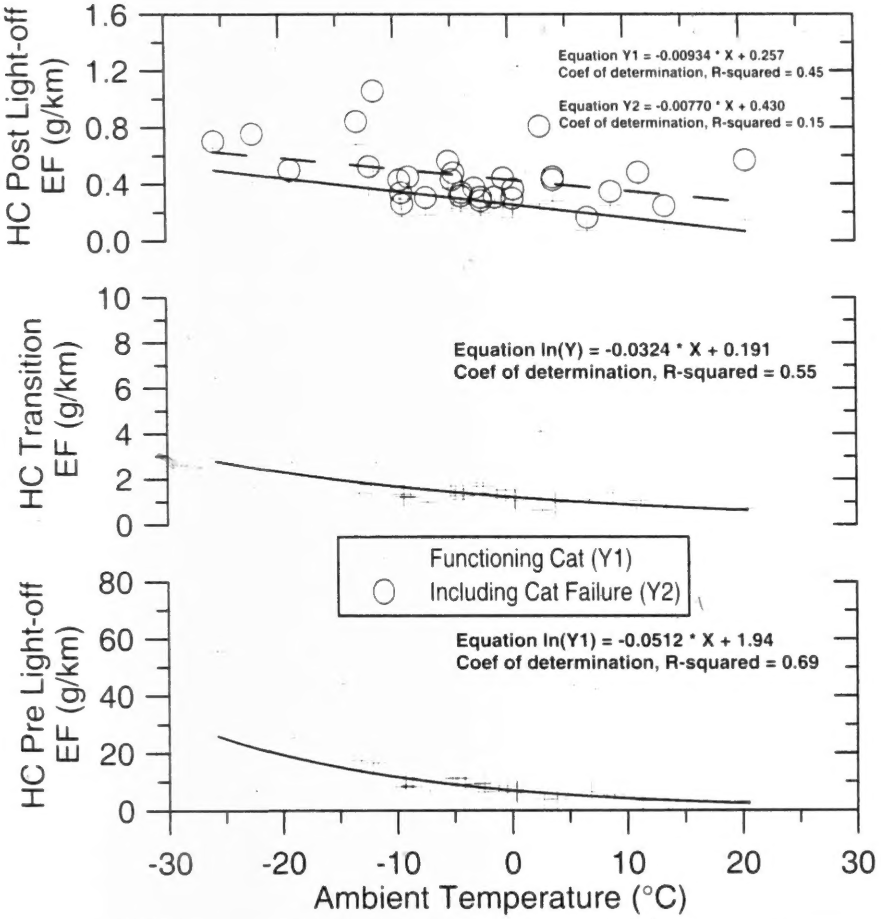

FIGURE 4-10 AMBIENT TEMPERATURE EFFECT ON HC EMISSION FACTORS (THREE EMISSION FACTOR MODEL)

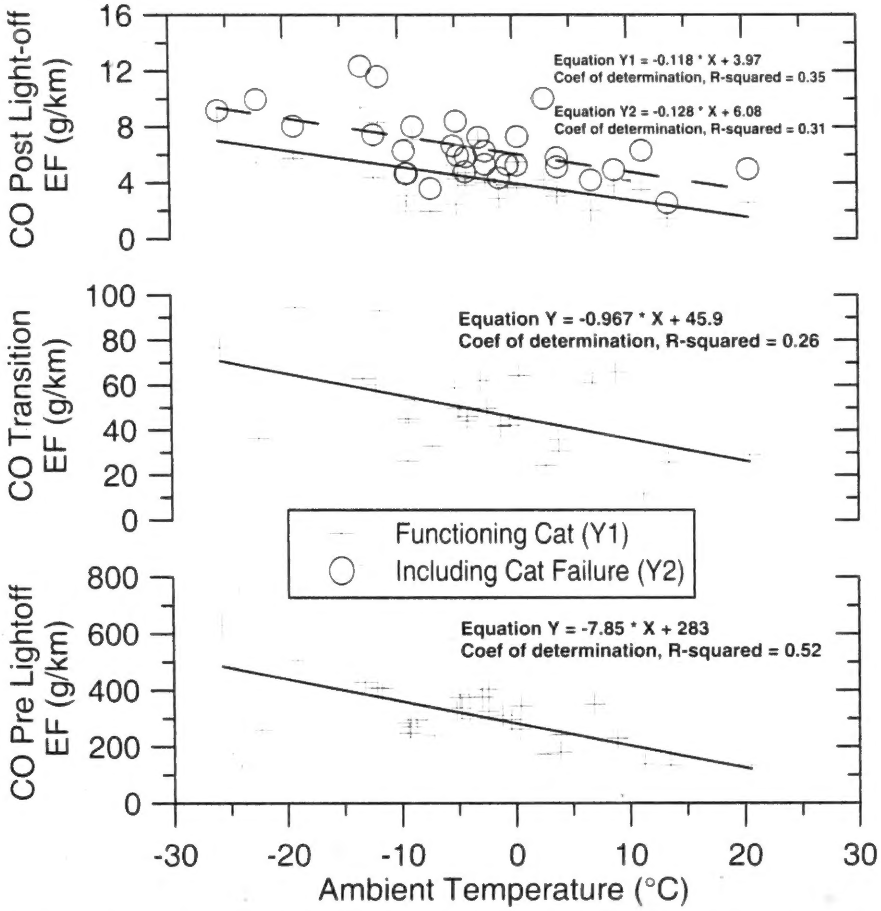

FIGURE 4-11 AMBIENT TEMPERATURE EFFECT ON CO EMISSION FACTORS (THREE EMISSION FACTOR MODEL)

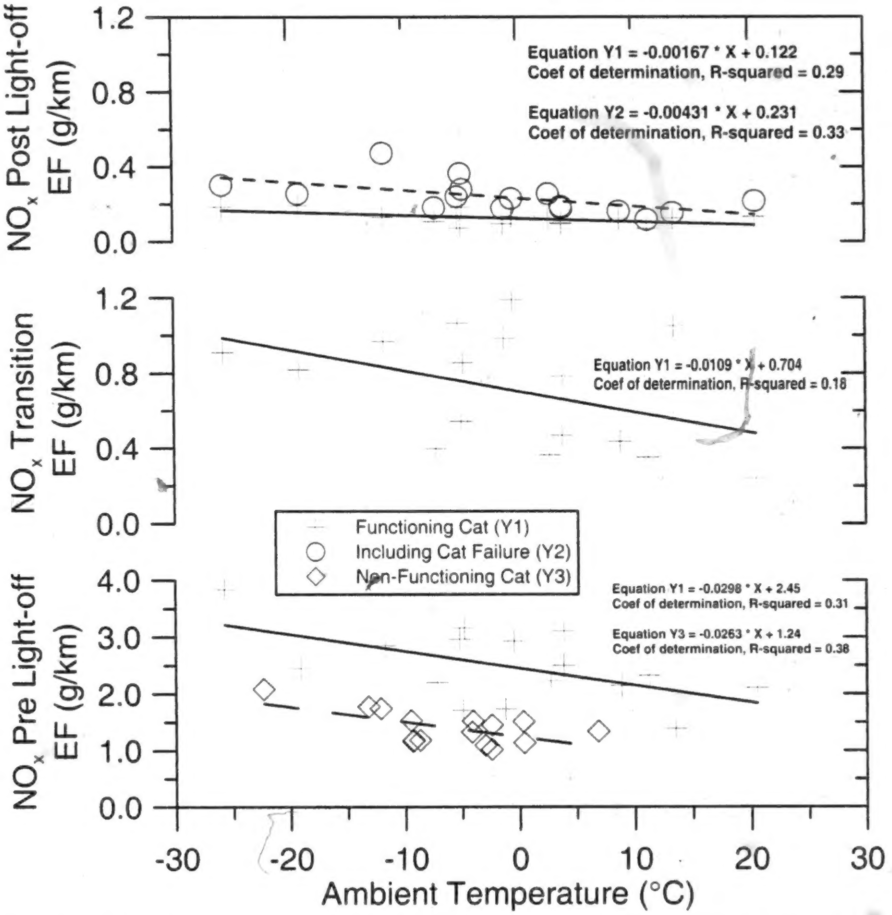

FIGURE 4-12 AMBIENT TEMPERATURE EFFECT ON NO$_X$ EMISSION FACTORS (THREE EMISSION FACTOR MODEL)

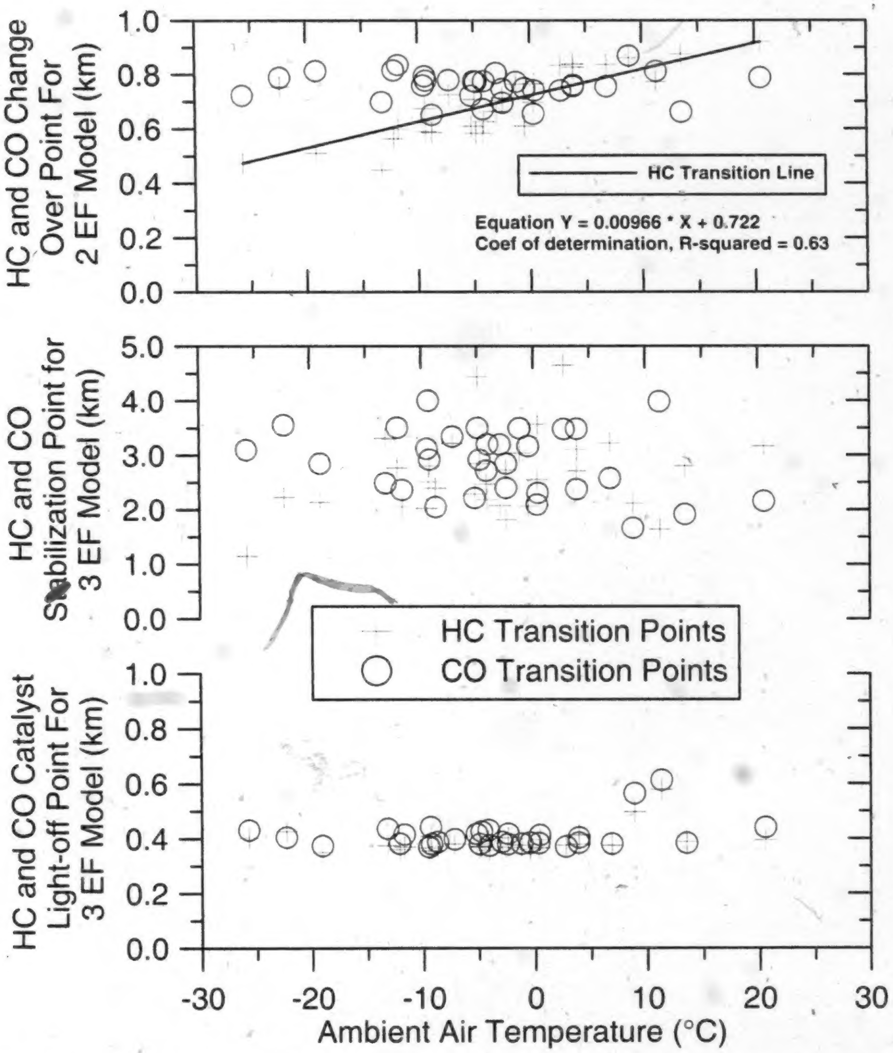

FIGURE 4-13 AMBIENT TEMPERATURE INFLUENCE ON HC AND CO CHANGE-OVER POINTS FOR THE TWO AND THREE EMISSION FACTOR MODEL

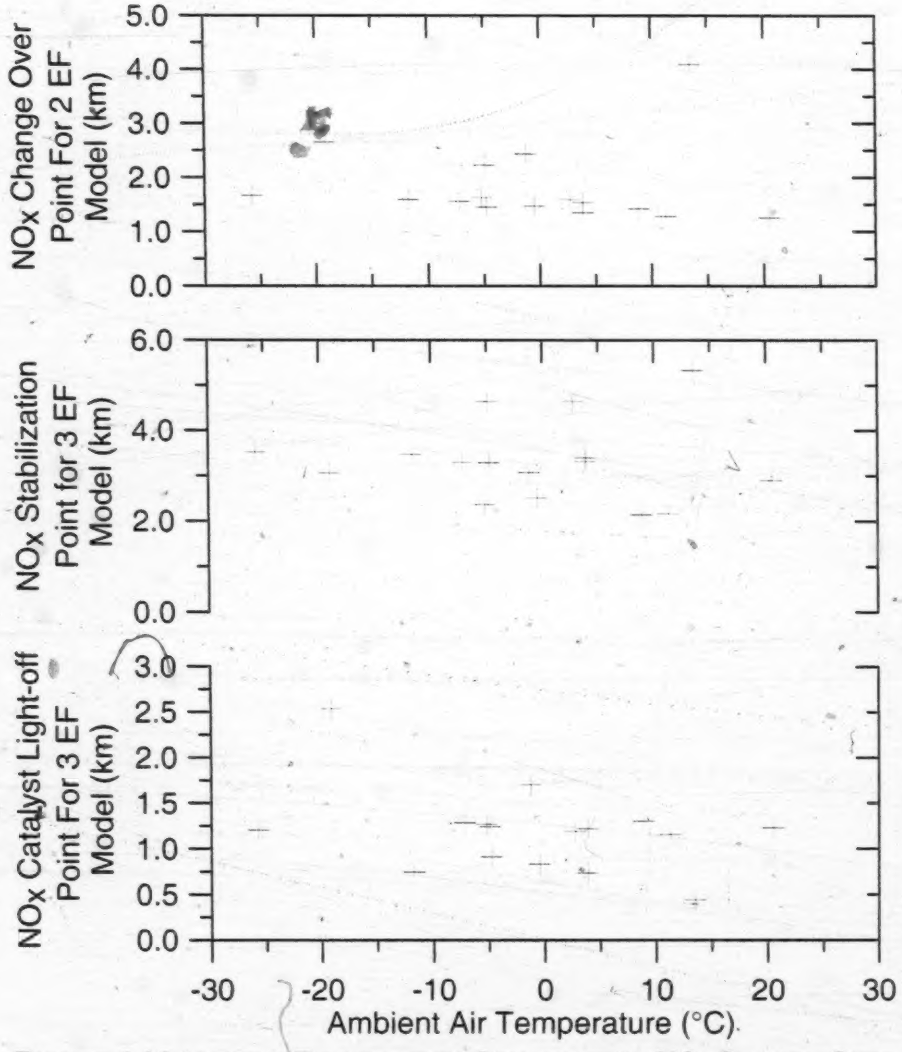

FIGURE 4-14 AMBIENT TEMPERATURE INFLUENCE ON NO$_X$ CHANGE-OVER POINTS FOR THE TWO AND THREE EMISSION FACTOR MODEL

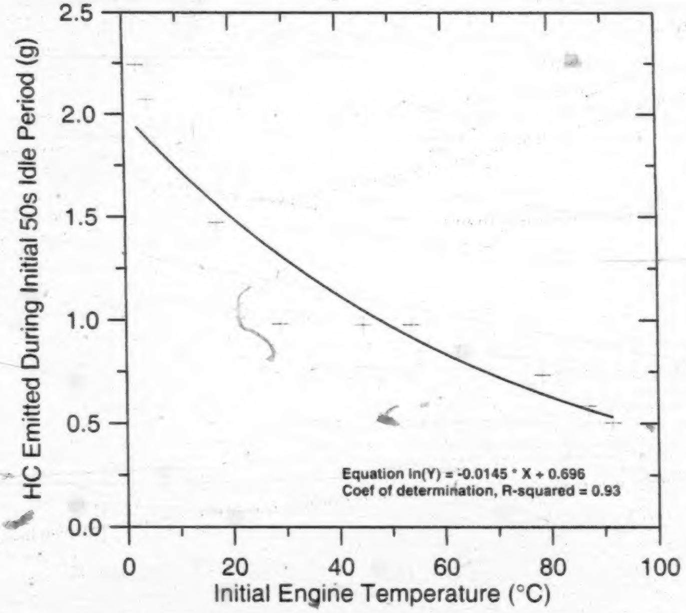

FIGURE 4-15 INITIAL ENGINE TEMPERATURE EFFECT ON HC EMISSIONS DURING A 50S IDLE PERIOD (-20°C AMBIENT TEMPERATURE)

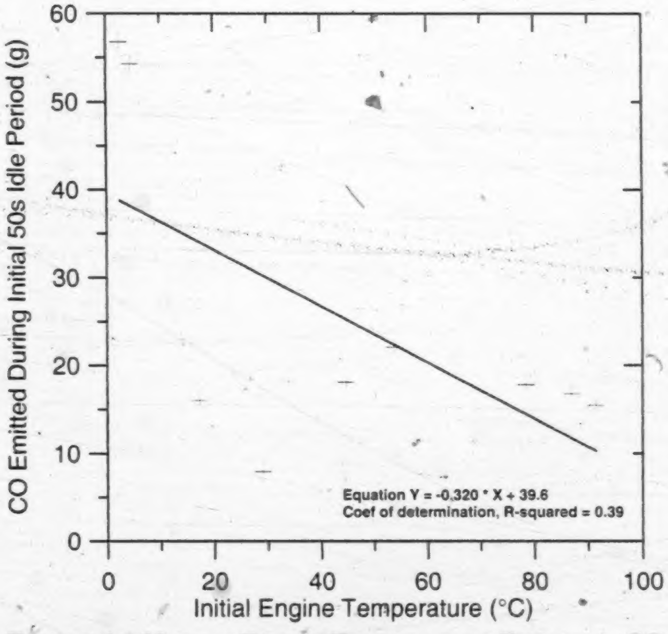

FIGURE 4-16 INITIAL ENGINE TEMPERATURE EFFECT ON CO EMISSIONS DURING A 50S IDLE PERIOD (-20°C AMBIENT TEMPERATURE)

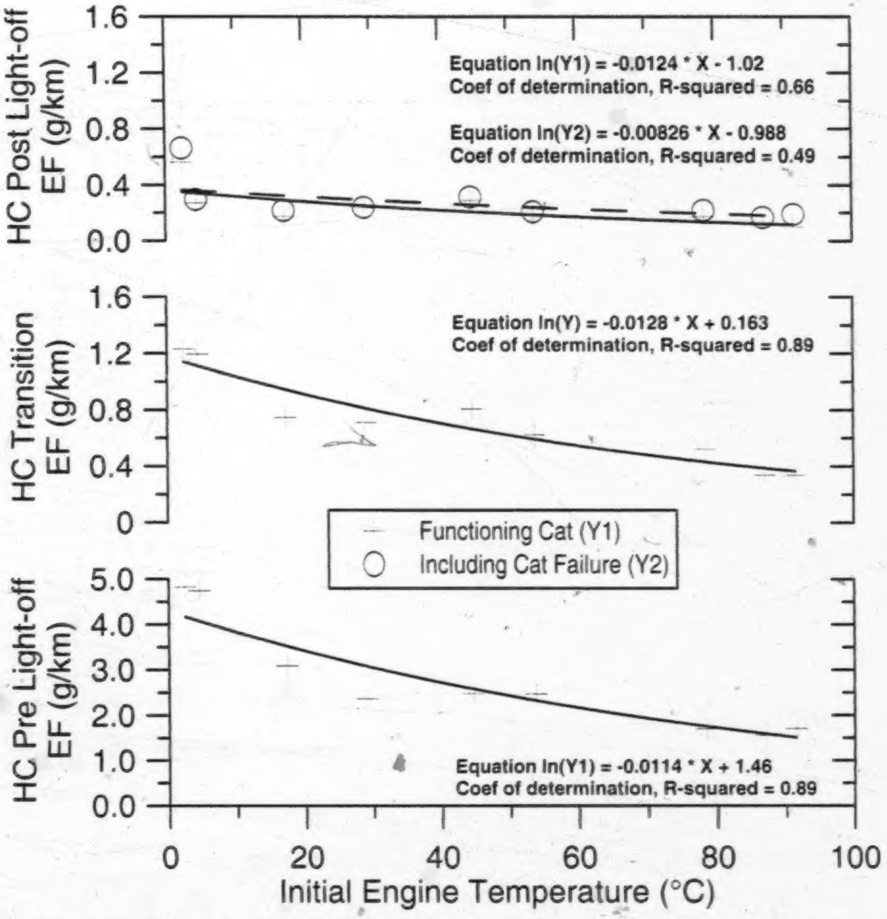

FIGURE 4-17 INITIAL ENGINE TEMPERATURE EFFECT ON HC EMISSION FACTORS (-20°C AMBIENT TEMPERATURE)

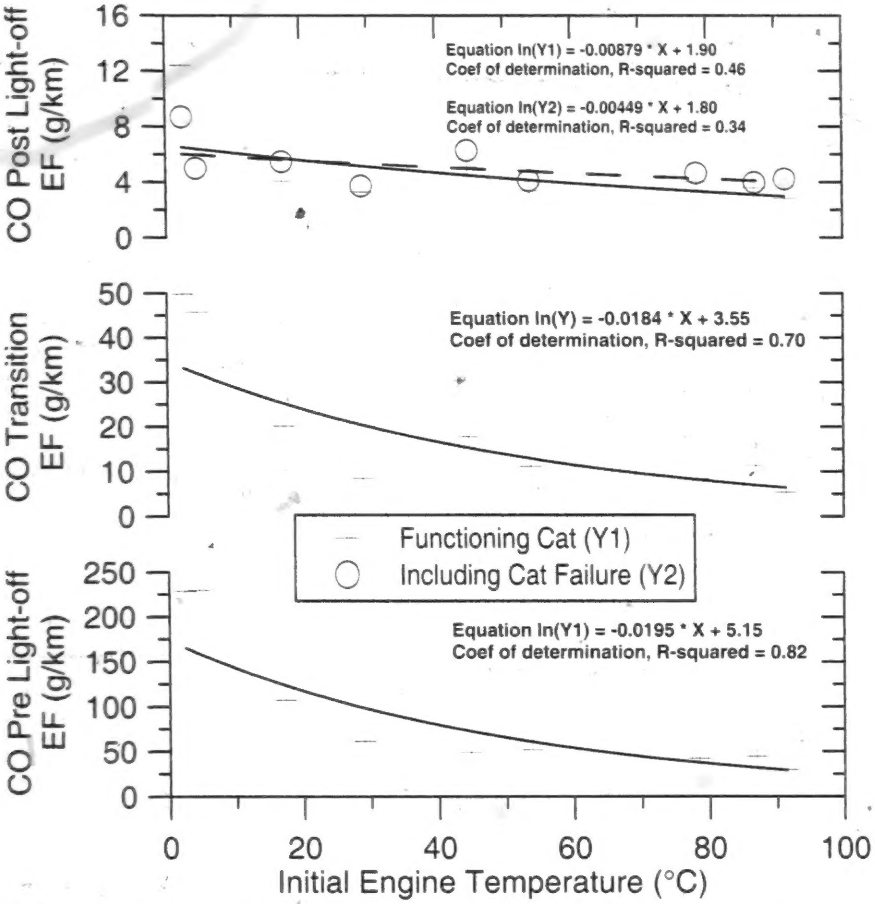

FIGURE 4-18 INITIAL ENGINE TEMPERATURE EFFECT ON CO EMISSION FACTORS (-20°C AMBIENT TEMPERATURE)

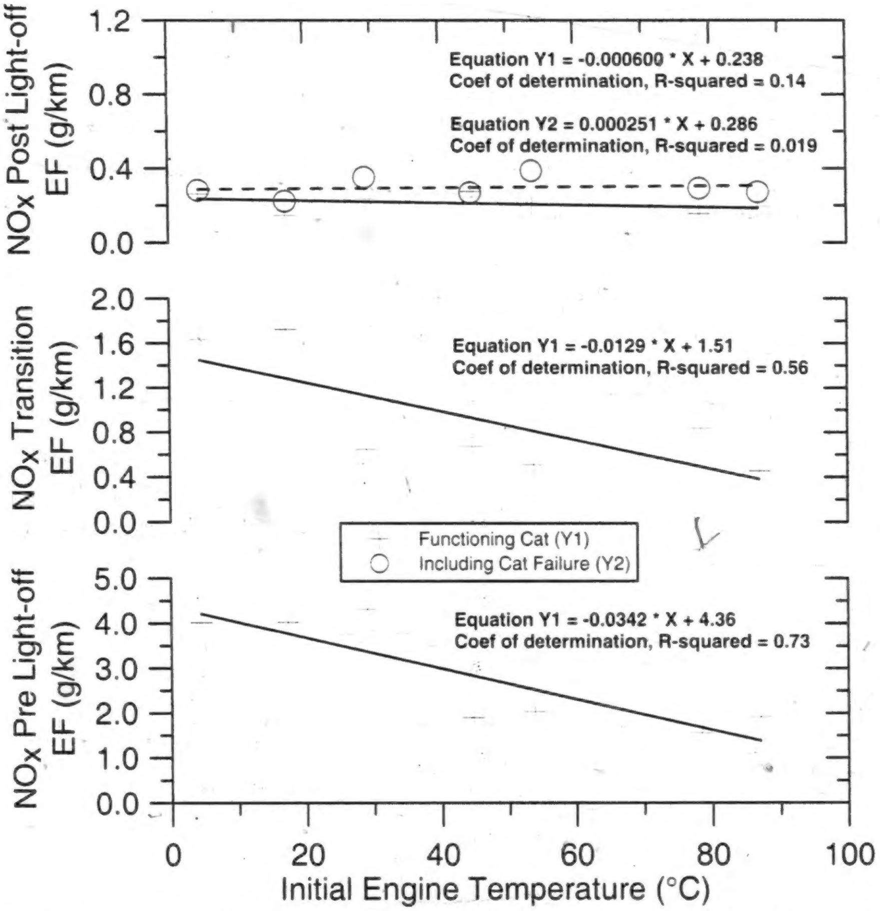

FIGURE 4-19 INITIAL ENGINE TEMPERATURE EFFECT ON NO_X EMISSION FACTORS (-20°C AMBIENT TEMPERATURE)

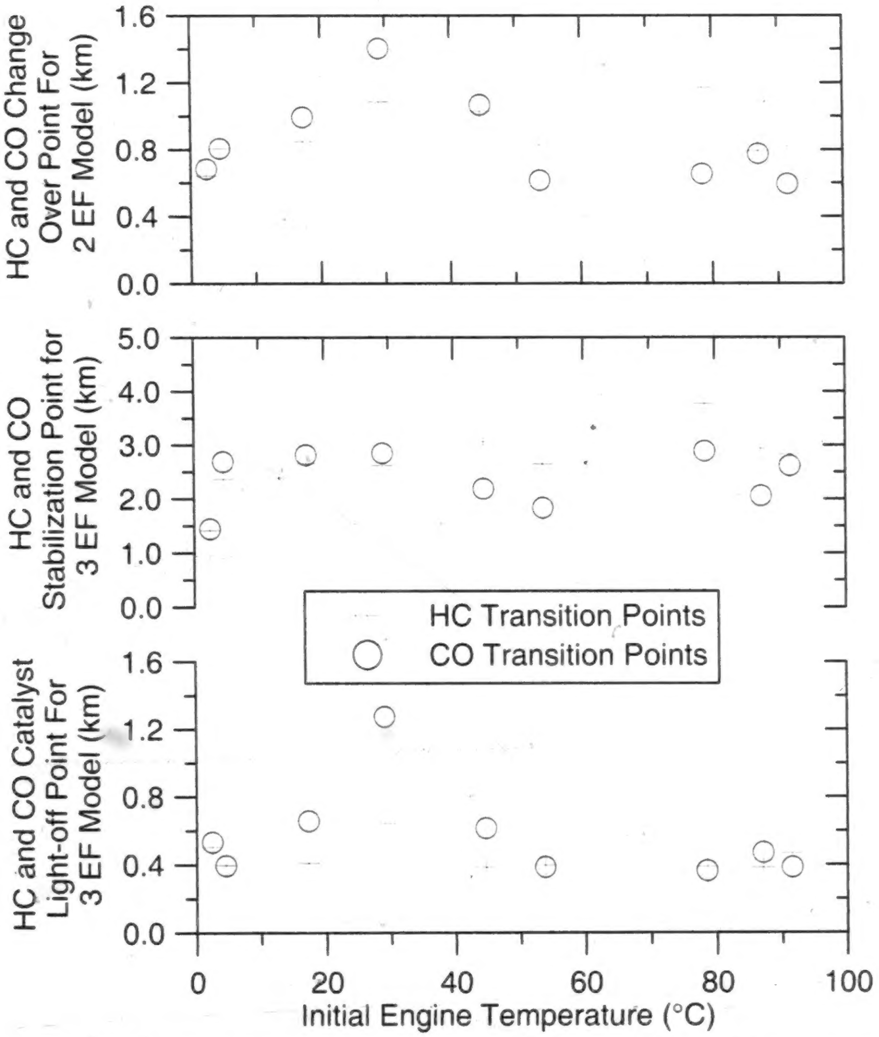

FIGURE 4-20 INITIAL ENGINE TEMPERATURE EFFECT ON HC AND CO CHANGE-OVER POINTS FOR THE TWO AND THREE EMISSION FACTOR MODELS

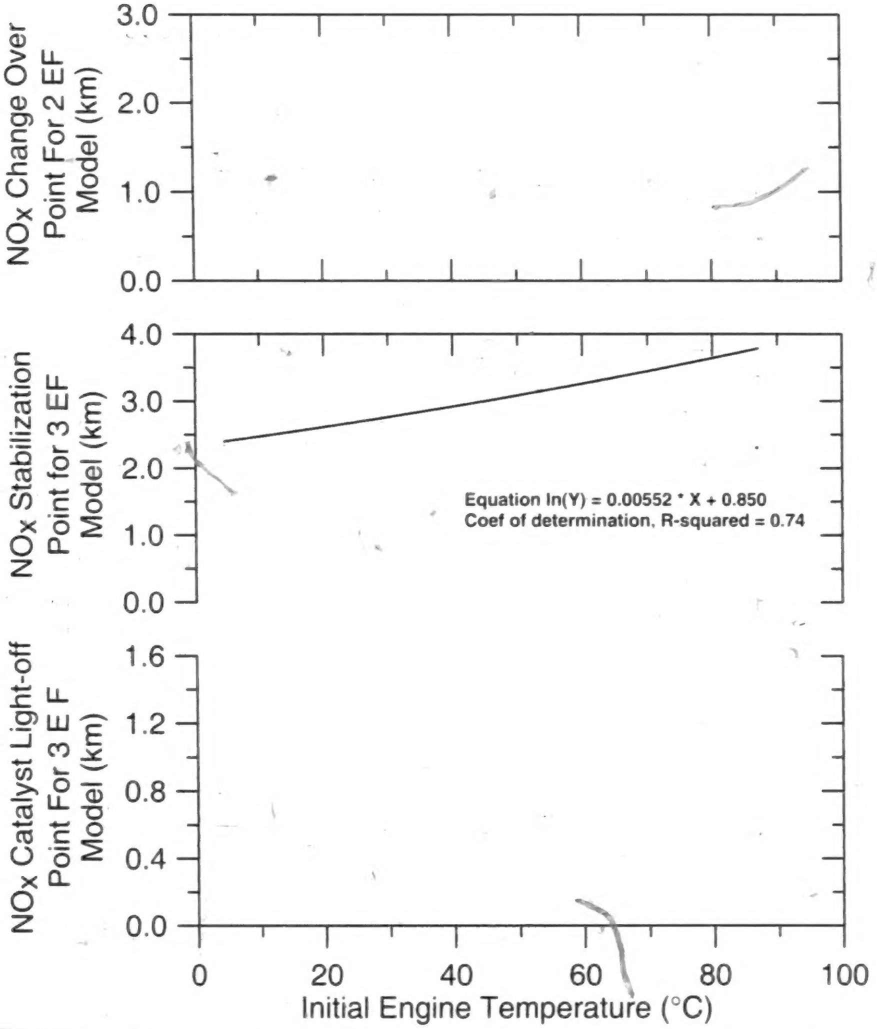

FIGURE 4-21 INITIAL ENGINE TEMPERATURE EFFECT ON NO_X CHANGE-OVER POINTS FOR THE TWO AND THREE EMISSION FACTOR MODELS

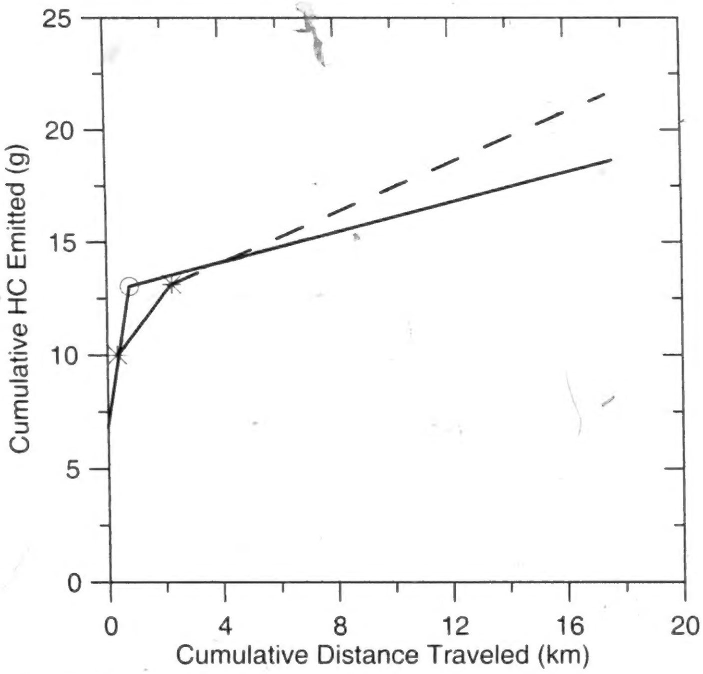

Figure 4-22 CUMULATIVE HC EMISSION PROFILE SHOWING LOSS OF HC EMISSION CONTROL AFTER TEMPERATURE STABILIZED

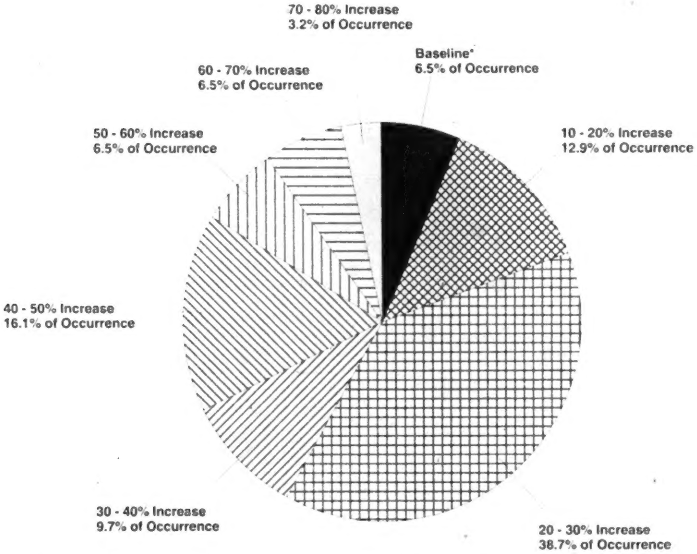

FIGURE 4-23 MAGNITUDE AND FREQUENCY OF HC EMISSION FAILURE (* - EMISSIONS WITH A FUNCTIONING EMISSION CONTROL SYSTEM)

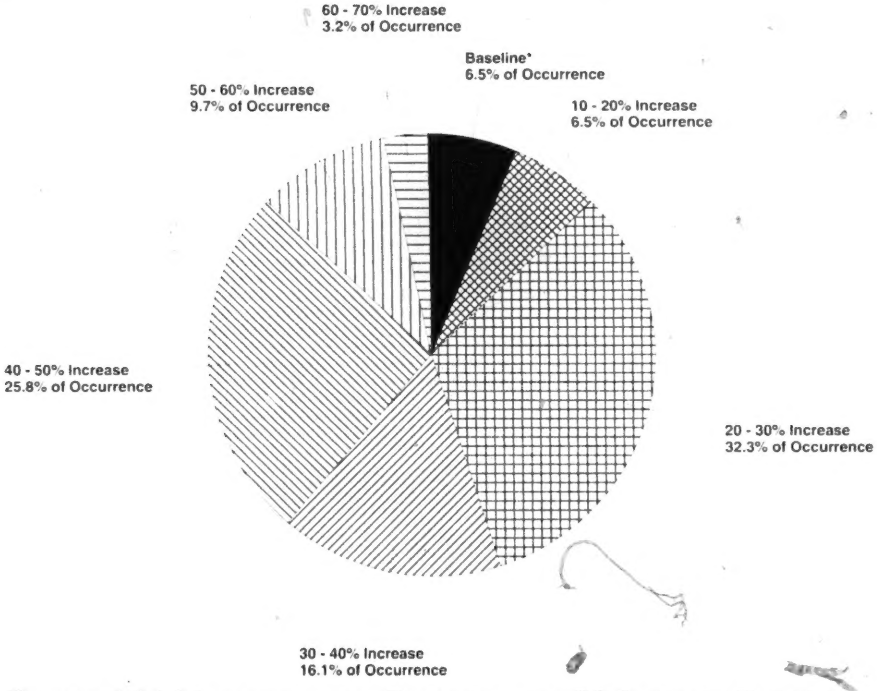

FIGURE 4-24 MAGNITUDE AND FREQUENCY OF CO EMISSION FAILURE (* - EMISSIONS WITH A FUNCTIONING EMISSION CONTROL SYSTEM)

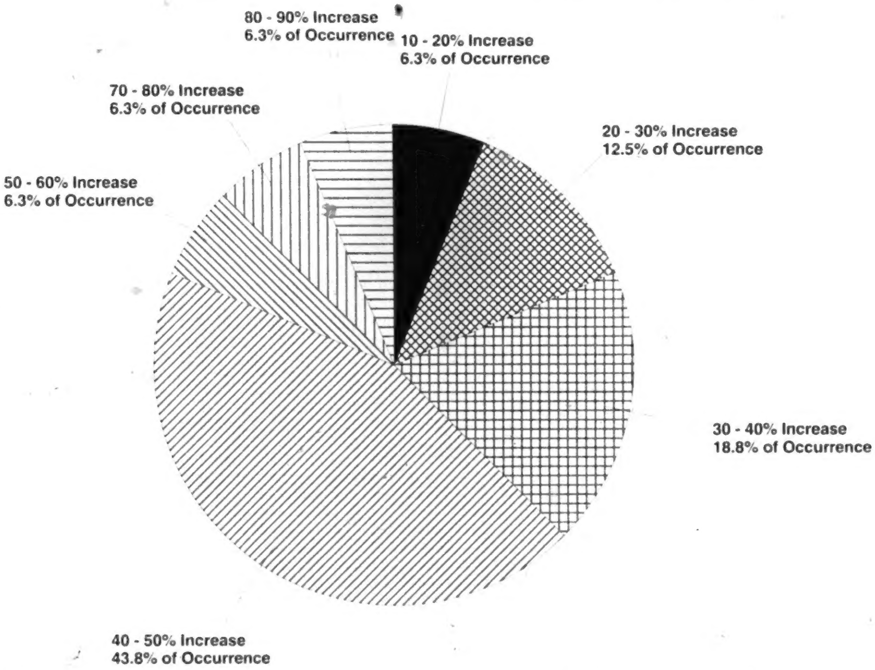

FIGURE 4-25 MAGNITUDE AND FREQUENCY OF NO_X EMISSION FAILURE

REFERENCES

1. St. Denis M.J., Winer A.M., "Prediction of On-Road Emissions and Comparison of Modeled On-Road Emissions to Federal Test Procedures Emissions," Environmental Science and Engineering Program. Environmental Health Sciences Department. School of Public Health. University of California, Los Angles. (310) 825 - 3161.

2. Hawirko J.D., Checkel M.D., "Real-Time, On-Road Measurements of Driving Behavior, Engine Parameters and Exhaust Emissions" SAE Technical Paper 2002-01-1714, Society of Automotive Engineers, 2001.

3. Goodwin R., Ross M.H., "Off-Cycle Exhaust Emissions from Modern Passenger Cars with Properly-Functioning Emission Controls," SAE Technical Paper 960064, Society of Automotive Engineers, 1996.

4. Watson H.C., Milkins E.E., Preston M.O., Chittleborough C., Beardsley P.A., "In-Use Vehicle Survey of Fuel Consumption and Emissions on Dynamometer and Road," SAE Technical Paper 850524, Society of Automotive Engineers, 1985

5. St. Denis M.J., Cicero-Fernandez P., Winer A.M., Butler J.W., Jension G., "Effects of In-Use Driving Conditions and Vehicle/Engine Operating Parameters on "Off-Cycle" Events: Comparison with Federal Test Procedure Conditions," Journal of Air and Waste Management Technical Paper, Vol 44, Pages 31-38, January, 1994.

6. Enns P., German J., Markey J., "EPA's Survey of In-Use Driving Patterns: Implications for Mobile Source Emission Inventories," USEPA Technical Report, 1993.

7. Laurikko J., Erlandsson L., Arbrahamsson R., "Exhaust in Cold Ambient Conditions: Considerations for a European Test Procedure," SAE Technical Paper 95923, Society of Automotive Engineers, 1995.

8. Laurikko J., Aakko P., "The Effect of Ambient Temperature on the Emissions of Some Nitrogen Compounds: A Comparative Study on Low-, Medium- and High Mileage Three-Way Catalyst Vehicles," SAE Technical Paper 950933, Society of Automotive Engineers, 1995.

9. Eccleston B.H., Hurn R.W, "Ambient Temperature and Trip Length – Influence on Automotive Fuel Economy and Emissions," SAE Technical Paper 780613, Society of Automotive Engineers, 1978.

10. Taylor G.W.R., Stewart S., "Cold Start Impact on Vehicle Energy Use," SAE Technical Paper 2001-01-0221, Society of Automotive Engineers, 2001.

11. Gurney M.D., Allsup J.R., "Predictability of Emissions from In-Use Vehicles at Low-Ambient Temperature and Alternate Driving Cycle Based on Standard Tests," SAE Technical Paper 890625, Society of Automotive Engineers, 1989 .

12. Larson R.E., "Vehicles Emission Characteristics Under Cold Ambient Conditions," SAE Technical Paper 890021, Society of Automotive Engineers, 1989.

13. Polak J.C., "Cold Ambient Temperature Effects on Emissions from Light-Duty Motor Vehicles," SAE Technical Paper 741051, Society of Automotive Engineers, 1974.

14. Ginberg L., Morgan L., "Effect of Temperature on Exhaust Emissions," SAE Technical Paper 740527, Society of Automotive Engineers, 1974.

15. Laurikko J., Nylund N. "Regulated and Unregulated Emissions from Catalyst Vehicles at Low Ambient Temperatures," SAE Technical Paper 930946, Society of Automotive Engineers, 1993.

16. Laurikko J., Nylund N.O., Sipila K.,"Automotive Exhaust Emissions at Low Ambient Temperature," Valtion teknillinen tutkimuskeskus, Tutkimuksia Statens tekniska forskingscentral, Forskingsrapporter Technical Research Centre of Finland, Research Reports, 1987.

17. Braddock J.N.,"Impact of Low Ambient Temperature on 3-Way Catalyst Car Emissions," SAE Technical Paper 810280, Society of Automotive Engineers, 1981.

18. Milkins E., Watson H., Comparison of Urban Driving Patters" SAE Technical Paper 830939, Society of Automotive Engineers, 1983.

19. Rijkeboer R.C., Hendriksen P., Hollemans B., van der Weide J., (1994) "Potential Impact of Four Different Car Fuels on the Dutch Environment" SAE Technical Paper 941914, 1994.

20. Kruse R.E., Huls T., "Development of the Federal Urban Driving Schedule," SAE Technical Paper 730553, Society of Automotive Engineers, 1973.

21. Mondt J.R., "Clearer Cars: The History and Technology of Emission Control Since the 1960s" Society of Automotive Engineers, Warrendale PA, 2000.

22. Stephens R.D., Giles M.T., Groblicki P.J., Gorse R.A., McAlinden K.J., Hoffman D.B., James R., Smith S., "Real World Emissions Variability as Measured by Remote Sensors," SAE Technical Paper 940582, Society of Automotive Engineers, 1994.

23. Staab J., Schurmann D., "Measurement of Automobile Exhaust Emissions under Realistic Road Conditions," SAE Technical Paper 871986, Society of Automotive Engineers, 1987.

24. Unal A., Dalton R., Frey H.C., Rouphail N.M., "Simultaneous Measurement of On-Road Vehicle Emissions and Traffic Flow Using Remote Sensing and an Area-Wide Detector," Paper # 99-712, 1999.

25. Stephens R.D., "Remote Sensing Data and a Potential Model of Vehicle Exhaust Emissions," Journal of Air & Waste Management, Vol 44, pp 1284-1292, 1994.

26. Salt W., Checkel M.D., "A Fully Functional Natural Gas Pickup Truck - The University of Alberta 1993 NGV Challenge," Department of Energy, Austin, 1993.

27. "User's Guide to Mobile 5 (Mobile Source Emission Factor Model)" Environmental Protection Agency, EPA-AA-TEB-94-01, May 1994.

28. "Determination of Start Emissions as a Function of Mileage and Soak Time for 1981-1993 Model Year Light-Duty Vehicles" Environmental Protection Agency, EAP420-R-01-058, M6.STE.003, November 2001.

29. Heywood, J.B., "Internal Combustion Engine Fundamentals" McGraw-Hill, 1988.

CHAPTER 5

ON-ROAD CHARACTERIZATION OF DRIVER BEHAVIOR AND ITS INFLUENCE ON VEHICLE EMISSION FACTORS

Chapter 4 examined the effect of ambient / initial engine conditions on emission factors. Chapter 5 extends the emission factor model by examining the effects of driving profiles, namely the non-zero average vehicle speed. This analysis made use of the same experiments, but separated each trip into different segments, depending on the traffic profiles. As a result, the correction factor / equations from the temperature analysis were implemented to adjust all of the segmented emission factors to a common temperature of +20°C. The resulting trends of the emission factors were then correlated to the non-zero average speed variable. This chapter presents the complete two emission factor model as functions of driving profiles and (ambient & initial engine) temperatures.

Chapter 5 is a paper which was written in the Society of Automotive Engineers format but will not be publish in this form. This stand alone paper includes a summary the work published in Chapters 3 & 4 and utilizes similar arguments and justifications for the development of an in-use and real-time measurement system.

ABSTRACT

This paper describes vehicle emission behavior and the effects of traffic patterns on vehicle emission factors. The paper also develops an emission profiling model consisting of (1) start/idling phases,(2) pre-light-off regions and (3) post-light-off operation. Vehicle operating parameters, fuel consumption and emissions were measured on-road using a portable system which was designed for ease of use with a range of vehicles, drivers and driving situations. The data reported come from repeated trips over a 17.4 km urban / suburban commute with a particular vehicle that could meet Tier 1 standards at normal conditions. As such, the resulting emission models do not represent the current on-road fleet. Instead, they show the importance of ambient temperature, initial engine temperature and traffic patterns in determining emissions. This leads to an appreciation to the value of on-road testing as a basis for emission inventories.

Truncated sections of commuting trips were analyzed to correlate emission factors to non-zero average vehicle speeds. (The influence of ambient / engine conditions and correction equations are presented in an accompanying paper, Chapter 4). The analysis shows that the emission factors are extremely sensitive to different driving patterns and that single-value emission factors based on standard certification tests do not necessarily provide an accurate representation of on-road vehicle emissions performance. Multiple emission factors are required to describe the pollution characteristics of vehicles operating in various traffic patterns. In this study the non-zero average vehicle speed was used as the parameter to describe various driving sequences. Strong correlations to non-zero average vehicle speeds were determined for the post-light-off emission

factors. Pre-light-off emission factors were found to correlate only to ambient temperatures. This paper develops a complete two emission factor model using the variable of ambient temperature (or initial engine temperature) and non-zero average vehicle speed to profile the emissions of the test vehicle.

5.0 INTRODUCTION

Automotive tailpipe emissions are known to contribute to urban air quality problems.(1) Emission inventories are used to estimate and predict the amount of pollution released into the atmosphere by automobiles. These inventories are generally based on a simple equation multiplying the number of current on-road vehicles, the number of vehicle miles traveled and sets of emission factors. The number of active on-road vehicles can be found from vehicle registries and the number of vehicle miles traveled can be estimated with traffic models. Currently, emission factors are determined from chassis dynamometer experiments and sometimes include information from remote sensing studies. These emission factors are known with less certainty (in terms of real-world applications), leading to some questionable emission inventory estimates. Engine and chassis dynamometer experiments offer an excellent controlled, repeatable and comparable experiment, however concerns have been raised with the representative nature of the emission factors determined with this procedure. Actual vehicle operation in any urban area encompasses a wider range ambient conditions and driving profiles(2-6) when compared to the standard certification tests. Given the highly tuned nature of current engine control systems, the actual in-use emission levels are sensitive to nonstandard ambient and operating situations.

This research examines the influence of driving profiles on exhaust emissions with an on-road, real-time measurement system using a high mileage vehicle that could meet Tier 1 emission levels under standard test conditions.

Ambient temperature conditions are known to influence vehicular exhaust emissions.(7-17) Relationships between "real-world" emission factors and ambient temperatures was presented in Chapter 4 with developed correlations and simple emission factor models.

Driving behavior is also known to have a large effect on vehicular emissions,(18,19) and is the main subject of this paper. The majority of the testing for current emission factors is based on a single driving sequence which happens to be the same cycle used for vehicle tuning and certification testing, (i.e. FTP 75). This test cycle was originally derived from an on-street speed-time trace,(20,21) (measured in 1973 Los Angeles traffic and edited to limit the peak accelerations to values that any vehicle could attain). However, given increases in traffic congestion and varying vehicle capability, there is some doubt about how representative this cycle is for current driving patterns. Also, given the highly tuned nature of current engine controllers, it is questionable how well emission factors measured on the precisely controlled FTP-75 dynamometer cycle represent emission performance with slightly different operating parameters on the road. It is important to consider that all dynamometer studies are only simulations of on-road driving behavior and resulting tailpipe emissions.

Remote sensing studies improve the real-life behavior of emission measurements by covering a broad spectrum of in-use vehicles, (sampling hundreds or thousands of vehicles per day).(22-25) However, they only provide measurements of instantaneous emissions at a specific location and provide no indication of the vehicle operating parameters or emissions under different operating situations.

It is the focus of this paper to use the emission factor correlations developed in the ambient temperature analysis (Chapter 4) to identify factor relationships for driving profiles using the non-zero average vehicle speed variable. The various driving profiles were obtained from individual sections of the commuter trip driven in all of the experiments as described in the other two papers (Chapters 3 & 4) of this series.(2) The result of this work is to model emission factors as functions of (1) driving patterns (non-zero average vehicle speed) and (2) ambient / engine temperatures. With these emission factors, the pollution profiles for this test vehicle can be estimated.

Since this research only considers a single drive cycle and test vehicle / driver combination, the results clearly do not represent those of the entire fleet. However, this study has allowed the development of an "in-use, real-time" measurement system and required processing algorithms to expand this research to various vehicles, thus providing a true in-use emission factor database of the current fleet.

5.1 EXPERIMENTAL SET-UP / CONFIGURATION

The arrangement of sensors and connections with the data acquisition system is shown schematically in Figure 5-1. The emission measurements were based on a Vetronix PXA - 1100 five-gas analyzer which used a combination of infrared absorption and fast response chemical cells to measure Oxides of Nitrogen (NO_x), Hydrocarbons (HC), Carbon Monoxide (CO), Carbon Dioxide (CO_2) and Oxygen (O_2). Air mass consumption rate was measured by a Siemens HFM 62B mass air flow (MAF) sensor which had been calibrated against an ASME standard nozzle. Instantaneous fuel consumption rate was inferred using an ECM AFRecorder 2400E fast response lambda sensor in combination with the mass air consumption rate. Measured vehicle parameters included speed, (measured by a signal conditioning circuit on the stock vehicle speed sending unit), and coolant temperature, (measured by an AD590 temperature probe in the manifold crossover water jacket). Ambient temperatures were measured by two AD590 temperature probes, one in the vehicle's intake system under-hood before the throttle valve, and one attached to the vehicle's radio antenna. Barometric pressure was measured using a lab barometer at one end of the trip. Communication with all of the instruments and senors was conducted through a Fujitsu laptop computer running National Instruments Labview 6i. The five-gas analyzer composition data was communicated over a serial line and the other parameters were measured as analog signals using a National Instruments PCMCIA DAQCard-AL-16E-4 data acquisition (DAQ) card. Further measurement system and processing details are provided in SAE paper 2002-01-1717(2) (Chapter 3)

5.2 EXPERIMENTAL VEHICLE

A 1992 GMC 2500-series, two-wheel drive, regular cab pickup with 5.7L (350ci), automatic transmission and long box bed was used for this study. This vehicle class represents a significant fraction of the Edmonton, Alberta on-road fleet and, due to original standards and age, provides an even more significant fraction of the on-road emissions. The dry vehicle weight was approximately 2,100 kg (4,700 lbs.) and, at the start of testing in early July of 2001, the odometer read approximately 187,000 km. At the end of the data collecting phase, June of 2002, approximately 10,000 km were accumulated on the test vehicle. To avoid the complications of a severely aged catalyst, a replacement OEM catalytic converter was installed near the start of the test period. Multimode dynamometer testing showed that the vehicle would probably meet US Tier 1 standards in this condition. (This test vehicle was originally the University of Alberta entry in the 1993 NGV Challenge.(26) Before this test period, the engine and emission control systems were returned to stock gasoline configuration.

5.3 EMISSION FACTORS AS FUNCTIONS OF AMBIENT TEMPERATURES

The developed measurement system directly calculated the instantaneous emission profiles (on a g/s basis) which provided detailed insight as to the second-by-second emission behavior of the test vehicle. However, this information is of little use in the calculation and representation of the emission factors. Measurement of actual vehicle emission factors (in g/km or g/mi) requires integration of the instantaneous emission rates to present the cumulative emission with distance traveled. The emission factors are then the slopes of such plots of cumulative mass emission against distance traveled. The intercepts of these profiles indicated the amount of pollution emitted during the initial idling phase (50s in these experiments).

A generalized algorithm was developed to consistently extract emission factors from the cumulative emission curves for the 31 commuter trips. The range of ambient temperature in the analysis was -25 to 20°C. Specific details of the analysis algorithm can be found in an Chapter 4 & Appendix E. Figure 5-2 illustrates an example cumulative HC emission trace. The two emission factors, defining the two emission factor model, are the slopes of the cumulative trace in the "pre-catalyst-light-off" and "post-catalyst-light-off" regions. Previous research (Chapter 4) has shown that two emission factors are sufficient for emission profiling.

5.4 EXAMPLE OF DRIVING PATTERNS AND RESULTING EMISSION FACTORS

Figures 5-3 and 5-4 illustrate two examples of driving patterns on vehicle exhaust. The two driving profiles were obtained from Segments II and III of the commuting profile used for this research as described in accompanying papers(2) (Chapters 3 & 4). Within these segments the emission control system was operational and the engine had reached a stabilized temperature. Segment I of the commute was similar to Segment III in length and traffic conditions (i.e. free-flowing sub-urban driving), but was the section in which the vehicle was in the "pre-light-off and transition" phase. From examining the lower plots (velocity-time traces) in Figures 5-3 and 5-4 a clear visual difference can be seen between the two sequences. As displayed in the congested Segment (Figure 5-3) an average vehicle speed of 17 km/hr was attained whereas the non-zero average vehicle speed was 23 km/hr. In contrast, the free-flow profile (Figure 5-4) had an average vehicle speed of 41 km/hr and a non-zero average speed of 48 km/hr.

Figures 5-5 and 5-6 illustrate the modal analysis of the two sequences presented in Figures 5-3 and 5-4. In this analysis the four modes consisted of Idle, Acceleration, Deceleration and Cruise and are defined in Table 5-1. Figure 5-5, displaying the modal analysis for the congested profile, shows that only 15% of the test time was accumulated in the cruise mode where as 26% was spent in the idle mode. Comparing the positive Acceleration times, a 2.3% increase was found for the free-flow segment. (Positive acceleration and cruise modes are the most critical since these modes represent significant energy demands and emission rates.) In contrast, Figure 5-6 illustrates that the free-flowing sequence spent 25% (a 10% increase) in the cruise mode and 16% (a 10% decrease) in the idle mode.

TABLE 5-1 DEFINITIONS OF THE FOUR MODAL ANALYSIS VARIABLES(27)

	Variable Name	Definition
1	Idle	Proportion of idle time ($v <= 3$ km/hr and $\|a\| >= 0.1$ m/s^2)
2	Acceleration	Proportion of acceleration time ($a > 0.1$ m/s^2)
3	Deceleration	Proportion of deceleration time ($a < -0.1$ m/s^2)
4	Cruise	Proportion of constant speed time ($\|a\| <= 0.1$ m/s^2)

Before examining the emission data, it should be noted that the test vehicle's engine had reached the operating temperature before the start of the congested section (i.e. Section II). In addition, since the two profiles (i.e. free-flowing and congested) were part of the same morning commute, the ambient temperature of 4°C was excluded as a variable affecting the emissions.

The cumulative emission profiles (as functions of distance traveled) are illustrated for the congested section of the commute in the upper plot of Figure 5-3. Note that graphs similar to these were used in the determination of the test vehicle's emission factor as functions of ambient temperature. Also, shown in this figure are the emission factors based on the slope of the cumulative emission profiles. As shown, the calculated emission factors were 0.85, 8.8 and 0.23 g/km for the HC, CO and NO_x emissions respectively. A similar diagram, with respect to the free-flowing traffic scenario, is shown in the upper plot of Figure 5-4. The calculated emission factors for this section are 0.18, 2.4, and 0.10 g/km indicating a 79, 73 and 57% decrease for the respective emission factors of HC, CO and NO_x. This analysis has shown a minimum 57% decrease in emission factors for a 35% increase in non-zero average vehicle speed.

The analysis of the commuting driving profiles has found:

1. Different driving profiles were found within the same commuting sequence. This overall driving sequence was repeated in all of the conducted experiments.
2. Different emission factors were found for different driving profiles.

5.5 METHOD TO ADJUST EMISSION FACTORS FOR AMBIENT TEMPERATURE

With the emission factors calculated as functions of ambient temperatures, (as presented in Chapter 4) curves fits were applied through the data sets for both the pre and post-light-off emission factors. These curve fits allowed emission modeling of the pre and post-light-off sections for any given ambient temperature.

To describe the emission factor in terms of another variable, it was necessary to adjust (or translate) all of the emission factors, obtained at different ambient conditions, to a common temperature. Any remaining trends or scatter would be due to other variables of the experiment. In this analysis the common temperature chosen was 20°C since this represented the FTP standard test conditions. As presented in an accompanying paper (Chapter 4), fit equations were found for both functioning and non-functioning emission control systems. The fit equations used in the translation analysis are for the fully functioning emission control system. A similar analysis could have been conducted for the experiments where a mid test emission control failure occurred, but were not considered here.

With the influence of ambient temperature accounted for, the other major contributor to vehicle emissions was traffic profiles. Numerous variables describing traffic conditions were examined including: kJ/km, number of stops per km, mean positive acceleration of the sequence, and average vehicle speeds. The tractive energy determined from the dynamic model (Illustrated in Appendix B) was originally to be used as the second descriptive variable. However, further analysis of these values indicated no distinctive differences between different driving patterns. This was a result of the parameters describing the dynamics of the test vehicle (i.e. competing magnitudes of aerodynamic and inertial resistances) and narrow operating range (i.e. one particular drive cycle). It is hoped that future work examining different vehicles will make use of this analysis. It was determined that for this data set / experimental conditions, that the average vehicle speed provided the most informative correlations. However, since the average vehicle speed is biased by idle times, the average non-zero vehicle speed was implemented as the descriptive parameter of the driving sequences. The following section presents the results of this analysis for both the pre- and post-light-off emission factors for both cold and warm start experiments.

5.6 RESULTS OF TEMPERATURE ADJUSTED EMISSION FACTORS AND INFLUENCE OF VEHICLE SPEED

The emission factor results presented in this section were all corrected to a simulated ambient temperature of 20°C. The emission factors are presented in two sections; one for the pre-light-off (cold-start applications) and one for the post-catalyst light-off regions. Pre-light-off emission factors were found from examining the first 400m of all commuter profiles. The distance of 400m was chosen since it was found that no catalyst-light-off occurred before 400m for any ambient condition. Post-light-off emission factors were determined from examining the Segments II and III of the commuting profiles. These sections allowed a wide range of driving characteristics to be analyzed with resulting emission factors. The emission factors presented here are averages for the entire sequence examined. That is, the mass of the emissions for the sequence was divided by the distanced traveled to give a g/km value. In addition, no filtering or distinctions are made between functioning and partially non-functioning emission control systems for the HC and CO emission factors. However, the NO_x emission factors are separated based on a working or failing emission control system. The data sets are based on the 31 commuter trips used in Chapter 4.

5.6.1 CORRELATION OF EMISSION FACTORS FOR THE PRE-LIGHT-OFF REGION WITH NON-ZERO AVERAGE VEHICLE SPEED

Figures 5-7, 5-8 and 5-9 illustrate the temperature corrected emission factors as functions of non-zero average vehicle speed for the pre-light-off region. These emission factors were determined from analyzing the first 400m of the cold start morning commutes. This distance was chosen since the data presented in the temperature analysis indicated that the catalytic converter started to oxidize both HC and CO after 400m into the test regardless of the ambient temperature. The reduction of NO_x emissions started to occur at 1.8 km into the commute. This analysis ensured that the reported emission factors were truly the pre-light-off values, and all correlations were attributable to a non-functioning emission control system. It was possible to have negative emission factors as a result of the translation process, thus all negative emission factors have been removed from the figures.

Figure 5-7 displays the corrected pre-light-off HC emission factors as a function of non-zero average vehicle speed. As seen in the figure, a horizontal cluster of data (below 5 g/km) is visible with no clear correlation over the narrow range of non-zero average vehicle speed (15 - 24 km/hr). One outlier, due to a cold start temperature of -26°C is shown occurring at 16.5 km/hr and indicates 26 g/km. The narrow vehicle speed range is a result of driving though the same traffic conditions every morning. The narrow vehicle speed range is also presented in Figures 5-8 and 5-9. Since no clear correlation exists from this analysis, it was concluded that (for this particular test vehicle and commuting sequence), the pre-light-off emission factors were only functions of ambient temperature. It is unclear what this analysis would have found if a different type of driving profile had been used for the first 400m and is the subject of further research.

Figures 5-8 and 5-9 illustrate the corrected pre-light-off CO and NO_x emission factors as functions of non-zero average vehicle speed. As with the HC analysis, no clear tend existed over the narrow average non-zero speed range. It was concluded that these emission factors are not functions of the non-zero average vehicle speed variable but are functions of (ambient or initial engine) temperature.

This analysis has clearly shown that no correlations exist between pre-light-off emission factors and average vehicle speeds for the cold-start scenarios. A similar conclusion was also found for the warm start experiments. In addition, since the warm-starts were only conducted at a single ambient temperature of -20°C, no relationships could be derived linking warm start pre-light-off emission factors to ambient temperature, but is also consideration for future work.

5.6.2 CORRELATION OF EMISSION FACTORS FOR THE POST-LIGHT-OFF REGION WITH NON-ZERO AVERAGE VEHICLE SPEED

Figures 5-10, 5-11 and 5-12 illustrate the temperature corrected emission factors as functions of non-zero average vehicle speed. These emission factors were determined by examining Segments II and III of the morning commute. As was described earlier, the catalyst had reached the light-off temperature at 400m into the commute for HC and CO and 1.8 km for NO_x emissions. Since, Section II started at 6.1 km into the commute, a fully (and hopefully stable) operating catalyst and a stabilized engine temperature were expected. This ensured that the emission factors reported described the post-light-off region of the commute.

Due to the small sample size of the warm start experiments tested at a single ambient temperature, the results of the warm start post-light-off emission factors were not calculated. For modeling purposes, the results of the post-light-off emission factors from the cold start study should be used. This is justified because the post-light-off emission factors should not be functions of initial engine temperature but are functions of the ambient conditions. This analysis presented in Chapter 4, illustrated strong correlations of the post-light-off emission factors with ambient temperature and little variation with initial engine temperature.

Figure 5-10 details a power correlation for the temperature corrected HC emission factors with the non-zero average vehicle speed parameter. In contrast to the previous analysis for the pre-light-off emission factors, a wider non-zero average speed range (15 to 55 km/hr) of 40 km/hr is presented. This was a result of analyzing Segment II (a congested section) and Segment III (a free-flowing scenario). As presented in the figure, a logical result of decreasing HC emission factors is found with increasing non-zero average vehicle speeds. A 22 times difference was found for the corrected HC emission factors over the average speed range of 15 to 55 km/hr. For low non-zero average vehicle speeds the following inferences can be made: 1) the vehicle was driven with a lower average velocity and hence 2) a more congested traffic condition was experienced. For congested traffic patterns more standing start acceleration events occur. It is during these numerous acceleration events where fuel enrichment strategies(28) occur and result in higher instantaneous HC emission rates and thus higher emission factors.

The temperature corrected CO emission factors are presented in Figure 5-11. As with the HC correlation, a power fit described the emission factors over the non-zero average speed range. Similarly, the CO emission factors decrease with increasing non-zero average vehicle speed for the same reasons as presented above. A 6 times difference was found for the corrected CO emission factors over an average speed range of 15 to 55 km/hr. This plot shows more scatter in the data set than was found for the HC emission factors, indicating the sensitivity of the CO emission factors to this and other emission influencing variables.

Figure 5-12 illustrates the temperature corrected NO_x emission factors for two situations: (1) a functioning and (2) a non-functioning emission control system. The first data set shown is for the experiments where the emission control system was operating and are indicated by crosses. This data set shows a weak linear dependance with non-zero average vehicle speeds. A 1.5 times difference was found for the corrected NO_x emission factors over an average speed range of 15 to 55 km/hr. The data, consisting of experiments where no NO_x reduction occurred are plotted with circles. As shown, there was large scatter in the data set and no true correlation to non-zero average vehicle speed was found. These emission factor differences were possibly occurring due to an aged O_2 sensor with drift and/or offset measurement problems. However, only the emission factors and correlations of the functioning emission control system will be used for modeling purposes.

The analysis of the adjusted emission factors correlated to non-zero average vehicle speeds has shown:

1. No correlations were found for the temperature adjusted pre-light-off emission factors for the warm or cold start studies. These emission factors will only be considered functions of the ambient temperature.
2. The temperature adjusted post-light-off emission factors were found to have strong correlations to the non-zero average vehicle speed variable. All emission factors were found to decrease (with varying degrees) with increases in average vehicle speeds.

5.7 DESCRIPTION OF THE TWO EMISSION FACTOR MODEL

The model presented here uses starting/idling emission values and two sets of emission factors to fully describe the emission profiles of the test vehicle for cold and warm start applications. One factor describes the pre-light-off emissions and one to estimate the post-light-off emissions. The experimentally determined emission factors were correlated with variables consisting of ambient temperature (or initial engine temperature) and non-zero average vehicle speed. The general algorithm of the model is presented in Figure 5-13. The model has two paths, one for cold and one for warm start applications. However, both paths merge at the calculation for the post-catalyst light-off emission factors for the reasons presented above.

The first step in predicting the vehicle emissions is to account for the amount of pollution emitted during the starting/idling phase described by the ambient or initial engine temperatures. The next step is to calculate the pre-light-off emission factor and the corresponding change-over point, which was found to correlate with the ambient or initial engine temperature. The post-light-off emission factor is first calculated as a function of the non-zero average vehicle speed. A temperature correction is applied to this factor accounting for the ambient temperature influence. Once these terms have been calculated, the results are summed providing an estimate of the pollution emitted by the test vehicle.

5.7.1 Idle Emissions for Cold and Warm Start Applications

As presented in Chapter 4, the duration of the idle time after a vehicle start-up was 50s. During this time, a total mass of accumulated pollutants was calculated. Tables 5-2 and 5-3 list the mass correlations with ambient and initial engine temperatures (variable name "Temp") respectively. Note that no NO_x values are presented due to the insignificant accumulations found during the idle periods.

Table 5-2 Cold Start/Idle Mass Accumulation Correlations for a 50s Idle Time (Ambient Temperature Range of -30 to +20°C)

	HC	CO
Mass Correlation (g)	Mass = exp(-0.0720*Temp + 1.08)	Mass = -2.70*Temp + 58.7

Table 5-3 Warm Start/Idle Mass Accumulation Correlations for a 50s Idle Time (Initial Engine Temperature Range of 0 to +90°C)

	HC	CO
Mass Correlation (g)	Mass = exp(-0.0145*Temp + 0.696)	Mass = -0.320*Temp + 39.6

5.7.2 PRE-CATALYST LIGHT-OFF EMISSION FACTORS AND CHANGE-OVER POINTS FOR COLD AND WARM START APPLICATIONS

Table 5-4 lists the cold start pre-light-off emission factor correlation equations and change-over points. Table 5-5 lists the pre-light-off emission factors and corresponding change over points as functions of initial engine temperature.

Once the appropriate emission factor has been calculated, this factor is multiplied by the distance to which the factor applies. That is, if the vehicle is driven a distance less than the experimentally determined change-over point, then no further analysis is required, and the predicted emissions are simply the idle and pre-light-off contributions. However, if the vehicle travels farther than the calculated change-over point (which is usually the case), then the pre-light-off emission factor is multiplied by the change-over point distance. The remaining distance is multiplied by the post-light-off emission factor.

TABLE 5-4 COLD START HC, CO AND NO_x PRE-CATALYST LIGHT-OFF EMISSION FACTOR CORRELATIONS (AMBIENT TEMPERATURE RANGE OF -30 TO +20°C)

Pollutant	Correlation Equation (g/km)	Applicable Distance or Correlation (km)
HC	EF = exp(-0.0512*Temp + 1.94)	Dist = 0.00970*Temp + 0.723
CO	EF = -7.85*Temp + 283	0.750
NO_x	EF = -0.0298*Temp + 2.45	1.80

TABLE 5-5 WARM START HC, CO AND NO_x PRE-CATALYST LIGHT-OFF EMISSION FACTOR CORRELATIONS (INITIAL ENGINE TEMPERATURE RANGE OF 0 TO +90°C)

Pollutant	Correlation Equation (g/km)	Applicable Distance (km)
HC	EF = exp(-0.0114*Temp + 1.46)	0.89
CO	EF = exp(-0.0195*Temp + 5.15)	0.84
NO_x	EF = -0.0342*Temp + 4.36	1.29

5.7.3 AVERAGE SPEED INFLUENCE ON POST-CATALYST LIGHT-OFF EMISSION FACTORS

The emission factor describing the emissions of the post-light-off region is calculated as a function of two variables. The first variable considered is the influence of the non-zero average vehicle speed, as presented in this paper. An appropriate non-zero average vehicle speed must first be determined which describes the traffic conditions to be modeled. Once this variable has been chosen, the resulting emission factors can be found by using the experientially determined correlations as presented in Table 5-6.

TABLE 5-6 POST-CATALYST LIGHT-OFF HC, CO AND NO_x EMISSION FACTOR CORRELATIONS FOR NON-ZERO AVERAGE VEHICLE SPEEDS OF 10 TO 60 KM/HR

Pollutant	Correlation Equation (g/km)
HC	EF = exp(-2.29*ln(Non-Zero Average Speed) + 6.80)
CO	EF = exp(-1.22*ln(Non-Zero Average Speed) + 5.71)
NO_x	EF = -0.00250*(Non-Zero Average Speed) + 0.336

5.7.4 AMBIENT TEMPERATURE CORRECTION OF THE POST-CATALYST LIGHT-OFF EMISSION FACTORS

With the post-light-off emission factors calculated as a function of non-zero average vehicle speed, the factor must be corrected for the second variable of ambient temperature. The ambient temperature correction equations are presented in Table 5-7 and were determined in the analysis of Chapter 4. The "EF_{20C}" terms describe the emission factors found from Table 5-6.

TABLE 5-7 COLD START HC, CO AND NO_x POST-CATALYST LIGHT-OFF EMISSION FACTOR CORRECTIONS FOR AN AMBIENT TEMPERATURE RANGE OF -30 TO +20°C

Pollutant	Correction Equation (g/km)
HC	$EF = EF_{20C} - 0.00940 * (\text{Ambient Temperature} - 20)$
CO	$EF = EF_{20C} - 0.118 * (\text{Ambient Temperature} - 20)$
NO_x	$EF = EF_{20C} - 0.00170 * (\text{Ambient Temperature} - 20)$

Once the emission factors have been corrected for the temperature conditions, they are multiplied by the remaining travel distance, as determined from the pre-light-off analysis. Finally the mass emitted at idle, during the pre-catalyst light-off region and the mass from the post-light-off region are summed to give the pollution estimate of the test vehicle for the simulated distance.

5.8 CONCLUSIONS

This paper has examined the influence of traffic conditions on the emission profiles (and resulting emission factors) for a single vehicle / driver configuration. The emission measurements were conducted in a real-time and in on-road applications to improve the analysis of real-world vehicle emissions.

This research has extended the development of the simple temperature emission factor model with the introduction of the non-zero average vehicle speed variable. The pre-light-off emission factors were found to correlate well with ambient temperature and with initial engine temperature. As was shown in the analysis, no correlations were found for the temperature corrected pre-light-off emission factors with non-zero average vehicle speeds. The temperature corrected post-light-off emission factors were found to correlate with non-zero average vehicle speed allowing the characterization of emission behavior with two variables: non-zero average vehicle speed and ambient temperatures. In general, the post-light-off emission factors for HC and CO were found to decrease with increasing non-zero average vehicles speeds. This was a result of fewer fuel enrichment events due to fewer accelerations from zero velocity. The NO_x emission factors were also found to decrease with non-zero average vehicle speed.

This paper has also presented the complete set of correlations to fully model the emission profiles for both cold and warm start applications. The model consists of three sections, the mass emissions of: (1) the start/idling phase, (2) the pre-light-off section and (3) the post-light-off region.

In addition, the main goal of this research has been to develop test equipment and analysis to algorithms to analyze other vehicles representing the current on-road fleet.

5.9 FUTURE WORK

With the development of the measurement system and algorithms to analyze the data, numerous other test vehicles will be explored. This will allow the emission characterization of newer vehicles with more sophisticated emission control systems. Older vehicles with aged or non-functioning emission control systems will be tested to determine their impact on air pollution. Finally, more research is required to determine the effect of initial engine temperatures (i.e. soak times) on emission factors.

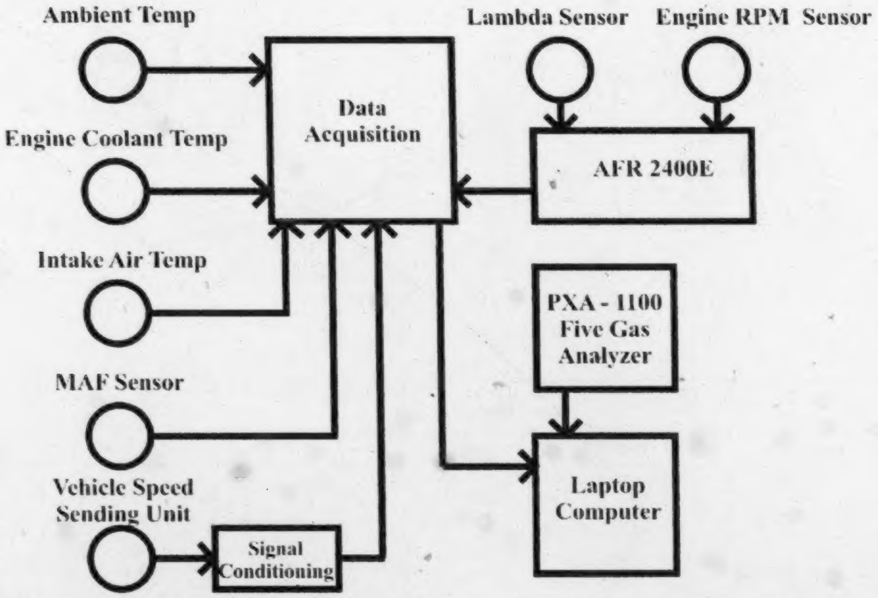

FIGURE 5-1 COMPONENTS OF THE ON-ROAD, REAL-TIME EMISSIONS SYSTEM

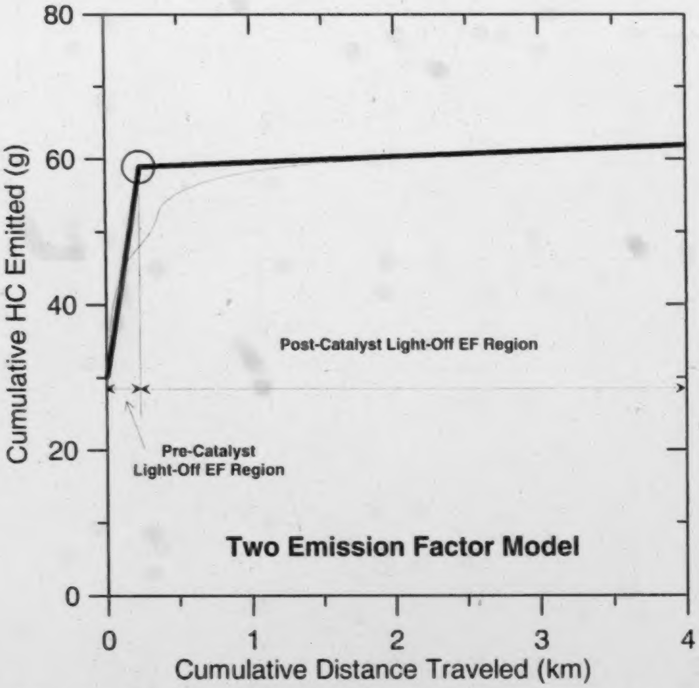

FIGURE 5-2 CUMULATIVE HC EMISSION PROFILE ILLUSTRATING THE TWO EMISSION FACTOR MODEL

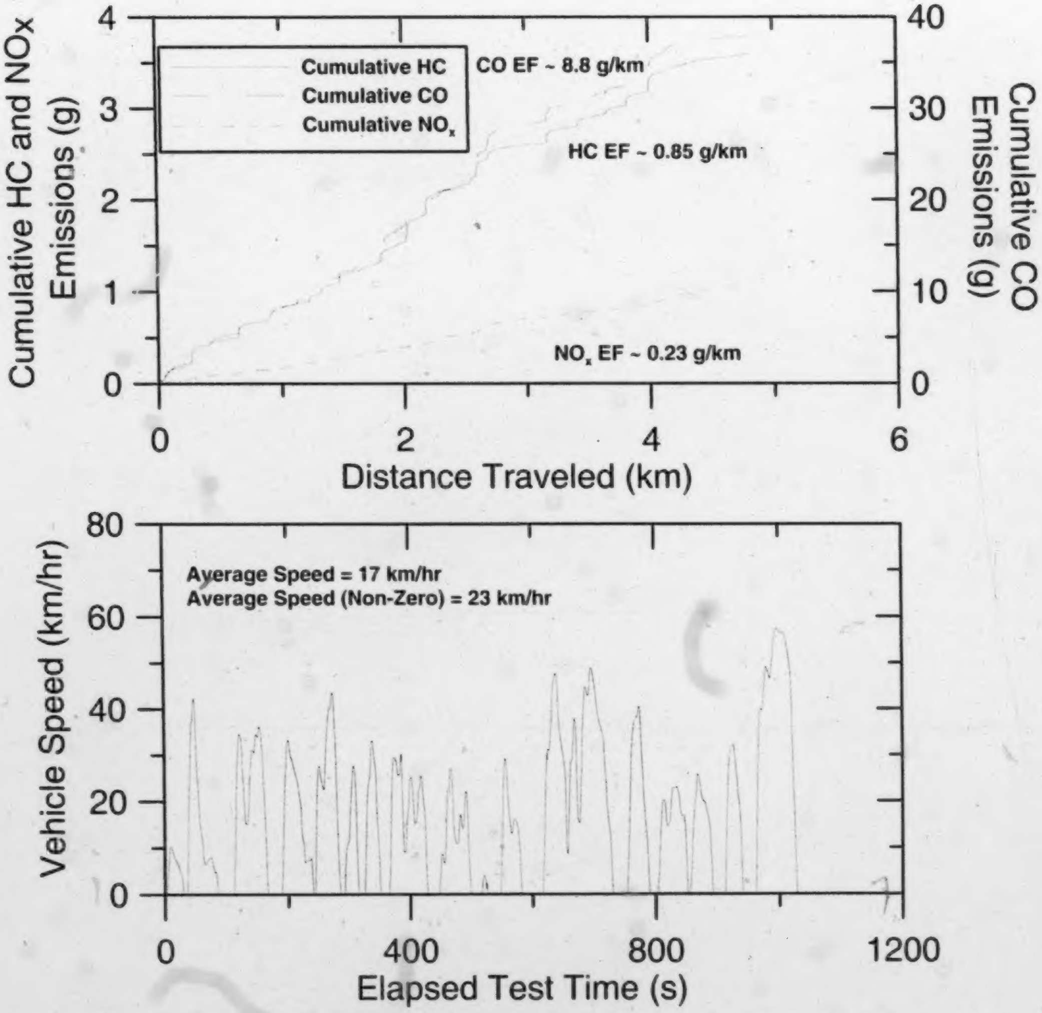

FIGURE 5-3 CONGESTED VELOCITY PROFILE WITH RESULTING EMISSION FACTORS (SECTION II OF COMMUTER TRIP)

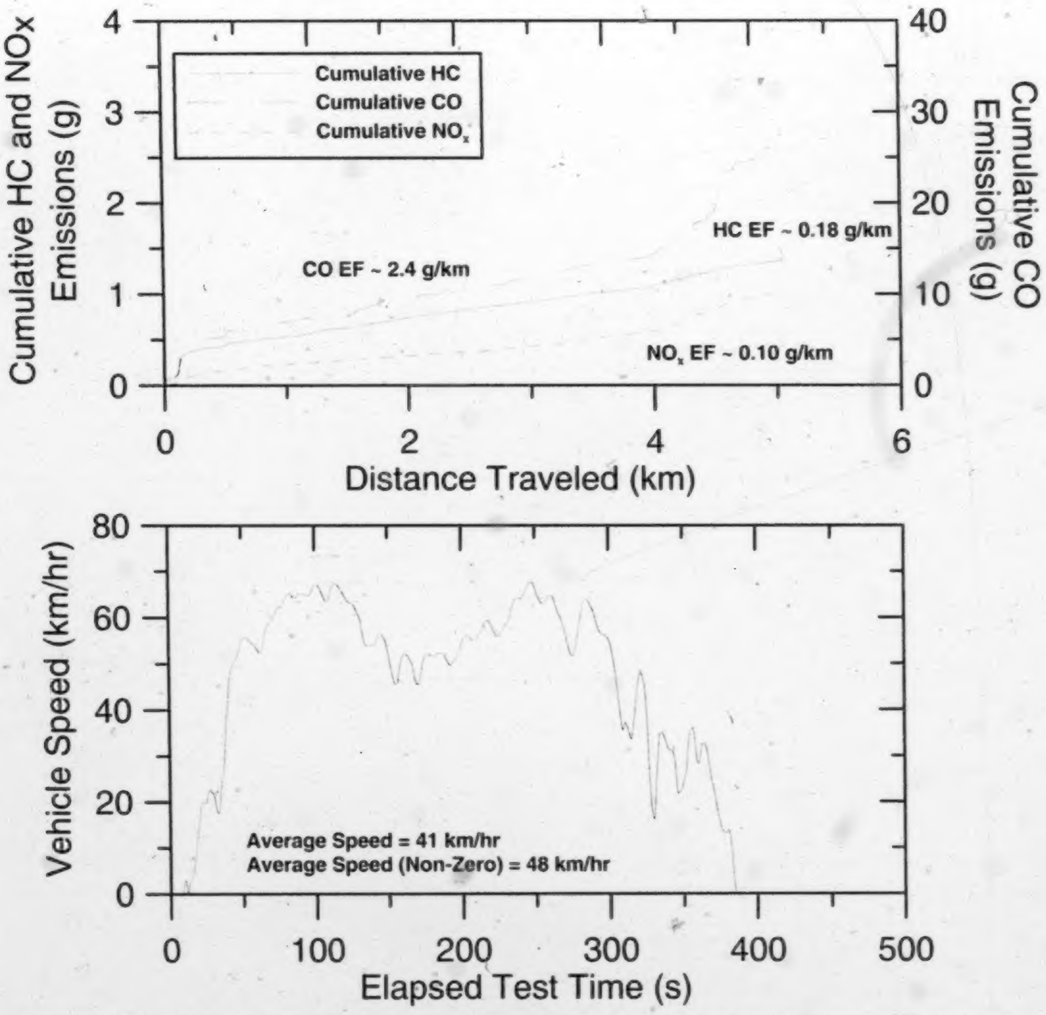

FIGURE 5-4 FREE-FLOWING VELOCITY PROFILE WITH RESULTING EMISSION FACTORS (SECTION III OF COMMUTER TRIP)

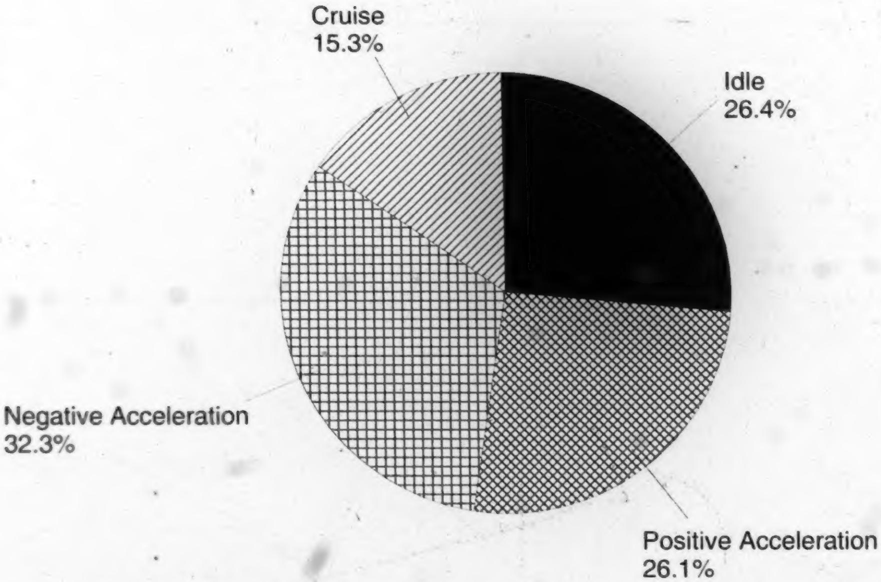

FIGURE 5-5 MODAL ANALYSIS FOR THE CONGESTED TRAFFIC PROFILE

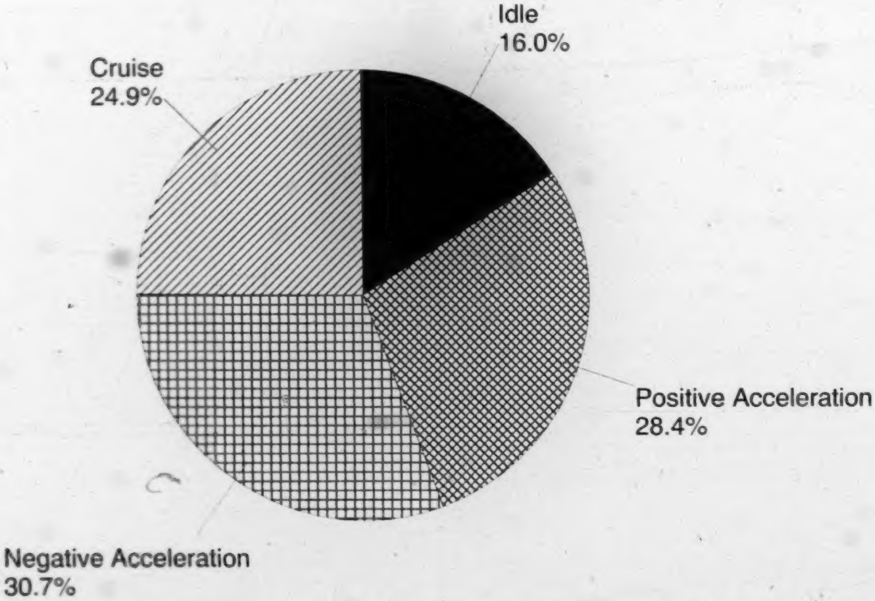

FIGURE 5-6 MODAL ANALYSIS FOR THE FREE-FLOWING TRAFFIC PROFILE

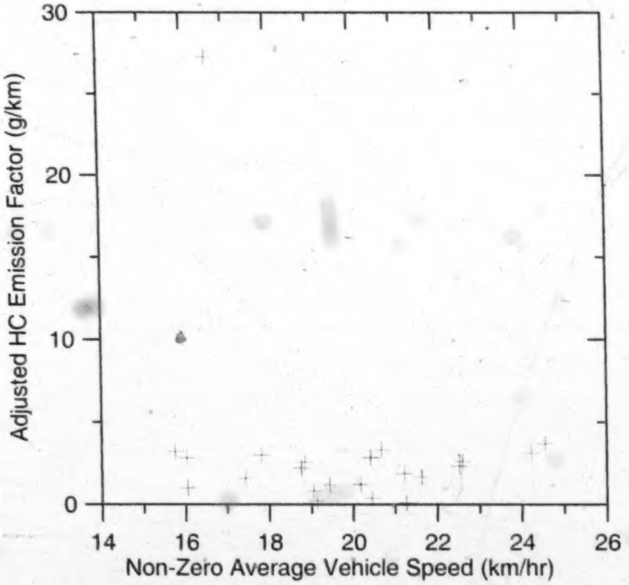

FIGURE 5-7 CORRELATION OF TEMPERATURE CORRECTED PRE-CATALYST LIGHT-OFF HC EF WITH NON-ZERO AVERAGE VEHICLE SPEED

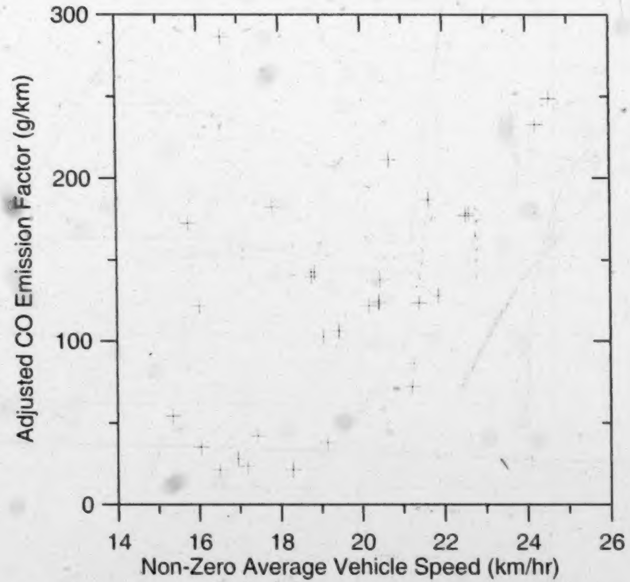

FIGURE 5-8 CORRELATION OF TEMPERATURE CORRECTED PRE-CATALYST LIGHT-OFF CO EF WITH NON-ZERO AVERAGE VEHICLE SPEED

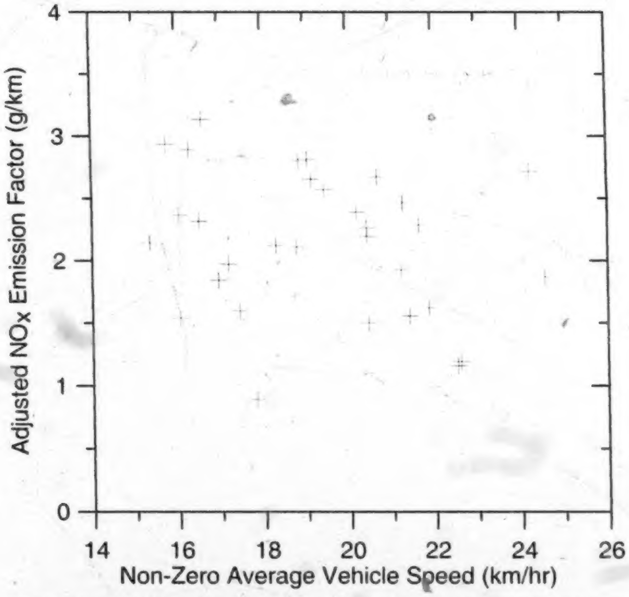

FIGURE 5-9 CORRELATION OF TEMPERATURE CORRECTED PRE-CATALYST LIGHT-OFF NO_x EF WITH NON-ZERO AVERAGE VEHICLE SPEED

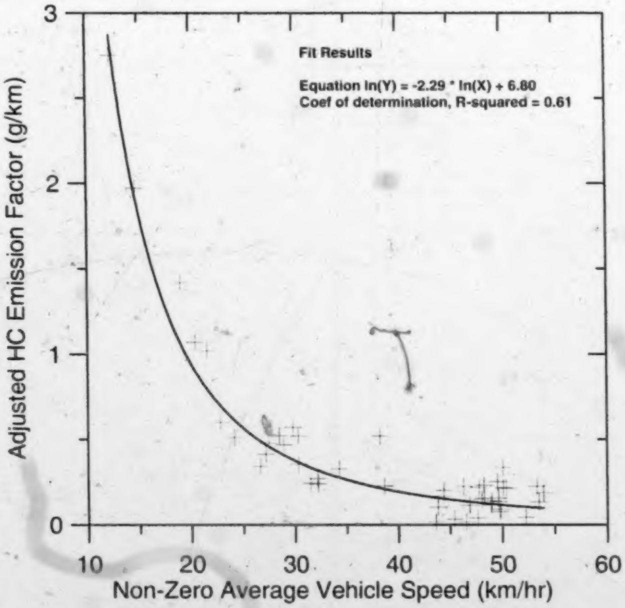

FIGURE 5-10 CORRELATION OF TEMPERATURE CORRECTED POST-CATALYST LIGHT-OFF HC EF WITH NON-ZERO AVERAGE VEHICLE SPEED

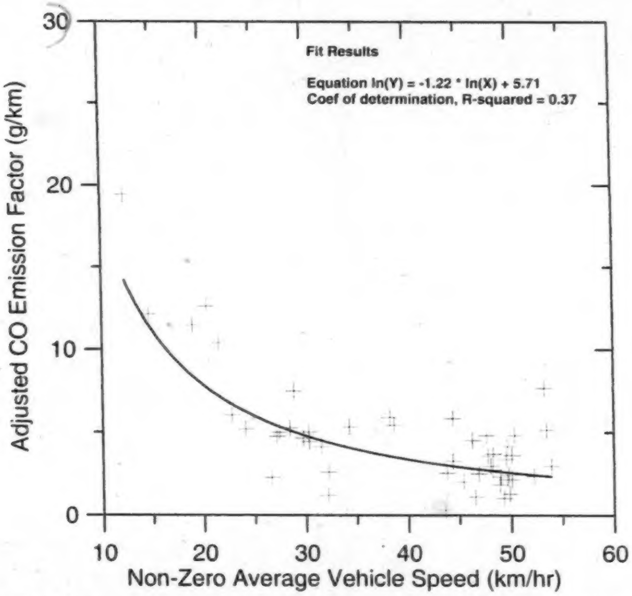

FIGURE 5-11 CORRELATION OF TEMPERATURE CORRECTED POST-CATALYST LIGHT-OFF CO EF WITH NON-ZERO AVERAGE VEHICLE SPEED

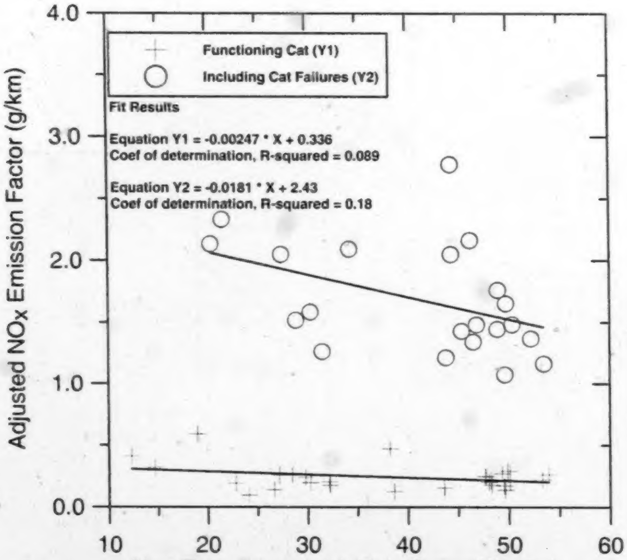

FIGURE 5-12 CORRELATION OF TEMPERATURE CORRECTED POST-CATALYST LIGHT-OFF NO_x EF WITH NON-ZERO AVERAGE VEHICLE SPEED

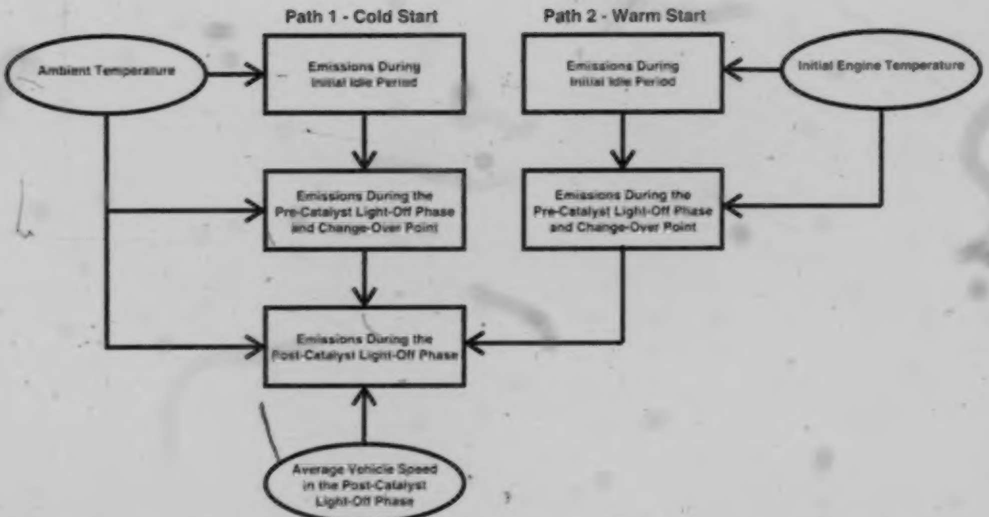
Path 1 - Cold Start
Path 2 - Warm Start
Ambient Temperature
Emissions During Initial Idle Period
Emissions During Initial Idle Period
Initial Engine Temperature
Emissions During the Pre-Catalyst Light-Off Phase and Change-Over Point
Emissions During the Pre-Catalyst Light-Off Phase and Change-Over Point
Emissions During the Post-Catalyst Light-Off Phase
Average Vehicle Speed in the Post-Catalyst Light-Off Phase

FIGURE 5-13 DERIVED ALGORITHM FOR EMISSION PROFILING USING EXPERIMENTAL EMISSION FACTORS

REFERENCES

1. St. Denis M.J., Winer A.M., "Prediction of On-Road Emissions and Comparison of Modeled On-Road Emissions to Federal Test Procedures Emissions," Environmental Science and Engineering Program. Environmental Health Sciences Department. School of Public Health. University of California, Los Angles. (310) 825 - 3161.

2. Hawirko J.D., Checkel M.D., "Real-Time, On-Road Measurements of Driving Behavior, Engine Parameters and Exhaust Emissions" SAE Technical Paper 2002-01-1714, Society of Automotive Engineers, 2001.

3. Goodwin R., Ross M.H., "Off-Cycle Exhaust Emissions from Modern Passenger Cars with Properly-Functioning Emission Controls," SAE Technical Paper 960064, Society of Automotive Engineers, 1996.

4. Watson H.C., Milkins E.E., Preston M.O., Chittleborough C., Beardsley P.A., "In-Use Vehicle Survey of Fuel Consumption and Emissions on Dynamometer and Road," SAE Technical Paper 850524, Society of Automotive Engineers, 1985

5. St. Denis M.J., Cicero-Fernandez P., Winer A.M., Butler J.W., Jension G., "Effects of In-Use Driving Conditions and Vehicle/Engine Operating Parameters on "Off-Cycle" Events: Comparison with Federal Test Procedure Conditions," Journal of Air and Waste Management Technical Paper, Vol 44, Pages 31-38, January, 1994.

6. Enns P., German J., Markey J., "EPA's Survey of In-Use Driving Patterns: Implications for Mobile Source Emission Inventories," USEPA Technical Report, 1993.

7. Laurikko J., Erlandsson L., Arbrahamsson R., "Exhaust in Cold Ambient Conditions: Considerations for a European Test Procedure," SAE Technical Paper 95923, Society of Automotive Engineers, 1995.

8. Laurikko J., Aakko P., "The Effect of Ambient Temperature on the Emissions of Some Nitrogen Compounds: A Comparative Study on Low-, Medium- and High Mileage Three-Way Catalyst Vehicles," SAE Technical Paper 950933, Society of Automotive Engineers, 1995.

9. Eccleston B.H., Hurn R.W, "Ambient Temperature and Trip Length – Influence on Automotive Fuel Economy and Emissions," SAE Technical Paper 780613, Society of Automotive Engineers, 1978.

10. Taylor G.W.R., Stewart S., "Cold Start Impact on Vehicle Energy Use," SAE Technical Paper 2001-01-0221, Society of Automotive Engineers, 2001.

11. Gurney M.D., Allsup J.R., "Predictability of Emissions from In-Use Vehicles at Low-Ambient Temperature and Alternate Driving Cycle Based on Standard Tests," SAE Technical Paper 890625, Society of Automotive Engineers, 1989 .

12. Larson R.E., "Vehicles Emission Characteristics Under Cold Ambient Conditions," SAE Technical Paper 890021, Society of Automotive Engineers, 1989.

13. Polak J.C., "Cold Ambient Temperature Effects on Emissions from Light-Duty Motor Vehicles," SAE Technical Paper 741051, Society of Automotive Engineers, 1974.

14. Ginberg L., Morgan L., "Effect of Temperature on Exhaust Emissions," SAE Technical Paper 740527, Society of Automotive Engineers, 1974.

15. Laurikko J., Nylund N. "Regulated and Unregulated Emissions from Catalyst Vehicles at Low Ambient Temperatures," SAE Technical Paper 930946, Society of Automotive Engineers, 1993.

16. Laurikko J., Nylund N.O., Sipila K., "Automotive Exhaust Emissions at Low Ambient Temperature," Valtion teknillinen tutkimuskeskus, Tutkimuksia Statens tekniska forskingscentral, Forskingsrapporter Technical Research Centre of Finland, Research Reports, 1987.

17. Braddock J.N., "Impact of Low Ambient Temperature on 3-Way Catalyst Car Emissions," SAE Technical Paper 810280, Society of Automotive Engineers, 1981.

18. Milkins E., Watson H., Comparison of Urban Driving Patters" SAE Technical Paper 830939, Society of Automotive Engineers, 1983.

19. Rijkeboer R.C., Hendriksen P., Hollemans B., van der Weide J., (1994) "Potential Impact of Four Different Car Fuels on the Dutch Environment" SAE Technical Paper 941914, 1994.

20. Kruse R.E., Huls T., "Development of the Federal Urban Driving Schedule," SAE Technical Paper 730553, Society of Automotive Engineers, 1973.

21. Mondt J.R., "Cleaner Cars: The History and Technology of Emission Control Since the 1960s" Society of Automotive Engineers, Warrendale PA, 2000.

22. Stephens R.D., Giles M.T., Groblicki P.J., Gorse R.A., McAlinden K.J., Hoffman D.B., James R., Smith S., "Real World Emissions Variability as Measured by Remote Sensors," SAE Technical Paper 940582, Society of Automotive Engineers, 1994.

23. Staab J., Schurmann D., "Measurement of Automobile Exhaust Emissions under Realistic Road Conditions," SAE Technical Paper 871986, Society of Automotive Engineers, 1987.

24. Unal A., Dalton R., Frey H.C., Rouphail N.M., "Simultaneous Measurement of On-Road Vehicle Emissions and Traffic Flow Using Remote Sensing and an Area-Wide Detector," Paper # 99-712, 1999.

25. Stephens R.D., "Remote Sensing Data and a Potential Model of Vehicle Exhaust Emissions," Journal of Air & Waste Management, Vol 44, pp 1284-1292, 1994.

26. Salt W., Checkel M.D., "A Fully Functional Natural Gas Pickup Truck - The University of Alberta 1993 NGV Challenge," Department of Energy, Austin, 1993.

27. Klingenberg H., "Automobile Exhaust Emission Testing," New York, Springer, 1996.

28. Heywood, J.B., "Internal Combustion Engine Fundamentals" McGraw-Hill, 1988.

CHAPTER 6

CONCLUSIONS

Chapter 6 states the general conclusions obtained from the work.

This MSc. Thesis was a study on quantifying vehicle emissions (emission factors) with a real-time, on-road measurement system. The emission factor results presented in the previous chapters do not represent those of the entire on-road fleet. However, this research showed that on-road emissions could be represented by a two emission factor model. The individual achievements included:

1. The development of an in-use and real-time measurement system.
2. The ability to predict emission factors (pre, transitional and post catalyst light-off) based on ambient / initial engine conditions and corresponding change-over points.
3. Correlation of the temperature corrected post-light-off emission factor to non-zero average vehicle speed.
4. A two emission factor model was developed. This model combined the temperature and non-zero average vehicle speed analysis to predict the emission factors.
5. The detection of emission system control failures and low test-to-test repeatability.

The first part of the research was to develop a portable measurement system which would allow real-time emission measurements to be made. After the system was designed, justification of the system was made with the analysis of a set of commuter trips. This analysis illustrated the ability of the system to capture the performance of the vehicle and widely varying emission / consumption traces.

The second goal of this study was to develop correlation equations relating the emission factors of the test vehicle to either the ambient temperature or the initial engine conditions. This analysis required development of algorithms to analyze the cumulative emission profiles. The designed algorithms provided unbiased emission factor values and change-over points. The resulting analysis proved that all emission factors (pre, transitional and post-catalyst light-off) increased with decreasing ambient / initial engine temperatures. It was also discovered that typical magnitude increases between the cold-start pre and post light-off emission factors were 100, 60 and 10 for the emissions of HC, CO and NO_x respectively.

The third accomplishment of this research was to relate the experimental emission factors to driving or traffic conditions. Initially the tractive power model was to be used as the second descriptive variable. An in-depth analysis illustrated that this parameter was unable to distinguish a congested sequence from a free-flowing traffic profile. This result was traced to competing aerodynamic and inertial resistance terms in the dynamic model for this particular test vehicle. Therefore, the average non-zero vehicle speed variable was used as the second variable. The temperature corrected post-light-off emission factors were found to strongly correlate to non-zero average vehicle speed. The pre-light-off emission factors were found to be only functions of ambient or initial engine temperature. Trends of decreasing emission factor magnitudes with increasing non-zero average vehicle speeds were found for all measured emissions.

The fourth achievement was the development of a two emission factor model. It allows the prediction of the test vehicle's emission factors for both cold and warm-starts. It either uses the ambient (or initial engine) temperature too calculated the pre-light-off emission factors. The post-light-off emission factors are further described by a second variable, the non-zero average vehicle speed, to allow variations in traffic patterns.

Finally, in in addition to the determination of the emission factors, numerous emission control anomalies were discovered throughout this research. Lean burn scenarios were found which resulted in low HC and CO emissions but led to increased NO_x levels. Numerous catalyst failures were measured in mid-trip experiments which led to short-term emission factor magnitudes similar to the pre-catalyst light-off values for all emissions. Lastly, complete catalyst failure situations were measured for NO_x emissions. These situations occurred with no loss in vehicle performance or indication to the driver. However the result of these occurrences implies low test to test repeatability and will result in large errors when estimating vehicle emissions.

With the development of the measurement system and algorithms to analyze the data, numerous other test vehicles could be explored. Both older and newer vehicles could be tested to determine the emission performance of different emission control systems. More research is required to determine the effect of initial engine temperatures (i.e. soak times) on the emission factors. Future work could also examine the effects of different driver and route combinations.

APPENDIX A

ACCOUNTING FOR THE TIME DELAY OF THE GAS ANALYSER

A time shifting algorithm was devised to match up the volumetric concentrations of the exhaust species to the instantaneously determined exhaust mass flow rates. Synchronization of these two data sets was essential in order to determine the correct mass flow rates of the corresponding emissions. As a result, a behavioural study of the PXA-1100 five gas analyser and associated sampling system was required to determine the appropriate time delay values and is presented in this Appendix.

The time shifting values used in this research were 8.0 and 10.0 seconds for the NDIR and electrochemical measurement techniques which incorporated:

1. Transport Delay. This delay accounted for the transit time of the exhaust sample from the tail pipe to the gas analyser.
2. First Order Time Constant. This time constant was based on the 2/3 transient rise time for a step change concentration. The 2/3 output value was chosen for comparison purposes since the time the instrument takes to respond to 2/3 of the final value is the first order time constant of the instrument.(1)

This appendix examines three delays of the emission measurement system. The first delay was associated with the time response of the gas analyser itself. The second delay was due to the transport of the exhaust sample from the tail pipe of the test vehicle to the gas analyser including the transient response of the analyser itself. The last delay considered was varying exhaust transit times through the exhaust system of the test vehicle. The following is a detailed explanation of the behaviour of the PXA-1100 and steps involved in determining the proper time delays. This analysis provides the methodology used to first estimate and finalize the time shifting values.

GAS ANALYSER DELAY TIME

The first test determined the response time of the PXA-1100 to a step change concentration without the use of the sample line. This experiment was conducted by allowing the gas analyser to first sample ambient air and then introducing the analyser to a known step change concentration. These known concentrations were placed into the inlet section of the gas analyser, thus allowing the response time of only the PXA - 1100 to be determined. Figures A-1 through A-5 illustrate the results for a set of repeated experiments.

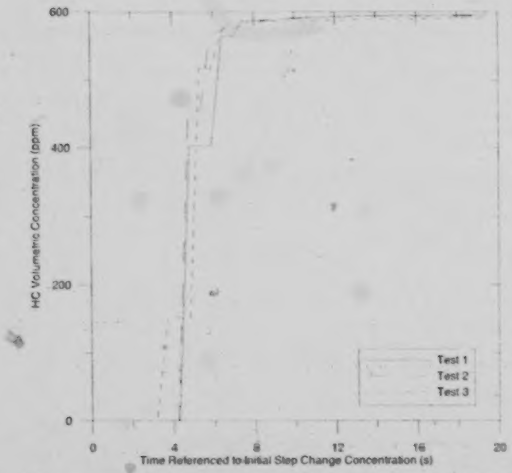

FIGURE A-1 RESPONSE TIME OF THE HC MEASUREMENT TO A STEP CHANGE CONCENTRATION WITHOUT SAMPLE LINE

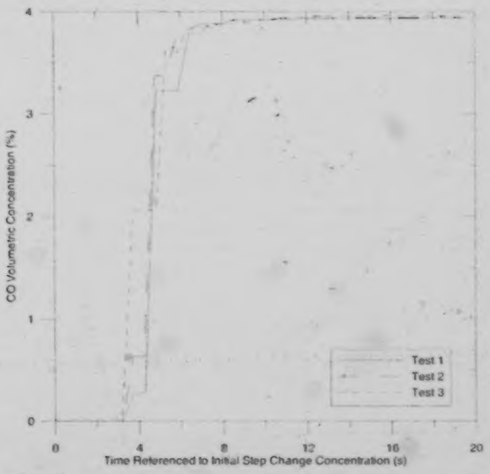

FIGURE A-2 RESPONSE TIME OF THE CO MEASUREMENT TO A STEP CHANGE CONCENTRATION WITHOUT SAMPLE LINE

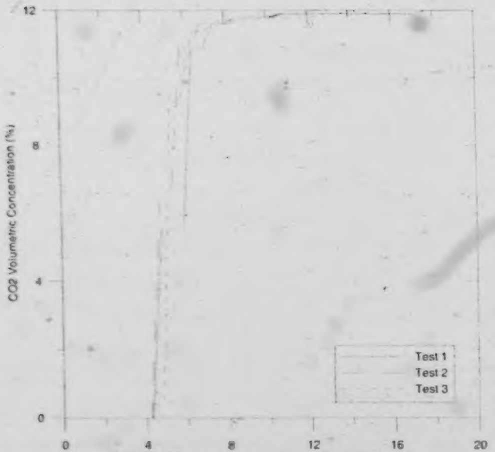

FIGURE A-3 RESPONSE TIME OF THE CO_2 MEASUREMENT TO A STEP CHANGE CONCENTRATION WITHOUT SAMPLE LINE

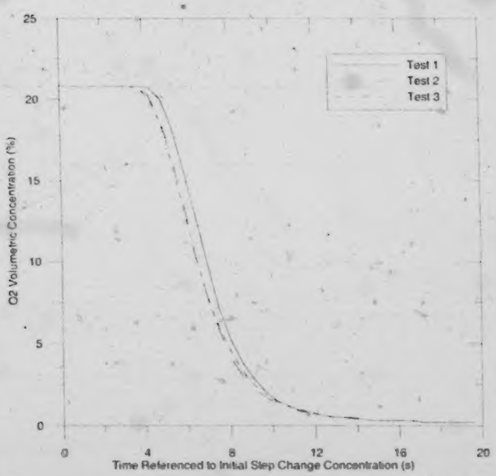

FIGURE A-4 RESPONSE TIME OF THE O_2 MEASUREMENT TO A STEP CHANGE CONCENTRATION WITHOUT SAMPLE LINE

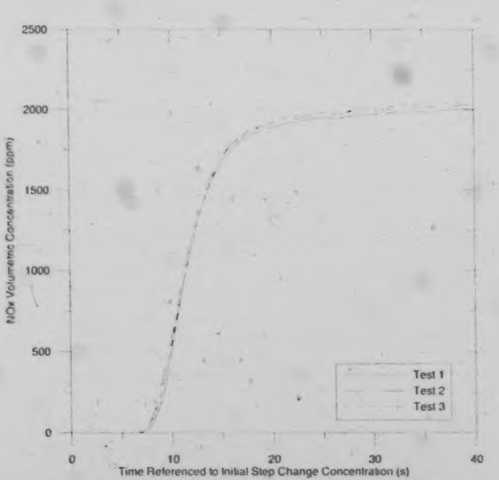

FIGURE A-5 RESPONSE TIME OF THE NO_X MEASUREMENT TO A STEP CHANGE CONCENTRATION WITHOUT SAMPLE LINE

Figures A-1 through A-3 illustrate the response times of the gas analyser for the gas concentration measurements of HC, CO and CO_2 respectively. The PXA-1100 instrument uses NDIR techniques to determine the concentrations of these species. As a result, it was expected that similar response times would be found since the three species are determined with the same measurement system. Examining these figures it is clear that the response time, for the sample to reach the NDIR measurement system was 4.2, 3.2 and 4.2 seconds for the HC, CO and CO_2 measurements respectively. The combined transit time (not including the sample line) and first order time constant of the NDIR measurement system to reach 2/3 of the final gas concentrations was found to be approximately 5.0 seconds for the three gas species.

Figures A-4 and A-5 display the behaviour of the analyser for the gas concentrations of O_2 and NO_x. These two measurements were made with independent electro-chemical detection cells with different response characteristics from the NDIR sample system described above. The transit times for the gas sample to reach the measurement cell were determined to be 4.0 and 6.2 seconds for the O_2 and NO_x measurements respectively. From these figures it can be clearly seen that the response time of the electro-chemical cell is substantially longer than that found for the NDIR system. For comparison purposes, the combined transit time (not including the sample line) and first order time constant of the chemical-electrical cells to reach 2/3 of the final values was found to be 7.5 and 12.5 seconds for the O_2 and NO_x measurements respectively. The time required to measure the final concentrations of both species was on the order of 20s.

GAS ANALYSER AND SAMPLE LINE DELAY TIME

With the response times of the gas analyser known, the effect of the sample line was considered next. Identical experiments to those conducted above were used illustrating the combined transit time (including the sample line) and first order time constant of the complete exhaust measurement system. Figures A-6 through A-10 present the results.

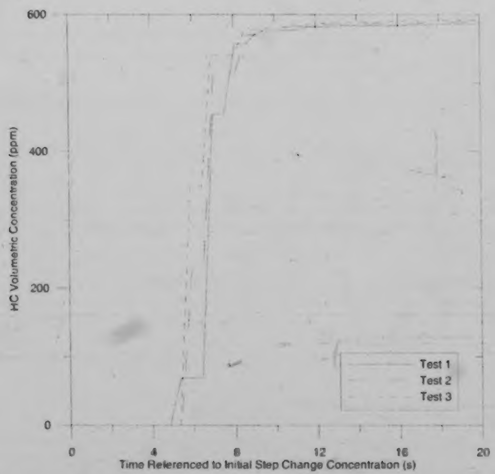

FIGURE A-6 RESPONSE TIME OF THE HC MEASUREMENT TO A STEP CHANGE CONCENTRATION WITH SAMPLE LINE

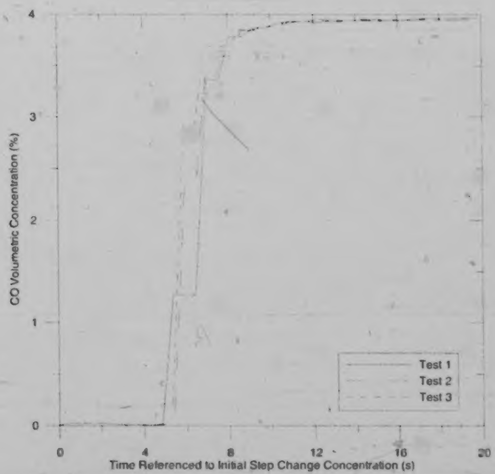

FIGURE A-7 RESPONSE TIME OF THE CO MEASUREMENT TO A STEP CHANGE CONCENTRATION WITH SAMPLE LINE

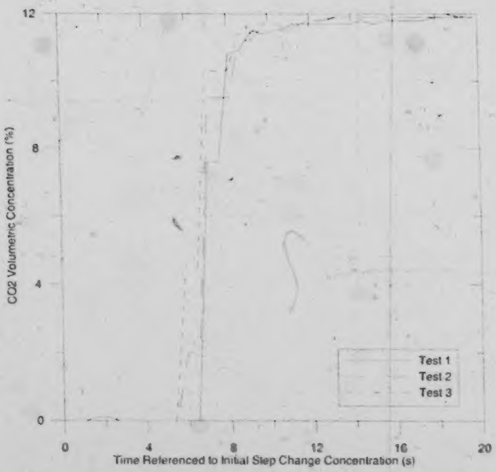

FIGURE A-8 RESPONSE TIME OF THE CO_2 MEASUREMENT TO A STEP CHANGE CONCENTRATION WITH SAMPLE LINE

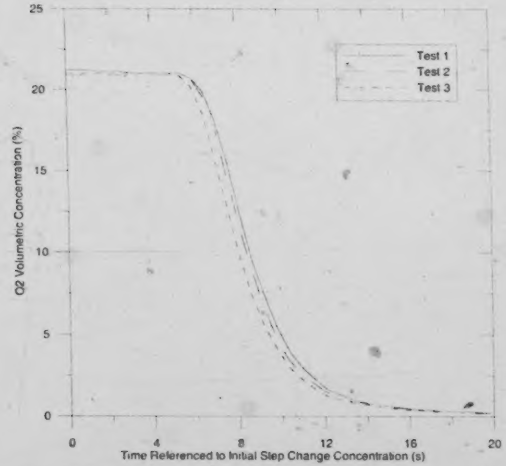

FIGURE A-9 RESPONSE TIME OF THE O_2 MEASUREMENT TO A STEP CHANGE CONCENTRATION WITH SAMPLE LINE

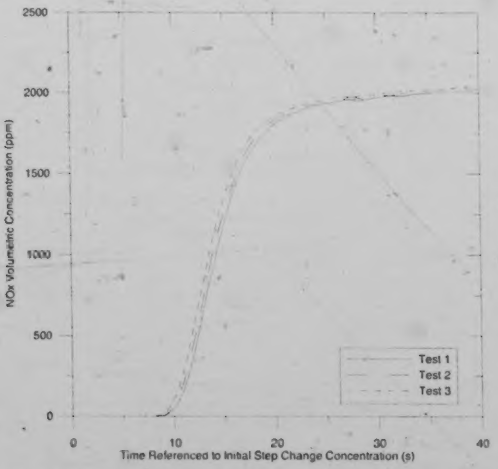

FIGURE A-10 RESPONSE TIME OF THE NO_X MEASUREMENT TO A STEP CHANGE CONCENTRATION WITH SAMPLE LINE

Figures A-6 through A-8 illustrate the response times of the NDIR measurement system operating with the sample line installed. The transit times for the gas sample to reach the measurement device (NDIR) was found to be 5.2, 5.0 and 5.2 seconds for the HC, CO and CO_2 measurements and are approximately 1.0, 1.8 and 1.0 seconds longer respectively, than the previous experiment. In addition, the time for the gas analyser to measure 2/3 of the final concentration was found to be 5.8 seconds for the three gas species. This was approximately 0.8 seconds longer than that determined with no sample line. This implies that the transit time from the tip of the sampling probe to the gas analyser could be estimated as 1 second.

Figures A-9 and A-10 illustrate the time response behaviour for the electro-chemical measurement cells operating with the sample line. The transit time for the sample to reach the measurement cells were determined to be 5.0 and 8.0 seconds for the O_2 and NO_x measurements. Comparing these values to the experiment conducted without the sample line, an increase of approximately 1.5 seconds was found. The times for the gas analyser to measure 2/3 of the final concentrations were found to be 9.0 and 15.0s respectively for the O_2 and NO_x measurement. Based on these measurements, the sample line increased the 2/3 response time by approximately 2.5s for the measurements made by the chemical cells.

FLOW IN THE SAMPLE LINE

Based on the above analysis of the analyser with and without the sample line, it was found that the transit time from the exhaust probe tip to the analyser averaged 1.5s. The sample line was approximately 7.0 m in length with an internal diameter of 4 mm. The velocity of the sample was therefore 4.7 m/s. If complete combustion is assume for the composition of exhaust at a temperature of 20°C, the Reynold number of the flow in the sample line would be 1300. This is less than the Reynolds number for turbulent flow of 2300.(2) It therefore be concluded that the flow in the sample line is laminar. If increased exhaust gas temperatures are analysed, the Reynolds number decreases due to the inverse relationship between temperature and the kinematic viscosity. It should be noted that a turbulent flow in the sample line is desirable for better transient response.

EXHAUST SYSTEM DELAY

The last delay time considered was due to the transport of the vehicle emissions through the exhaust system of the vehicle. Because this delay continuously varied due to changing power requirements placed on the engine, a simulation was conducted which assumed typical exhaust temperatures and pressures to estimate the exhaust volume flow rates. The volume of the exhaust system was also estimated, thus allowing the transport time to be approximated for typical mass air flow rates. The results are presented in Table A-1, for three experimental mass air flow rates and 5 typical exhaust gas temperatures. As illustrated in Table A-1, the resonance times for idle conditions (MAF of 8 g/s) range from 0.88 to 0.65s for estimated exhaust gas temperatures of 300 to 500 °C respectively. If a typical steady state cruise MAF rate of 53 g/s is examined, resonance times ranging from 0.12 to 0.10s for exhaust temperatures of 300 to 500 °C.

TABLE A-1 VARIOUS EXHAUST SYSTEM RESONANCE TIMES FOR EXPERIMENTAL EXHAUST VOLUME FLOW RATES

	Exhaust Gas Temperature (°C)				
MAF (g/s)	300	350	400	450	500
8.0	0.88	0.81	0.75	0.70	0.65
24	0.29	0.27	0.25	0.23	0.22
53	0.13	0.12	0.11	0.10	0.10

Since these values are based on estimated exhaust gas temperatures and pressures, an experiment was devised to quantify these resonance times. The experiment entailed running the engine at two different MAF rates and inducing a miss fire in the engine. This resulted in a HC emission spike and the corresponding delay time was recorded. The results of these two experiments are shown in Figures A-11 and A-12. Figure A-11 illustrates the total time delay for the HC spike to leave the engine and travel through the exhaust system and be detected by the gas analyser at an idle condition (MAF = 12.5 g/s). This time delay was found to be approximately 6s for three repeated experiments. Figure A-12 illustrates the same delay but with a higher MAF rate of 40.0 g/s and shows a 5s delay. The results of this experiment prove the validity of the simulated exhaust system transit times and indicate transport variations on the order of 1s.

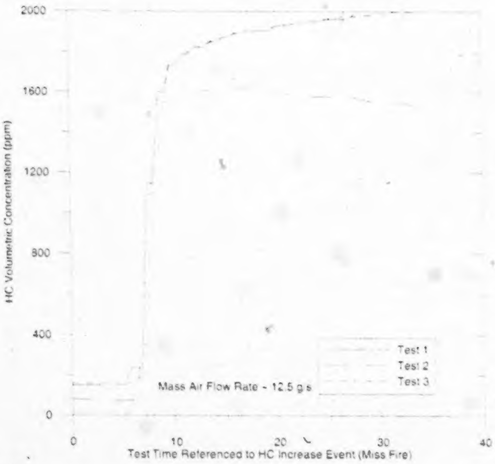

FIGURE A-11 EXHAUST SYSTEM DELAY TIME AT A MAF RATE OF 12.5 G/S

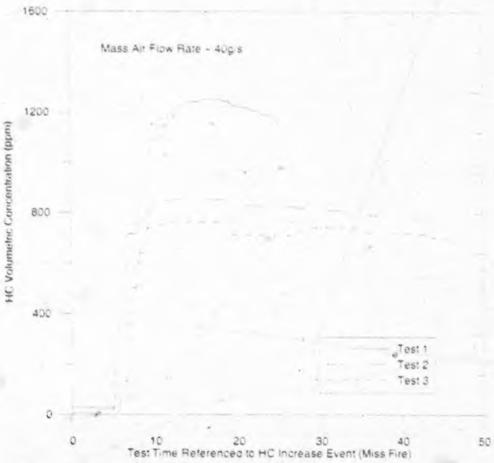

FIGURE A-12 EXHAUST SYSTEM DELAY TIME AT A MAF RATE OF 40.0 G/S

IMPLEMENTATION OF THE TIME SHIFTING ALGORITHM

With the sample delay times known and estimates for the exhaust gas resonance time, a time shifting algorithm was devised to correlate the volumetric concentration data with the instantaneously calculated exhaust mass flow rate. The values determined above were used as initial values for the time shifts. Since the species measured with the NDIR measurement system showed similar delay times, the three gases of HC, CO and CO_2 were initially shifted together at a time delay of 5.0 s. Similarly, the measurement of O_2 and NO_x were also shifted together, as a result of comparable delay times, at an initial time delay of 9.0 s. These constants were then used to determine the instantaneous mass flow rate of the emissions and were then cross-correlated with measurements known to affect the pollutant rates such as vehicle speed and mass air flow parameters. This led to the final conclusion that appropriate time shifts were 8.0 and 10.0 s for the NDIR and chemical cell measurement devices respectively.

To illustrate the effect of time shifting the volumetric concentrations, Figures A-11 through A-15 show the measured mass flow rate of air and the shifted mass flow rate of the associated pollutant for the first 20s of a data set. Also plotted on these figures are the effects of a large and a zero time shift scenario. Ideally, the MAF rate and mass emission rates should correlate, i.e. changes in mass air flow should correspond to changes in the mass emission rates of the measured pollutants.

Figure A-13 displays directly how the HC mass rate correlates to the MAF rate using a time shift of 8.0s for the NDIR measurement system. As expected, increased MAF rates lead to increases in the mass emission rates of HC. This figure also shows the effect of no time shift, leading to inaccurate emission rates for the first 8s and a large time shift of 12s leading to discrepancies after 16s of elapsed test time. These discrepancies can be attributed to correlating the wrong volumetric concentrations to the instantaneous exhaust flow rate.

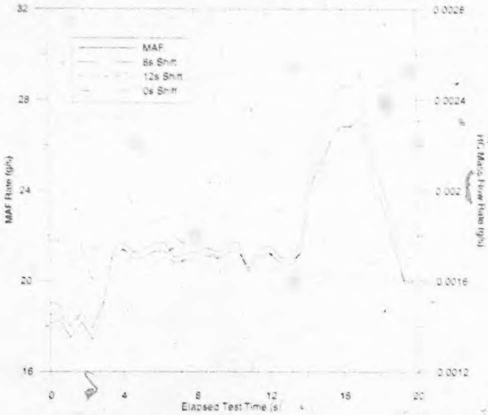

FIGURE A-13 THE EFFECTS OF VARYING TIME SHIFTING CONSTANTS ON HC EMISSIONS

Figure A-14 displays the MAF rates and CO mass emission rates, for the same 20s data set also with an increased time shift of 12s and a zero time shift. The time shift applied to this measurement was 8.0s. Due to the various mechanisms contributing to the formation and reductions of CO, no single correlation can be seen. However, this figure still illustrates that the mass flow rate of CO emitted is related to the variations in the MAF rate. Specifically, prior to 4s of elapsed test time, a significant increase in MAF occurs at the same time as a decrease in the mass emission rate of CO describing a leaning of the air fuel mixture. In addition, at approximately 14s elapsed test time, a dramatic increase in the MAF corresponded to an increase in the CO emission rate. This implies the engine was operating in a fuel enrichment mode. Together, these events illustrate the correct use of time shifting values. Also, shown in this figure are the results of a 12 s and zero time shift. Obviously, neither one of these two shift times correlate well with the MAF rate, but it does illustrate the sensitivity of the CO time shift value.

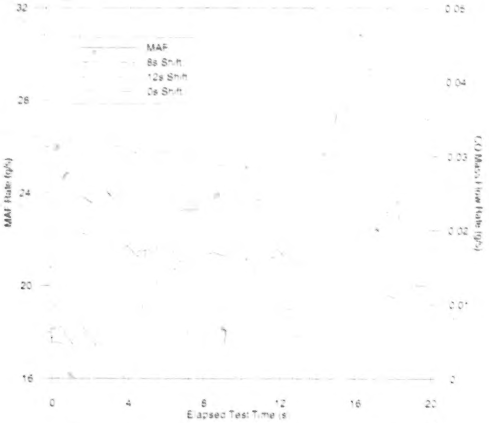

FIGURE A-14 THE EFFECTS OF VARYING TIME SHIFTING VALUES ON CO EMISSIONS

Figure A-15 focuses on the CO_2 emission rate and the effects of various time shifts. As portrayed in the diagram, the mass emission rate of CO_2 directly correlates to the MAF rate with the NDIR shift time of 8.0s. In addition, no real differences are seen by applying a 12 and zero second time shift and are attributed to the large continuous concentrations of CO_2 in the exhaust

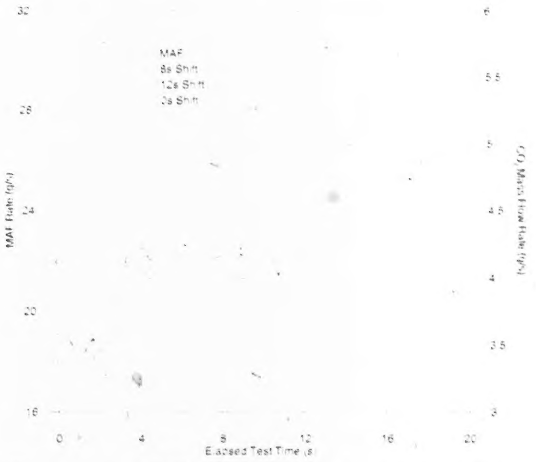

FIGURE A-15 THE EFFECTS OF VARYING TIME SHIFTING VALUESS ON CO_2 EMISSIONS

Figure A-16 presents the O_2 mass flow rate based on an electro-chemical measurement cells and the effects of various time shifts. As was described above, both the O_2 and NO_x measurements were shifted together at 10.0s. From this plot, no correlations exist between the MAF rate and O_2 mass emission rate. This result was expected since, the catalyst was probably operating during this small data set duration thereby removing oxygen from the exhaust. It is important to note that while no correlations exist for the three time shifts shown, the shifts can affect the final integrated result.

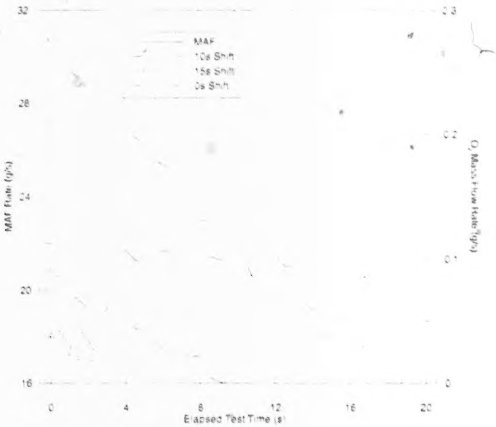

FIGURE A-16 THE EFFECTS OF VARYING TIME SHIFTING VALUES ON O_2 EMISSIONS

Figure A-17 displays the NO_x mass emission rates for the chosen shift time and a 15 and zero second time shift. As with the O_2 measurement, the NO_x measurement is determined by an electro-chemical cell and was shifted by 10.0 s. Examining this figure, it is clear that the NO_x mass emission rate correlates with the MAF rate using the applied shift. This direct correlation was expected since NO_x emissions are formed from increasing the temperature and pressure inside the combustion chamber. As a result, as more air is allowed into the chamber a corresponding increase in NO_x emissions is expected. Recalling the fuel enrichment protocol occurring at 14s, a lag in NO_x emissions is visible in this region. This result was expected since the increased amounts of fuel was introduced into the combustion chamber as indicated by increased CO output. As a result, lower combustion temperatures were attained leading to a lag between the CO and NO_x emission with MAF rates. However, after the enrichment process ended, the NO_x emissions peaked where as the CO emission decayed, indicating a leaning of the air fuel mixture. Detection of this event illustrates the integrity of the measurement system and shifting algorithms. Lastly, the effect of different time shifts can be visually seen and did not correlate well with the MAF rate.

FIGURE A-17 THE EFFECTS OF VARYING TIME SHIFTING VALUES ON NO_x EMISSIONS

SENSITIVITY OF MASS EMISSIONS RATES TO CONSTANT TIME SHIFT VALUES

Because of the varying exhaust gas resonance times of which are not accounted for in the time shifting algorithm and experimentally determined shift values, an analysis was conducted to determined the effect of deviations from the constant time shifting parameters. This analysis was conducted by examining a small data set and applying different shifting constants around the determined values. Table A-2 displays the percent differences calculated for a particular data set which was also divided into three segments. As shown in the table, the maximum errors induced in the exhaust specie measurements were found to be 1.36, 2.35, 0.16, 27.0 and 3.24% for the HC, CO, CO_2, O_2 and NO_x respectively. Figures A-18 through A-22 illustrate typical results for the five measured exhaust gas species showing the effects of various time shifts applied to the same data set.

TABLE A-2
ILLUSTRATION OF MAXIMUM PERCENT DIFFERENCES DUE TO DIFFERENT TIME SHIFTS

	HC	CO	CO_2	O_2	NO_x
Segment I	0.46	0.90	0.16	5.1	1.4
Segment II	1.4	1.5	0.01	27	3.2
Segment III	1.4	2.4	0.12	1.3	1.9
Full Trip	0.67	0.85	0.090	4.3	1.8

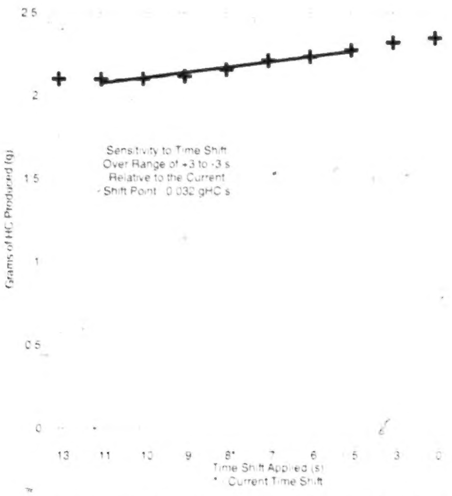

FIGURE A-18 SENSITIVITY OF THE HC MASS CALCULATION TO VARIOUS TIME SHIFT CONSTANTS

The effect of various time shifting values for the HC measurements are displayed in Figure A-18. From this figure a positive slope can be seen around the current shift point of 8.0 seconds. The slope of the line indicates that the measurement of total HC will deviate by 0.032 grams for every second deviation from the current time shift of 8.0s. Based on this simulation, this corresponds to an additional 1.42% error in the total HC measurements.

Figure A-19 illustrates a similar analysis for the measurement of CO. Examination of the figure shows that a positive and negative slope are found. Concentrating on slope encompassing the current shift point of 8.0s, a value of -0.289 grams of CO per second of shift time is calculated. This translates into a 1.44 % error in the final calculation of the total mass of CO.

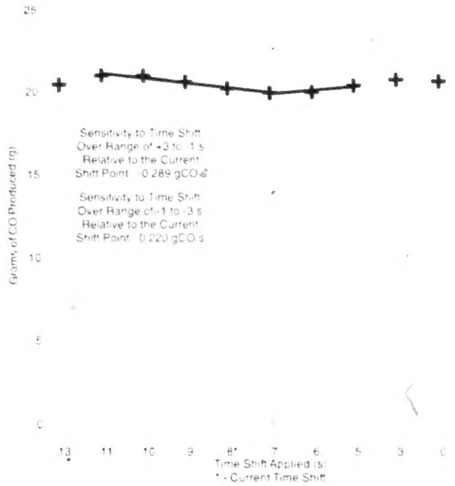

FIGURE A-19 SENSITIVITY OF THE CO MASS CALCULATION TO VARIOUS TIME SHIFT CONSTANTS

The sensitivity of varying time shifts to measurements of CO_2 is illustrated in Figure A-20. This figure displays the insensitive nature of the CO_2 measurement to varying time shifts. The slope of the line encompassing the 8.0s current time shift was determined to be -0.234 grams of CO_2 per second. This corresponds to an additional error of 0.011% in the determination of total CO_2 produced.

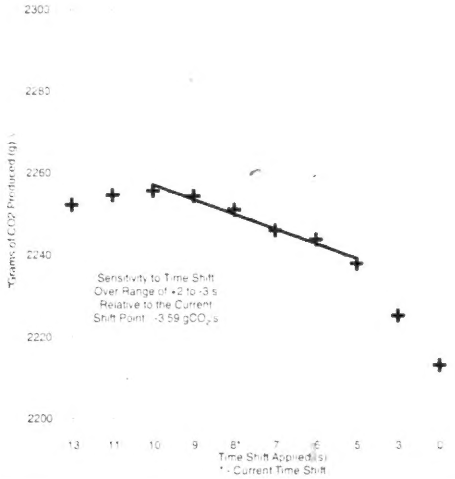

FIGURE A-20 SENSITIVITY OF THE CO_2 MASS CALCULATION TO VARIOUS TIME SHIFT CONSTANTS

Figure A-21 illustrates the effect of various time shifts applied to the O_2 measurement. As shown in the figure, a large slope, relative to the total O_2 magnitudes, of 0.108 grams of O_2 per second error was calculated. This implies a 24% additional error in the final calculation of O_2. While this error is large depending upon the error in the time shifting constant, the determination of the total O_2 is not required with great accuracy.

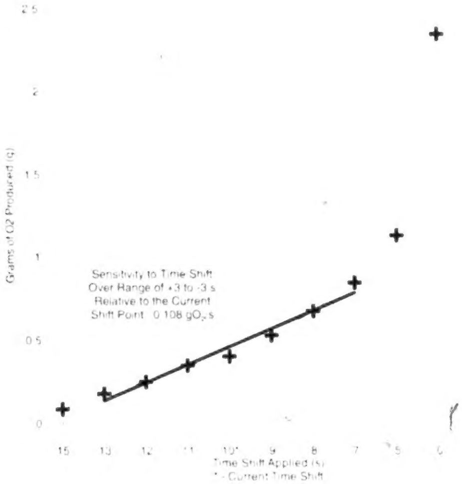

FIGURE A-21 SENSITIVITY OF THE O_2 MASS CALCULATION TO VARIOUS TIME SHIFT CONSTANTS

Illustrating the effects of the various time shifts to the total calculations of total NO_x emitted are shown in Figure A-22. This slope, found in the region of the current shifting point was calculated to be -0.035 grams of NO_x per second. This results in an additional 3.18% error in the calculation of total NO_x emitted.

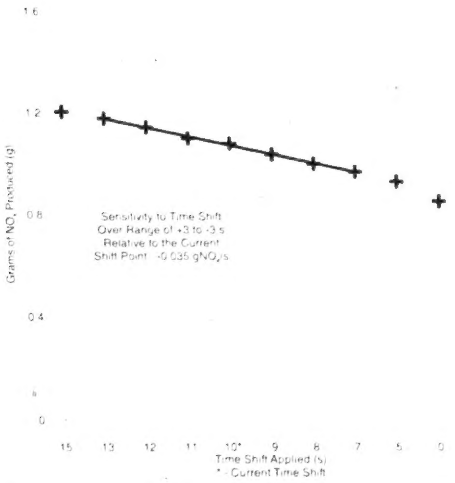

Figure A-22 Sensitivity of the NO_x Mass Calculation to Various Time Shift Constants

SAMPLE DATA ILLUSTRATING THE EFFECTIVENESS OF THE TIME SHIFT ALGORITHM

To illustrate the effectiveness of the time shifting algorithm, Figure A-23 illustrates a sample data set containing an acceleration trace, and an original and shifted NO_x emission profile. As described earlier, the NO_x emissions correlate well with vehicle acceleration. As seen in the original NO_x values no correlation exists, however once the time shift has been applied the NO_x emission trace correlates well with the associated acceleration profile. This correlation adds confidence to the time shifting procedure.

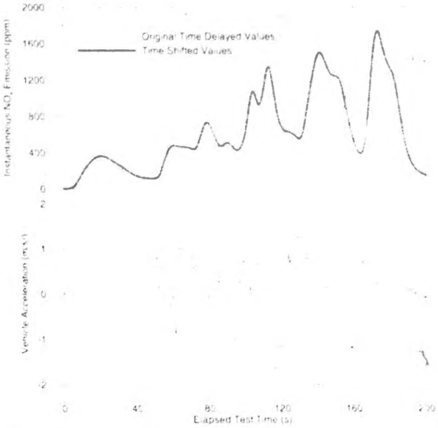

Figure A-23 Illustration of an Original and Shifted NO_x Emission Trace and the Correlation to Vehicle Acceleration

Figures A-24 and A-25 illustrate correlation relationships between the instantaneously measured mass flow rate of exhaust and the "instantaneously" calculated mass flow rates of HC and NO_x respectively. These figures expand the 160 to 200s window of Figure A-23. As shown in Figure A-24, the HC mass flow rate is strongly correlated to the exhaust mass flow rate. This indicates that confidence in the time shifting procedure for the NDIR measurements. However as illustrated in Figure A-25, there is an apparent delay in the NO_x mass flow rate compared to the exhaust mass flow. This indicates that there is some uncertainty in the final NO_x measurements.

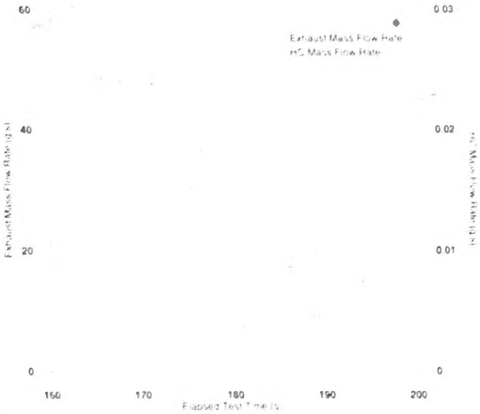

FIGURE A-24 CORRELATIONS OF EXHAUST AND HC MASS FLOW RATES

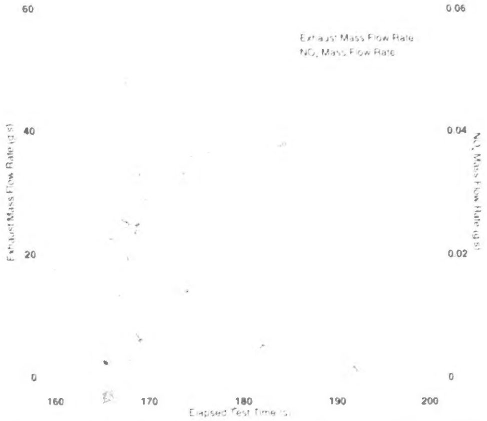

FIGURE A-25 CORRELATIONS OF EXHAUST AND NO_x MASS FLOW RATES

A final example of the time shifting procedure is shown in Figure A-26 illustrating two air to fuel (A/F) ratio measurements. The first A/F trace was obtained with a fast response lambda sensor mounted in the exhaust pipe of the test vehicle. The second time shifted trace, was obtained as a calculated value from the PXA - 1100 gas analyser. These calculated A/F values were shifted by the same constant as were the species measured with NDIR measurement system (i.e. 8.0s). Other than the initial discrepancies occurring from 0 to 20s due to calculation difficulties, a close correlation exits between the two measurements. In addition, the shifted A/F measurement even correlated to the "fuel-cutoff" strategy further strengthening the chosen time shifting values.

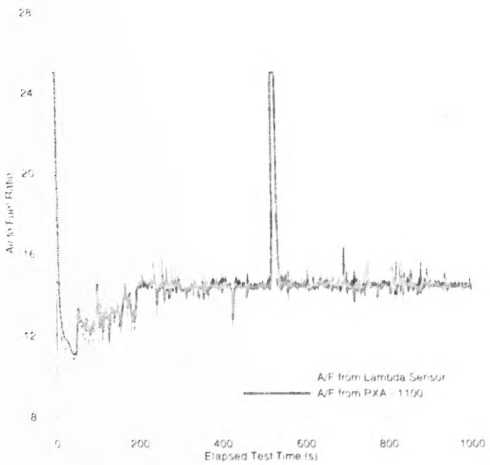

FIGURE A-26 CORRELATION OF A MEASURED AND TIME SHIFTED A/F VALUES

CONCLUSIONS

Based on the above analysis, an adequate time shifting algorithm was developed and implemented. The algorithm accounts for the first order time constant of the gas analyser and sample line transport time determined to be 8.0s for the NDIR and 10.0s for the electro-chemical cell measurements. It was found that the NDIR instantaneous mass flow rates correlated strongly with the exhaust mass flow rate. However, the electro-chemical cell measurements, specifically NO_x, lagged behind the exhaust mass flow rate. This indicates that there are some uncertainties in the final NO_x and O_2 measurements. In addition, the effects of varying exhaust volume flows rates were examined and found to vary with 1.0 second. Since the developed algorithm does not attempt to correct for this delay, an error analysis was conducted to account for the varying exhaust volume flow rates.

REFERENCES

1. Doebelin E.O., "Measurement Systems Application and Design," McGraw-Hill, New York, 1966.

2. White F.M., "Fluid Mechanics," McGraw-Hill, New York, 1994.

APPENDIX B

VEHICLE DYNAMIC MODEL

In order to help understand driving behavior in terms of vehicle power demands, a dynamic vehicle model was implemented. This model allowed the energy requirements of the vehicle to be calculated and provided insight as to specific power demands placed on the vehicle by the driver. Once the specific power/energy demands were known, classification of driver behavior could be attainable; in addition, estimations of the emission factors expressed in g/kWh could be determined. This appendix describes the equations and the methodology to determine the Cd (the drag coefficient), and Cr (rolling resistance coefficient) for any given test vehicle.

The vehicle dynamic model calculated the tractive power defined as the power transmitted to the road by the automobile. The model accounted for the aerodynamic, rolling and inertial resistances of the vehicle as shown in Figure B-1. All other losses, such as drive train inefficiencies, were accounted for because of the dynamic nature of the model.

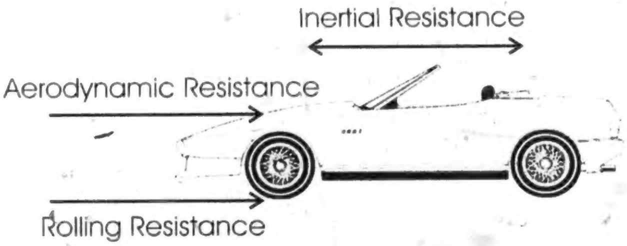

FIGURE B-1 SCHEMATIC OF DYNAMIC VEHICLE RESISTANCES

GENERAL CALCULATION OF THE VEHICLE TRACTIVE POWER

The forthcoming equations provide the methodology to calculate the tractive vehicle power. Equation 1 illustrates the simplicity of the tractive power calculation that was determined at each time step of the recorded data file. This allows not only the instantaneous tractive power levels to be calculated but also the instantaneous energy (Power * Time Step) requirements placed upon the test vehicle. Lastly, the positive power trace can be integrated against time to provide the total positive tractive energy requirements for the driving sequence.

$$Power = Speed \times \frac{(Aero + Rolling + Inertial)}{1000} \qquad \textbf{(1)}$$

Where:

Power = Vehicle Tractive Power [kW]
Speed = Vehicle Speed in [m/s]
Aero = Aerodynamic Resistance [N]
Rolling = Rolling Resistance [N]
Inertial = Inertial Resistance [N]

CALCULATION OF THE AERODYNAMIC RESISTANCE

To account for the aerodynamic drag component of the dynamic model, the drag coefficient (Cd), vehicle frontal area, air density and the vehicle speed were required. Note that the frontal area was based on the vehicle's maximum road height and width measurement (excluding the mirrors). Since the open area under the vehicle and mirror surfaces are not accounted for, the current accepted method in determining the frontal area is to take 80% of the road height and width product. The method to determine the drag coefficient and frontal area as a single value will be explained in the coast down test (CDT) section. Equation 2 was used to determined the resistance due to the aerodynamic drag.

$$Aero = \frac{Cd \times FA \times \rho \times (Speed)^2}{2} \quad (2)$$

Where:

Aero = Vehicle Aerodynamic Rolling Resistance [N]
Cd = Drag Coefficient
FA = 80% of Test Vehicle's Frontal Area [m^2]
ρ = Air Density [kg/m^3]

CALCULATION OF THE ROLLING RESISTANCE

The rolling resistance of the vehicle is determined with Equation 3 and requires the rolling resistance coefficient (Cr) and mass of the test vehicle. The determination of the rolling resistance coefficient will be illustrated in the coast down test section.

$$Rolling = 9.81 \times Cr \times Mass \quad (3)$$

Where:

Rolling = Vehicle's Rolling Resistance [N]
Cr = Rolling Resistance Coefficient
Mass = Test Vehicle's Mass [kg]

CALCULATION OF THE INERTIAL RESISTANCE

Finally, the inertial resistance component of the model is calculated with Equation 4 and requires the mass and instantaneous acceleration of the test vehicle. With the velocity/time trace obtained either from an actual drive profile or from a CDT, the acceleration values can be determined using a numerical differentiation scheme as illustrated in Equation 5. This formula calculates the current acceleration (i) based on the previous (i - 1) and next (i + 1) velocity/time values.

$$Inertial = Mass \times A \quad (4)$$

Where:

Inertial = Vehicle's Inertial Resistance [N]
A = Instantaneous Vehicle Acceleration [m/s^2]

$$A(i) = \frac{V_{i+1} - V_{i-1}}{T_{i+1} - T_{i-1}} \quad (5)$$

Where:

V = Vehicle Velocity [m/s]
T = Time [s]

With all of the individual components of the dynamic model known, Equation 1 can then be used to determine the resulting instantaneous tractive power estimates in kW at each time step of the data file. Figure B-2 illustrates a typical speed and power trace for a congested type of traffic profile consuming 4300 kJ of positive tractive energy.

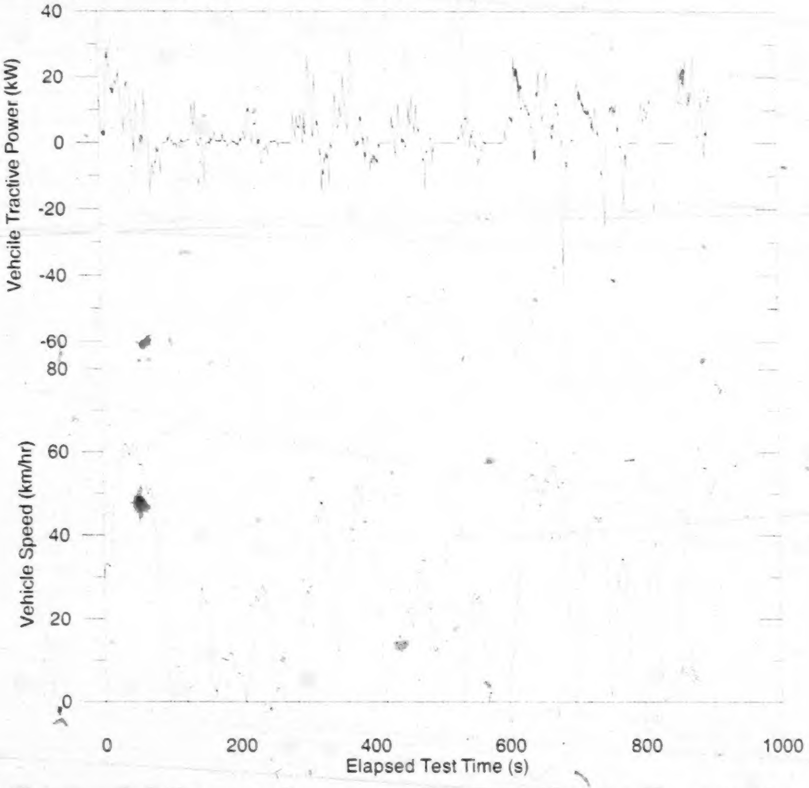

FIGURE B-2 TYPICAL SPEED AND TRACTIVE POWER TRACE FOR A CONGESTED DRIVING SEQUENCE

COAST DOWN TEST PROCEDURE

As previously discussed, the parameters of Cd×FA and Cr can be determined from a vehicle CDT. This procedure involves utilizing a flat section of roadway where the test can safely be conducted; rural highways are usually sufficient. A completely flat roadway is not necessary since the road gradient can be accounted for as will be shown in Equation 6. The first step is to accelerate the vehicle up to a speed of 100 to 120 km/hr. Once this velocity is attained, the vehicle transmission is placed into neutral and allowed to coast down, while the vehicle speed is recorded using the data acquisition system. In addition to recording the vehicle's speed, the ambient conditions of temperature and pressure and vehicle mass is also required for the analysis. For the research conducted in this thesis, a sample velocity trace of a CDT is illustrated in Figure B-3. To account for wind effects, it is advisable to conduct the test in both directions and average the calculated coefficients, described in the next section.

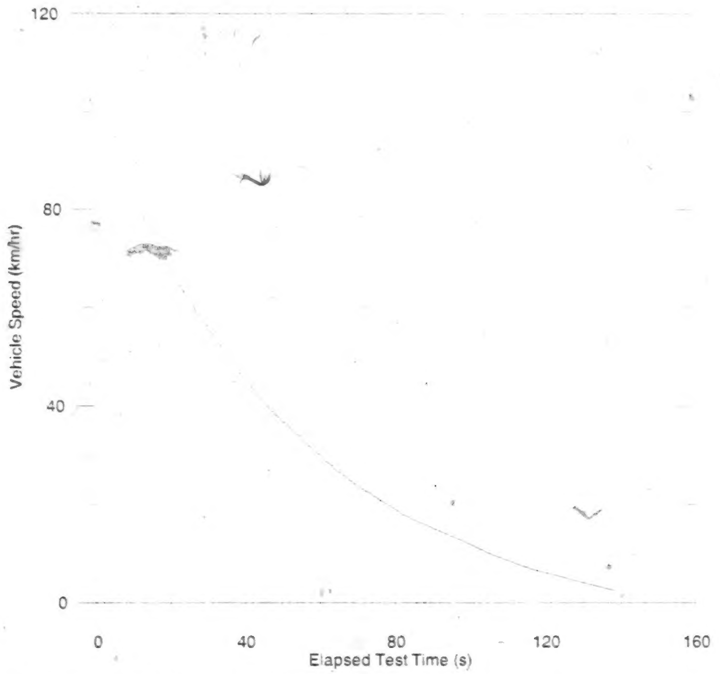

FIGURE B-3 TYPICAL SPEED-TIME TRACE OF COAST DOWN TEST FOR THE 1992 GM 3/4 PICK-UP TRUCK

ANALYSIS OF COAST DOWN VELOCITY PROFILE

To determine the coefficients of Cd×FA and Cr for use in the previous equations, a linearization equation was used.(1) As shown in Equation 6, the parameters of Cd ∗ FA and Cr are explicitly determined as the slope and y-intercept respectively. In addition, if the road gradient is known, it can be accounted for by the variable θ.

$$\left(-\frac{A}{g}-\sin\theta\right) = CdA\left(\frac{\rho V^{2}}{2mg}\right) + Cr \qquad \textbf{(6)}$$

Where:

A = Vehicle's Acceleration (Determined in Equation 5) [m/s^2]
g = Acceleration due to Gravity [9.81 m/s^2]
θ = Roadway Gradient (If applicable) [radians]
Cd×FA = Combination of the Drag Coefficient and Vehicle Frontal Area
ρ = Air Density [kg/m^3]
V = Vehicle Velocity [m/s]
m = Vehicle Mass [kg]
Cr = Rolling Resistance Coefficient

ANALYSIS AND EXPLANATION OF COEFFICIENTS FOR THE TEST VEHICLE

The vehicle used in the research was a 1990 GM 3/4 ton pick up truck with a mass of 2100 kg and a corrected frontal area (i.e. 80% of width×height) of 2.66 m^2. CDTs were conducted in ambient temperature conditions ranging from -25 to +15°C to determine the effect of ambient conditions on the Cd×FA and Cr coefficients. An example of a linearized data set (as determined with Equation 6) is presented in Figure B-4. This sample data was obtained on Feb 7, 2002 when the ambient condition was approximately -12°C. As illustrated in this plot large scatter is noticeable, and two sets of slope/intercept values are apparent.

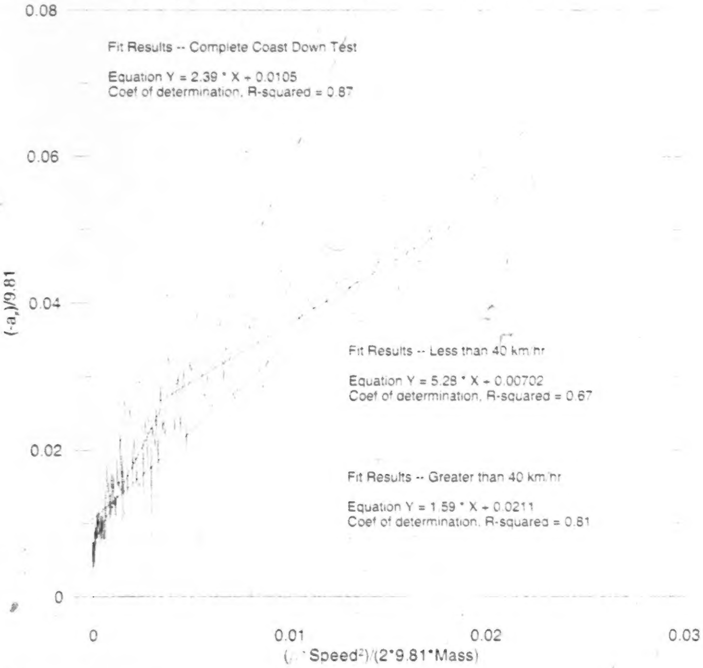

FIGURE B-4 LINEARIZED COAST DOWN TEST ILLUSTRATING BREAK POINT VELOCITY MODEL

No clear and precise conclusions were found for the two sets of intercept/slope values. However, explanations for the disjointed data are a speed dependent rolling resistance factor, varying tire properties at different speeds or possibly unaccounted road gradient variations. It is important to note that this trend was found in other processed coast down experiments for this particular test vehicle. It is questionable whether this anomaly would be found for different vehicles since this finding was not reported by Yates.(1) Because of the shape of the linearized data sets, two analysis methods were implemented to examined the data. The first method involved fitting a piecewise linear equation system to best represent the data and to infer the Cd×FA and Cr parameters. This involved selecting a break point vehicle speed where the two slopes were noticeably different and a resulting two parameter model could be developed. From examining the all of the processed CDTs, it was found that the best overall break point speed was 40 km/hr and would correspond to approximately 0.0035 on the x-axis of Figure B-4. The second method involved fitting a linear equation to the entire data set as proposed by Yates. Figure B-4 also presents the fit equations for the break point and the single linear fit models.

As illustrated in Figure B-4, the fit for the complete CDT had the highest r-squared value of 0.87 compared to 0.67 and 0.82 for the lower than and higher vehicle speeds of 40 km/hr respectively. The Cd×FA coefficient for the complete CDT was calculated to be 2.39. For vehicles speeds lower than 40 km/hr, a Cd×FA value of 5.28 was determined which was 45% larger than when compared to the Cd×FA for the complete data set. Similarly, for vehicle speeds greater than 40 km/hr a Cd×FA value of 1.59 was calculated which was 67% lower than for the complete data set value. Analysis of the Cr coefficient for the complete CDT was determined to be 0.0105. For vehicle speeds lower than 40 km/hr a Cr value of 0.0070 was determined which was 67% lower than the Cr coefficient for the complete CDT. For vehicle speeds greater than 40 km/hr a Cr value of 0.0212 determined and was 49% larger when compared to the complete data set value. This analysis presents the competing nature of the coefficients determined with the piecewise functions. That is, for vehicle speeds less than 40 km/hr large Cd *FA (5.28) and low Cr (0.007) values were determined. Conversely, for vehicle speeds greater than 40 km/hr low Cd×FA (1.59) and high Cr (0.02) values were calculated. With no clear indication of the science behind this un-intuitive behavior, it was determined to use the parameters calculated with the complete data set. In addition, coefficients determined with the single linear regression fit the accepted ranges of Cd and Cr values. The accepted Cd (Cd×FA / FA) range for passenger cars are 0.3 to 0.9. Acceptable Cr values, depending on tire configurations, vehicle speed and road properties should fall within 0.01 to 0.08.(2-8)

The results of this analysis for all of the experimentally conducted CDTs are shown in Table B-1. This table illustrates all of the individual Cd×FA and Cr coefficients and averages for each set of CDT runs. In addition, the five sets of CDTs were conducted in a chronological order. That, is the first test was conducted approximately five minutes after a cold start where the vehicle had been "soaked" at the ambient condition for a minimum of 12 hrs. The remaining tests were carried out as the engine/vehicle went through the warm-up phase. This was done to ensure the effects of the cold lubricating oils were captured and used in the overall average values.

TABLE B-1 PROCESSED CDA, CD AND CR VALUES DETERMINED FROM COAST DOWN TESTS

CDT #	1	2	3	4	5	6	Average	Std. Dev.	Rel. Dev.
	Feb 7, 2002 (Ambient Temperature -12°C)								
Cd×FA	2.39	2.53	2.36	2.10	2.32	1.75	2.24	0.26	0.11
Cd	0.899	0.950	0.888	0.789	0.874	0.656	0.843	0.10	0.11
Cr	0.010	0.010	0.012	0.012	0.010	0.011	0.011	0.0090	0.08
	March 7, 2002 (Ambient Temperature -23°C)								
Cd×FA	2.36	2.32	2.13	1.89	n/a	n/a	2.18	0.19	0.09
Cd	0.866	0.873	0.801	0.711	n/a	n/a	0.818	0.070	0.09
Cr	0.010	0.012	0.012	0.016	n/a	n/a	0.013	0.0021	0.17
	March 8, 2002 (Ambient Temperature -22°C)								
Cd×FA	2.21	1.97	1.92	2.44	n/a	n/a	2.14	0.21	0.10
Cd	0.830	0.742	0.720	0.919	n/a	n/a	0.830	0.079	0.10
Cr	0.010	0.014	0.010	0.011	n/a	n/a	0.011	0.0016	015
	March 20, 2002 (Ambient Temperature -26°C)								
Cd×FA	2.97	2.51	2.66	n/a	n/a	n/a	2.71	0.19	0.07
Cd	1.12	0.943	1.00	n/a	n/a	n/a	1.02	0.072	0.07
Cr	0.015	0.021	0.015	n/a	n/a	n/a	0.017	0.0028	0.17
	May 29, 2002 (Ambient Temperature +15°C)								
Cd×FA	2.67	2.22	1.90	2.33	n/a	n/a	2.28	0.28	0.12
Cd	1.00	0.834	0.712	0.874	n/a	n/a	0.856	0.10	0.12
Cr	0.006	0.010	0.010	0.010	n/a	n/a	0.0090	0.0017	0.19

Table B-2 displays the set of averaged coefficients from the five sets of coast down experiments. This table also indicates the relative deviation for the Cd×FA, Cd and Cr values that were used in the calculation of vehicle tractive power. The Cd×FA for this test vehicle was calculated to be 2.31 with a relative deviation of 10%. The Cd coefficient was determined to be 0.87 with a relative deviation 10% indicating a strong repeatability in the Cd values. The Cr coefficient was calculated to be 0.0121 with a relative deviation of 24%.

TABLE B-2 FINAL OVERALL AVERAGED DRAG AND ROLLING RESISTANCE COEFFICIENTS

	Cd×FA	Cd	Cr
Average	2.31	0.868	0.0121
Standard Deviation	0.23	0.09	0.03
Relative Deviation	0.10	0.10	0.24

SENSITIVITY OF THE TRACTIVE POWER ENERGY CALCULATIONS

An analysis was conducted to determine the individual contributions of the three parameters (i.e. aerodynamic, rolling or inertial) to the overall positive tractive energy. This analysis was based upon selecting a single complete driving sequence and examining the individual positive energy contribution from each of the contributing terms. The results of the analysis for a 12 900kJ commute are presented in Figure B-5 illustrating the percentages of accumulated positive tractive energy. Clearly, the aerodynamic and inertial contributions are the dominating influences since they consumed 35 and 37% of the positive tractive energy. The rolling resistance was only responsible for 28% of the total consumed positive energy. This illustrates importance of the experimentally determined Cd coefficient, since over one third of the energy consumed using this coefficient. This implies that the positive tractive energy is very sensitive to the aerodynamic drag contribution. Since the amount of energy consumed due to the rolling resistance was still comparable to the aerodynamic and inertial resistances, it can be said that the energy calculation is sensitive to the Cr coefficient as well. This has the implies that the Cd and Cr coefficients should be known with high accuracy due to the equally split nature of the energy calculation.

FIGURE B-5 INDIVIDUAL ENERGY CONTRIBUTIONS TO OVERALL POSITIVE TRACTIVE ENERGY

CONCLUSIONS

From the previous discussion, a vehicle dynamic model was used to calculate the vehicle tractive power requirements for a 1992 GM 3/4 ton pick up truck. The equations provide estimates of the aerodynamic, rolling and inertial resistances and actually calculate the amount of power transmitted to the road by the vehicle. Vehicle coast down procedures and a linearization equation presented by Yates(1) allow the coefficients of Cd and Cr to be experimentally determined for use in the tractive power calculations. In addition, the sensitivity analysis presented for this test vehicle operating with the experimentally determined Cd and Cr values, showed that these coefficients must be know with high accuracy due to the equally split nature of the energy calculation. With the methodology presented above, this procedure / analysis can be easily conducted for any other test vehicle.

REFERENCES

1. Yates A.D.B., Mkwanazi S., "Methodology For Determining Octane Response At Different Altitudes For Vehicles Equipped With Knock Sensors" SAE Technical Paper 2002-01-1663, Society of Automotive Engineers, 2002.

2. Gregory L., Daniel L. "Deriving Wheel HP and Torque from Accelerometer Data" SAE Technical Paper 2000-01-3544, Society of Automotive Engineers, 2000.

3. Johnson T.V., "Gasoline Vehicle Emissions - SAE 1999 In Review" SAE Paper 2000-01-0855, Society of Automotive Engineers, 2000.

4. White R.A., Korst H.H., "The Determination if Vehicle Drag Contributions from Coast-Down Tests" SAE Technical Paper 720099, Society of Automotive Engineers, 1972.

5. Gillespie T.D., "Fundamentals of Vehicle Dynamics" Society of Automotive Engineers, USA, 1992.

6. Checkel M.D., Brownlee A., Doblanko L. "Pollution Inventories using Second-bySecond Vehicle Modelling and Traffic Planning Models" Combustion and Global Climate Change, Combustion Canada, Natural Resources Canada, 1999.

7. Checkel M.D. "Emission Function for Motor Vehicle Emission Audits Based on Traffic Modelling" Presented at CI/CS Spring Technical Meeting, Waterloo, May 27-2, 1996.

8. Yung V., Checkel M.D., "Energy Use and Emissions Effects of Operating a Hybrid Vehicle," Presented at The Combustion Institute, Canadian Section, May 25-28, 1997.

APPENDIX C

REAL TIME EMISSION CALCULATIONS

This appendix describes the equations utilized to determine the instantaneous emission rates in various formats.

This Appendix describes the formulas and equations utilized at each time step in the data analysis to calculate the exhaust emission rates.

All calculations were based on the following chemical equation:

$$C_xH_y + A(O_2 + 3.76N_2) \rightarrow BC_6H_{14} + DCO + ECO_2 + FO_2 + GNO + HN_2 + IH_2O \quad \textbf{(1)}$$

Where:

$$B = \frac{[HC]}{1000000} \quad \textbf{(2)}$$

$$D = \frac{[CO]}{100} \quad \textbf{(3)}$$

$$E = \frac{[CO_2]}{100} \quad \textbf{(4)}$$

$$F = \frac{[O_2]}{100} \quad \textbf{(5)}$$

$$G = \frac{[NO_x]}{1000000} \quad \textbf{(6)}$$

$$H = 1 - B - D - E - F - G \quad \textbf{(7)}$$

$$A = \frac{G + 2 \times H}{2 \times 3.76} \quad \textbf{(8)}$$

$$I = 2A - D - 2E - 2F - G \quad \textbf{(9)}$$

$$x = 6B + E + D \quad \textbf{(10)}$$

$$y = 14B + 2I \quad \textbf{(11)}$$

The mass based Air to Fuel ratio was calculated using the following formula:

$$Air\,/\,Fuel = \frac{A \times 4.76 \times 28.97}{(x + 12.00) + (y \times 1.01)} \qquad \textbf{(12)}$$

The hydrogen to carbon ratio of the fuel was determined from:

$$H\,/\,C = \frac{y}{x} \qquad \textbf{(13)}$$

To determine the rate of emission in units of g/s, the molecular weight of the exhaust was calculated as follows:

$$\begin{aligned} MW_{exh} &= 86.1 \times B + 28.0 \times D + 44.0 \times E + 32.0 \times F \\ &\quad + 30.0 \times G + 28.0 \times H + 18.0 \times I \end{aligned} \quad [\text{g/mol}] \qquad \textbf{(14)}$$

The calculation of the pollutants, in units of g/s, was determined from:

$$Poll_{g/s} = \frac{P \times MW_p \times (Airflow + Fuelflow)}{MW_{exh}} \quad [\text{g/s}] \qquad \textbf{(15)}$$

Where:

P = E, or F, or G, or I, or J

MW_p = the molecular weight of the associated pollutant

Airflow = Mass flow rate of air entering the engine determined from the Siemens HMF 62B

Fuelflow = Airflow divided by the Air to Fuel ratio measured from the AFR-2400E

To calculate the pollution in g/kW-hr, the following formula was used:

$$Poll_{g/kWhr} = \frac{Poll_{g/s} \times 3600}{Power} \quad [\text{g/kW-hr}] \qquad \textbf{(16)}$$

Where:

$\text{Poll}_{g/s}$ = any one of the five exhaust emissions measured calculated as above
Power = instantaneous tractive power determined in Appendix B

The calculation to determine the pollutants in terms of g/gfuel was as follows:

$$Poll_{g/gfuel} = \frac{Poll_{g/s}}{Fuelflow} \qquad [\text{g/g}_{\text{fuel}}] \qquad \textbf{(17)}$$

APPENDIX D

ERROR ANALYSIS

This appendix presents the equations of the error analysis consisting of three sections. The first section examines all of the equations and errors associated with the measurement and computation of the instantaneous error values. It emphasizes the error in the grams per second emission calculations. The second section describes the calculations and resulting errors for the dynamic vehicle model used to estimate the tractive power vehicle requirements. The last section details the analysis of the emission factors and associated errors. The error analysis uses standard error estimation techniques for all equations described.

SECTION 1 - ERROR ANALYSIS OF THE INSTANTANEOUS RATE EQUATIONS

All equations described in this section are calculated at each time step in the analysis. This section examines the calculations required to determine the instantaneous emission rates and errors. All emission calculations are based on the following chemical equation describing the combustion of a fuel with air:

$$C_xH_y + A(O_2 + 3.76N_2) \rightarrow BC_6H_{14} + DCO + ECO_2 + FO_2 + GNO + HN_2 + IH_2O \quad \textbf{(1)}$$

Where B, D, E, F and G are determined from the PXA - 1100 gas analyzer and converted to mole fractions, assuming ideal gas behavior, with the following formulas:

$$B = \frac{[HC]}{1000000}$$

$$D = \frac{[CO]}{100}$$

$$E = \frac{[CO_2]}{100}$$

$$F = \frac{[O_2]}{100}$$

$$G = \frac{[NO_x]}{1000000}$$

To calculate of the amount of nitrogen, N_2, in the products one kilomole of dry-based products is assumed and determined from:

$$H = 1 - B - D - E - F - G \quad \textbf{(2)}$$

The error in the amount of N_2 calculated is given by:

$$\varepsilon H = \left[(\varepsilon B)^2 + (\varepsilon D)^2 + (\varepsilon E)^2 + (\varepsilon F)^2 + (\varepsilon G)^2\right]^{1/2} \quad \textbf{(3)}$$

Where:

$\varepsilon B = \varepsilon D = \varepsilon E = \varepsilon F =$ 5% of Reading

$\varepsilon G =$ 32 ppm $\in$ 0 - 1000 ppm

60 ppm $\in$ 1001 - 2000 ppm

120 ppm $\in$ 2001 - 4000 ppm

The amount of air required to balance the products of combustion, or term A, can be calculated from a nitrogen balance. Again, the concentrations of the exhaust species are represented in terms of moles fractions. The resulting calculation is:

$$A = \frac{G + 2 \times H}{2 \times 3.76} \tag{4}$$

The error associated with this calculation is determined with:

$$\varepsilon A = \left[(\varepsilon F)^2 + (\varepsilon B)^2\right]^{1/2} \tag{5}$$

The last term to calculate on the right-hand side of the chemical expression, Equation 1, is the amount of water (H_2O) produced during the combustion (i.e. I). It is determined from an oxygen balance and computed using:

$$I = 2A - D - 2E - 2F - G \tag{6}$$

The error in the calculated amount of water is determined from:

$$\varepsilon I = \left[(\varepsilon A)^2 + (\varepsilon D)^2 + (\varepsilon E)^2 + (\varepsilon F)^2 + (\varepsilon G)^2\right]^{1/2} \tag{7}$$

With all of the coefficients known on the right-hand side of Equation 1, the molecular weight of the exhaust can be computed by multiplying the mole fractions by the corresponding exhaust specie molecular weight given by:

$$MW_{exh} = 86.1 \times B + 28.0 \times D + 44.0 \times E + 32.0 \times F + 30.0 \times G + 28.0 \times H + 18.0 \times I \tag{8}$$

Now, the error in the molecular weight of the exhaust can be determined from:

$$\varepsilon MW_{exh} = \left[(\varepsilon B)^2 + (\varepsilon D)^2 + (\varepsilon E)^2 + (\varepsilon F)^2 + (\varepsilon G)^2 + (\varepsilon H)^2 + (\varepsilon I)^2\right]^{1/2} \tag{9}$$

The error in the mass fuel flow rate (MFF) is found next. This calculation is based on assuming an error in the mass air flow (MAF) rate of 1.0 g/s and an error in the air to fuel (A/F) ratio measurement of 0.25 units. The MFF is determined from:

$$MFF = \frac{MAF}{A/F} \tag{10}$$

Where:

MAF = Mass Air Flow Rate [g/s]
A/F = Air to Fuel Ratio

The error in the instantaneous MFF calculation can be found from:

$$\varepsilon MFF = MFF\left[\left(\frac{\varepsilon MAF}{MAF}\right)^2 + \left(\frac{\varepsilon A/F}{A/F}\right)^2\right]^{1/2} \qquad \textbf{(11)}$$

Where:

εMAF = Error in the Mass Air Flow Rate (i.e. 1.0 g/s)
εA/F = Error in the measured A/F (i.e. 0.25)

Finally, the calculation used to determine the instantaneous rate of emissions was:

$$\dot{M}_{poll} = \frac{Poll \times MW_{poll} \times (MAF + MFF)}{MW_{exh}} \qquad \textbf{(12)}$$

Where:

Poll = B, or D, or E, or F, or F
MW_{poll} = Molecular Weight of Associated Pollutant [g/mol]

The error in the instantaneous mass emission of any pollutant rate is given by:

$$\varepsilon\dot{M}_{poll} = \dot{M}_{poll}\left[2\times\left(\frac{\varepsilon Poll}{Poll}\right)^2 + 2\times\left(\frac{\varepsilon MW_{exh}}{MW_{exh}}\right)^2 + \left(\frac{\varepsilon MFF}{MFF}\right)^2 + \left(\frac{\varepsilon MAF}{MAF}\right)^2\right]^{1/2} \qquad \textbf{(13)}$$

Where:

εPoll = Error in the corresponding pollutant (i.e. εB or εD or εE or εF or εG)

If the appropriate substitutions are made the error in the instantaneous mass emissions can be expressed as:

$$\varepsilon\dot{M}_{poll} = \dot{M}_{poll}\left[2\times\left(\frac{\varepsilon Poll}{Poll}\right)^2 + 2\times\left(\frac{\varepsilon MW_{exh}}{MW_{exh}}\right)^2 + 2\times\left(\frac{\varepsilon MAF}{MAF}\right)^2 + \left(\frac{\varepsilon A/F}{A/F}\right)^2\right]^{1/2} \qquad \textbf{(14)}$$

This equation expresses the importance of the error in the Poll, MW_{exh} and MAF terms due to the factor of two.

The instantaneous distance traveled D [m] at each time step, was determined knowing the velocity v [m/s], and the differential time t [s]:

$$D = v \times t \qquad \textbf{(15)}$$

Noting that the error in the measured velocity was 0.25km/hr or 0.069 m/s and no error in the time measurement, the error in the instantaneous distance is given by:

$$\varepsilon D = D\left(\frac{\varepsilon v}{v}\right) \tag{16}$$

Where:

εv = Error in the measured velocity (i.e. 0.069 m/s)

To determine the error in the integrated results, excluding the total emissions described previously, the instantaneous errors were first multiplied by the corresponding time steps. This provided the error in the associated measurement at each time step in the experiment. With these errors known, the following equation can be used to estimate the error in the final integrated result:

$$\varepsilon X = \sqrt{\sum_{1}^{n} \left(\varepsilon X_{inst}\right)^2} \tag{17}$$

Where:

εX = Total Error of Integrated Result
εX_{inst} = Error in the Instantaneous Result

To calculate the error in the totals of the emission produced, two factors were considered. The first source of error was due to measurement accuracies as described above. This error was processed by determining the error at each time step, i.e. the results from Equation 14 were multiplied by the corresponding time step. The second source of error was due to the use of a constant time shifting parameter. An analysis conducted in Appendix A, determined the maximum variations due to deviations in the time constants. The results of the analysis indicated that the calculated mass of emissions had an additional error of 1.36, 2.35, 0.16, 24.0 and 3.24% for the HC, CO, CO_2, O_2 and NO_x respectively. This error was determined by computing the mass of the emissions at each time step and multiplying this result by the corresponding percentage error. As a result, the error calculation describing the uncertainty in the total mass of any pollutant was:

$$\varepsilon M = \sqrt{\sum_{1}^{n} \left[\left(\varepsilon M_{inst}\right)^2 + \left(\varepsilon TS\right)^2\right]} \tag{18}$$

Where:

εM = Error in Total Mass of Pollutant [g]
εM_{inst} = Error in the Instantaneous Mass of Pollutant [g]
εTS = Error due to the Time Shift Algorithm [g]

SECTION 2 - ERROR ANALYSIS OF THE VEHICLE DYNAMIC MODEL

The equation used to estimate the vehicle tractive power requirements were based on three terms corresponding to the aerodynamic, rolling and inertial resistance of the test vehicle. The overall equation applied at each time step is given by:

$$Power = \frac{Speed \times (Aero + Rolling + Inertial)}{1000} \tag{19}$$

Where:

Power = Vehicle Tractive Power [kW]
Speed = Vehicle Speed [m/s]
Aero = Aerodynamic Drag [N]
Rolling = Rolling Resistance [N]
Inertial = Inertial Resistance [N]

The "Speed" term found in Equation 19 was the measured vehicle speed in units of m/s with associated error of 0.069m/s. The next term in the calculation of the tractive power requirement was associated with aerodynamic drag given by:

$$Aero = \frac{Cd \times FA \times \rho \times (Speed)^2}{2} \tag{20}$$

Where:

Cd = Drag Coefficient
FA = Corrected Vehicle Frontal Area [m^2]
ρ = Air Density [kg/m^3]

The error associated with the determination of Cd $*$FA is given by:

$$\varepsilon Cd \times FA = Cd \times FA\left[\left(\frac{\varepsilon Cd}{Cd}\right)^2 + \left(\frac{\varepsilon FA}{FA}\right)^2\right]^{1/2} \tag{21}$$

Where:

εCd $*$FA = Error in the Drag Coefficient Multiplied by the Corrected Frontal Area
εCd = Error in the Drag Coefficient
εFA = Error in the Test Vehicle Frontal Area [m^2]

Note that the Cd term is a constant corresponding to the vehicle drag coefficient. In this error analysis, it was estimated that the error in the Cd coefficient was 10%. Equation 21 has a term associated with the frontal area of the test vehicle, with measurement error. The frontal area of the vehicle was calculated based on:

$$FA = 0.8 \times W \times H \tag{22}$$

Where:

W = Test Vehicle Width [m]
H = Test Vehicle Height [m]

Allowing for an error of 5.0% in width and height of the test vehicle, the error associated with the calculation of this term is given by:

$$\varepsilon FA = FA\left[\left(\frac{\varepsilon W}{W}\right)^2 + \left(\frac{\varepsilon H}{H}\right)^2\right]^{1/2} \tag{23}$$

Where:

εW = Error in the Width Measurement [m]
εH = Error in the Height Measurement [m]

The second term in Equation 20 dealing with the density of the ambient air, ρ [kg/m^3], of which was calculated by:

$$\rho = \frac{P \times T}{R} \tag{24}$$

Where:

P = Atmospheric Pressure [kPa]
T = Atmospheric Temperature [K]

Assuming no error in the R (ideal gas constant for air) term, and knowing the error in the ambient pressure of 0.013kPa and the temperature of 0.5°C, the error associated with the calculation of the air density is given by:

$$\varepsilon\rho = \rho\left[\left(\frac{\varepsilon P}{P}\right)^2 + \left(\frac{\varepsilon T}{T}\right)^2\right]^{1/2} \tag{25}$$

Where:

ερ = Error in the Air Density Calculation [kg/m^3]
εP = Error in the Pressure Measurement (i.e. 0.013kPa)
εT = Error in the Temperature Measurement (i.e. 0.5°C)

Finally, the error in the aerodynamic drag was determined to be:

$$\varepsilon Aero = Aero\left[\left(\frac{\varepsilon Cd \times FA}{Cd \times FA}\right)^2 + \left(\frac{\varepsilon\rho}{\rho}\right)^2 + \left(\frac{\varepsilon Speed}{Speed}\right)^2\right] \qquad \textbf{(26)}$$

Where:

εAero = Error in the Aerodynamic Drag Calculation [N]
εSpeed = Error in the Vehicle Speed (i.e. 0.069 m/s)

If the substitutions are made, the error in the aerodynamic drag can be expressed as:

$$\varepsilon Aero = Aero\left[\left(\frac{\varepsilon Cd}{Cd}\right)^2 + \left(\frac{\varepsilon W}{W}\right)^2 + \left(\frac{\varepsilon H}{H}\right)^2 + \left(\frac{\varepsilon\rho}{\rho}\right)^2 + \left(2 \times \frac{\varepsilon Speed}{Speed}\right)^2\right]^{1/2} \qquad \textbf{(27)}$$

Equation 27 illustrates the importance of knowing the vehicle speed with high accuracy due to the multiplication of the error by a factor of 4. The second term in the calculation of the vehicle tractive power requirement was associated with the rolling resistance of the vehicle and is calculated as:

$$Rolling = 9.81 \times Cr \times Mass \qquad \textbf{(28)}$$

Where:

Cr = Rolling Resistance Coefficient
Mass = Test Vehicle's Mass [kg]

Note that the error in the Cr term, corresponding to the rolling resistance coefficient was assumed to be known to within 10%. Also, the error in the mass of the vehicle was 100kg. The error calculation for the rolling resistance of the vehicle was defined as:

$$\varepsilon Rolling = Rolling\left[\left(\frac{\varepsilon Mass}{Mass}\right)^2 + \left(\frac{\varepsilon Cr}{Cr}\right)^2\right]^{1/2} \qquad \textbf{(29)}$$

Where:

εRolling = Error in the Rolling Resistance Calculation [Nm]
εMass = Error in the Mass of the Test Vehicle [kg]
εCr = Error in the Rolling Resistance Coefficient

The last term in the calculation of the vehicle tractive power was associated with the inertial resistance of the test vehicle and is given by:

$$Inertial = Mass \times A \qquad \textbf{(30)}$$

Where:

A = Test Vehicle's Acceleration [m/s^2]

Since the error in the vehicle speed measurement was determined to be 0.069m/s, the resulting error in the vehicle acceleration was calculated to be $[0.069*2]^{1/2} = 0.098$ m/s^2. The error in the inertial resistance of the vehicle was then determined from:

$$\varepsilon Inertail = Inertail\left[\left(\frac{\varepsilon Mass}{Mass}\right)^2 + \left(\frac{\varepsilon A}{A}\right)^2\right]^{1/2} \qquad \textbf{(31)}$$

Where:

εInertial = Error in the Inertial Resistance Calculation [N]
εA = Error in the Acceleration Calculation [m^2]

Finally, the vehicle tractive power was calculated from:

$$Power = \frac{Speed \times (Aero + Rolling + Inertial)}{1000} \qquad \textbf{(32)}$$

The estimate of the vehicle tractive power error is given by:

$$\varepsilon Power = Power\left[3 \times \left(\frac{\varepsilon Speed}{Speed}\right)^2 + \left(\frac{\varepsilon Aero}{Aero}\right)^2 + \left(\frac{\varepsilon Rolling}{Rolling}\right)^2 + \left(\frac{\varepsilon Inertial}{Inertial}\right)^2\right]^{1/2} \qquad \textbf{(33)}$$

Where:

εPower = Error in the Tractive Power Calculation

And, if all of the above substitutions are made, the error in the tractive power can be expressed as:

$$\varepsilon Power = Power\left[\begin{array}{l} 7 \times \left(\frac{\varepsilon Speed}{Speed}\right)^2 + \left(\frac{\varepsilon Cd}{Cd}\right)^2 + \left(\frac{\varepsilon W}{W}\right)^2 + \left(\frac{\varepsilon H}{H}\right)^2 \\ + \left(\frac{\varepsilon \rho}{\rho}\right)^2 + 2 \times \left(\frac{\varepsilon Mass}{Mass}\right)^2 + \left(\frac{\varepsilon Cr}{Cr}\right)^2 + \left(\frac{\varepsilon A}{A}\right)^2 \end{array}\right]^{1/2} \qquad \textbf{(34)}$$

Equation 34 illustrates that the main source of error in the tractive power calculation is due to the error in the vehicle speed measurement. The tractive energy and associated error can be determined by multiplying the tractive power and calculated error by the time step. Since only the positive tractive power levels are meaningful in terms of correlations, removing the negative power values was necessary. The remaining values could then be integrated to determine the quantity of positive energy (kJ) used throughout the test. The positive tractive energy and corresponding errors could then be transferred into units of kWhrs by dividing the results by 3600. The error associated with this calculation was determined as follows:

$$\varepsilon E = \sqrt{\sum_{1}^{n} \left(\varepsilon E_{inst}\right)^2} \qquad \textbf{(35)}$$

Where:

εE = Error in the Total Positive Energy [kJ]
εE_{inst} = Error in the Instantaneous Positive Energy [kJ]

SECTION 3 - ERROR ANALYSIS OF EMISSION FACTORS

With all of the above expressions and formulas known, the error in the calculated emission factors could be determined. The first factor, representing the amount of fuel consumed or pollution emitted on a grams/km basis was determined from:

$$EF_{g/km} = \frac{X_g}{Dist_{km}} \qquad \textbf{(36)}$$

Where:

$EF_{g/km}$ = Emission Factor Expressed in g/km
X_g = Total mass of Pollutant [g]
$Dist_{km}$ = Distance Traveled [km]

The error associated with this emission factor is found by:

$$\varepsilon EF_{g/km} = EF_{g/km}\left[\left(\frac{\varepsilon X_g}{X_g}\right)^2 + \left(\frac{\varepsilon DIST_{km}}{DIST_{km}}\right)^2\right]^{1/2} \qquad \textbf{(37)}$$

Where:

$\varepsilon EF_{g/km}$ = Error in the Emission Factor [g/km]
εX_g = Error in the Total Mass of Pollutant [g]
$\varepsilon Dist_{km}$ = Error in the Total Distance Traveled [km]

The second emission factor, representing the amount of pollution emitted on a grams per kg_{fuel} consumed basis is calculated from:

$$EF_{g/kgfuel} = \frac{X_g}{Fuel_{kg}} \tag{38}$$

Where:

$EF_{g/kgfuel}$ = Emission Factor Expressed g/kg_{fuel}
$Fuel_{kg}$ = Amount of Fuel Consumed [kg]

The error associated with this emission factor calculation is given by:

$$\varepsilon EF_{g/kgfuel} = EF_{g/kgfuel}\left[\left(\frac{\varepsilon X_g}{X_g}\right)^2 + \left(\frac{\varepsilon Fuel_{kg}}{Fuel_{kg}}\right)^2\right]^{1/2} \tag{39}$$

Where:

$\varepsilon EF_{g/kgfuel}$ = Error in Emission Factor $[g/kg_{fuel}]$
$\varepsilon Fuel_{kg}$ = Error in the Amount of Fuel Consumed [kg]

The last emission factor represents the amount of pollution emitted on a grams per kilo-Watt-hour (kWhr) basis. This calculation was performed on a subset of the recorded data pertaining to situations when the vehicle was in a positive tractive power level only and is determined by:

$$EF_{g/kWhr} = \frac{X_g}{E_{kWhr}} \tag{40}$$

Where:

$EF_{g/kWhr}$ = Emission Factor Expressed g/kWhr
E_{kWhr} = Amount of Energy Consumed [kWhr]

The error associated with the calculation of this emission factor is given by:

$$\varepsilon EF_{g/kWhr} = EF_{g/kWhr}\left[\left(\frac{\varepsilon X_g}{X_g}\right)^2 + \left(\frac{\varepsilon E_{kWhr}}{E_{kWhr}}\right)^2\right]^{1/2} \tag{41}$$

Where:

$\varepsilon EF_{g/kWhr}$ = Error in Emission Factor
εE_{kWhr} = Error in the Amount of Energy Consumed

CONCLUSIONS

This Appendix has provided the equations required to determine the error in the required emission factor calculations. The analysis first began with the equations required to determine the error in all of instantaneously measured/calculated results. In addition, a separate section was devoted to the error in the vehicle dynamic model. Finally, all of the errors were consolidated and the final error in the emission factors could be determined.

APPENDIX E

DETERMINATION OF EMISSION FACTORS AND CHARACTERISTIC POINTS

The focus of this research was to calculate accurate emission factors (EF) of any given test vehicle. With these experimentally determined emission factors, detailed models were attainable which encompassed temperature and driving pattern corrections. These models were then capable of describing the amount, by mass, of pollution emitted by the test vehicle. However, due to the complex nature of the emissions produced by any given vehicle, a standardized algorithm was required to determine the emission factors for various sections of the emission profile. This appendix describes the procedure and resulting analysis used to determine the emission factors for both two and three parameter models. Since the method and resulting analysis is generalized, it can be applied to any instrumented test vehicle. This discussion will only consider emission factors expressed in g/km, since this is the most versatile and recognized form. However, this analysis could also be applied to emission factors in the form of g/kg_{fuel} *or g/kWhr.*

BACKGROUND OF EMISSION FACTORS

Currently, emission factors are determined from chassis dynamometer experiments using Constant Volume Sampling (CVS) systems. These procedures involve a test vehicle following a particular driving cycle, the FTP - 75 in North America. The resulting emissions are collected into three different bag samples, corresponding to the three regions of the driving cycle as shown in Figure E-1.(1) These bag samples are then post analyzed to determined the total mass of each pollutant. The emission factors are then calculated by dividing the total mass of each pollutant by the distance traveled during the corresponding bag sample. Finally, the emission factors are weighted (i.e. 43% for the cold start, 57% for the warm start and 100 % for the stabilized sections) resulting in a single emission factor representing the pollution characteristics of that particular test vehicle. However, as described earlier in this thesis, a more accurate model of vehicle emissions is attainable if first the emissions are measured in-real time and in on-road situations. Secondly, different emission factors are utilized to describe the emission profiles of the vehicle for the different phases of vehicle operation. The use of multiple emission factors complicates the procedure of defining the transition points between different emission factors. The appendix illustrates a method to determine multiple emission factors and the corresponding change-over points.

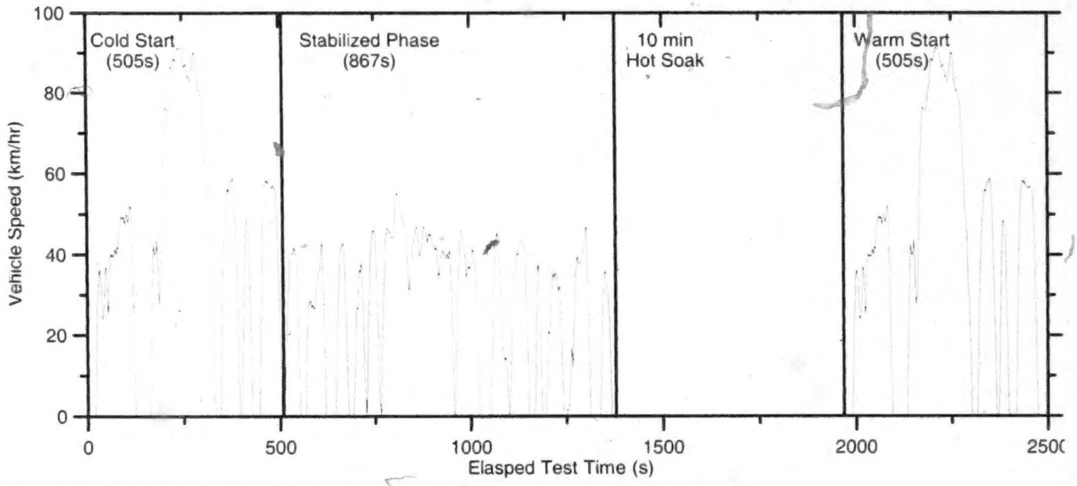

FIGURE E-1 THE FTP 75 CERTIFICATION DRIVING SEQUENCE(1)

DESCRIPTION OF EMISSION PROFILES FOR THE TEST VEHICLE

To better understand the issues faced with the determination of the emission factors for the test vehicle, Figure E-2 illustrates a sample plot showing the cumulative HC, CO and NO_x emissions with distance traveled for a particular test run conducted at an ambient temperature of -26°C. As seen in this figure two distinctive slopes are visible pertaining to the pre-catalyst light-off and post-catalyst light-off regions. In addition, a zone separating the previous two emission profiles, or transition region, is also visible. Clearly, the changeover points for the emission profiles could be found by intuition alone. For instance, the initial slope of the cumulative HC emission profile, describing the pre-light-off emission factor seems to end at 0.4 km when the profile bends into the transition zone. Similarly, the post-light-off region emission factor seems to start at approximately 2 km into the driving sequence. With these two points defined, an analysis of the resulting emission factors could be conducted by calculating the slope of the three curves defined by the two change-over points. This HC emission factors calculated using this method was 79, 3, 0.7 g/km for the pre, transition and post light-off regions respectively. A similar analysis of the CO and NO_x emissions are presented in Figure E-2; note that the different changeover points were used for the NO_x emissions. However, (1) with various people working on this project, (2) the possibility of different emission profiles for various vehicles and (3) numerous data files to analyze, the use of a standardized algorithm was required.

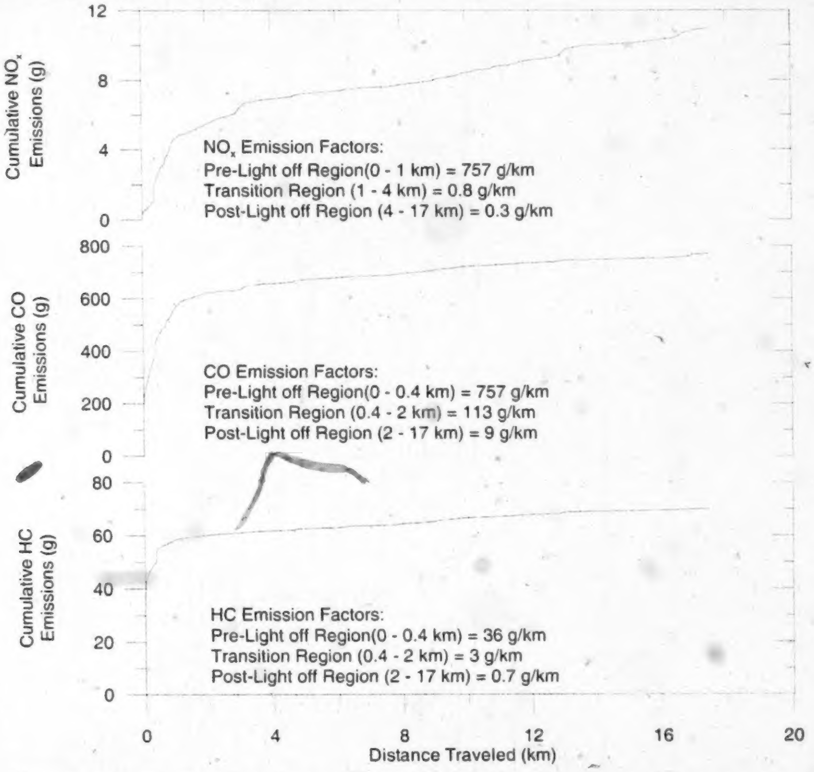

FIGURE E-2 CUMULATIVE HC, CO, AND NO_X EMISSIONS FOR AN AMBIENT TEMPERATURE OF -26°C

DESCRIPTION OF ALGORITHM

SMOOTHING ROUTINE

In order to aid in the processing of the cumulative emission profiles, a smoothing routine was devised to act as a low pass filter to remove some of the visible discontinuities seen in Figure E-2. To preserve the integrity of the data set, that is, to not skew or shift the changeover points, a short time period of 60s was used in the rolling average procedure. In addition, the 60s time window allowed the capture and smoothing of emissions data produced from acceleration, cruise and deceleration sequences throughout the original data set.

LINEAR FITTING PROCESSES

Since these cumulative diagrams were running totals of the emissions produced by the test vehicle plotted against the distance traveled, the required emission factors (represented in g/km) could be directly determined from the slopes of a linear regression analysis. This is similar to the intuitive method presented earlier. To remove some of the biasing effects, a MATLAB program was written to automate the process. However, as not clearly illustrated in the previous sample plots, it was observed that large discontinuities were sometimes seen in the data sets, usually resulting from the loss of catalyst conversion effectiveness. In order to accommodate these issues, some user inputs were still required in the linear regression analysis.

To fit a linear line to the pre-catalyst light-off region it was necessary for the user to choose a starting and ending point for the regression algorithm to begin and end. The starting point was easily defined as the first point on located on the y axis at a zero traveled distance, or y-intercept value. The emission profiles all include a y-intercept value because the test vehicle was started and allowed to warm-up for approximately 50s before driving, thus accumulating emissions were produced without accumulating any travel distance. The second point however, required some examination of the emission profile by the user to decide where the profile became non-linear; however, to help compensate for the biasing of results, the MATLAB routine used a regression analysis to fit a linear line between the two selected end points. The program was designed to then start at the y-intercept location and compare the original y value to that obtained with the linear fit. The routine continued to check and compare the original and linear fit y values, stepping to the right and extrapolating the linear fit if required, until a discrepancy of 2% was found. Once this deviation was calculated, a second algorithm was implemented to continue checking the differences for an additional 200 data points to ensure the correct changeover point was found. This algorithm was necessary since it was possible for a deviation greater than 2% to occur in between the selected endpoints due to sudden variation in the emission profiles. Figure E-3 illustrates a pre-catalyst light-off fitted data set for the HC emission profile presented earlier. The resulting emission factor was determined to be 56 g/km with an intercept of 33 g. The point at which the linear line deviated by more than 2% from the original data set was found to be 0.40 km; marked by a star.

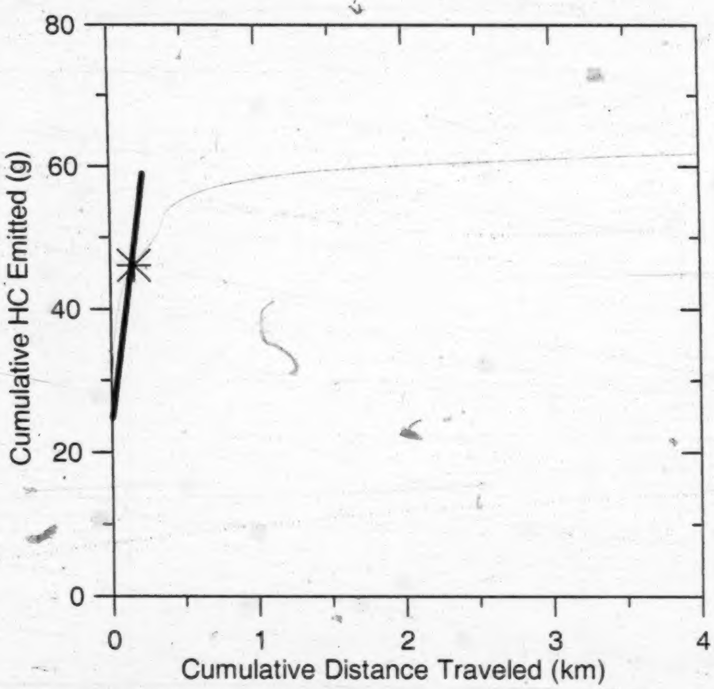

FIGURE E-3 LINEAR REGRESSION ANALYSIS FOR THE PRE-LIGHT-OFF HC EMISSION FACTOR

To determine the emission factor of the post-catalyst light-off section of the emission profile, a similar algorithm to that described previously was used. The program first required to the user to identify a point just after the non-linear transition region. It also asked the user to select an end point for the linear regression analysis. From examining numerous emission profiles, it was not always possible to select the final point in the data set as the end point for the linear curve fit. As a result, based on the users analysis of the post-catalyst light-off emission trace, a point was selected which best represented a linear profile. Once the two end points were chosen, the program began comparing the original y values to the y values obtained with the linear regression line starting from the furthest right selected end point. Thus, the algorithm would continue searching toward the transition zone and calculate the discrepancies between the y values. As before, once a 2% deviation was found, the code continued to search past this point to ensure it was the correct derivation location. Figure E-4 illustrates the linear fit to the post-light-off HC emission profile present earlier. The resulting emission factor was determined to be 0.6 g/km. The point at which the linear line deviated by more than 2% from the original data set was found to be 1.3 km; marked by a star.

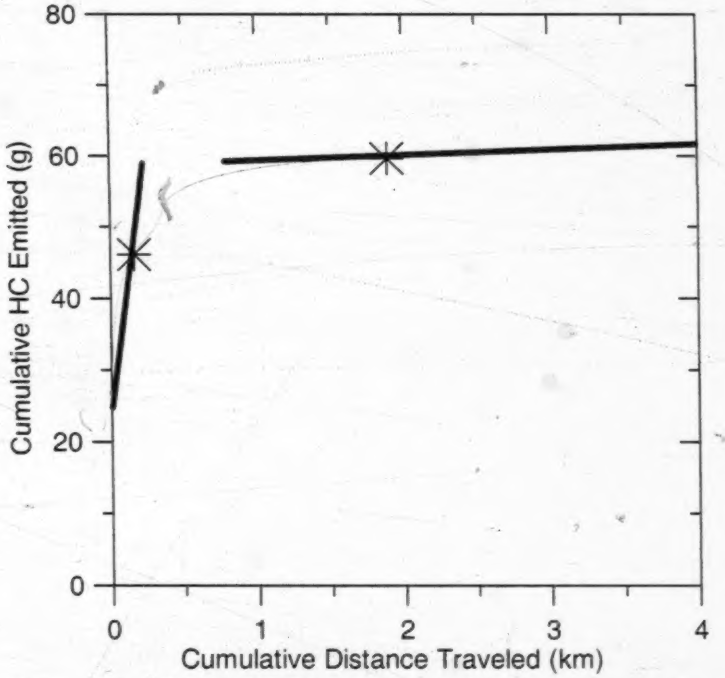

FIGURE E-4 LINEAR REGRESSION ANALYSIS FOR THE POST-LIGHT-OFF HC EMISSION FACTOR

TWO PARAMETER VEHICLE EMISSION MODEL

The above analysis illustrates the general algorithm to determined the emission factors for a two emission factor model. This implies that the linear equations for the pre-catalyst and post-catalyst light-off regions can be intersected and used to describe the emission performance of the vehicle, for this particular set of ambient and driving conditions. As shown in Figure E-5, the intersection point, indicated by a 'o', of the two linear equations was determined to be 0.48 km. As a result the emission behavior of the vehicle can be completely described by a set of piecewise equations for each of the required emissions as shown in Table E-1. For instance, if the vehicle were to travel only 0.45 km *(0.45km was chosen to illustrate the effects of the pre-light-off emission factor only)*, an expected 58 g (32.6 + 0.45 * 55.7) of HC would be emitted. If the vehicle traveled 50 km, 91 g (32.6 + 0.478 * 55.7 + 0.65 * (50-0.478)) of HC could be expected. Comparing these calculated emissions to a single emission factor of 4.0 g/km (determined from the total mass of HC for the entire trip divided by the total trip distance) represented a total of 1.8 and 200 g for the two simulated trips. This presents a difference of 97% and 120% for the 0.45 and 50 km trips respectively.

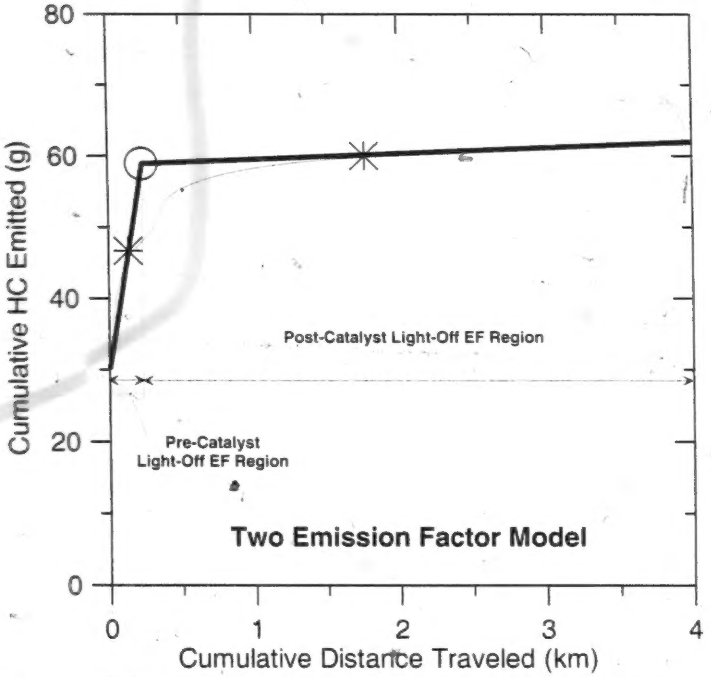

FIGURE E-5 ILLUSTRATION OF THE INTERSECTION POINT OF THE LINEAR REGRESSION ANALYSIS FOR THE TWO EMISSION FACTOR MODEL

TABLE E-1 LINEAR EQUATION FIT COEFFICIENTS FOR THE TWO EMISSION FACTOR MODEL

	Pre-Light Off Region			Post-Light Off Region	
	Range (km)	Slope (g/km)	Intercept (g)	Range (km)	Slope (g/km)
HC	0 to 0.478	55.7	32.6	0.478 to x	0.65
CO	0 to 0.717	632	172	0.717 to x	8.74
NO_x	0 to 1.64	3.84	0.205	1.64 to x	0.185

THREE PARAMETER VEHICLE EMISSION MODEL

As described above, a simple two parameter model can be designed by intersecting the two linear fit equations. But as illustrated in Figure E-5, this model while a vast improvement over the single emission factor descriptions, tends to over predict the emissions in the transition regions. To help improve the accuracy of the emission factor models, a third linear fit can be used to describe the emissions in the transition zones. This fit is conducted by linearly connecting the two previously determined change-over points (i.e. the two points determined in the pre and post-light-off regions where the deviation was greater than 2%) and calculating the slope of this line, representing the transition region emission factor. Figure E-6 details the three parameter emission factor model for the HC emission profile described earlier. Similarly, the emission profiles of this test vehicle can be described by a set of piecewise linear equations. Since this method only differs by the selected changeover points, the equations describing the emissions for the pre and post-light-off regions do not change but are re-presented in Table E-2. Table E-2 also illustrates the new changeover points for the pre and post-light-off emission regions and also displays the slope of the transition region. These equations result in mass HC estimates of 55 g and 91 g for the 0.45 and 50 km trip lengths. These values have 5% and 0% differences when compared to the two emission factor model and 97% and 36% when compared to the single emission factor model. Note that both the two and three emission factor model will yield identical results in the post-light-off region.

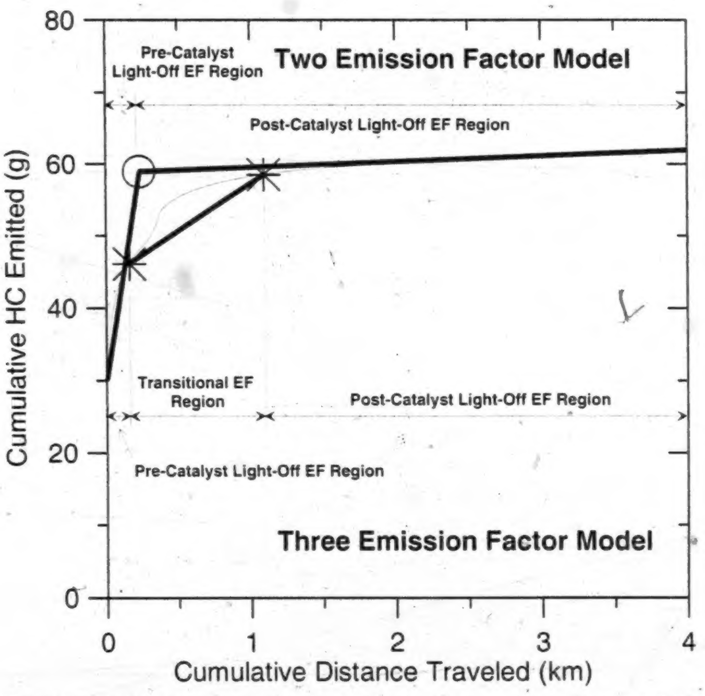

FIGURE E-6 ILLUSTRATION OF THE TWO AND THREE HC EMISSION FACTOR MODEL

Table E-2 Linear Equation Fit Coefficients for the Three Emission Factor Model

	Pre-Light Off Region			Transitional Region		Post-Light Off Region	
	Range (km)	Slope (g/km)	Intercept (g)	Range (km)	Slope (g/km)	Range (km)	Slope (g/km)
HC	0 to 0.403	55.7	32.6	0.403 to 1.31	6.06	1.31 to x	0.620
CO	0 to 0.431	632	172	0.431 to 3.01	78.5	3.01 to x	8.74
NO_x	0 to 1.17	3.84	0.205	1.17 to 3.52	0.920	3.52 to x	0.18

Emission Control Anomalies

The emission factors determined above, were computed with the designed algorithm and explained on an example which included no emission control anomalies. It was found that for this particular test vehicle that the emission control strategy at times could fail, and the emission profiles would resemble those of an un-functioning catalytic converter. Two cases were notice upon examination of the cumulative emission profiles. The first situation was one in which the emission control strategy was lost for the HC, CO and NO_x emissions once in the stabilized region, as illustrated in Figure E-7 for an example HC case. To deal with this type of emission anomaly, the same algorithm described above was first used to determine the pre and post-catalyst light-off points. That is the linear regression analysis was utilized within the two regions. The main difference was that the size of the linear region in the post-light-off zone was truncated to not include the rise in the cumulative HC emission profile due to the emission control failure. Then, a linear line was used to join the stabilized catalyst operation point to the final HC mass value, as shown with the dashed line. The slope of this line was then used as the post catalyst light-off emission For this example the HC emission factor found with the original algorithm was calculated to be 0.38 g/km. The emission factors determined with the dashed line (providing a better representation of the true emission performance) was determined to be 0.56 g/km which is a 47% increase.

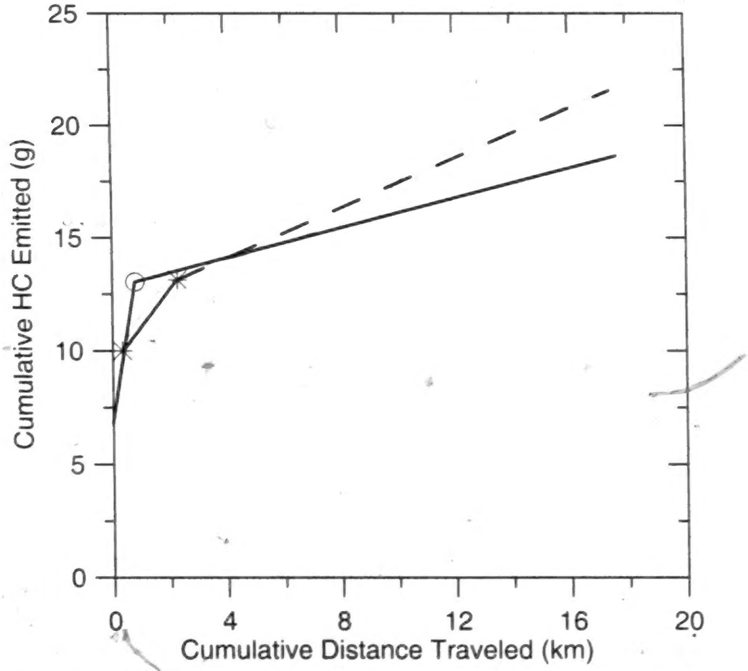

FIGURE E-7 LOSS OF HC EMISSION CONTROL WITHIN THE STABILIZED REGION

The second emission control anomaly concerned the reduction of NO_x emissions. It was found that for certain experiments with this test vehicle, the catalytic converter was unable to reduce the amount of NO_x emissions produced from the engine. This resulted in no catalyst light-off and corresponding NO_x emission profiles as displayed in Figure E-8. These situations were handled by using a linear regression analysis applied to the entire cumulative plot and calculating a single NO_x emission factor for the entire trip.

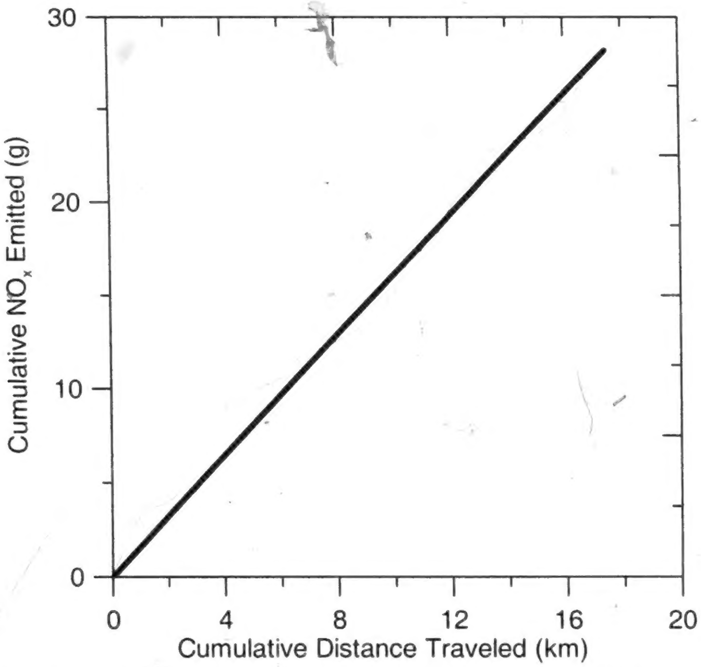

FIGURE E-8 NO NO$_x$ EMISSION CONTROL FOR THE ENTIRE EXPERIMENT

CONCLUSIONS

The above analysis has illustrated a detailed method/procedure for determination of the emission factors from the smoothed cumulative plots. As previously mentioned, this analysis only focused on the g/km emission factor, but could easily be extended to emission factor representing g/kg$_{fuel}$ and g/kWhr. Also, as was presented in the analysis, the use of a two emission factor model greatly improved the accuracy of the estimated mass production when non-standard trip distances are examined, that is 0.45 and 50 km runs. The accuracy was further improved, with the use of the three emission factor model for distances traveled into the transition region.

REFERENCES

1. Kingenberg K., "Automobile Exhaust Emission Testing" Springer-Verlag, Berlin Heidelberg, 1996.